Universitat Rovira i Virgili

Departament d'Enginyeria Electrònica, Elèctrica i Áutomàtica

Design, Fabrication and Characterization of Thick-Film Gas Sensors

PhD thesis

Presented for PhD qualification by:

Peter Tsolov Ivanov

Director of the thesis:

Xavier Correig Blanchar

June 10th 2004

Tarragona, Spain

Dedicated

to my parents Tsolo and Radijanka

&

my wife Marta

INDEX

ACKNOWLEDGEMENTS

During the work on this thesis, I have been lucky to work in a research group that has helped me a lot and made this period really very pleasant. I would like to thank them all, but particularly my thesis director Dr. Xavier Correig, who has been constantly by my side, advising, supportig, and easing the moments of indecision. Thank you, Xavier, for supervising my first steps in research and for being the best director anybody could imagine!

A PhD thesis is nothing if it is not accepted by the scientific community. And the only possible acceptance is that the results be published in international journals. As I was not a writer, when I began this thesis, I would like to express my particular gratitude to Dr. Eduard Llobet for helping me to get started and for reviewing hundreds of manuscripts again and again.

I would also like to thank all the people of the Department of Electronic Engineering of the URV, particularly Xavier Vilanova, Josep Pallarés, Lluís Marsal, Jesus Brezmes, - all my colleagues, my doctoral companions, especially Mariana, who helped me in many things, not only in my work.

I want to express my gratitude to Isabel Gràcia and Carles Cané for providing me with the micro-machined substrates I used throughout the work. Without these materials the whole PhD thesis would not have been possible.

Jean-Pierre, thank you for allowing me to attend your university and to work with a lot of excellent people and good equipment. I appreciate the time you spent with me, guiding me and helping me during my stay.

Neither must I forget Jaromir Hubalek, my first doctoral companion, who helped me start out in research and introduced me to the methods used for fabricating thick-film gas sensors.

I would also like to thank M. Moncusi and C. Bittencourt for their help in the structural analysis I needed for my samples. Thank you for helping me to discover the invisible and to explain the unexplainable.

I would like to thank the Rovira i Virgili University and the Ministry of Education Culture and Sports (Spain) for doctoral fellowships and the CICYT for project number TIC2000-1598-C02.

Finally, I would like to thank my wife, Marta Ros, for being by my side throughout these years and for helping me to overcome all the difficulties I met on my way. Thank you, Marta, for helping me always to look ahead! Without your help, the writing of this thesis would not have been possible.

RESUME OF THE DOCTORAL THESIS

Title: Design, Fabrication and Characterization of Thick-Film Gas Sensors
Doctorate: Peter Tsolov Ivanov
Director: Xavier Correig Blanchar

Solid-state gas sensors have proved to be very promising for monitoring the emission of air pollutants because they are a low cost option for constructing gas analysers. Some problems associated to this approach, especially their deficient selectivity and high power consumption, remain unsolved. The aim of this doctoral thesis is to develop new sensors and sensor matrices that can improve the selectivity of metal oxide gas sensors and decrease their power consumption.

The methodology used here consists of creating sensor matrices made from sensors with different selectivities. As the sensor response is different at different working temperatures and as the different dopants or catalytic filters accelerate or reduce the sensor response, the different sensors give different reactions. If these reactions are combined, sensor groups capable of discriminating between different pollutants can be obtained with the help of pattern recognition techniques.

The thesis begins by reviewing the methods used for fabricating gas sensors and discussing the problems caused by the poor selectivity of metal oxide gas sensors and the methods for increasing their selectivity. Then, the screen-printing technique is introduced and described. The experiments were performed with three different types of gas sensor substrates (ceramic, silicon microhotplate and silicon-on-insulator microhotplate) and more than 15 active layers (undoped and doped with gold, platinum, silver, titanium and paladium tin dioxide and tungsten trioxide sensitive layers). A wide variety of volatile compounds (ammonia, ethanol, acetone and benzene), gases (carbon monoxide, nitrogen dioxide, methane and hydrogen sulphide) and some binary mixtures were measured. The results obtained from quantitative and qualitative gas analysis using the sensor response from a simple 4 sensor based matrix led to the optimal sensor/sensor matrix for gas/binary mixtures.

The results showed that, with the help of fuzzy ARTMAP neural networks, it is possible to identify and simultaneously quantify the gases analysed by using only one MHP-chip (four sensors) with the same active layer. The doped SnO_2 and WO_3 sensors showed different response to the tested pollutants. Composing carefully the sensor matrix and defining well the working temperature we were able to discriminate, with a high success rate, between the different test gases with no need for pattern recognition techniques.

The main conclusion that can be drawn from this thesis is that sensor matrices can be used, coupled to dynamic pattern recognition techniques, to significantly increase the selectivity of metal oxide sensors. The simplicity of the methods implemented makes them suitable for developing low-cost gas analysers and hand-held e-noses.

The research carried out during this doctoral thesis resulted in 15 articles being published in international journals, 10 communications at international conferences and 3 communications at a Spanish national conference.

Date: June 10th 2004 Signature:

I. INTRODUCTION

After decades of neglecting the effects that ever-increasing industrial, agricultural and military activities can have on human health and ecosystems, there is an urgent need world-wide to find solutions that comply with newly reinforced environmental regulations. However, surveying, protecting or even cleaning-up the environment is enormously expensive and time consuming. Recent developments in chemical sensors have provided simple, yet efficient strategies suited to environmental applications. Indeed, chemical sensors are often cheap, reliable, real time and field-portable alternatives that do not compromise detection sensitivity. Despite the huge number of publications on chemical and biological sensing, not all of the current findings have been developed into commercial devices. This is partly due to the complexity of the environmental matrix, which can cause interference, and partly to the fact that the sensor has to integrate electronics, mechanical design, hardware and software.

In the European Union, in response to the Fifth Action Programme targeting the protection of public health and quality of ambient air, the European Commission published Directive 96/62/CE, the aim of which was to set up and identify the ambient air quality objectives. The monitoring of air quality in every state member makes it possible to obtain the best available set of data on atmospheric pollution. As a following step, the European Commission has launched the Sixth Environment Action Programme. One of its main approaches is to find solutions for environmental monitoring and control.

The diversity and complexity of contaminated matrices along with the broad concentration range of target pollutants within them can pose difficult sampling and sample preparation problems, especially for field analytical methods. However, research in the area of chemical and biological sensors is very active and their success depends on making small, low-cost, long-life devices such as micro-systems, autonomous sensing devices and wireless systems. These can often have the advantage of low reagent consumption and low waste production. Microsystems can also be batch-fabricated, making them inexpensive as sensors.

In the last few years, the Department of Electronics of the Rovira i Virgili University has been focussing on this field of knowledge, and has obtained significant results in the fabrication and characterization of semiconductor gas sensing materials, as well as in the development and testing of gas sensor devices. Joint work with National Centre of Microelectronics, Barcelona (Spain) and with the Catholic University of Louvain, Louvain-la-Neuve (Belgium) have made it possible for us to work with their newest sensor substrates in an attempt to create reliable and selective sensors, with low thermal inertia and energy use. The partnership with the Technical University in Brno (Check Republic) has enabled us to produce highly sensitive and time-stable active layers with excellent properties and different reactions to the tested species. The enriching collaborations with the Scientific Resource Service of the Rovira i Virgili University in Reus and the Interdisciplinary Laboratory of Electronic Spectroscopy Notre-dame de Paix in Brussels (Belgium) have been of great importance for improving our knowledge about the structural characterization of the fabricated sensing layers.

The aim of this doctoral thesis is to develop small thick film gas sensors with low power consumption and improved selectivity, which can be used for low-cost hand-held gas analysers (especially for air quality control) and electronic noses. The approach adopted here creates sensor matrices from microhotplate sensors with different selectivities. As the sensor response is different at different working temperatures, measuring the sensor reaction at a set of operating temperatures makes it possible to create a database, which can then be used in statistical and neural pattern recognition algorithms.

At the very beginning, we learned to deposit thick film metal oxides like SnO_2 and WO_3 onto different substrates like alumina, silicon microhotplates and silicon-on-insulator microhotplates with very high technological efficiency. The function of the catalysts and of the noble metal doping is widely studied. We chose the screen printing instead of the

conventional sputtering technique, because it permits us to obtain thicker layers with high porosity and better sensitivity. As our work was closely related to a joint project with the Spanish Commission for Science and Technology, whose basic objective was detection of ammonia, after the initial test with tin dioxide, which is the most usually used material for gas detection, we proceeded to use tungsten trioxide, because of its high affinity to ammonia.

This thesis has been organized as follows:
Chapter II *State of the art of gas sensors* presents the state of the art of semiconductor gas sensors and summarises the mechanisms by which sensors react to gases in the air. The role of the metal oxide, of the catalysts and of the operating temperature is discussed. The major problem caused by the poor selectivity of metal oxide gas sensors is presented and various methods for solving it are reviewed. Finally the most commonly used metal oxides (tin dioxide and tungsten trioxide) for fabricating active layers are presented. Several concepts concerning the improvement in the sensitivity of active layers are discussed.

In chapter III *Thick film technology for gas sensor fabrication* we make a detailed description of the screen-printing technique, which is the main technique used for fabricating our gas sensors. This chapter reviews the thick-film processes used for fabricating our sensors. It begins with a detailed review of thick-film technology and presents the whole substrate fabrication process. All the processes are briefly explained and then they are implemented for the different substrates used.

In chapter IV *Fabrication of thick film gas sensors on Al_2O_3 substrate* we present the fabrication steps for producing the main elements of the sensor substrate (electrodes, heater and temperature resistor). Particular attention is paid to the pastes produced for the active film. The deposition of the active layer on alumina substrates and the annealing processes used are also described. The chapter continues with the wire bonding procedure and sensor packaging and testing. How to minimize the power consumption of the heating element is also discussed. Different techniques for physically characterizing the fabricated active layers were used. We present some analyses with these techniques, and we also discuss the results obtained. These studies improve our understanding of the main physical and chemical sensing phenomena that take place in the sensing material. Finally, we describe the measurement systems used for the chemical test and the experiments performed. We began our investigation with a simple sensor fabricated on both sides of alumina substrate. With this

sensor type we present detailed studies of various pure and doped active layers. The influence of the doping method and the use of catalytic filters are also shown.

In chapter IV *Fabrication of thick film gas sensors on microhotplate and silicon on insulator substrate* we discuss about one of the most promising sensor substrates based on silicon microhotplates and silicon-on-insulator microhotplates. Initially the different sensor substrates are presented. Then we go on with the introduction of the different pastes used for the active layers. The physical structural composition of the active layers obtained is very important. For this purpose we use Scanning Electron Microscopy, Energy-Dispersive X-ray Spectroscopy, Atomic Force Spectroscopy, X-ray Photoelectron Spectroscopy and Raman Spectroscopy. The objective of these analyses is to obtain information about the material structure, which may be related to its detection properties. For these reasons, detailed studies are made, especially for the layers loaded with noble metals. The nano-crystalline properties of these sensing layers were also investigated. The most significant results from the analyses with these techniques are presented. Three different types of sensors are used. At the beginning we introduce the silicon substrate, with which we try to solve the problem of the adhesion of the thick film paste to the silicon. Once we successfully solve this problem, we implement screen-printing technology to fabricate thick-film gas sensors on microhotplates. For power consumption to be even lower, we use sensors based on silicon-on-insulator substrates with deposited thick film layers. For all of the fabricated sensors, we present measurements with gases and volatile compounds such as CO, NO_2, benzene, ammonia, ethanol, and acetone. These species are chosen because of their negative effects on the environment and human beings. The results of quantitative and qualitative gas analysis using microhotplate-based sensors and different pattern recognition methods are also discussed.

The PhD thesis finishes with the *Conclusions* drawn from the work done and from the studies performed during the investigation. The results obtained from the thesis are summarized and briefly discussed.

In *Appendix A*, a concise review of the frequently used techniques for physically characterizing active layers is made. In *Appendix B* we summarize all the information obtained from the measurements of different sensor sets. A *Reference list, List of our publications* and *Participation in international and national congresses* is attached to the end of the thesis.

II. STATE OF THE ART OF SEMICONDUCTOR GAS SENSORS

Semiconductors are between one of the most common used types of sensor, in which semiconductor materials are mainly responsible for sensor operation. Acoustic sensors are used to determine wave amplitudes, phases, polarization, spectra and wave velocity. Electrical and magnetic sensors, used in positional control, detect the electromagnetic field, charge, potentials, current, fluxes, conductivity and permeability. Mechanical sensors are used to detect position, velocity and acceleration (linear, angular), force, stress and strain, mass density, moment, torque, speed of flow, shape, roughness, orientation, stiffness, viscosity and material structure. Optical sensors are used in cameras and night-vision systems. Temperature and flow sensors are used in air conditioning and automotive systems. Chemical and biological sensors are used in biological diagnostic systems to detect biomass characteristics. The list of applications is enormous, and it is growing yearly. It is of particular importance that the sensor characteristics should be known: response speed, sensitivity, measuring range, (short-term/long-term) stability, resolution, selectivity, ambient conditions, allowed overload characteristics, operating lifetime, output format, size, weight and cost for each measurand.

Currently, there is a considerable demand for low-cost, accurate, and reliable sensors for industrial and consumer product applications. This study deals with chemical sensors and how they work. In this chapter, we consider semiconductor-based chemical sensors for gas

detection, their basic features and parameters. First, we provide an overview of the materials that can be used as the active layer, including metal oxide, mixed oxide and organic substances, and we go on to deal with the problem of selectivity and how it can be enhanced. Then we discuss how sensor arrays and catalytic additives can be used to improve sensor sensitivity and selectivity. We describe thick- and thin-film deposition technology and, in particular, thick-film gas sensors. At the end, a state-of-the-art summary of the active material is given for SnO_2 and WO_3-based gas sensors.

II.1 Need of semiconductor gas sensors

Nowadays, there is great interest in using sensing devices to improve the environmental and safety control of toxic gases. There is also a great need for these kind of sensors for optimizing combustion reactions in the emerging transport industry, and domestic and industrial applications.

The most commonly used gas sensor devices can be divided into three big groups depending on the technology applied in their development: solid state, spectroscopic and optic. Spectroscopic systems make a direct analysis of the molecular mass or vibrational spectrum of the target gas. They can quantitatively measure the composition of the different gases with good precision. Mass chromatography and mass spectrometry are maybe the most important gas sensor spectroscopic systems. Optical sensors measure absorption spectra after the target gas has been stimulated by light. They require a complex measurement system: a monochromatic excitation source and an optical sensor to analyse the absorbed spectra. Expensive analytical techniques (such as infrared spectroscopy, ultraviolet fluorescence, chromatography, etc.) are used to analyse gases instead of techniques based on chemical sensors. The gas chromatograph (GC) is very often combined with a mass spectrometer (GC-MS) for separating and identifying compounds. Through mass spectroscopy, the molecular mass and typical fragmentation of an unknown volatile can be obtained and compared with reference libraries. Infrared spectroscopy using Fourier transform methods can also be combined with a gas chromatograph (GC-FTIR). Due to its ability to differentiate between isomers, it can complement GC-MS [1]. To detect odours, the gas chromatographic separation of volatiles can be combined with sensory analysis of individual peaks, using a split gas-stream GC-technique [2]. All these techniques are very precise, sophisticated and require a technician with a lot of experience to work with the equipment in order to obtain usable results.

While spectroscopic and optic systems are too expensive for domestic use and sometimes difficult to implement in reduced spaces such as car engines, the so-called solid state sensors have great advantages. They are small, so they can be portable, they are low-power consuming, they are inexpensive because of the considerable production of semiconductor technology and they can be used in complex systems such as sensor arrays. Furthermore, these sensors are capable to work on-line without need of specially trained operators. They are based on the change in the physical and/or chemical properties of their sensing materials when exposed to different gas atmospheres. Although a huge number of materials can be used to implement these devices, this study will focus only on the ones with semiconductor properties, and more specifically on those using WO_3 and SnO_2 as sensing materials. The major disadvantages of this type of sensors, especially their lack of selectivity and time-stability will be discussed later in this chapter.

The conductivity of the sensing material in semiconductor gas sensors changes in the presence of a particular gas. The working temperature at which these devices are most efficient depends on the gas atmosphere and on the properties of the sensor material selected in every case. As these temperatures range from 200 to 800ºC, far above room temperatures, a heating system must be implemented in the sensor devices. A simple semiconductor gas sensor consists of a substrate (where the sensor material is supported), inteerdigitated electrodes (to measure the conductivity changes), a measuring resistor (to control the sensor temperature) and a heater (so that the optimum sensing temperature can be reached). Nowadays, new metal-oxides, temperature cycling, catalytic filters and doping combinations are being investigated in an attempt to solve problems of the sensitivity and selectivity of solid state gas sensors.

II.2 Basic considerations

In 1938, Wagner and Hauffe discovered that atoms and molecules interact with semiconductor surfaces, and influence such surface properties as conductivity and surface potential. The effect of the ambient atmosphere upon the electrical conductance of semiconductors was described by Brattain and Bardeen (1953), Heiland (1954) and Morrison (1955). Subsequently, Seiyama *et al* (1962) and Taguchi (1970) applied this discovery to gas detection by producing the first chemo-resistive semiconductor gas sensors [3].

The most suitable semiconductor materials for this type of sensor are metal oxides. Unlike other semiconductors which, under long-term or cycled heating in air, undergo irreversible

chemical transformations by forming stable oxide layers, metal oxides bind oxygen on their surface in a reversible way. Metal oxide sensors have been commercially available for many years. The leading manufacturer is Figaro Engineering in Japan. The type of metal-oxide sensor sold by Figaro is known as the "Taguchi sensor", named after the developer of the SnO_2 sensor. Metal oxide sensors operate by decreasing the resistance of a layer of ceramic SnO_2 if a combustible gas is present in the ambient atmosphere.

II.2.1 Oxygen sensing (bulk type mechanism)

Much of the interest in developing low-cost oxygen sensors stems from the need to monitor the exhaust gases from internal combustion engines. In such environments there are simultaneous changes in the partial pressure of oxygen and of a number of other gases as the ratio of air to fuel in the ignition mixture (the lambda ratio) is altered. Oxygen sensors used in this application are thus sometimes referred to as "lambda sensors". A particularly sensitive application arises when the system is required to operate in the fuel lean region. Semiconducting oxides that have been explored as lambda sensors generally respond to changes in oxygen partial pressure at high temperatures (700°C and above) by exploiting the equilibrium between the composition of the atmosphere and the bulk stoichiometry. In general, the relationship between oxygen partial pressure and the electrical conductivity of a mixed valence oxide sensor may be represented by:

$$\sigma = A\exp(-E_A/kT).P_{O_2}^{1/N} \qquad \text{(II.1)}$$

where σ is the electrical conductivity, A is a constant, E_A is the activation energy for conduction, P_{O_2} is oxygen partial pressure and N is a constant determined by the dominant type of bulk defect involved in the equilibrium between oxygen and the sensor.

Equation (II.1) makes it clear that the lower the value of N, the more sensitive the electrical conductance will be to changes in oxygen partial pressure. Also the lower the value of E_A, the lower the sensitivity of the response will be to temperature fluctuation. The first material seriously investigated for use as a bulk-equilibration sensor for oxygen was titanium dioxide, which is n-type over the oxygen partial pressure range of interest. Oxygen sensors were prepared as thick films of $BaTiO_3$. They had the advantage of simplicity and their transient responses were faster than those with the conventional stabilised zirconia potentiometric alternative. However, titanium dioxide has an activation energy for conductivity of around 1.5 eV which translates into a 100% resistance change for a 40°C shift in temperature around

600°C. Thus considerable uncertainty is introduced to the measured value of lambda as the temperature varies. Initially two means of overcoming this problem were proposed: either the sensor could be provided with a printed heating track in addition to the oxygen sensitive element so that the operating temperature of the device could be held constant a little above the maximum temperature attained by the local ambient or the sensor could be incorporated in a voltage divider network in series with a thermistor so that temperature variation could be compensated.

An alternative solution would be to replace titanium dioxide with a material that combines useful oxygen sensitivity with activation energy of almost zero. Now the measured dependence of conductance on oxygen partial pressure for many semiconducting oxides follows the form of the data for $BaTiO_3$. The material is n-type at low oxygen partial pressure but above certain minimum conductance values the material is p-type. An important feature of the data shown here and the equivalent characteristic for several perovskite structure oxides is that, in the p-type range, the isothermal data lines are very much closer together than in the n-type range. In other words, the temperature dependence of conduction is considerably less in the p-type than in the n-type range. The reasons for this characteristic are quite interesting. In general, as the temperature is raised at a fixed oxygen partial pressure, the oxides of transition metals lose oxygen. And if they are in the p-type range of oxygen partial pressure, conductivity will tend to decrease. This effect is contrary to the thermal promotion of charge carriers and it makes it possible to dope the oxide to such an extent that the two effects cancel each other out and the temperature changes have hardly any effect on the conductivity.

Two points should be made. First, this balance of thermal effects must not alter the effect of changes in oxygen partial pressure at a fixed temperature. Secondly, such a balance is only possible for oxides in the p-type regime, where the thermal activation of charge carriers and the stoichiometry effect are opposed. For $BaTiO_3$, the thermal activation and stoichiometric effects are not quite in balance so the activation energy is small but not zero. A family of doped perovskite structure ferrates has been found, however, where the balance is achieved and the activation energy is almost zero over a considerable temperature range. Materials such as $BaFe_{0.8}Ta_{0.2}O_3$ retain substantial oxygen sensitivity and thus should be useful in the construction of oxygen sensors without the need for additional temperature control or compensation elements.

II.2.2 Minority gases in air (surface type mechanism)

The second major category of gas detection for which semiconducting oxides are used is in an atmosphere of fixed oxygen partial pressure (air) to detect minor concentrations of potentially hazardous gases. Bulk changes in oxygen stoichiometry are not relevant to this type of application and the materials are normally held at temperatures between 300-500ºC, where useful surface reactions proceed at a sufficient rate.

The central surface reaction that controls most gas responses of semiconducting oxides operating in air at temperatures between 300-500°C involves changes in the concentration of surface oxygen species such as O_2- (figure II.1).

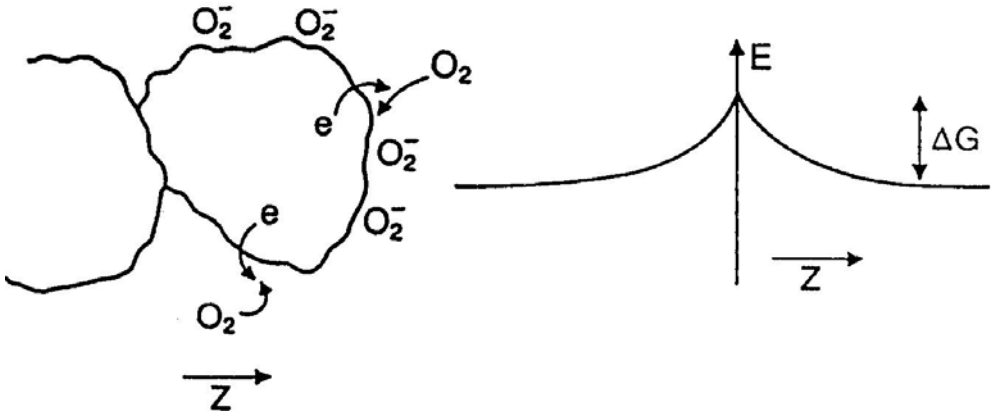

Figure II.1. Charge exchange associated with the chemisorption of oxygen at a semiconductor surface and the potential distribution across a grain junction

The formation of such ions by oxygen adsorbed at the gas/solid interface abstracts electrons from the bulk of the solid. The oxygen can thus be thought of as a trap for electrons from the bulk. In the case of an n-type semiconductor such as SnO_2, the electrons are drawn from ionised donors via the conduction band, so the charge carrier density at the interface is reduced and a potential barrier to charge transport, ΔG, is developed. As the surface charge increases, the adsorption of further oxygen is inhibited. The adsorption rate slows down because the charge must be transferred to the adsorbate over the developing surface barrier, and the coverage saturates at a rather low value. At the junctions between the grains of the solid, the depletion layer and associated potential barrier make high resistance contacts, which dominate the resistance of the solid.

Thus at temperatures between 300-500°C semiconducting oxides can be used as gas sensitive resistors to monitor as impurities in air any gases that can react in such a way that they alter

the quantity of charge trapped at the surface. For example, in the presence of a reactive gas such as carbon monoxide, a surface catalysed combustion like:

$$2CO + O_2- \rightarrow 2CO_2 + e- \quad \text{(II.2)}$$

may occur so the surface coverage of adsorbed oxygen ions may decrease. Likewise, the resistance may decrease as a consequence of the reduction in the surface potential barrier height and the depletion length. The surface barrier height, ΔG, depletion layer width d_{sc} charge Q_s associated with oxygen surface coverage, and donor density N_D are related as follows:

$$d_{sc} = Q_s/N_D e \quad \text{(II.3)}$$

$$\Delta G = Q_s\, 2/2\varepsilon_o \varepsilon e N_D \quad \text{(II.4)}$$

In the case of a p-type oxide, adsorbed oxygen acts as a surface acceptor state, abstracting electrons from the valence band and increasing the charge-carrier (hole) concentration at the interface. Any decrease in the surface coverage of oxygen ions, for example caused by reactions such as the one shown in reaction (II.2), decreases the charge-carrier concentration and hence increases the resistance of the material.

So materials can be classified as n-type or p-type according to whether their resistance increases or decreases when they are exposed to a reducing gas in an atmosphere of fixed oxygen partial pressure (air). The resistance of some semiconducting oxides is also found to respond to the introduction of oxidising gases, such as chlorine and nitrogen dioxide, in air. It is very unlikely that these gases will react with surface oxygen ions. More likely are direct chemisorption reactions such as

$$NO_2 + e^- \rightarrow NO_2^- \quad \text{(II.5)}$$

On the basis of reactions such as these, it is expected that responses would take place in the opposite sense to those with reducing gases. A consistent pattern of response type would be as shown in Table II.1.

Material	Reducing gases	Oxidising gases
n-type	Resistance falls	Resistance rises
p-type	Resistance rises	Resistance falls

Table II.1. Resistance responses expected for reducing and oxidising gases on n and p-type semiconducting oxides

One further mechanism by which the resistance of a semiconducting oxide may be modified as a result of gas reactions involves the effect of water molecules. The resistance of tin dioxide is dependent on the ambient moisture content at temperatures up to 600°C. Between 300 and 600°C the response to changes in moisture level is quite reversible. For this reason, whenever a surface-catalysed reaction leads to the formation of water, such as:

$$2H_2 + O_2^- \leftrightarrow 2H_2O + e^- \quad \text{(II.6)}$$

both the reaction product and the release of electrons can contribute to the resistance response.

The most commonly used metal oxide material in resistive sensors is SnO_2. When a metal oxide crystal such as SnO_2 is heated at a particular high temperature in air, oxygen is adsorbed on the crystal surface with a negative charge, as was discussed before. Then, donor electrons in the crystal surface are transferred to the adsorbed oxygen, which leaves positive charges in a space charge layer. This creates surface potential, which serves as a potential barrier against electron flow (Figure II.2 left).

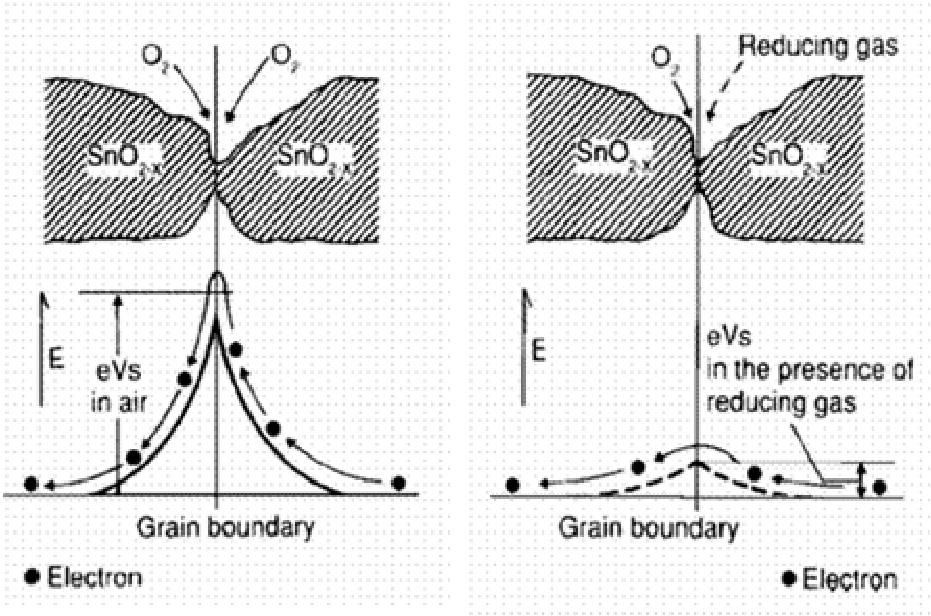

Figure II.2. Model of inter-grain potential barrier: in the absence of gas (left); in the presence of gas (right)

Inside the sensor, the electric current flows through the conjunction parts (grain boundary) of SnO_2 micro crystals. At grain boundaries, adsorbed oxygen forms a potential barrier, which prevents carriers from moving freely. The electrical resistance of the sensor is attributed to this potential barrier. In the presence of a deoxidizing gas, the surface density of the

negatively charged oxygen decreases, so the barrier height at the grain boundary is reduced (Figure II.2 right). This decreases the sensor's resistance. The relationship between sensor resistance and the concentration of deoxidizing gas can be expressed by the following equation over a certain range of gas concentration:

$$R=AC^{-\alpha} \quad \text{(II.7)}$$

where R is the electrical resistance of sensor; A, α are constants; and C is the gas concentration.

In summary there are a number of ways in which semiconducting oxides between 300-500°C can provide resistance responses to the introduction of impurity gases into an air ambient:

- ✓ Reducing gases can react to reduce the concentration of surface oxygen ions
- ✓ Oxidising gases can undergo direct reaction
- ✓ Reaction products such as water can have an effect.

The foregoing brief survey of mechanisms by which semiconducting oxides provide responses to changes in atmospheric composition emphasises the detailed electronic properties of the bulk and the reactivity of the solid surface and thus leads to an expectation that the characteristics of gas sensors will be strongly influenced by the selection of materials.

In gas sensitive resistors operating at 500°C or below, the material most commonly used to measure impurity gases in air is tin dioxide. Tin dioxide sensors, though often useful in particular alarm functions, have generally been found to suffer from a lack of selectivity. Many reducing gases and increases in relative humidity give rise to conductance increases on tin dioxide. This characteristic has limited the commercial development of gas sensors and considerable efforts have been expended to find oxide materials with specific responses. Many materials have been found to respond like gas sensitive resistors and the responses of some materials can be far more selective than tin dioxide. Because the response mechanism depends on an optimum combination of the electronic properties (bulk) and catalytic properties (surface), different materials are expected to show a wide variety of behaviour. It should therefore be possible to engineer properties to some degree. Doping of the parent structure oxide with alternative metal ions should make it possible to adjust the electronic properties and the addition of second-phase matter at the oxide surface should make it possible to modify the catalytic properties.

An important outcome of the work on alternative materials has been the demonstration of an analogy with the function of the bulk equilibration mechanism of transition metal oxides in the monitoring of oxygen. Just as a semiconducting material can be switched from n-type to p-type by equilibration with an atmosphere of higher oxygen partial pressure it can also be switched by the interaction of reducing gases at the oxide surface if the materials have a sufficient surface/volume ratio.

A simple model of these effects indicates that when the bulk donor density is low enough, the average grain size small enough and the surface acceptor state density high enough, the grains are fully depleted of conduction electrons. So depending on the surface density of the acceptor states, the conductivity may pass through a minimum value or not. Increasing the concentration of hydrogen sulphide decreases the density of surface oxygen ions past the point where the dominant charge carriers switch from holes to electrons. This type of effect has been demonstrated with a variety of gases on a variety of oxides.

As in the case of bulk equilibration sensors for oxygen, the conductance minimum can be negotiated by systematic substitution and it is possible to operate a sensing material well away from this condition. Close to the conductance minimum there is potential for ambiguity but the characteristic change of sign that it produces may be put to good use.

II.2.3 Catalysts (basic assumptions)

Metal oxide gas sensors often use a catalyst deposited on the surface of the semiconductor to accelerate the reaction and increase the sensitivity. The catalyst increases the chemical reaction without itself changing. It does not change the free energy of the reaction but lowers the activation energy. For example, Pt can be considered as the catalyst in the oxidation of hydrogen. Without Pt, the reactions would be as follows:

$$\begin{aligned} H_2 &\rightarrow 2H \\ O_2 &\rightarrow 2O \\ 2H + O &\rightarrow H_2O \end{aligned} \qquad \text{(II.8)}$$

The first two equations require a huge input of energy and will not happen at moderate temperatures. On the other hand, with Pt available as a catalyst, the possibilities are the following:

$$\begin{aligned} H_2 + 2Pt &\rightarrow 2Pt - H \\ O_2 + 2Pt &\rightarrow 2Pt - O \\ 2Pt - H + Pt - O &\rightarrow 3Pt + H_2O \end{aligned} \qquad \text{(II.9)}$$

The first reactions require very little energy input. A hydrogen molecule adsorbed on the Pt surface readjusts its bonds to form Pt-H groups. The Pt effectively dissociates the hydrogen molecule and presents the hydrogen in the active form. Thus, the overall reaction has very low activation energy and can proceed at relatively low temperatures. If the sensor depends on such a reaction, the catalyst will lower the response time.

A promoter is a second additive, one that improves the catalyst's performance. The obvious mechanisms for promoting action are: stabilizing the surface so the reaction cannot irreversibly change the surface; inducing phase changes in the catalyst so that it provides the more active phase; stabilizing the surface area; or stabilizing the favourable valence state (such as Cu^{+} rather than $Cu+Cu^{2+}$).

The catalyst chosen influences the selectivity of the sensor. The ideal case is that the catalyst combination catalyzes the oxidation of the gas of interest but not that of any of the other combustible gases. Unfortunately, these cases are not easy to find. However, there is some selectivity. Arrays of sensors with different catalysts are used to detect a spectrum of gases.

Transition metal oxides, such as TiO_2, SnO_2, WO_3, In_2O_3, etc. appear to be the best candidates for semiconductor gas sensors [4]. The sensitivity of these devices is based on the dependence of the conductivity of metal oxides on the surrounding atmosphere. Nevertheless, if these devices are to be developed to the full, their characteristics should be improved by introducing metal additives [5], which enhance the material sensitivity and selectivity, and decrease the response time and the operating temperature of the sensitive layer [6, 7]. To increase the sensitivity and selectivity, one of the most widely used methods has been to add catalytically active metals, such as Pt and Pd [8-10] or even Au [11], which have been claimed to promote chemical or electronic sensitizations [12, 13]. Adding other elements such as Sb or La mainly changes the doping level, thus modifying the bulk Fermi level position and, hence, the equilibrium carrier population at the grain surfaces. Adding different metallic species to semiconductor gas sensing materials will improve the detection of a particular gas in every specific case. Table II.2 summarizes the most widely used sensing semiconductor materials with their specific metal loading and the corresponding target gases.

Target Gas detected	Metal Additive/SC used
CO	Ag /WO_3, Fe_2O_3, Pd / SnO_2, Pt / SnO_2
CH_4	Pt /SnO_2, Pd / SnO_2
H_2	Pt / SnO_2, Pd / SnO_2, Pt / TiO_2, Nb / TiO_2
NH_3	WO_3, Ag/WO_3, $Cr_{1.8}Ti_{0.2}O_3$, Pt / TiO_2,
O_2	In_2O_3, Pd / SnO_2, Nb / TiO_2, TiO_2
C_2H_5OH	Pt / TiO_2, Pd / SnO_2, Nb / TiO_2
NO_2	WO_3 ,In_2O_3, $LaFeO_3$, Pd / SnO_2, Pt / SnO_2

Table II.2. Sensing semiconductor materials and corresponding target gases [14-21]

Generally, conductometric or resistive sensors cannot explicitly identify an unknown gas or mixture of gases because they are not inherently selective. These sensors, and particularly those that have been developed for reducing gases, usually respond to many compounds. This dilemma of cross-sensitivity is particularly acute when dealing with hazardous industrial chemical agents, explosives, food substances, and so forth, because they are chemically complex. Rapid and accurate identification may be critical for making decisions that affect the safety of personnel and equipment, or the productivity of a manufacturing process.

One theoretical method of synthesizing selectivity or minimizing cross-sensitivity, proposed by Cliffort [22], is to assemble an array of sensors with differential sensitivities to different gases and to solve a series of simultaneous equations to derive the concentrations of all target species. Since this proposal, many investigators have studied various sensor arrays. The success of the approach depends on the degree to which the sensor array gives a unique response for each target gas. Several strategies can be used to create a sensor array: different sensing materials, catalysts, thermal gradients or thermal cycling, and filters (Figure II.3.).

Figure II.3. Gas sensor array of commercial gas sensors

Target gases can be both recognised and quantified as long as only one target substance is present, or if the universe of possibilities is simple enough and the sensor system is sensitive enough. However, a more realistic and therefore more difficult dilemma is how to discriminate among dynamically changing mixtures of compounds.

Another important property is that the presence of metallic additives can also modify the growth kinetics [23, 24]. It has been found that the addition of platinum and palladium can induce important changes in the growth kinetics of SnO_2 nano-powders [25]. For both additives, the SnO_2 grain size depended on the metal concentration. The higher the concentration was, the lower the resulting grain size. In contrast, gold did not introduce any significant change. The size of the nano-powders obtained with gold did not depend on the gold concentration.

The amount and distribution of the metal is one of the parameters that most affects sensitivity. Figure II.4 shows a schematic representation of some additive distribution patterns.

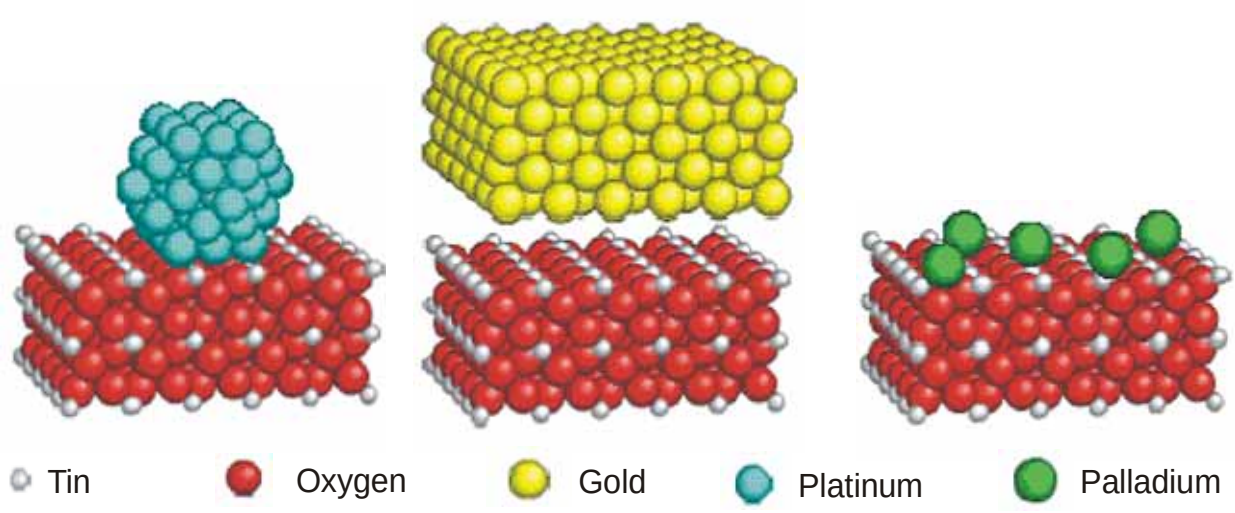

Figure II.4. Schematic representation of additive distributions on sensing material structure (SnO_2): left - superficial clustering, showing a Pt nano-cluster on a SnO_2 surface; centre - macro-agglomerated metal, showing metal additive clusters (Au) as big as metal oxide grains; right - atomically ultra-dispersed metals, with several Pd atoms on a SnO_2 surface

When loading metal additives into semiconductor materials it is generally expected to use metals, which can promote the desired chemical reactions. A metal cluster or nano-cluster formation is also expected to be found on the surface of semiconductor nano-powders, such as

those observed in the case of Pt and Pd [26]. Although this is the general situation in additive disposition, these metals can also be distributed in other ways. Sometimes, when the metal is loaded in low concentrations it can be dispersed as mono-atomic centres. The additive metal is then ultra-dispersed or atomically dispersed on the semiconductor's surface, as found in the case of Pd on SnO_2 [27]. On the other hand, metal distribution can lead to the formation of macro-agglomerated metal clusters as big as semiconductor grains, as found in the case of Au loaded onto SnO_2 [28]. All these additive disposition patterns will be briefly described below, and it will be explained how each one leads to gas sensing and catalysis.

II.2.3.1 Metal diffusion inside the semiconductor bulk

The first option for additive distribution is metal diffusion inside the semiconductor bulk, occupying interstitial or substituting positions or inducing structural changes in metal oxide structure. At present, there is a considerable interest in the effect of chemically inequivalent foreign atoms on the surface reactivity of the metal oxides. It is highly desirable to chemically incorporate the foreign atoms without changing the crystallographic structure of the metal oxides.

II.2.3.2 Superficial clustering

From the point of view of catalysis, it is generally expected that metal additive loading will involve the formation of nano-clusters on the metal oxide surface. Several authors have pointed out that this mainly happens in the case of noble metal loadings. The diameters of these nano-clusters typically range from 1 to 8 nm. Both Pt and Pd provide effective catalytic adsorption sites for oxygen and reducing gases, and nucleate on metal oxide surfaces. The main difference between Pt and Pd is that Pd forms a stable compound with oxygen whereas Pt does not at the temperatures used in sensing [23]. As a result, part of the Pt remains in a metallic state in air, providing not only catalytic adsorption sites for oxygen but also helping activated oxygen species to spill over onto the metal oxide surface where they get ionosorbed by trapping electrons from the metal oxide. This increase in the density of ionosorbed oxygen species explains the large resistance observed for the Pt-SnO_2 film. Under a reducing gas environment, the metallic Pt provides preferential catalytic adsorption sites for reducing gas. The surface-adsorbed reducing gas further dissociates into more active species at a faster rate and spills over onto the metal oxide surface to react with ionosorbed oxygen. This explains the rise in sensitivity and fall in response time for Pt-SnO_2 films.

On the other hand, Pd forms a stable oxide in air. Several studies have reported that Pd can oxidise at temperatures as low as 300 ºC in oxygen and consequently, at higher temperatures (450-500ºC), PdO is the predominant species and is responsible for the catalytic activity. It has also been observed that the work function of the metal oxide changes due to the change in the oxidation state of Pd, as happens in the case of Pd/SnO_2 [23]. In other words, Pd in the oxygen phase acts as an electron acceptor and traps the charge from the metal oxide conduction band. This trapped charge, along with that of the ionosorbed oxygen, further depletes the electrons from the metal oxide surface, which causes a rise in resistance. Since the depletion of carriers is related to the density of trapped charge at the surface, Pd clusters must be a few nano-meters in size if they are to affect the resistance.

As we explained, the addition of small amounts of noble metals such as Pd and Pt to the metal oxide used for gas sensing can promote not only gas sensitivity but also the rate of response. The promoting mechanisms are not the same for all metals, as Yamazoe et al. demonstrated with their XPS studies on three different promoters - Ag, Pt and Pd - in the early 90s [23]. They recognized a notable difference among by whether these additives affected the work function of the metal oxide (Pd) or not (Pt) and proposed two types of sensitization mechanisms:

Electronic sensitization (Pd)

Electronic sensitization comes about by a direct electronic interaction between the metal additive and the semiconductor surface. When the oxidation state of the metal additive changes with the surrounding atmosphere, the electronic state of the semiconductor will also change accordingly. More specifically, the typical additives of this type (Pd) are known to form stable oxides (PdO) in air, while they are easily reduced to metals with a reducing gas. The oxidized metal produces a strong electron-depleted space-charge layer inside the semiconductor, inducing shifts in its work-function. However, this electron interaction is ruptured when the oxidized additive is reduced to metal. The absence of the electronic interaction between Pt and SnO_2 seems to reflect that Pt cannot form a stable oxide under these conditions [23].

Chemical sensitization (Pt)

Chemical sensitization takes place via a spill-over effect, which is now rather familiar in catalytic chemistry. The promoter in this case activates a test gas to facilitate its catalytic

oxidation on the semiconductor surface. In other words, the promoter does not affect the resistance of the element directly, and the gas-sensing mechanism is essentially the same as when the promoter is not used. The promoter increases the gas sensitivity as it increases the rate of the chemical processes, and this decreases the concentration of the negatively charged adsorbed oxygen. This is why the effect is called chemical sensitization [23].

Obviously Pd particles can be distributed rather uniformly on the spherical surface of each metal-oxide particle. In air, the metal additive exists as PdO clusters, which draw electrons from the metal-oxide particle underneath and produce an electron-depleted layer in the particle. On exposure to an inflammable (reducing) gas, PdO is reduced to Pd, and there is a corresponding decrease or disappearance of the space-charge layer. In this way, PdO nano-clusters act as a receptor to the reducing gas, which is otherwise provided by the adsorbed oxygen. The electron affinity of PdO nano-clusters is far stronger than that of the adsorbed oxygen, which means that gas sensitivity is far higher when working with additive loaded than with unloaded SnO_2.

II.2.3.3 Metal macro-agglomeration

Metal distribution can be also carried on forming macro-agglomerated metal clusters as found in the case of Au loaded to SnO_2 [28]. In the tipical case, Au not only nucleates to form small nano-clusters on metal oxide surfaces, but it also forms large independent clusters which are sometimes as big as the metal-oxide grains (between 50 and 200 nm in diameter). Since the effective area of large metal forming clusters is lower in gas reactions, it is of particular interest to reduce the number of clusters and increase the dispersion of Au nano-clusters on the SnO_2 surface.

II.2.3.4 Metal ultra-dispersion

When the metal is loaded in low concentrations it can be dispersed as mono-atomic centres. The additive metal is then ultra-dispersed or atomically dispersed on the semiconductor surface, as in the case of Pd on SnO_2 [27]. Composite systems consisting of metal particles interacting with a semi-conducting substrate are an electron transport system with interesting properties. At very low concentrations, when the metal may be dispersed as atomic impurities, the metal may act as a donor or acceptor in the semiconductor. At higher metal concentrations, percolating transitions dominate the electrical behaviour of the system.

II.3 Sensor characteristics

A number of behavioural tendencies have been established for the metal oxide sensor. Sensitivity to gases varies with the temperature and is maximum at different temperatures when the gases and oxides are different. Response times are highly dependent on temperature (they are shorter at high temperatures), and the responses to gases are non-linear as a function of concentration. Changes in the ambient temperature cause changes in the sensor response. Another common feature is that water vapour affects both the conductance in air and the sensitivity to other gases. This is why it is preferable to work in a controlled atmosphere. Another possibility is to find materials that are less dependent on humidity or to compensate for this dependence by characterising the sensor response to different humidity values. The objective of the characterization is to establish the optimum operating conditions, and the reproducibility and reliability of the sensor. This involves determining the spread in the various operating parameters for different sensors and different operating conditions, and ascertaining the stability of these parameters.

For most semiconductor devices, there will be a spread in the characteristics measured. This is because both the chemical and the physical properties of the semiconductor are affected by the presence of trace impurities. The surface reactions, on which the sensors are totally dependent, are also affected by variations in surface topography. The method used to fabricate the device can also affect the characteristics. The situation can be further complicated when additives are introduced into the oxide to improve some aspect of performance; both the amount of additive and the method of introduction can be critical.

II.3.1 Operating temperature

The characteristics of any semiconductor sensor are likely to be highly temperature dependent, so all measurements should be carried out at a number of temperatures. The temperature range of interest will have been determined during the preliminary work and will be different for different oxides and for different analyte gases. For some devices, and particularly at lower temperatures, conductance takes quite a long time to reach a steady state. Hence, measurements must be made only after sufficient time has been allowed at a given temperature for the conductance to reach a steady value. It has also been suggested that the behaviour of the sensor can be somewhat dependent on the recent history of the sensor. It is therefore advisable, at least in the early stages, to obtain data when temperature is both increasing and decreasing over the range of interest. Semiconductor chemical sensors work at

elevated temperatures, although there are sensors that work at room temperature. This is why we can say that they work in the range from ambient temperature (approximately 25ºC) to temperatures of 900°C.

II.3.2 Conductance

The principal parameter measured is the conductance or resistance of the semiconductor, whether it is in thin film, polycrystalline thick film, single crystal or any other physical form. Since it is unlikely that the conductivity will be uniform throughout the material, and because the measured parameter is in fact the surface resistance, it is meaningless to compute the absolute parameters of conductivity or resistivity.

II.3.3 Calibration curve

This is the curve obtained when the sensitivity to a gas is plotted as a function of the concentration. Since the temperature of operation may be fixed by the findings on sensitivity and selectivity, it may not be necessary to obtain this curve at all temperatures for all gases and for all sensors.

II.3.4 Base line

This is defined as the conductance in clean, dry air, except when measuring the effect of moisture on the sensitivity to other gases or vapours. In this instance, the base line is defined as the conductance in clean air with the specified amount of water vapour added.

II.3.5 Sensitivity

Sensitivity is the device characteristic that perceives the variation in the physical and/or chemical properties of the sensing material when exposed to gas. If it is to be improved, the sensing material must be the most appropriate and the temperature optimum. As several authors have suggested, working with nano-structured materials will give a higher surface area to the gas [29, 30]. Taking into account that sensing reactions take place mainly on the sensor's layer surface, the semiconductor particle size, the catalytic filters and the doping will be some of the first requirements for enhancing the sensitivity of the sensor. The sensitivity to a given concentration of a gas is defined as: (resistance in gas R_g – resistance in air R_a)/(R_a) expressed as a percentage, i.e. (R_g-R_a)/Rx100 %. The sensitivity to the gases and gas mixtures of interest must be measured over the whole temperature range; this gives most of the

parameters required to fully characterize the sensor. From the study of sensitivities, an optimum temperature can be determined.

II.3.6 Response and switch-on time

In gas detection, response time is usually defined as the time taken to achieve 90 % of the final change in conductance following a step change in gas concentration at the sensor. This is because the response is often very fast initially but has a long-drawn-out tail before the steady value is reached. The shape of the curves can vary from one gas to another. The response time is an important parameter since it can determine the applicability of the sensor. Unfortunately it is probably one of the most difficult of all the operating parameters of the sensor to measure.

The switch-on time is the measure of the time taken for the conductance to reach a steady state, in air or in a gas mixture, after the sensor is switched to the operating temperature from cold. This parameter is important if the device is to be used in an intermittent mode, i.e. it is only raised to the operating temperature when a measurement is required. It is much less important when the device can be maintained permanently at the operating temperature, in which case it only governs the length of time required, after switch-on, before a measurement can be made. This parameter can often limit the use of metal oxide devices since, at low temperatures, the rates of deposition of some adsorbed species can be slow and the time taken to achieve a steady state therefore precludes intermittent operation. However, at high temperatures such an operation is sometimes feasible.

II.3.7 Selectivity

Selectivity is the capacity of a sensor to discriminate between gases in a mixture. The basic problem of metal oxide gas sensors is that the conductivity value can be almost the same for different gas species and concentrations. It is well known that these kinds of sensors suffer from lack of selectivity and drift [31]. A lot of sophisticated and extremly expensive technics could be used for improvement the sensor selectivity [32]. The problem consists that they are very often influenced by water vapour, so changes in the moisture content of the atmosphere could interfere drastically the gas sensing. The selectivity of semiconductor gas sensors can be improved in a number of ways and the most important and most widely used methods will be described below. These include the following strategies:

Improvement of the sensitive material

- Use of new metal oxides that are more sensitive to target gases and less responsive to temperature
- A better control of the film microstructure using nano-metric oxides, in order to increase the active area
- Use of new catalysts/doping
- New technologies for material deposition

The sensitivity and the optimum operating temperature of sensors are correlated to the sensitive material and the material deposition techniques. The amount of catalysts/doping on the sensor surface also influences sensitivity. In general, sensitivity is enhanced either by doping, which modifies the carrier concentration and mobility, or by micro-structural changes such as reducing the oxide particle size to the nano-metric scale [33]. For example, the most commonly used oxide, SnO_2, can be sensitised to different gases by selecting an optimal operating temperature for the target gases, by making micro-structural modifications or by using doping and catalysts.

In practice, selectivity is achieved by enhancing gas adsorption or promoting specific chemical reactions via catalytic or electronic effects using bulk doping, surface modification methods and the addition of metallic clusters or oxide catalysts [34, 35]. For instance, the selectivity of chemical sensors can be strongly influenced by the addition of metal clusters such as platinum and palladium, which increase the sensor selectivity to reducing gases. Other studies have shown that gold, when deposited on transition metal oxides, has important applications in the catalytic oxidation of CO to CO_2 at room temperature, and functions as a selective gas sensor for CO and H_2 [36, 37]. The selectivity of metal oxide gas sensors increased when gold was used as the doping substance, like Au-WO_3 for NH_3. Penza et al. [38] have shown that sensitivity and selectivity can be significantly improved by adding thin layers of noble metals such as palladium, platinum or gold to the surface of WO_3 films operating at low temperatures. Maekawa et al. [39] have shown that the sensitivity of Au-doped WO_3 sensors is high at low concentrations of ammonia in the air.

Nano-structured materials present new opportunities for enhancing the properties and performance of gas sensors because their surface-to-bulk ratio is higher than that of coarse micro-grained materials. They are essential if gas sensitivity is to be high. The sensitivity of

semiconductor oxide materials has been improved by reducing particle size, and greatly improved properties have been reported for sizes in the 10-50 nanometre range [40, 41].

Measurements performed in the dynamic operation mode

- AC operation mode
- Modulation of the gas concentration
- Thermal modulation of the working temperature of the sensor

Measuring in the AC operation mode at different frequencies has been investigated as a method for dynamically characterising sensors. Gutierrez et al. [42] have found that the peaks that appear in the impedance plots of tin oxide gas sensors in the presence of reducing gases are a function of the nature of the adsorbed species. Amrani et al. [43] have conducted research in the use of AC measurements of conducting polymer sensors in the presence of various chemical species. They showed that for a single sensor element, characteristic patterns can be found over a very wide frequency range.

Another strategy that has been used is to modulate the gas concentration. Some studies have modelled the transient behaviour of SnO_2-based thick-film sensors in response to abrupt changes in the gas concentration [44, 45]. It has been demonstrated that the study of the dynamic sensor response makes it possible to increase the selectivity of a sensor array [46]. However, modulating the concentration of the gas/gases measured requires a complex measurement system and it is difficult to apply in practice.

Another way of increasing the selectivity of gas sensors is to operate them in a temperature modulation mode. Temperature modulation improves the selectivity and sensitivity of sensors as each gas has a characteristic conductance versus temperature profile for each type of sensors. The problem is that the stress to which the sensor is subjected dramatically reduces the sensor's lifespan [47].

New methods of conditioning and pre-treating gas mixtures before sensing

- Catalytic filters that burn out interfering species
- Separation columns (e.g. chromatographic columns)
- Techniques of selective concentration (e.g. carbon traps or polymer-coated fibres)

Unlike conventional doping methods for metal oxide gas sensors, selectively permeable ceramic coatings are used to tune the gas reception of the sensor elements. The selective effect of these membranes is twofold. First, gas molecules are specifically adsorbed at the membrane surface and, second, if these molecules are larger their diffusion through the membrane is chemistry dependent. Additionally, the coating can be used as a protective shield against corrosive components in the analyte medium. The effect of membranes on the properties of coated gas-sensor elements has been extensively investigated [48]. By covering the sensor structure with a porous layer of a refractory ceramic (e.g. Al_2O_3 or even Ga_2O_3), the gas diffusion through this ceramic is filtered and the cross sensitivities to organic solvents are almost completely eliminated. Althainz et al. [49] have developed selectively permeable SiO_2 and Al_2O_3 coatings to customise the selectivity and improve the stability of SnO_2 conductivity sensors for the detection of organic gases in air. Park et al. [50] achieved selectivity to a specific gas by depositing a catalytic filter layer over the SnO_2 sensing element. Using a Nb_2O_5 filter layer, they fabricated hydrocarbon sensors and alcohol sensors with excellent selectivity. For selective sensing to combustible gases, Portnoff et al. [51] proposed catalytic filtering technology in which ambient gases must pass through the catalytic filter before reaching the active region of the sensing film. They reported that the selectivity could be improved for the more thermochemically stable gases by properly selecting and preparing the catalytic material.

Feng et al. [52] also suggested that the gas diffusion process could be controlled for selective sensing. According to their research, because of the difference in the diffusivities of various gases selectivity could be further improved by controlling the diffusion process. Schwebel et al. [53] showed that Au-dispersion could considerably enhance the CO sensitivity because the reactive solvents were burned and only the more stable CO reached the sensor surface. The cross influence of ethanol was almost completely eliminated, with no deterioration in the response behaviour of the CO sensor. Know et al. [54] reported a highly selective C_3H_8 gas sensor: they combined Pd and Pt catalysts in the filtering technology and controlled gas diffusion with a SiO_2 insulating layer.

The Electronic Sensor Technology Company [55] has used in its "Znose" in addition to the adsorption/desorption system, a chromatographic column, to increase the sensitivity, and fundamentally, the selectivity of sensors. The compounds are discriminated in the column, to

which different temperatures are applied. As a matter of fact, it is a chromatograph in which the detector is substituted by a gas sensor. The main disadvantage of this system is its cost.

Selective preconcentration techniques, such as purge and trap or solid phase microextraction, can be used to improve the lack of selectivity of the electronic nose instead of the more common non-preconcentrated static headspace. Purge and trap is one way of extracting and concentrating volatile organic compounds (VOCs). It was originally developed for the analysis of organic volatiles in water samples. The process involves passing a stream of an inert gas through the sample to carry away the organic volatiles, which are then trapped from the gas stream onto the surface of a trapping material. Since it was developed, the principles involved in purge and trap analysis have been applied to a wide variety of samples including foodstuffs, polymers, pharmaceuticals, soils and arson debris.

The purge and trap technique has already been used to improve the selectivity of the sensors, particularly as a filter for ethanol [56], i.e. the ethanol contained in the samples was not adsorbed by the porous polymer material and, therefore, was not delivered to the sensors. Consequently, the sensors were not blinded by the ethanol content and could respond to other components.

Use of sensor arrays with pattern recognition techniques

To overcome the selectivity problem of sensors, the most widely used strategy has been to construct multisensor systems. The success of artificial olfaction depends not only on the development of new sensor technologies, but also on the availability of powerful pattern recognition software. These e-nose instruments are commercially available nowadays and used for assessing quality in the food, beverage and cosmetic industries, etc.

Attempts to measure odours with electronic instruments were first made as early as the 1950s [57], but the modern field of artificial olfaction began in 1982 with the work of Persaud and Dodd [58], who used a small array of gas-sensitive metal oxide devices to classify odours. Since then, there has been a steady increase in the number of systems using chemical sensor arrays. These systems are composed of several types of gas sensors, i.e. they use an array of sensors with partially overlapping sensitivities, capable to obtain different response to the tested odours [59].

The sensor signals encode chemical information about the gas or gas mixture. Each sensor in the array defines an axis in a multidimensional space where gases can be represented as points positioned in this space, according to sensor responses. Pattern recognition uses multivariate techniques to elucidate relationships in the multidimensional space of sensor response.

The most common approach for fabricating a sensor array is to develop sensors with different dopants as sensing materials [60]. The literature available in the area of gas sensors on the development of selective gas sensor systems puts particular emphasis on sensor arrays that use tin oxide in association with various dopants [61]. A few examples of this approach are reviewed below.

Low concentrations of NO_2, CO and toluene have been detected by Cané et al. [62] with a micromachined gas sensor array consisting of three devices working at different temperatures. Yan et al. [63] designed a sensor array with four specifically designed SnO_2 and γ-Fe_2O_3 sensors and used an improved back-propagation algorithm to accurately distinguish ethanol and gasoline.

Many attempts have been made to develop electronic nose systems for applications in the fields of food, drinks, cosmetics, environmental monitoring, etc. [64]. Particular attention has been paid to the cost, size and portability of these systems. Hong et al. [65] fabricated and characterised a portable electronic nose system using an oxide semiconductor gas sensor array and back-propagation artificial neural network. The sensor array consisted of six thick-film gas sensors (Pd-doped WO_3, Pt-doped SnO_2, TiO_2-Sb_2O_5-Pd-doped SnO_2, TiO_2-Sb_2O_5-Pd-doped SnO_2 + Pd-coated layer, Al_2O_3-doped ZnO and $PdCl_2$-doped SnO_2). The system was successfully applied to identify 26 car exhaust gas mixtures.

II.3.8 Stability

Stability is a characteristic that takes into account the repproducibility of device measurements after long use. To avoid the effects of non-repeatability after repeated use, several gas sensor manufacturers [66] submit these materials to a thermal pre-treatment, which decreases subsequent material instabilities. During these treatments, samples are submitted to high calcination temperatures (from 400 to 1000ºC for 1 to 24 hours) to prevent instabilities in their working life, during which they are continuously heated at 200-400ºC. The gas sensor should be stable in a variable ambient atmosphere, but it should also be

reversibly unstable in the presence of the gases to be detected. These requirements are difficult to meet simultaneously. Slow changes in the properties of the bulk material or in the near-surface region are almost inevitable. These changes, which are the result of changes in the ambient atmosphere or in temperature, are called drift.

A long-term drift problem with SnO_2-based sensors provides a good example of drift [67]. After a SnO_2/Pd-based sensor has been held at room temperature for a time and then heated to the operating temperature, a high conductivity spike is observed. This temporary high conductivity occurs whether or nor a combustible gas is in the ambient atmosphere. The conductivity spike, lasting about a minute or two, can be useful, because when it disappears one can be certain that the sensor is operating, and the disappearance indicates that the level of combustible gas is low. However, although this high conductivity spike almost vanishes after a few minutes, a residual excess conductivity is retained for days or weeks after storage at room temperature. If a low combustible gas partial pressure has to be measured reasonably accurately, the sensor must be "burned in" for several days until the initial spike has decayed to a value low enough to be considered negligible background. The probable reason for this spike is the adsorption of combustible gases from the atmosphere while the sensor is stored at room temperature. This temperature is too low to support catalytic oxidation of the contaminating gases. When the sensor is heated to the operating temperature, the pre-adsorbed gases react with the surface oxygen ions, inject electrons and give a false signal.

II.3.9 Long-term effects

Changes over long operation times in both the base line and sensitivity are very important, when one sensor is used. These changes determine the frequency at which calibration checks should be carried out and the frequency at which the sensors may have to be replaced. They can only be determined over long periods of time and there is no valid method for accelerating the process. It is, therefore, important to set up, at an early stage, separate long-term characterization experiments in which the sensors are operated both continuously and intermittently. Measurements in both air and in gas mixtures should be made periodically over a period of time.

II.4 Active layer deposition technology

Various processing schemes have been tested effectively, even though only on a laboratory scale. Processing techniques should be able to afford the desired oxide composition with

specific doping and the minimum number of processing steps. Film processing techniques are grouped in two main categories: thin-film deposition processes such as sputtering, evaporation (i.e. physical vapour deposition – PVD) and chemical vapour deposition (CVD), for thicknesses in the range 0.005-2μm, and thick-film deposition processes such as screen printing, drop coating and tape casting for thicknesses greater than 10μm. Thermal spraying can be used to deposit coatings of metals, ceramics and cermets that are thicker than ~50μm. Below are summarised the different processing methods used for synthesising gas sensor films [68].

II.4.1 Thin-film technology

Thin solid films are fabricated by depositing individual atoms on a substrate. Historically Bunsen and Grove first obtained thin films in a vacuum system in 1852. Thin films are now widely used. By varying the deposition process, and modifying the film properties during deposition, a range of unusual properties can be obtained which is not possible with bulk material. The difference in the principle between thin-film sensors and those obtained from sintered powder layers is clear. In both cases, the main measuring processes are the same: oxygen chemisorption and reaction with the reducing gases. In thin films, the electric conductivity is modulated in the external region of the layer in contact with the gases, while in sintered layers this modulation is performed in their interior, on the grains whose surface comes into contact with the gases.

Thin films are synthesized from atoms or small groups of atoms. These ultrafine particles are generally effectively quenched on a substrate during film growth, and this non-equilibrium aspect can lead to the formation of exotic materials. An amorphous phase, which is not characteristic of the bulk material, can also be observed in thin films. Other structures found in the growth of thin films are an island structure of ultra-thin layers and a fiber structure. Any thin film deposition process involves three main steps: production of the appropriate atomic, molecular or ionic species; transport of these species to the substrate through a medium; and condensation on the substrate, either directly or via chemical and/or electrochemical reaction. A postdeposition annealing at temperatures higher than the deposition temperature may modify the grain size. The higher the annealing temperature, the larger the grain size is.

Thin films are generally <1 μm thick. Many chemical and physical methods of thin-film deposition are available. In chemical vapour deposition (CVD), gaseous compound precursors

are mixed and heated in a vacuum chamber as they approach the deposition surface. The precursor molecules diffuse to and are adsorbed onto the substrate surface where they react to form the deposited material. Volatile reaction by-products are then desorbed and transported away. CVD methods provide excellent film-coating conformity over uneven surfaces. RF magnetron sputtering (i.e. PVD) consists of bombarding the source material (sputtering target) with magnetically enhanced discharged plasmas. This erodes surface atoms, which travel across a vacuum chamber and condense on the substrate. Variations of CVD techniques, such as plasma-enhanced CVD (PECVD) and atmospheric-pressure CVD (APCVD), have been used to produce both nanopowders and nanostructured thin films. Physical vapour deposition (PVD) techniques using either evaporation or a sputter source have also been extensively used. The process, called low-pressure flame deposition (LPFD), is based on the combustion flame-chemical-vapour condensation process used to produce oxide nano-particles with minimal aggregation.

Considerable emphasis is given to developing solution-based thin-film deposition techniques as an economical alternative to the more expensive chemical vapour deposition and reactive sputtering processes. However, the quality of the film produced by vapour deposition processes remains superior.

The sol-gel technique consists of a system going from a liquid sol (colloidal suspension of miniature solid particles in a liquid) to a viscous gel in which the suspended particles are organised in a loose, but definite three-dimensional arrangement. The thin film gel is dried (this process can be repeated several times to achieve the required film thickness) and finally sintered. Gel layers can be formed by spin-coating (the solution is poured onto the substrate surface, which is then spun to expel fluid and create a uniform thickness), by dip-coating (the substrate surface is dipped into the solution) and by spray-coating (the solution is sprayed onto the sensor surface).

Spray pyrolysis, using an atomising nozzle of 300μm, has recently been used to deposit SnO_2 films that were 50-300 nm thick. Tin chloride was dissolved in ethanol or deionised water and sprayed at a deposition temperature between 300-550 ºC. Mukhopadhyay et al. [69] developed a modified chemical solution-based technique, where a thin adherent film of tin sulfide is formed on a ceramic substrate by reacting sodium sulfide and tin chloride. Subsequently, the tin sulfide film was reacted in air to produce SnO_2.

II.4.2 Thick-film technology

In most applications one of the greatest justifications for the existence of thick-film technology is the need to combine different electronic technologies, but in advanced sensor applications it is dominant. The single chip solution is often treated as a holy grail by designers, but so far it has rarely made sense, though demand is always driving developers of technologies towards providing such solutions, and it is an active area of research. Thick-film technology was first introduced more than 30 years ago. Nowadays there is a big amount of companies which are using this technology: Envin Scientific, Zellweger Analitics, Trafag and Oliver IGD, (gas sensors); GfG, OLDHAM, Industrial Scientific Corporation, GMI, BW technologies, Draeger Industrie and KANE (gas detectors); B+B Thermo-Technic and M&C Products (gas sampling probes) [70].

One of the most important thick-film deposition methods is screen-printing, which is similar to that used for ceramics, textiles, etc. Thick-film paste can be formulated to paint or print an active layer onto a substrate [71]. To formulate the paste, finely milled metal oxides or other sensing materials are combined with small amounts of glass frit of a similar size (for adhesion to the substrate), catalysts (if desired), and an organic vehicle to form a printable paste. The particle size of the constituents varies, although for screen printing powders it should be 0.5 μm or less in diameter. The paste is spread on the substrate by means of a screen made from non-rusting steel mesh, polyester or nylon, mounted on a metallic frame. The screen is coated with an ultraviolet-sensitive emulsion. These regions were drawn by photographic methods. The screen is maintained at 0.5 mm from the substrate surface in the screen-printing machine. The paste is pushed through the defined regions by pressure from a spatula. The paste is printed onto a ceramic substrate, typically alumina, dried, and fired at temperatures between 500 and 1000° C for one or more hours. Standard printable thick-film materials for resistive heaters and conductor lines may be applied to the substrate before or after the sensor layer (normally pastes of noble metals like Pt and Au).

Tape casting is a forming technique for producing thin, flat ceramics. The method was originally developed for producing electronic ceramics (insulating substrates and packages and multilayer capacitors). Ceramic slurry is spread evenly onto a flat horizontal surface by means of a ‘doctor blade’. Once dry, the flexible ‘green tape’ is cut, laminated or shaped and sintered. The thickness of the tape is generally in the range 25 μm to 1 mm, but tapes as narrow as 5 μm can be produced.

Another thick film method is drop-coating. A particular thickness can be obtained by varying the number of drops that are deposited. This method is highly dependent on solution viscosity and density. Once the solution is deposited, the solvent evaporates by itself or with the help of gentle firing. Other techniques for thick-film deposition certainly exist, but they are of little interest to this study and, therefore, not discussed.

II.5 Active layer materials

One of the most important and growing applications of sensors fabricated using thick-film and related techniques is the detection and monitoring of gases. The materials of choice for this application are semiconducting oxides which make it possible to use reactions that involve molecular chemistry confined to the surface layer of atoms. The electrical consequences of this chemistry, however, are manifest through a considerable volume of the solid. When the surface reactions are followed by a bulk change in stoichiometry the resistance of the entire device is modified. In other instances, surface reactions may modify the conductance only to a depth of the order of a micron or so. However, if the oxide presents in a high surface to bulk form (e.g. in a porous thick film), the device may still be enormously sensitive to atmospheric composition. In either case semiconductor gas sensors functioning as gas sensitive resistors are a simple, low cost and rugged means of atmospheric monitoring.

The effectiveness of gas sensors prepared from thick films of semiconducting oxides depends on such factors as the nature of the reaction taking place at the oxide surface, the temperature, the catalytic properties of the surface, the electronic properties of the bulk oxide and the microstructure. It is of course possible to present semiconducting oxides for gas sensing in forms other than thick films. However, thick-film methods offer a route to small-scale devices at a cost that is likely to be lower than that of the thin-film equivalent. Good control over thickness and microstructure is possible and, although response time is likely to be longer than for a thin-film structure at the same temperature, the lifetime is expected to be longer.

II.5.1 Metal oxides

The primary mechanism responsible for gas reactions with metal oxide semiconductors in air at elevated temperatures is the surface type mechanism for minority gases in air. Solid state doping can make the metal oxide *n*- or *p*-type, as desired, although many materials predictably switch behaviour from *n*- type to *p*-type as the partial pressure of oxygen increases [72].

Basically we used two different metals in our studies:

- SnO_2 is sometimes called a transparent metal and is widely used as a gas sensor. Of the well-known and well-used oxide semiconductors (SnO_2, TiO_2, GeO_2, Cu_2O, Ag_2O, In_2O_3, Tl_2O_3, ZnO, $BaTiO_3$, $SrTiO_3$, $LaCrO_3$, WO_3, etc.), SnO_2 is one if the most representative broadband semiconductors in which s and p electrons propagate with a large mobility. SnO_2 has the rutile structure shown in Figure II.4 (up).
- WO_3 is lemon-yellow metal widely used in gas sensor applications. It is solid, with a density of 7200 kg/m^3 and with a high melting and boiling point (1470°C/1840°C), respectively. WO_3 has the structure shown in Figure II.5 (down).

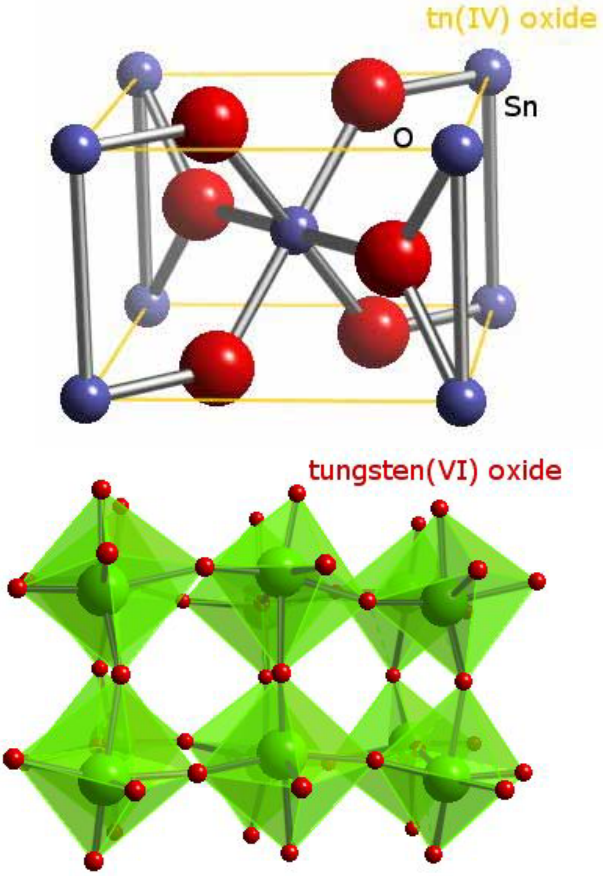

Figure II.5. Structural composition of SnO_2 and WO_3

The most popular metal oxide material used in resistive sensors is tin oxide. Many sensitive gas sensors and detectors have been created, particularly by Figaro Engineering Inc., one of the leading sensor producers since 1968. The sensing material in Taguchi gas sensors is metal oxide, most typically SnO_2. A diagram of the Figaro sensor can be seen in figure II.6. This sensor consists of a small ceramic tube coated with tin oxide and a suitable catalyst. A heater coil maintains the tin oxide temperature (between 200 and 500° C). The signal is the

resistance measurement between the two electrodes at opposite ends of the tube. The power consumption of the Figaro sensors ranges from 0.6 to 1.2 W.

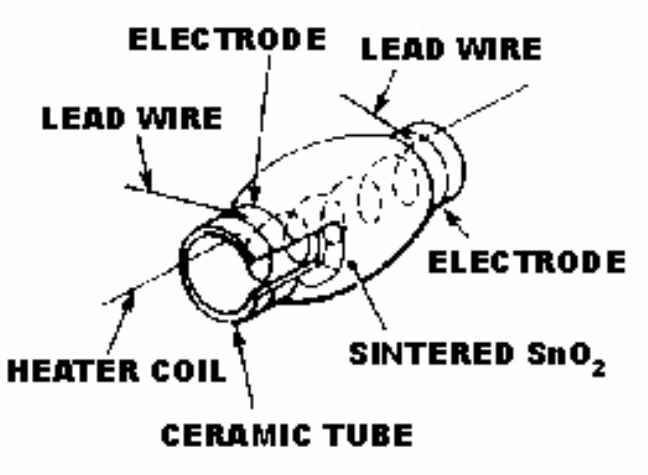

Figure II.6. Schematic of the Figaro sensor

Another sensor distributed by Sinostone, Chicago, is based on SnO_2/Fe_2O_3 [73]. Indium oxide (In_2O_3) is the basis of commercial sensors developed for detecting hydrogen sulphide [74]. In this case, thin films are particularly attractive because less precious metal is used per sensor. The first sensor prototypes were modified ceramic trim potentiometers with the potentiometer used as a heater. In subsequent developments, oxidized silicon wafers were chosen for the substrate material. The design was a single thin-film deposition system with integrated thermistors. In the final version, the thermistor was replaced by a platinum heater wire connected as one leg of a common Wheatstone bridge circuit from which an error signal was used to keep the heater at constant temperature. Another commercial sensor, distributed by Steinel [75] is based on Ga_2O_3 and is used to detect ozone and CO.

Some n-semiconductor materials have been extensively studied to detect changes in the partial pressure of oxygen, carbon dioxide, and other stable gases. One example is a titania (TiO_2) sensor [76]. Resistance changes in non-stoichiometric TiO_2 provide a means of quantifying the oxygen partial pressure. Other metal oxide thick films for oxygen sensors include for example CeO_2 [77].

The major advantages of metal oxides are reversibility, durability, low cost and robustness. The materials and manufacturing techniques easily lend themselves to batch fabrication. Unfortunately, several disadvantages limit their more widespread use in sensors and continue to challenge sensor development. Metal oxide sensors generally require a high temperature to

measure gas response, which often means that power consumption is high (although newer fabrication techniques produce a much smaller sensor area that dramatically reduces power consumption). Metal oxide sensors are not highly selective and considerable effort has been made to devise materials and methods of operation to improve specificity. These sensors are generally not appropriate for applications in vacuum or inert atmospheres, and most commercial devices are not sensitive enough for sub-ppm detection. Baseline sensor drift may require periodic calibration for certain applications. Time response, even with the use of dynamic signal analysis, is often too slow for real time feedback and control applications. Table II.3 shows several materials used for resistive gas sensors, including metal oxides [72].

Material	Target gases	Implementation
Commercial sensors		
SnO_2	Carbon monoxide, alcohols, methane, ethane and propane	Porous sintered tube
SnO_2+Fe_2O_3	Hydrogen, butane, carbon monoxide, propane, ethane, methane	Sintered pellet
TiO_2	Oxygen	Sintered pellet
$Cr_{2-x}Ti_xO$	Carbon monoxide, hydrocarbons	Sintered pellet
GaO, 4 wt% Cu	Butane, isobutene	Sintered pellet
Prototype sensors		
$BiFeO_3$, $Bi_4Fe_2O_9$, $Bi_2Fe_4O_9$	Ethanol, acetone, natural gas, petrol vapour	Sintered pellet
CeO_2	Oxygen	Thick film
PbPc, 10 wt% RuO_2, 2 wt% Pd	Cl_2, NO_2, H_2, CO	Thick film
$Sr_{1-y}Ca_yFeO_{3-x}$	Phosphine	Thick film
TiO_2	Trimethylamine	Thick film
WO_3	2-methylpyrazine	Porous sintered tube
ZnO	Hydrogen, phosphine	Thick film

Table II.3. Examples of materials used for resistive gas sensors

Relatively simple binary metal oxides, such as Ga_2O_3 and WO_3, are some of the most promising new metal oxides. Additionally, there are numerous ternary, quaternary, and complex metal oxides, including the so-called heteropoly metallates. In the group of the ternary metal oxides, the perovskites contain numerous promising candidates (for example, $SrTiO_3$, $BaTiO_3$ and $BaSnO_3$). These materials have been produced and investigated in pure and doped forms. Ga_2O_3 became well known because of its sensitivity to monitoring combustible gases such as CO, H_2 and CH_4 [78]. Sensitivity to CH_4 is reported to be high at temperatures above 800°C. At these temperatures, the sensitivity to other combustible gases is considerably lower. Thus, Ga_2O_3 may be used as a selective CH_4 monitor at temperatures above 800°C.

WO_3 and TiO_2 have been used to detect nitrogen oxides. However, the typical operating temperatures vary significantly. The sensitivity to NO with WO_3, for example, increases as the temperature decreases. Typical operating temperatures are around 300°C [79]. The NO sensitivity of TiO_2-based sensors, however, is usually maximum at 450ºC [80]. A marked sensitivity to NH_3 is reported for WO_3. The combined measurements of NO and NH_3 is of interesting practical importance. The reduction of NO_x emissions may be monitored during selective catalytic reduction with NH_3.

II.5.2 SnO_2 based sensors

Since Seiyama *et al* first proposed using oxide semiconductors to detect flammable gases [81] and the subsequent manufacturing of the first commercially sintered SnO_2 Taguchi Gas Sensor (TGS) [82], SnO_2 has been subjected to extensive research as a solid state gas sensor [83]. Taguchi sensors based on tin dioxide are widely applied for detecting oxidizing and reducing gases. Signal drift is a severe problem with these devices.

Several authors have attributed drift effects to changes in the oxygen deficiency of SnO_2 [84, 85]. Others have studied the kinetics of oxygen exchange by two different methods: an electron paramagnetic resonance relaxation technique and a conductivity relaxation technique [86]. They concluded that the kinetics of the drift processes is determined by the surface exchange reactions of oxygen on SnO_2 rather than by the chemical diffusion of oxygen. Other researchers proposed a theory that explained the dependence of the gas sensitivity of SnO_2 films on film thickness and operating temperature.

On the basis of a previous study by Gardner [87], Vilanova *et al* developed a model for the electrical conductance transient behaviour in thick-film SnO_2 sensors [88, 89]. They proposed two models, which showed that the transient behaviour of a thick-film SnO_2 sensor exposed to a step change in gas concentration is diffusion-limited.

Other papers discuss a method of quantitatively analysing volatile organic compounds using both transient and steady-state responses of thick-film tin oxide gas sensor arrays [90, 91]. An array of four TGS-type, non-selective, SnO_2 gas sensors and pattern recognition techniques were combined to discriminate and quantify single vapours and binary mixtures of ethanol, toluene and o-xylene. The system recognized the single vapours with a success rate of 100 % and quantified the identified vapour with a success rate of 95 %. The system quantified binary mixtures with a success rate of 83 %. Another of their studies deals with similar topics [92].

Other authors have studied the abnormal current-voltage characteristics of WO_3-doped SnO_2 oxide semiconductors [93]. They developed a novel method for detecting reducing gases that used the self-heating mechanism of the sensing layer without an additional heater. This method was used to detect C_2H_5OH.

The fact that there are so many deposition techniques available has led many to study how they influence gas sensing properties. By attaching an ultra-thin metal activator (Pt, Pd or Au), the response time was reduced to less than one tenth of its value. Hellmich *et al* [94] investigated the sensitivity of micromachined gas sensor elements to CO, NO, NO_2, CH_4, H_2O and oxygen partial pressure changes. They found that changes in the bias voltage could be used to systematically modify the cross-sensitivity of identically prepared sensor elements. Tin oxide-based gas sensors prepared by the sol-gel process were studied by Rella *et al* [95]. Pure and Pt-doped films were investigated and the sensitivity of the second type was improved. Responses to carbon monoxide (CO), ethanol (C_2H_5OH) and methanol (CH_3OH) were reported.

Highly selective SnO_2 ethanol sensors were reported by Molas *et al* [96]. The deposition technique was drop-pipetting. The gases tested were ethanol, ammonia, benzene and methane. All the sensors showed high selectivity to ethanol, but the ones annealed in N_2 were more sensitive than those annealed in air.

It has been suggested that WO_3/SnO_2 ceramics is an effective sensing material for monitoring offensive odours or pollutant gases [97]. Miniaturized thick-film gas sensors were fabricated by screen-printing. The long-term stability and sensitivity to several gases of two types of sensor materials, W-doped SnO_2 and WO_3-mixed SnO_2, were compared. Small amounts of W doping (0.1 mol%) in SnO_2 largely improved the long-term stability. W (0.1 mol%)-doped SnO_2 gas sensors were more sensitive to acetone and alcohol than WO_3 (5 wt%)-mixed SnO_2 gas sensors. On the other hand, WO_3 (5 wt%)-mixed SnO_2 gas sensors were more sensitive to cigarette smoke because of their larger W content.

Lee *et al* compared SnO_2 thick- and thin-film gas sensors [98]. Thin films were prepared on polished alumina substrates using a cold-wall, horizontal, low-pressure metal organic chemical vapour deposition (MOCVD) system. Thick films were prepared by spin coating metal organics on alumina substrates, followed by metal organic decomposition (MOD). Both sensors showed good sensing reproducibility and stability under 1 % H_2 gas, and an enhancement in the sensitivity of the thick film. The enhancement seemed to originate from its microstructure. The greater surface area as well as the exposed grain boundary area caused by the pore structure allowed higher densities of the adsorbed oxygen species, thereby increasing the resistance in air and the gas sensitivity of the thick film. The dense columnar structure, which formed only near the surface, responds to the reducing gas molecules. The sensitivity to 1 % CO was degraded in the thick-film sensor and was almost negligible for the thin-film sensors. The time response was also enhanced in the thick-film sensor when the charge carrier diffusion was inhibited.

II.5.3 WO_3 based sensors

WO_3 proved to be good at detecting NO_x, NH_3 and other gases. Nitric oxide (NO) and nitrogen dioxide (NO_2) are two of the most dangerous air pollutants. Currently about one-half of all NO_x emissions into the environment are from power plants and industrial boilers. NO_x gas, which is the precursor to nitric and nitrous acid, causes acid rain and photochemical smog and is a critical factor in the formation of ozone in the troposphere. Ground level ozone is a severe irritant, responsible for the burning eyes, choking and coughing associated with smog. Ozone often damages lungs, aggravates infections and is particularly harmful to children. Elevated ozone levels can also inhibit plant growth and cause widespread damage to trees and crops. Therefore, exceeding critical NO_x levels poses immediate health and environmental problems. In fossil fuel combustion, NO_x is formed by high temperature chemical processes

involving both the nitrogen present in the fuel and the oxidation of nitrogen in air. Typically, the NO_x emissions consist of 90-95 % NO with the remainder being N_2O and NO_2.

Ammonia is the most abundant alkaline component in the atmosphere. It plays an important role in atmospheric chemistry and has given rise to serious environmental concerns. A considerable amount of the acid in the atmosphere generated by the oxidation of sulphur dioxide and nitrogen oxides is neutralized by ammonia. As a result, ammonia is a major constituent of atmospheric aerosols. On the other hand, ammonia promotes the oxidation rate of sulphur dioxide dissolved in hydrometeors. When ammonia comes into contact with soil, the resulting acidification and nutrient imbalance destroy or change the natural vegetation. Another aspect about ammonia emission is odour hindrance. It has been shown that ammonia is not the main component responsible for odour hindrance, but it has been observed that there is a relation between odour hindrance and ammonia emission.

Tomchenko *et al* investigated the sensitivity of WO_3 thick-film gas sensors to NO_x [99]. The fabrication method applied was screen-printing. The sensors showed good sensitivity to NO over the range of temperatures investigated (100-300°C). The sensitivity decreased, their response times increased slightly and their recovery times decreased as the operating temperature increased. The sensitivity also decreased as the thickness of the WO_3 films increased. They also investigated these films doped with Bi_2O_3. The results showed that sensitivity to low NO concentrations (2-300 ppm) was good at 300°C. One year later, the same sensors were fabricated with a RuO_2 heater [100]. The sensors were highly sensitive to NO in air but were unresponsive to common interfering gases such as carbon monoxide and methane. Subsequently, Tomchenko reported WO_3-Bi_2O_3 mixed screen-printed thick films with various Bi_2O_3 contents (3-50 wt%) as a sensing material for NO gas sensors [101]. He demonstrated that the Bi_2O_3 influence on gas-sensitive electrical properties of the mixed tick films was ambiguous and depends on Bi_2O_3 contents. WO_3-Bi_2O_3 (3 wt%) thick films are more sensitive to NO than pure WO_3 thick films. On the other hand, increasing the Bi_2O_3 content further decreases the NO sensitivity.

Other authors investigated how the process condition affects the sensing properties of WO_3 thick films [102]. They changed the firing temperature and annealing atmosphere. The sensor fired at 700°C and operated at 100°C had excellent sensor properties and its operating temperature was lower than in other reports. Yang *et al* [103] investigated the effects of

various binders, such as polyvinyl alcohol (PVA), silica sol and Al_2O_3, on the sensing and electrical characteristics of WO_3-based n-type semiconductor gas sensors. Grain size varied slightly according to the binders used. The electron concentration of WO_3 films at about room temperature and the temperature dependence of film resistance in normal air did not show any systematic dependence on the binders. In NO gas, however, the optimum operating temperature and the sensitivity of the films at this temperature were observed to depend greatly on the binders. The resistance of the WO_3 films showed an exponential temperature dependence on NO_x gas in the temperature range of 110-375°C. The sensors with Al_2O_3 binders gave the best response and recovery times for 30 ppm NO_x. Another sensor for NO_x was studied by Lee and co-workers [104]. TiO_2 was added to WO_3 and then synthesized by sol-coprecipitation of WCl_6 and $TiCl_4$ solution with ammonium hydroxide and surfactant. Tungsten trioxide and titanium oxides were also synthesized by sol-precipitation from WCl_6 and $TiCl_4$, respectively. After calcining these materials, the sensors were fabricated by screen-printing. The nanocrystalline sensor based on TiO_2 added to WO_3 showed excellent sensitivity to low level NO_x concentrations (0.5-30 ppm), fast response and recovery, and good selectivity at 350°C.

In [105], micro-hotplates were used to fabricate WO_3 gas sensors In this study, the micro-hotplate was made out of a $Si_3N_4/SiO_2/Si_3N_4$ diaphragm, 0.6 nm thick and with an area of 1.5x1.5 mm^2. The power required to maintain the device temperature of 300 °C was about 60 mW. The response of the film to NO_2 gas was fast and the linearity between sensitivity and NO_2 concentration was good in the concentration range 0-30 ppm. The response time was about 1-2 min.

One major problem is the environmental load produced by agriculture. It has been shown that most of the ammonia emission into the atmosphere comes from livestock wastes. The combination of a thick-film ammonia sensor with an accurate ventilation rate sensor was studied to measure and control the total ammonia emission from individual livestock buildings [106]. The sensor was made using conventional screen printing techniques and measured up to 150 ppm ammonia at 450°C.

Several oxide semiconductor ammonia gas sensors have been proposed and developed. Maekawa *et al* [107] showed that Au-loaded WO_3 sensors were highly sensitive to low concentrations of ammonia gas in air. Takao *et al* [108] investigated the sensing properties of

the In_2O_3-doped MgO ammonia sensor and examined some double layer sensors with a catalyst on the sensing layer. The resistance of all these n-type oxide semiconductor gas sensors is decreased by exposure to ammonia gas, which is similar to the case of reducing gases. Yun and co-workers [109] investigated a FeO_x-WO_3-SnO_2 oxide semiconductor thick-film gas sensor with high sensitivity, the resistance of which increased when exposed to low concentrations of NH_3. They also presented a novel method for detecting ammonia gas quite selectively by using a sensor array with two sensing elements.

Another sensor reported by Llobet *et al* [110] is based on WO_3 deposited onto a silicon substrate by means of the drop-coating method. Then the films were annealed in dry air at two different temperatures (300 and 400°C) for 3 h. The devices were sensitive to ammonia vapours when operated between 250 and 350°C. The optimal operating temperature of the highest sensitivity to ammonia was found to be 300°C. The response time was typically 15 and 10 s for sensors working at 300 and 350°C, respectively.

There is also a potential need for an ammonia sensor in combustion exhaust control in power plants, where NO_x is removed by chemical treatment with NH_3. If an ammonia sensor is available to monitor the residual NH_3 after the process, it is possible not only to economize the consumption of NH_3 but also to minimize the harmful emission of NH_3 into the environment. Sensors using WO_3 were sensitive to both NH_3 and NO. NO sensitivity was selectively eliminated by adding MoO_3 to the elements [111].

Wang *et al* [112] studied WO_3-based sensing material for NH_3 and NO detection. The measurement of the NH_3 and NO sensing properties of the material revealed that WO_3+Mg, WO_3+Zn, WO_3+Mo and WO_3+Re characterized better responses to NH_3 and NO than pure WO_3. Marquis *et al* [113] engineered a small, robust, sensitive and selective sensor array to detect NO_x and NH_3 emissions. They observed that the electrical conductivity of WO_3 films doped with gold (Au) improves when they are exposed to NO and NH_3.

Penza *et al* [114] reported a WO_3 sensor array. The active layer was activated by evaporated Pd, Au, Bi and Sb catalysts. The sensors were characterized for such gases as H_2S, SO_2, CH_4 and NO. The array was exposed to a H_2S test gas concentration followed by dry air. The gases were separated well and the separation was tested with a principal component analysis (PCA) method.

Another semiconductor-type H_2S gas sensor was developed with silicon-based microfabrication and micromachining technology [115]. Platinum, gold and Au-Pt were then deposited onto WO_3 as the activator layer. Under 1 ppm H_2S the individual sensitivities of the Pt and Au-Pt doped WO_3 gas sensors were 23 and 5.5, respectively. These results show that the Pt-doped film has an excellent response. Ultra-fine tungsten oxide powder, made by evaporating tungsten metal by an electric arc discharge in a reactive atmosphere, was used to obtain highly sensitive H_2S devices [116]. The mean grain size of the film grown in this way was 40 nm. The film had excellent sensing properties when exposed to low concentrations of H_2S in air at room temperature. The sintering temperature was found to be important for the gas sensing properties of the WO_3 thick-films. The optimum sintering temperature was found to be about 500°C.

WO_3 films are also sensitive to SO_2. Shimizu and co-workers investigated the SO_2 sensing properties of several semiconductor metal oxides and found that WO_3 has the highest sensitivity at 400°C [117]. At this temperature, they observed an increase in resistance, but the film resistance decreased in SO_2 at temperatures higher than 500°C. The effects of metal additions were also tested. The addition of 1wt% Ag was most effective for improving the sensitivity at 450°C. In the case of 1wt%Ag/WO_3, however, the sensor resistance decreases throughout the temperature range studied. Interference of NO_2 with the SO_2 sensitivity was found to be more significant in the case of 1wt%Ag/WO_3.

As we have already stated, one of the most commonly used methods to the improve sensor selectivity is to use dopants. Noble metal additives such as Pt, Pd or Ag are often added to metal oxide semiconductor gas sensor materials to enhance sensor response to a particular gas or class of gases [118]. Other metals, such as Be, Mg, Ca, Sr and Ba, have been used with tin film to enhance the performance of an alcohol-selective sensor [119]. Consommé soup has also been qualitatively analysed [120]. Sensors of pure WO_3 and SnO_2 exposed to 2-methylpyrazine at temperatures between 200 and 500°C gave mild or little response. When WO_3 and SnO_2 films were loaded with noble metals (0.4 wt%), not only did sensor sensitivities improve but also the output of a WO_3-Rh sensor at 300°C was highly correlated to vapours of three grades of consommé soup and could possibly replace a human tester.

Additives are either dispersed on the semiconductor surface or they are impregnated throughout the material. In order to load these metallic additives onto the semiconductor metal

oxide, a wide variety of technologies have been used. Table II.4 shows the most commonly used technologies.

Technology used for additive loading	**Metal Additive/SC**
Laser induced pyrolisis	Nb, V, Ta / TiO_2
Sputtering	Ce, Nb, Cr, Cd / TiO_2, Pt, Pd, Au / SnO_2
Impregnation	Pt / TiO_2, Pt, Pd / SnO_2, Pd / MgO
Sol-gel	Pd / SnO_2, Nb / TiO_2
Microwave	Pt, Pd / SnO_2
Electron beam evaporation	Pt, Pd / SnO_2
Pulsed laser	Pt / TiO_2, Pt, Pd / Si, C
Metal vapor synthesis	Pt, Pd
Flowing gas mixture	Pd / Ln_2O_3
Photoreduction + precursor adsorption	Pt / TiO_2

Table II.4. Most common technologies used for metal additive loading [121-127]

The characteristics or behaviour of a gas can show how to enhance the sensitivity of the semiconductor material. For example, sensitivity to acidic gases, such as H_2S, or basic gases, such as NH_3, increases when corresponding acidic or basic oxides, respectively, are incorporated to form adsorption sites for the gases [128]. Similarly, sensitivity for other target gases can sometimes be increased by adding compounds with which the target will react.

II.6 Conclusions

This chapter begins with some basic considerations about semiconductor gas sensors and goes on to discuss how materials and catalysers affect the sensor reaction mechanism: bulk type (oxygen) / surface type (minority gases in air). The basic sensor characteristics are summarised and the various strategies used to enhance the selectivity of metal oxide gas sensors reviewed. These include improving the sensitive material, measuring in the dynamic operation mode, conditioning and pre-treating gas mixtures before sensing with new methods, using sensor arrays with pattern recognition techniques and intelligent sensors. The most widely used active layers SnO_2 /WO_3 for gas sensors and the most appropriate doping for these active layers are also discussed.

III. THICK FILM TECHNOLOGY FOR GAS SENSOR FABRICATION

The features and potential of thick-film technology has made it one of the leading solid-state sensor technologies. This chapter reviews the thick-film processes used for fabricating our sensors. All the processes are briefly explained and then they are implemented for the different substrates used. The history of thick-film technology dates back to the 1950s. It soon became clear that the result of fabricating components simultaneously with different technologies could open up a whole new field in electronics. In the mid 1960s, thick-film processing was capable of producing fine-line conductor geometries, thereby allowing a high component packing density on a single substrate. The essence of today's modern thick-film process is almost identical to that used thirty years ago [129]. The versatility of semi-conducting materials and the miniaturization of VLSI pattering techniques promise new sensors with better capabilities and performance-to-cost ratio than those of conventionally machined devices. Integrated circuit technology allows thousands of electronic circuits to be batch-fabricated simultaneously in a single processing sequence. By optically repeating the patterns on the substrate, many units are fabricated with just one application of the process. For most metal oxides, Al_2O_3 is the most suitable substrate material, but in recent years other substrates such Si and micro-hotplates have been investigated. These devices have several advantages: they are small, they perform well because of the precise dimensional control

during fabrication and they are cheap. What is more, their thermal inertia is very low and their power consumption low [130-135].

Nowadays, the thick-film technology is the most widely used technology for gas sensors fabrication. It is employed by company like FIGARO and FIS, leaders in the gas sensor production. The main goal of this chapter is to explain in what this technology consists of, as it will be the technology used for the fabrication of the gas sensors described in this thesis.

III.1 Basic assumptions

A thick-film circuit is normally considered to consist of layers of special inks (or pastes) deposited onto an insulating substrate. By adding integrated circuits, and sometimes films made by other technologies, a hybrid circuit is produced. One of the key factors that distinguishes a thick-film circuit, is the method of film deposition - screen-printing -which is possibly one of the oldest forms of graphic art reproduction. The deposition process for a thick-film circuit is essentially identical to that used for traditional silkscreen printing. The main differences lies in the screen materials and the degree of sophistication of the printing machine. A typical thick-film screen consists of a finely woven mesh of stainless steel (nylon or polyester) mounted under tension on a metal frame. The mesh is coated with a ultra-violet (UV) sensitive emulsion onto which the circuit pattern can be formed photographically. The finished stencil has open mesh areas through which the desired pattern can be printed and is held in position at a distance of around 0.5 mm from the top surface of the substrate. The ink is placed on the opposite side of the screen and a squeegee traverses the screen under pressure, thereby bringing it into contact with the substrate and also forcing the ink through the open areas of the mesh. The required circuit pattern is thus left on the substrate.

The next stage of the process is to dry the film and remove the organic solvents from the paste. This task can be performed in a conventional box oven but it is more common to use an infrared belt drier. After this stage, the dried film is relatively immune to smudging and the substrates can be handled. Sometimes it is permissible to screen print the next layer directly after the drying stage, but this really depends on the nature of the inks being deposited.

The films themselves contain fine powders, which must be exposed to high temperatures if they are to form a solid, composite material. This is often referred to as sintering, and takes place in a belt furnace, where such parameters as peak temperature, dwell time and throughput

speed can be controlled. Some inks are very sensitive to variations in these parameters whilst others are not. All thick-film inks contain glass. During the firing cycle, the glass melts and forms a mechanical key at the film-to-substrate interface. It also provides a suitable matrix for the active material of the film. The result is a fired composite film, which is firmly bonded to the substrate. Further screen-printed layers may be added after firing if necessary.

For thick-film circuit applications, further production stages are needed. The active devices are usually mounted and wire bonded out to a suitable substrate. The penultimate processing stage involves packaging the thick-film circuit. The hybrid circuit designer is faced with a wide range of different packages and must take great care when choosing between them. The decision will largely be influenced by the application of the circuit, but the usual engineering compromise of quality and cost prevails. After the circuit has been fabricated, the final step is to assess the quality and ensure that the performance is within specification.

Generating the artwork for thick-film screens was once a time consuming task. The master pattern was produced by such methods as tape strips and decals, drawing and inking, and cut-and-peel techniques and with such materials as Rubylith and Stabilene. Each of these methods has its own advantages but, in general, it is difficult to achieve sharp edges, positional accuracy and uniform density. Correcting for even the most minor errors can prove to be a tricky and often time consuming task. Modern desk-top computer systems have excellent graphic facilities and allow a variety of input devices to be used. There are many commercially available software drawing packages (Cadence, Corel draw etc.) which enable the thick-film engineer to produce computer-generated artwork in a fraction of the time needed with some of the manual techniques described above.

Once the design has been completed on a suitable software package, the next step is to verify that the design rules regarding track width, track spacing, etc. are not violated. Different thick-film manufacturers will have different design rules depending on the quality of the processing facilities available to them. However, some sophisticated software packages are available specifically for thick-film design. They make it possible, amongst other things, to automatically check the layout against a set of design rules, which can be modified to suit each individual user's processing capabilities. Assuming the computer layout conforms to the design rules, the next phase in the design process is to generate a hard copy of the design. The exact form of this copy can take one of several forms depending on the equipment used. For

example, many thick-film screen manufacturers will accept artwork in either positive or negative form scaled up to 2, 4, 5 or 10 times the required size. This was certainly a common method for screen generation when cut-and-strip processes were used, because the magnified artwork is subsequently reduced photographically thereby minimising any errors which may have occurred in the original artwork. With the advent of accurate photo-plotters, it is now possible to take the layout and accurately reproduce it on photographic film directly, so that it can be developed and fixed ready for screen manufacture. Alternatively, conventional office equipment such as laser printers and plotters can be readily used to generate magnified images of the required layout with sufficient quality to be sent directly to the screen manufacturer.

III.2 Screens

The screen defines the pattern of the printed film and also meters the amount of paste that is deposited. It is a very important part of the screen printing equipment, and is essentially a stencil through which the paste is forced during the printing process. The most common type of screen consists of a frame, normally cast aluminium, onto which a finely woven mesh is stretched. The mesh itself is usually based on a plain weave pattern. Some important properties of the screen mesh are: the size and density of the strands (usually quoted in terms of lines per inch), the tension, the orientation and the material. The selection of a suitable mesh count for a screen is a very important criterion. Factors that may influence this choice include the required line definition of the pattern and the type of paste being used. For general-purpose work a typical mesh count might be 200 strands per inch. The mesh opening depends on the mesh count and the filament diameter. For a given mesh count, the smaller the filament diameter, the larger the mesh opening, so a greater volume of ink will be deposited onto the substrate. Hence, the mesh opening provides one of the means of controlling the thickness of the deposit. Figure III.1 shows a cross-section of a mesh and defines some of the terms used.

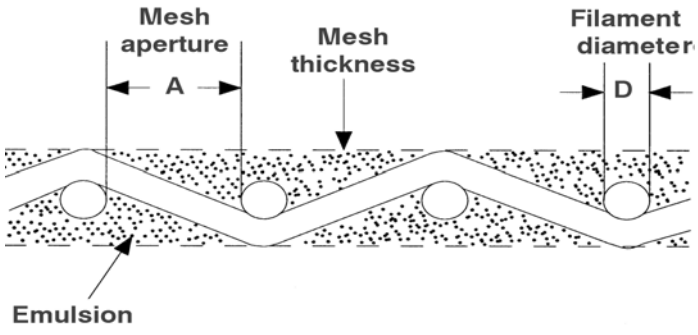

Figure III.1 Cross-section of a mesh

One common term is the percentage of open mesh area, which is defined as follows:
Percentage open area = $100A^2/(A+D)^2$, where A is the mesh aperture and D is the filament diameter. Some ordinary mesh types are detailed in Table III.1.

Mesh count	Wire diameter (μm)	Open area (%)
105	**76.2**	**46.9**
165	**50.8**	**44.9**
200	**40.6**	**46.2**
250	**40.6**	**36.0**
280	**30.5**	**44.1**
325	**27.9**	**41.3**
400	**25.4**	**36.0**

Table III.1 Common mesh types

The screen mesh can be aligned in several orientations. The most common mesh angles are 45°, 90° and 22.5°. A number of factors need to be considered when choosing the mesh angle. A 45° mesh provides maximum flexibility for the stretched fabric but may produce a serrated edge on conductor lines, which are aligned in parallel or at 90º to the direction of the squeegee. It is possible that a 90° mesh angle may cause a fine line to disappear altogether if the filament coincides with the line. In view of these matters the 22.5-30° mesh angle was adopted as a compromise.

The screen emulsion is usually polyvinyl acetate or polyvinyl alcohol sensitized with a dichromate solution. Some screen manufacturers apply the emulsion by hand coating, which can accurately produce a standard range of thicknesses (typically 13 to 23 microns).

III.2.1 Mesh materials

The three most common materials used for thick-film screen meshes are:

- ✓ Polyester
- ✓ Nylon
- ✓ Stainless steel

They all have their own advantages and disadvantages but, likewise, they must meet some fundamental requirements for all screen fabrics. The screen acts as a metering device to control print thickness. That is why the mesh material must make sure that the printed deposit is uniform. The mesh material must be precisely woven and have uniform mesh apertures.

The fabric should also be flexible enough to enable good contact all over the substrate. The fabric needs to be resilient so that the mesh returns to its original position after the printing stroke. The squeegee itself is in contact with the fabric for most of the printing stroke, so the finish of the fabric must be slippery and smooth so that the resistance to the squeegee is minimum. The mesh material must also be chemically stable and very resistant to attack from the various solvents and other chemicals used in the thick-film process. Finally the fabric must have an economic working lifetime and suitable mechanical support for the emulsion.

As mentioned above, a common fabric is polyester. It is flexible and can be used for printing onto uneven surfaces. It is also much more resilient than nylon and stainless steel. The elastic properties of polyester are better than those of stainless steel but cannot match those of nylon. The registration and definition properties are generally good. Polyester screens have a long life time and give low squeegee wear.

Nylon is the most elastic of the three screen fabrics, which can be an advantage in certain circumstances. Unfortunately, this also means that the open areas of the screen tend to deform during a print stroke, thereby resulting in elongated images. Another disadvantage of nylon is that its low resilience means that high viscosity inks should not be used. The mesh tends to stick to the substrate and not peel off, which results in poor print quality.

The main advantages of stainless-steel screens are that they produce high standards of line definition and registration and also good control of ink deposition. The mesh filaments can be drawn finer than those of nylon or polyester and can therefore provide a higher percentage of open area for a given mesh count. Stainless steel is ideal for printing onto flat surfaces but, because of its poor flexibility and resilience, it is much more difficult to use on uneven surfaces. It is generally recommended that stainless steel screens be used for printing on small areas where high definition and registration are needed.

III.2.2 Screen fabrication

Screens produced with the desired pattern exposed onto the screen emulsion are ready for printing. The screen frames are usually made of cast aluminium and serve to hold the mesh fabric taut, and the stencil firm and in place during printing. They are available in sizes ranging from 10 x 10 cm up to 3 x 3 m. The most common sizes are between 20 x 20 cm and 60 x 60 cm. The mesh is attached to the frame by either crimping it around the frame edge or

by using adhesives. The screen fabric must be tensioned before it is attached to the frame and this is usually done by clamping a large sheet of fabric around the edges and stretching in all directions to maintain uniform shape and tension. A tension gauge is used to measures the deflection over a fixed area with a known applied force. When the tension is correct, the mesh is attached to the frame. Adhesive mounting is the most common method used and the exact nature of the adhesive will affect the length of the setting time. Some adhesives make it possible to heat the screen and thus reduce the setting time. Care must be taken, however, to ensure that there is no loss of tension due to the differential expansion coefficients between the mesh fabric and the screen. It is advisable not to exceed temperatures of around 50ºC. The light-sensitive emulsion can be deposited by one of three methods:

- ✓ direct emulsion method
- ✓ indirect film method
- ✓ direct film method.

Direct emulsion involves directly coating the mesh by hand, and it is a skilled process. The process for making indirect film screens differs from the direct method in that the sensitised emulsion film is attached to a clear sheet of polyester backing. The photographic positive is exposed to the emulsion under ultra violet light, washed and then carefully pressed onto the underside of the screen using a soft roller. After a few hours, when the emulsion has dried, the polyester backing can be removed and the screen is ready to be used. With the direct film method the sensitised emulsion film and polyester backing are initially placed onto the still unexposed screen. After drying, the backing is removed and the emulsion is exposed in a similar manner to that used with the direct emulsion method.

The accuracy and definition of the exposed image largely depend on the quality of the photopositive from which it was formed. Therefore, the photopositive must be of high contrast and definition. Another source of error, which can occur during the exposure of the screen, arises if the emulsion side of the photopositive is not in direct contact with the screen surface. This can result in poor edge definition and undercutting of the desired image. Exposure usually takes place in a special cabinet, with an ultra-violet light source of such a wavelength that the screen emulsion polymerises. Exposure time is a function of the intensity of the UV source, distance between the light and the screen, the type and thickness of the screen emulsion and the type of pattern being produced.

III.3 Deposition equipment

Screen-printing is the transfer of pastes, through a fabric screen onto a substrate. This transfer occurs when the paste comes into contact with the substrate surface and is pulled through the screen. The high shear action of the squeegee passing over the screen allows this transfer to occur. The paste is deposited in a pattern that is defined by the open areas in the emulsion of the screen. Some essential screen printing parameters will be mentioned below and a detailed explanation will then be given:

✓ **Snap off**. The distance between the bottom of the screen and the top of the substrate surface. Also referred to as breakaway. This parameter can be set by lowering the screen until it contacts the substrate. The screen is then raised until the bottom is separated from the substrate by a desired distance. The snap-off can be observed in Figure III.2, while some typical snap-off values in relation to the screen size are presented in table III.2.

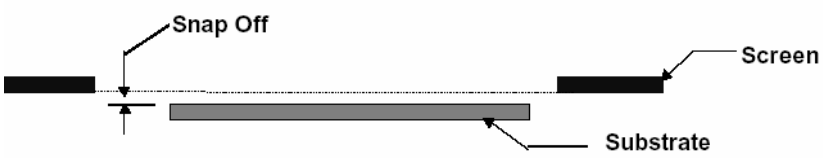

Figure III.2. Snap-off

Screen size		Typical snap-off	
5 x 5 inches	**127 x 127 mm**	**0.025 inches**	**0.635 mm**
5 x 7 inches	**127 x 178**	**0.025**	**0.635**
8 x 10 inches	**203 x 254**	**0.040**	**1.02**
12 x 12 inches	**305 x 305**	**0.060**	**1.5**

Table III.2. Typical snap-off values

✓ **Attack angle**. Angle between the leading edge of the squeegee and the substrate surface. It controls the transfer of the material to the substrate.

✓ **Down-stop**. Mechanical limit of stopping squeegee travel. This parameter is set by lowering the squeegee to come into contact with the substrate (this is the zero point). Then the mechanical limit is set lower than the substrate (75 - 125μm).

✓ **Squeegee pressure**. Force required to push squeegee up from its lowest position in the "print" mode.

✓ **Squeegee speed**. The speed at which the squeegee travels across the screen.

✓ **Squeegee durometer**. Hardness level of the squeegee. Different colours will indicate the durometer number. The relation between colour and hardness may vary between vendors.

✓ **Emulsion**. Photosensitive polymer on the bottom of the screen. It forms a gasket between the screen and substrate. A pattern is formed in the emulsion when the artwork is in contact and exposed to UV light. The unexposed pattern is washed away with deionised water.

✓ **Emulsion thickness**. The thickness of the emulsion applied to the screen.

✓ **Mesh size**. The number of openings in a screen. A 325-mesh screen has 325 openings per linear inch.

✓ **Flood printing**. Printing done with the screen completely covered with paste. This is typical of high-volume operations.

✓ **Peel**. The release of the screen from the printed area.

✓ **Planarity**. Parallelism between the screen and substrate.

Figure III.3 shows the constituent parts of a screen printer. The screen fabric is attached to the screen frame, which is firmly held in a chase.

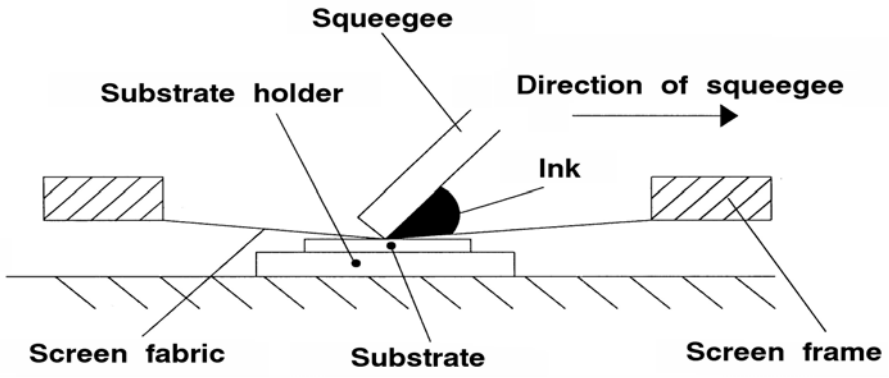

Figure III.3. Part of a screen printer

The screen is separated from the substrate by a snap-off gap of around 0.5 mm, which gives rise to the term off-contact printing process. The substrate is held in position by either a vacuum chuck or by a special jig, both of which are usually referred to as the substrate holder. The platform upon which the substrate holder is mounted can be adjusted in the vertical plane at both ends in order to ensure that the substrate is parallel to the screen. The screen position can be finely adjusted for registration purposes. The printing medium is applied to the upper surface of the screen and the flexible rubber squeegee is traversed across the stencil. As the squeegee is passed across the screen, the mesh fabric is pressed into contact with substrate surface. The ink is forced through the open areas of the screen mesh. Directly behind the squeegee, the screen peels away from the substrate and leaves behind a deposit of ink, in the

required pattern, on the substrate surface. A screen printing machine is shown in figure III.4, where the essential parts can be clearly distinguished.

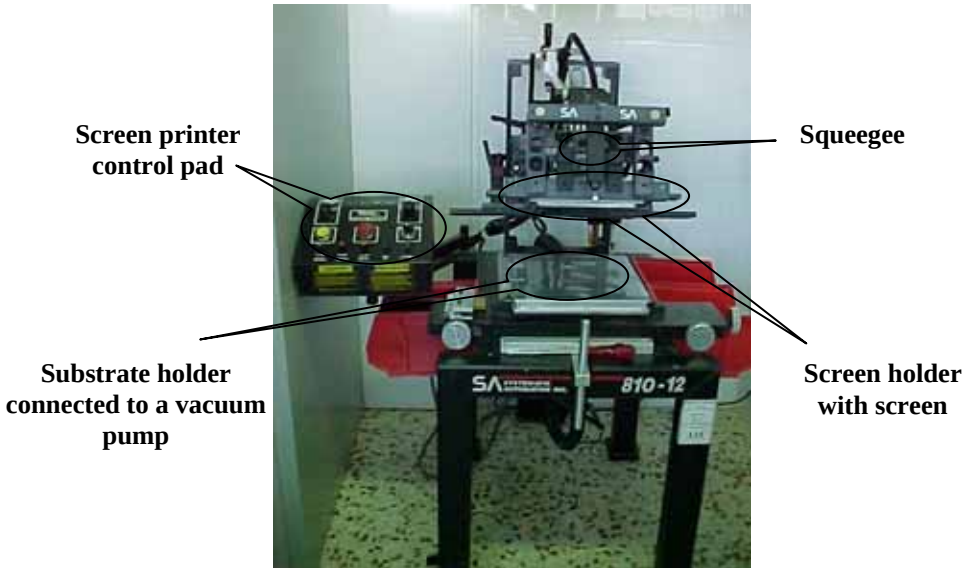

Figure III.4. Screen printer (Model: System Automation Inc. 810-12)

The screen mounting provides a means of holding the screen firmly so that it does not move during the printing cycle. It also provides a means for accurately positioning the screen for registration purposes. Typically, a positional tolerance accuracy of around 25 microns in the vertical and lateral directions is achievable. Although it is essential that the screen be held firmly in position, it is also necessary that it may be easily removed and replaced. If the screen is held in a chase, which is basically a screen carrier, it can be taken out and relocated accurately in the same position.

The function of the substrate holder is to register the substrate accurately below the screen and also to keep it firmly fixed in position during printing. The acceptable tolerances for the positioning and repeatability of the substrate holder are similar to those for the screen mounting. The two most common ways of holding the substrates are with a vacuum chuck or a recessed jig. In a vacuum chuck arrangement, the substrates are registered by butting two of their edges against two datum faces. The alternative is a recessed chuck, which is fitted with locating pins and a clamping edge. The depth of the recess is around 100 microns less than the thickness of a substrate.

The squeegee is essentially a flexible blade whose function is to transfer the paste through the screen and onto the substrate. During printing, the squeegee forces ink through the open areas

of the mesh and, by virtue of the surface tension between the film and substrate, the required pattern is transferred to the substrate as the screen and substrate separate. The squeegee's shape, material and pressure are all factors which dictate the life of the screen and the squeegee. Clearly, the squeegee must be resistant to the solvents and inks used in thick-film processing. Polyurethane and neoprene are common materials. Figure III.5 gives two examples of cross-sections of typical squeegees.

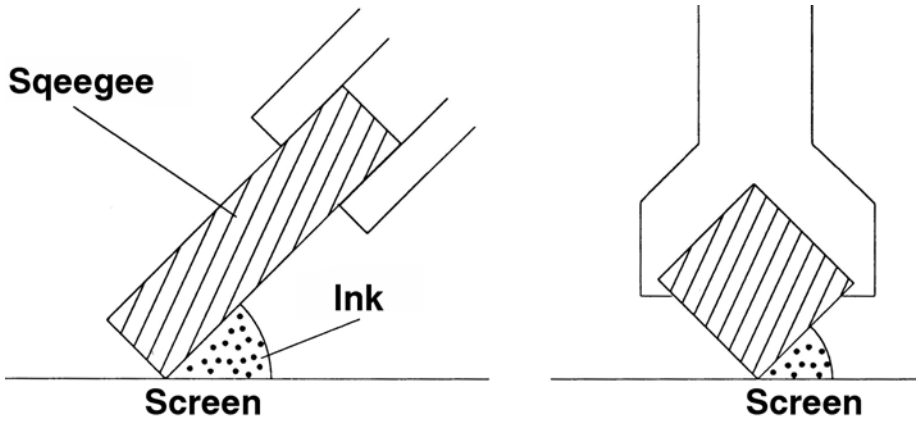

Figure III.5. Examples of different squeegee constructions

The angle of attack between the squeegee blade and the screen is usually around 45°. By using a rectangular cross section it is possible to prolong squeegee life as each of the four edges may be rotated periodically. The optimum durometer hardness of squeegees is in the range 50-70.

Squeegee down pressure can be adjusted, usually by spring loading. Other methods like pneumatic, dead weight and torsion bar loading can be found on some printing machines. It is essential to have accurate control over the squeegee pressure so that print thicknesses are accurate and repeatable.

The squeegee holder is sometimes mounted rigidly, but often it is a floating type:that is to say, it is pivoted so that it can align itself parallel to the screen. Although some printers print on both the forward and the return stroke, many operate with single direction printing as this gives improved registration. In order to return the ink to the starting position for the next print, a device called a flood blade is used. This is usually made of metal and is positioned perpendicular to, and slightly above, the screen. At the end of a print stroke, the squeegee is automatically lifted away from the screen and the action of the flood blade leaves a thin layer of ink over the surface of the screen ready for the next print stroke.

One of the most important aspects of thick-film inks is the viscosity, which must be accurately controlled if the quality of the film deposition is to be high. Figure III.6 shows how the viscosity of a typical thick-film varies at different stages during the printing cycle.

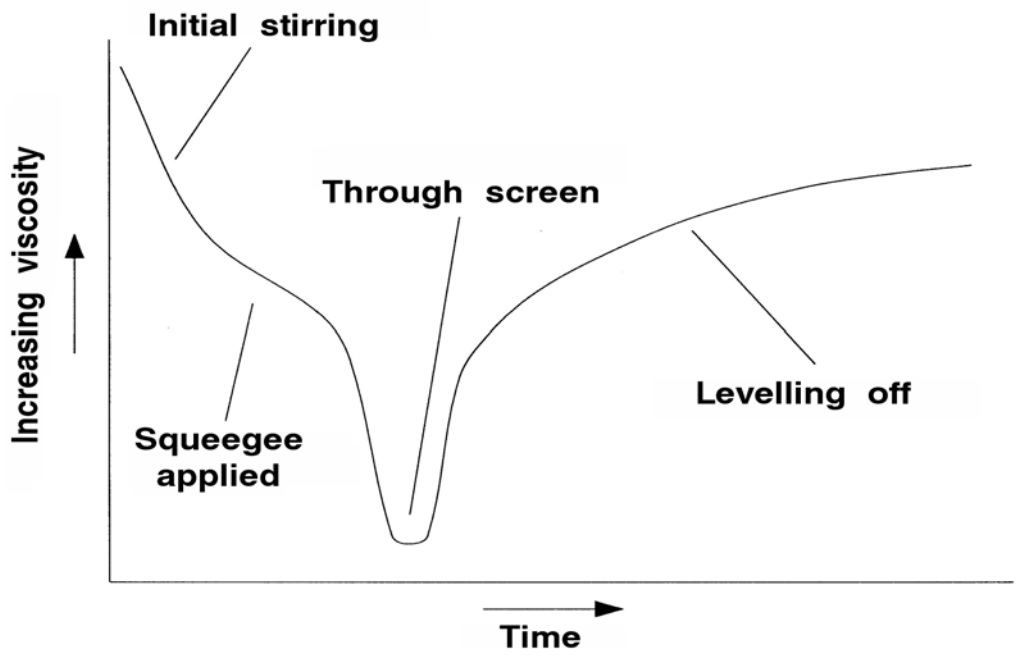

Figure III.6. Variation in the paste viscosity at different stages of the printing cycle

Firstly, we must consider the general requirements for thick-film pastes in terms of the ink rheology. The characteristics required of the ink viscosity depend on the printing stage. When the ink is being forced through the screen, viscosity must be low. After printing, however, viscosity must be high because the film must retain its printed geometry and not run. For ideal (Newtonian) fluids, the viscosity is independent of the shear rate and only varies with temperature. However, for a thick-film paste the viscosity must change with the pressure applied. The classification for fluids of this type is termed pseudo-plastic.

III.4 Monitoring of the film thickness

Film thickness needs to be carefully monitored and controlled and a number of techniques can be used to do so. Clearly it is desirable to measure the thickness at an early stage in the thick-film process so that any errors can be quickly corrected. For this reason, the film should be measured soon after printing or drying. However, it is also advisable to check the final fired thickness of the inks periodically. For newly printed layers it is preferable to use a non-contact measurement method as the film lacks surface stability in these stages. The instrument used for the contact method may well affect the thickness being measured.

One example of a non-destructive method for quickly determining the approximate thickness of freshly printed films is to focus an optical microscope on the substrate and then refocus it on the surface of the film. The distance that the microscope platform has moved can be read from a calibrated micrometer attached to the platform. Multiple readings will increase accuracy, but it should be noted that this technique is only capable of indicating the mean film thickness. This method may also be used for dried and fired films.

For a more detailed measurement of the thickness of fired and dried films a device called a surfometer can be used. A sharply pointed stylus is drawn over the surface of the film to be measured. A displacement transducer translates the vertical motion into an electrical signal, which can be displayed graphically on either a computer screen or a chart recorder. One advantage of a computer-based system is that digital signal processing can be performed on the transducer signal to remove noise, compute the mean sample thickness, etc. Generally the stylus is made from a hard material like sapphire or diamond and is therefore unsuitable for measuring the thickness of wet films. However, it is now possible to use an elipsometer, which can replace the conventional stylus and transducer head, thereby providing a non-contact, accurate technique for obtaining detailed measurements of wet, dried or fired films.

III.5 Annealing

The basic constituents of thick-film ink are:

- ✓ active material
- ✓ glass frit
- ✓ organic carrier

The active material is essentially a finely divided powder with a typical particle size of a few microns. Nowadays, a lot of powders with nanometric grain size are very commonly used for gas sensor fabrication, because better sensing properties of the active layer could be obtained. Conductor pastes will contain a precious metal or metal alloy like silver, platinum, gold, palladium and their alloys. Resistor inks contain metal oxides, while the dielectric pastes usually have ceramic powders as the active material. The glass frit acts as a binder, which holds the active particles together and bonds the film to the substrate. Lead borosilicate glasses are often used for this purpose. The organic carrier gives the paste the desired viscosity for screen-printing. Generally, the vehicle usually contains a resin dissolved in a solvent together with a surfactant to ensure that the solid particles disperse.

III.5.1 Drying process

After printing the film is allowed to stand in air for a few minutes so that the ink can level off and settle. This levelling off permits mesh marks to fill and some of the more volatile solvents to evaporate slowly at room temperature. As indicated in the section above, the film thickness can then be measured, if desired, with a non-contact technique. After this, the inks are subjected to a forced drying process. The object of the drying stage is to remove the organic solvents and make the printed film adhere to the substrate and relatively immune to smudging. The organic agent is still present in the ink at this stage. Drying takes place at temperatures between 70-180ºC in either a conventional box oven (Figure III.7) or a moving belt infra-red furnace.

Figure III.7. Conventional box oven (Model: Techno Print HA-02)

After drying, the inks can be overprinted with another thick-film layer or we can proceed directly to the firing stage.

III.5.2 Firing process

The high temperature firing cycle is designed to remove the remaining organic binders from the film, to develop the electrical properties of the ink and also to bond the ink to the substrate. Temperatures of up to 1000ºC are required to achieve these objectives. The electrical properties of some inks are very sensitive to the firing conditions and for this reason accurate control over the processing parameters is needed. Most thick-film furnaces are moving belt furnaces containing a number of heating zones. Figure III.8 shows a typical thick film furnace, where the parameters such as belt speed, peak firing temperature and firing time are controlled. Large industrial furnaces may have up to twenty separate zones and a belt width of up to 1m. More typically, furnaces have three or four zones and a belt width of around 10-15 cm.

Figure III.8. Thick film furnace (Model: BTU Engineering Corporation SP-8)

The heating zones inside the furnace are generated by resistance windings of materials like nichrome. Each zone has a separate temperature controller associated with it. A muffle tube traverses the length of the inside of the furnace and the belt is drawn through this tube. The belt itself is usually of the metal chain mesh-type and is capable of withstanding the high temperatures within the furnace. It is driven by a variable speed motor that can provide belt speeds of up to 15 cm per minute.

Figure III.9 depicts a typical firing profile, where three distinct regions are evident. Firstly, the temperature slowly ramps up towards the peak firing temperature. During this time the remaining organics are removed, at temperatures of around 350-400ºC. As the temperature reaches 600-800ºC, the glass frit softens. Glass is an unusual material in that it does not have a definite melting point but tends to go through a transition stage over a wide temperature range. The second noticeable region is the hot zone where the temperature remains constant for about 10 minutes. During this time, the active material sinters and various reactions take place. The electrical properties of the film begin to develop. The cooling stage allows the glass to solidify and the substrate emerges from the furnace close to room temperature.

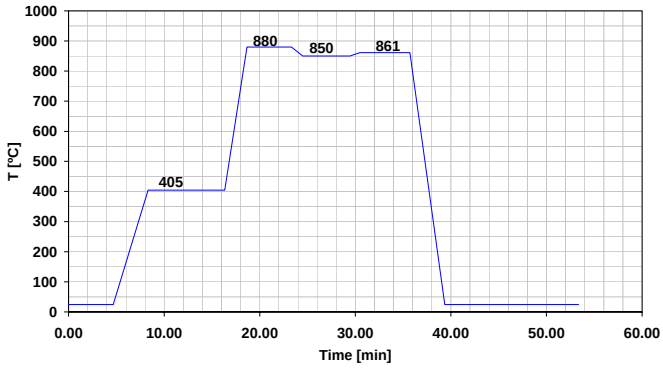

Figure III.9. A typical firing profile for thick film inks

Sometimes it is necessary to fire substrates in a controlled atmosphere. For example, a flow of clean, filtered air will produce a high quality film with repeatable characteristics. Some materials like copper and nickel will oxidise if fired in air and can only be processed in an inert atmosphere such as nitrogen.

III.6 Thick film materials

The range of materials available for thick-film technology is determined by their capacity to be both printed and fired. Established thick-film technology is based on three classes of material supplied in the form of printing inks. Their classification and function are determined by the resistivity, and the three original classes are conductors, resistors and dielectrics. Emerging sensor technology prescribes a whole new range of materials with desirable properties of interaction with the external world. These new materials are naturally less developed and optimized than the established ones, and they therefore tend to lack some of the more desirable properties.

An important property in manufacture is adhesion, and in commercial inks this tends to be optimized so that structures bond strongly to the substrate. In specially developed sensor inks, we sometimes have to compromise in order to achieve the desired interaction properties. The other major property is the coefficient of thermal expansion, which needs to be matched to the substrate to prevent large thermally induced stresses during manufacture.

In general, thick-film structures are created by printing patterns in inks composed of an organic carrier, a low softening temperature glass frit in the form of a finely divided powder and a characterizing ingredient. For conductors, the characterizing ingredient is a finely divided noble metallic powder (gold, silver, platinum or Ag/Pd). After processing, the metallic particles fuse to form continuous electrical paths through the carrier glass. Sheet resistivities of the order of 10 $m\Omega/cm^2$ are typical. In sensor applications, conducting inks have an important function in the formation of electrode patterns, which range from simple rectangular structures to interdigitated pairs. Platinum is also used for resistance thermometry and for combined heaters and thermometers in areas such as gas sensing, where control at a variety of temperatures is an important technique.

Dielectric inks are mainly used as insulants, either at crossovers or when a conducting substrate, such as stainless steel, has been employed. The characterizing ingredient is

generally a ceramic material such as particulate alumina. One of the vital requirements of the dielectric structure is that it must be free from pin holes, so multiple printing can be used. Because other structures are often superimposed upon the dielectric layer, the surface finish should be smooth. Sheet resistivities will normally be of the order of $T\Omega/cm^2$.

III.7 Substrates and substrate properties

The substrate is an important part of any thick-film process. The material needs to be robust, and the thermal conductivity is normally high and the electrical conductivity very low. It must also be easily shaped, but stable at firing temperatures as high as 1000°C. Classically, alumina has been used for this purpose. For normal electronic purposes, the substrate structure is a rectangle that can be mounted in a standard package. An important substrate sub-structure is the gap. This is normally used for isolation. In gas sensor arrays, for example, the various elements of the array may operate at different temperatures. The high conductivity of the normal substrate material militates against this provision, so it is usual to isolate elements from each other by means of laser cut slots.

Substrates mainly provide the mechanical support and electrical insulation for thick-film hybrid devices. The substrate can affect both the processes and the final characteristics of the devices. The properties of a potential substrate material should take into account the following aspects of circuit design and operation. Some engineering concerns are:

- ✓ Dielectric constant. This constant determines the capacitance, which is associated with different film elements screened onto the substrate. Capacitance effects are directly proportional to the dielectric constant and they affect the speed of the signals and the power needed for their propagation.
- ✓ Dielectric strength. The dielectric strength determines the voltage breakdown properties of the substrate.
- ✓ Dissipation factor. This factor determines the electrical losses in the substrate, and may be particularly important in high frequency and microwave circuits.
- ✓ Thermal conductivity. The thermal conductivity determines the thermal properties of the device. It is becoming more and more important as miniaturization becomes more widespread, because a "cold" component is more reliable than a "hot" one. Very high thermal conductivity is particularly useful for thermal sensors, while low conductivity is suitable for bolometric sensors.
- ✓ The thermal coefficient of expansion (TCE). This coefficient is a major factor in

determining the compatibility between the substrate and the added components. It has a significant effect on film adhesion and the temperature coefficients of resistivity and capacitance. If not properly matched, during the lifetime and in presence of thermal excursions, it can have a catastrophic effect on the integrity of the added components, including the thick film conductors and resistors.

- ✓ Volume resistivity: determines the electrical insulation between the circuit elements on the substrate.

Some of the manufacturing concerns related with the substrates are listed below:

- ✓ Ability to withstand high temperatures: typically between 500 and 1000°C.
- ✓ Mechanical strength: important for easy handling and basic for several sensors.
- ✓ Surface finish: important for good line definition and printed film uniformity.
- ✓ Camber: there should be a minimum distortion or bowing of the substrate. Excess can result in screening problems in thick-films and photo-processing problems in thin-films.
- ✓ Visual defects: surface defects such as small pits or burrs can result in circuit defects such as open circuits and pin holes.
- ✓ Compatibility of materials: the surface should be chemically and physically compatible with the chemicals and material used in fabrication. Generally speaking, the chemical inertness of ceramic substrates is particularly useful for sensors designed to work in very aggressive media.
- ✓ Low cost of producing large quantities.
- ✓ Tolerance: should be possible to achieve the suitable tolerances in overall dimensions.

Although none of the substrates available today fulfils all these requirements, the considerable number of existing materials can provide acceptable solutions for all applications. Most of the substrates used in thick-film technology are ceramic materials such as alumina, beryllia, magnesia, zirconia. Some of them are described below.

III.7.1 Beryllia (BeO)

The thermal conductivity of beryllia is approximately the same as that of alumina at room temperature. The combination of high strength and high thermal conductivity also gives beryllia good shock resistance. This material is mainly used in applications requiring rapid heat removal. Its TCE is slightly higher than that of Al_2O_3, while its dielectric constant is slightly lower.

III.7.2 Aluminium nitride (AIN)

Aluminium nitride is one of the new materials with improved thermal conductivity. It is very promising as a non toxic replacement for beryllia since its thermal conductivity is high, between 4 and $4.5x10^{-6}$/K, which is very close to that of silicon. Its thermal shock resistance is very good, its flexural strength is high, its chemical inertness is very good and its hardness is low, which makes both machining and laser scribing possible.

III.7.3 Porcelain enamelled steel substrates (PES)

The need for high thermal dissipation combined with great mechanical ruggedness in harsh environments has led to the development of a variety of metal core substrates. In addition to their inherent strength, vibration and shock resistance, and good thermal properties they have such potential advantages as excellent electromagnetic and electrostatic shielding properties. The metal can be inexpensively machined to produce complex three dimensional/odd shape parts with virtually no limitation on size. Porcelain enamelled steel substrates are based on a low carbon steel plate covered by a glassy or glass-ceramic layer 100 to 200 μm thick. After machining or punching, the steel is enamelled either by dipping, electrostatic spraying or electrophoretic deposition with a low alkali glass and fired at 950-1000°C. At this temperature, the glass forms a very smooth glassy surface on the substrate. The newest materials use crystallisable glass, which allow several re-firings at 850°C without re-softening.

III.7.4 Glass-ceramic substrates

These substrates are prepared by lamination and thermal treatment of several sheets of green (not yet fired) tapes on which the interconnection network has been screen-printed. Tape materials are glass-ceramic compositions like $MgO\text{-}Al_2O_3\text{-}SiO_2$ and are characterized by excellent sinterability at rather low temperatures (850°C to 1000°C), low dielectric constants, high fracture strengths, and low thermal expansion. The rather low sintering temperature makes it possible to use low resistivity conductive materials such as Cu, Ag, Au, Pd-Ag, leading to multilayer structures suitable for high-speed electronics. Moreover some characteristics of these materials, such as their TCE and dielectric constants, can be tuned by simply changing the nature of the basic components and/or their ratio. Usually the relative dielectric constant of the low-temperature cofired dielectrics is between 3 and 8 and the TCE between 4 and 8 x 10^{-6} /K. Unfortunately the thermal conductivity is about ten times lower than that of alumina. The fact that these sheets can be shaped in complex three-dimensional

structures makes them particularly interesting for the sensor area.

III.7.5 Alumina (Al_2O_3)

Alumina is the most suitable material for thick-film substrates, because it combines suitable physical and chemical properties with economic advantages. The industrial standard is now the 96% Al_2O_3 composition, which is used in approximately 90% of worldwide manufactured circuits. The additional 4% weight fraction of the content makes complete densification possible without grain growth and also makes it possible to optimize the electrical properties. The most common additives are magnesia and silica. Magnesia inhibits the growth of alumina grains (crystallites) by segregation at the alumina boundaries, which prevents them from moving. Silica is useful since the interaction between SiO_2 and Al_2O_3 gives rise to a new inter-grain phase (mullite), which binds the whole system. The elastic moduli and mechanical strength of alumina ceramic are high, which means that it is one of the strongest refractory oxides. These properties are particularly important for the implementation of several pressure and displacement thick-film sensors. The material characteristics are detailed in Table III.3.

Electrical characteristics of Al_2O_3	
Relative dielectric constant (at 1 mhz)	9.6
Dielectric strength (KV/mm)	12
Dissipation factor (x 10^{-4})	3
Volume resistivity (Ω.cm)	$>10^{14}$
Thermal characteristics	
Expansion coefficient (10^{-6}/ºC)	7.1
Thermal conductivity (W/mk)	20.9
Maximum temperature (ºC)	1500
Mechanical characteristics	
Bulk density (g/cm^3)	3.8
Flexural strength (mpa)	274
Young's modulus (gpa)	314
Poisson's ratio	0.23
Water absorption (%)	0

Table III.3. Al_2O_3 characteristics

III.8 Optimising structures

In some circumstances, we aim to adjust the geometry to optimize a property of the whole structure. Meandering and interdigitation are important examples in sensor fabrication.

III.8.1 Meander

In general, the purpose of a meander is to optimise the total resistance of the structure. This may be necessary if we need the occasional larger resistor and wish to avoid an extra printing stage with different ink. Heaters can be printed from platinum inks, and they also act simultaneously as resistance thermometers. In this case, the meander optimizes resistance and preserves some uniformity of heating over the area. The meander comprises a repetition of a basic L-shaped unit.

The total length of the meander, in terms of overall dimensions l and w and spacing d, is given by the following equation:

$$L = l\,(w + d\,)\,/2\,d \qquad \text{(III.1)}$$

If we ignore the smallest term, we obtain,

$$L \approx w\,l/2d \approx A/2d \qquad \text{(III.2)}$$

which gives a resistance of,

$$R \approx \rho_s\,A/2d^2 \qquad \text{(III.3)}$$

for a given surface resistivity ρ_s.

A typical minimum feature size would be of the order of 0.3 mm, so a useful rule of thumb for the maximum resistance obtainable with a given ink is

$$R \approx 5\,\rho_s\,A \qquad \text{(III.4)}$$

Thus, compared with a square, the meander increases resistance by 5A , where A is expressed in mm^2.

III.8.2 Interdigitation

The purpose of interdigitation is to optimize the electrical admittance between two conducting structures in order to exploit the properties of a material deposited over them by printing. Normally we seek to optimise either the conductance or the capacitance, but in some

applications the whole complex admittance is of value. In both cases the geometrical relationship is similar. If we let *P* represent the quantity we wish to measure (admittance, conductance or capacitance), then this quantity is related to the geometry by

$$P = k\,L/d \qquad \text{(III.5)}$$

where *d* is the spacing and *L* is the total electrode length. The constant *k*, includes a geometric factor and the relevant property of the superposed material (e.g. ε_r). Like meandering, interdigitation involves the repetition of basic units. The total length, *L,* for a given total area is *A /2d*, but what we need to optimize is *L/d*, or

$$P=kA/2d^2 \qquad \text{(III.6)}$$

Thus, for a typical minimum feature size of 0.3 mm, the rule of thumb is similar to the one above: in comparison with a square inter-electrode space the gain is of the order of 5*A,* where *A* is in mm^2.

These results emphasise that the optimising structures only have appreciable advantages when their total area is much greater than the square of the minimum feature size. We note again that the power dissipation per unit area is also a constraint.

III.9 Conductor pastes

The functions of thick-film conductors are so varied that no one composition is suitable for them all. Conductors play an important role in thick-film devices and the combination of properties is highly complex for both the paste composition and the fired films. Their conductivity, solderability, adhesion, and bonding capability must be excellent since they are the final connection between the circuit and the outside world.

Most of the characteristics of thick-film conductors depend on the composition of the functional phase in the paste, which consists of finely divided particles of:

- ✓ precious metals, particularly Ag, Au, Pd, Pt.
- ✓ base metals such as Al, Cu, Ni, Cr, W, Mo.

The particle size, size distribution, and particle shape have a significant influence on the electrical and other physical properties of the fired film conductor. Conductor based on Pt are

mainly used for heaters or resistive temperature detectors (RTDs). Some of the properties of the most commonly used conductor pastes are shown in Table III.4

Material	Sheet resistance ($M\Omega/cm^2$)	Wire bonding	Soldering	Remarks
Ag	1.5-2	Thick Al wire	All soft solders	Ag migration
AgPt	3-5	Thick Al wire	All soft solders	Ag migration
AgPd	10-60	Al wire	All soft solders	Good resistance
Au	3-8	Au or Al wire	Low melting solders	No metal migration
AuPt	20-100	Au wire	All soft solders	No metal migration
AuPdPt	10-100	Au wire	All soft solders	No metal migration
Cu	2-3	Au wire	All soft solders	High conductivity

Table III.4. Conductor pastes

To sum up, when choosing a conductor paste we have to be aware of the following paste parameters: electrical conductivity, solderability, solder leaching behaviour, bondability (Au or Al wire), electro-migration, adhesion in various working conditions (e.g. thermal aging, thermal cycling or shock, etc.), line definition (i.e. smallest printable line width and gap), compatibility with other pastes, working temperature, maximum allowable firing temperature and price.

Sheet resistance of fired conductors

With the exception of metal-organic conductors, the thickness of which is in the range of thousands of Angstroms, the usual thickness is between 10-20μm. It can be observed that the resistivity of films based on a single element is lower than that of films based on binary or ternary alloys, as happens in bulk metals. Moreover, the resistivities of thick films are usually larger than those of the parent bulk metals and may have quite a range of values, because the microstructure of thick-film conductors is not completely dense and includes voids and glass particles (Figure III.10).

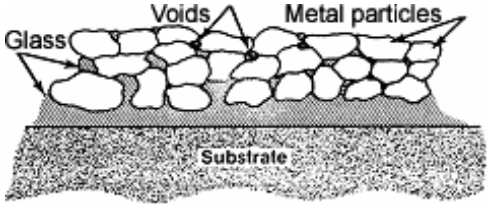

Figure III.10. Simplified view of the cross section of a thick-film conductor

The resistivity of the fabricated layer is also controlled by:

✓ the relative fraction of glass or other compounds included in the composition to bind the metal particles to one another and to the substrate.

✓ the density of the resulting composite, i.e. the number of residual voids in the structure after the organic vehicle has been fired out.

✓ the processing conditions, mainly temperature and time at peak temperature, which define not only the distribution and location of the binder and the number of the voids but also the interactions between metal and binder and between film and substrate.

Adhesion to the substrate

One of the most important factors that affects fired thick-film adhesion is the chemistry of the permanent binder. Three binder types are commonly used in thick-film conductors:

✓ Glass ($Pb/B_2O_3/SiO_2$ with Bi_2O_3 as fluxing agent). In glass-bonded systems (fritted conductors), the glass typically migrates to the substrate-metal interface during firing. Intrusions of glass extend from the substrate into the metal film, and sometimes to the surface of the conductor, to form a mechanical bond. In excessively high firing temperature profiles, glass may "float" on the conductor surface and result in poor solderability, poor adhesion and wire bondability. The chemical and physical properties of the substrate play an important role in determining how the glass binder phase wets the substrate surface and is attached to it. Variation in surface chemistry, grain size, and smoothness of the substrate can cause wide variation in thick-film conductor performances.

✓ Oxide (fritless conductors). Small amounts (0,1-1 %) of chemically active oxides like CuO, CdO or NiO, added to the paste, react at high temperatures with alumina substrates to form oxides like $CuAlO_2$, which provide adhesion.

✓ Glass+oxide. A combination of glass and oxides is used but the amount of glass is much lower than in the fritted systems. Adhesion is believed to be related to a combination of the effects mentioned above.

To understand the functionality of Bi_2O_3 in greater detail, its chemistry was explored for typical conditions in actual use. These experiments suggest that molten solders are reducing agents that are sufficiently strong to reduce bismuth oxide to bismuth metal, according to the following chemical reactions:

$$3\,Sn + Bi_2O_3 \rightarrow 3SnO + 2Bi \qquad \text{(III.7)}$$

$$3\,Sn + Bi_2O_3 \rightarrow 3SnO_2 + 4Bi \qquad \text{(III.8)}$$

Since bismuth oxide is part of the permanent binder phase in a fired thick-film conductor, a reduction of Bi_2O_3 to Bi metal destroys the glass network and reduces adhesion.

Bondability of thick-film conductors

Gold conductors (and sometimes also Pt/Au and Pd/Au conductors) have several unique performance characteristics that make them essential in certain applications. In fact, semiconductor devices can be bonded directly to the gold conductors by the formation of a gold/silicon eutectic between the gold conductor surface and the back of the silicon chip. Gold conductors are also excellent for most types of wire bonding. They are ideal for applications in which semiconductors are attached by "chip-and-wire" techniques. Wire bonding with aluminium wire is also possible on Ag, Pt/Ag, and Pd/Ag with reliable results. To obtain good yields during wire-bonding, the surface of the conductor must be very uniform, without oxidations and glass.

Paste price

Table III.5 compares the price of the most commonly used conductive pastes. The price of a hypothetical Ag-based conductor is considered to be 1.

Metal/Alloy	Relative price
Ag	1
Ag/Pt	1,8-3
Ag/Pt/Pd	2-4
Ag/Pd	1,6-4
Au/Pt	40
Au	30-40
Cu	2

Table III.5. Price of the most commonly used conductive pastes

The actual cost for the user depends not only on the type and amount but also on the coverage factor. This factor is defined as the area of the substrate covered by 1 gram of the paste, screen-printed according to the manufacturer's specifications.

III.10 Active phase preparation concepts

The preparation of a paste for screen printing thick films requires knowledge from several

disciplines, including polymer chemistry and rheology, sol-gel preparation, electrochemistry, solid state physics and chemistry. Any paste (also commonly referred to as ink) for electronic thick-film passive components or sensing elements contains at least two ingredients: an organic vehicle and a functional material or active ingredient which is intended to dominate the electric and sensing properties of the layer. A third ingredient is also commonly used —either a glass frit or an oxide— which bonds the fired films to their corresponding substrate. The typical methods of manufacturing thick-film pastes contain the following two steps. First, the weighted fractions of the constituents (organic vehicle, inorganic powders and metal-organic compounds) are roughly mixed in a plenary mixer (Figure III.11). This method can also be used if an active powder with a smaller grain size is required.

Figure III.11. Plenary mixer (Model: FRITSCH-Pulverisette 6)

In this stage, the vehicle wets the powders and large agglomerations are broken. The second stage can be carried out manually or with the three-roll mill, which is composed of three in-line rolls separated by small adjustable gaps. In this stage, the mixture is converted to a printable paste with suitable properties.

III.10.1 Organic vehicles

"Organic vehicle" is a generic term that describes a blend of volatile solvents and polymers or resins, which are needed to provide a homogeneous suspension of the particles of the functional materials and a rheology that is suitable for the printing of the film configuration. The vehicle is a temporary, sacrificial ingredient, which should be completely removed in the following steps of the process, during which the microstructure of the deposits is formed. The composition of the organic vehicle determines (or helps to determine) the shelf life of the paste, its drying rate on the screen, the change in printability with ambient temperature, the

resolution of fine lines, some electrical properties of the fired films and their cosmetic appearance.

The cooperative effects and the relationships between the properties (density, wettability, surface energies, viscosity etc.) of the organic vehicle and inorganic constituents of the paste contribute to the static and dynamic properties of the paste. Moreover, the solvents should not be so volatile that after a short time they leave a hard unprintable paste on the screen mesh but, at the same time, they should evaporate early in the drying phase of the process. Finally, the fluid properties (rheology) of the vehicle should prevent penetration through the screen when the paste is at rest, but should enable printing to be fast under the squeeze pressure and the film to settle quickly in the desired configuration on the substrate without bleeding or smearing from the defined geometry.

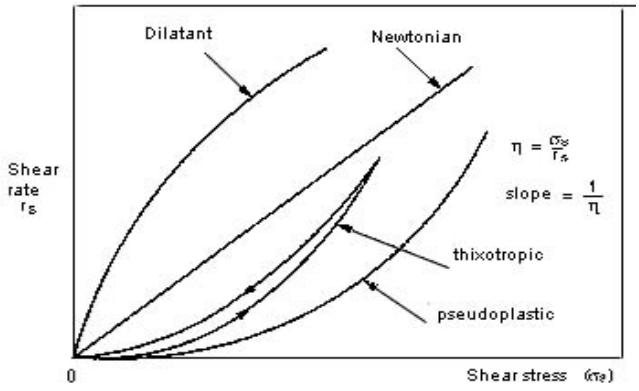

Figure III.12. Response of fluids to shear

The pseudo-plastic and moderate thixotropic properties of the paste, which are two of the four possible rheological behaviours of materials shown in figure III.12, make this behaviour possible. This figure shows the relationships between the shear stress and the shear rate of fluids. Shear stress versus the pressure (or force per unit area measured in Pascal, Pa) applied to a viscous fluid to cause its movement on a plane and shear rate (r_s) is the velocity (v) of the relative shift of two planes, separated by fluid for a distance (x), divided by the distance itself ($r_s=\delta_v/\delta_x$). The viscosity of the fluid η is the ratio between these two quantities, i.e. $\eta=\sigma_s/r_g$.

In a Newtonian fluid, η is a constant quantity. In a dilatant fluid, however, the η value increases with σ. Apparently the required behaviour of printable pastes is not met in either case, which is why these fluids cannot be used. Pseudoplastic and thixotropic fluids behave similarly, in that η increases when shear stress is applied. Thixotropy, however, involves

hysteresis. Very simple organic vehicle formulations can be used to prepare model pastes that are suitable for both basic studies and feasibility tests. They are usually blends of terpineol-type solvents and cellulose-type resins, like α-terpineol and butylcarbitol (as the solvents) and some ethyl cellulose (the polymeric viscosifier). The relative fractions of these ingredients are varied according to the types and amounts of the inorganic materials of the paste. These simple vehicles perform well with many solid systems in a variety of printing conditions and environments. However, requirements of fine line resolution (e.g. lines about 125 μm wide), fast printing rates, smooth surfaces and the like have stimulated the development of complex vehicles.

III.10.2 Metals

The size and shape of metal particles strongly affect the characteristics of the fired films, e.g. in terms of sinterability, densification, conductivity, solderability. Finely divided metal particles, such as spheres, flakes or drops, are usually blended in the pastes with a mean size lower than 5 μm, and sometimes in the range from 0.1 to 0.5 μm. It is virtually impossible to obtain these features by comminuting mass-produced metals and alloys. Chemical routes are suitable, however, the most common being precipitation (or co-precipitation i.e. precipitation of multiple systems) from appropriate solutions of metal salts, decomposition of metallorganic compounds, and spray pyrolysis. Precipitation is the most common approach. Several methods have been described in the patent literature for both precious (e.g. Au, Pt, Pd, Ag) and base metals. For example, precious-metal compounds like nitrates, chlorides, bromides or cyanides can be dissolved in a suitable solvent such as water or hydrocarbon solvents. Reducing agents are added to precipitate the metal or the alloy. The main parameters affecting the precipitation rate, the coarsening of the particles and their shape are the concentrations of the solution, pH and temperature. The precipitate is filtered off and dried. After size classification (e.g. sedimentation, surface area measurement by gas absorption, scanning electron microscopy and checking the powder composition for contaminants), the powder can be blended with the other constituents of the paste.

The typical dimensions of the conductive lines prepared with these pastes are the following: width between 0.5 mm and 0.125 mm and thickness between 10 and 20 μm, with a surface roughness of 0.1-2 μm. Line resolution can be better, and the thickness and roughness lower with the metal powders provided by spray pyrolysis and metallorganic compounds.

In spray pyrolysis, the metal salts are dissolved in water, acetate, carbonates, etc. The solution is atomised and introduced in a heated reactor with a conveying gas. The starting material, gas flow rate and reaction temperature are the most influential properties of the process. Almost spherical, submicron-sized pure grains can be obtained, which make it possible to prepare thin (a few μm thick) smooth films. Metallo-organic (MO) compounds (also known as resinates, since the early products were derived from natural resins) consist of molecules in which a central atom is linked to ligands through a hetero-atom (e.g. O, N, P, S). Metallo-organic compounds can be synthesized so that thermal decomposition produces fine metal powders or films (0.1 to 0.3 μm thick) without going through the powder stage. Both opportunities have been exploited in thick-film technology. These films can give a line resolution as low as 15 μm. The main interest of these MO-based pastes is that they be used to manufacture thick-film print heads, metallized solar cells and high density interconnections, but emerging applications also encompass thick-film sensors, e.g. gas sensors. One very important use of MO-compounds is that small amounts in thick-film pastes can adjust the electrical properties of thick-film resistors for both circuits and sensors.

III.10.3 Metal oxides

The approaches used to prepare metal-oxide powders for thick-film pastes include precipitation, MO-decomposition, spray pyrolysis, and many more: solid state reactions, thermal evaporative decomposition of precursors (similar to spray pyrolysis but without the conventional convective heating with flowing gases), oxidation of metal powders in air or oxygen and sol-gel. Precipitating a single component or a multi-component system is a common method for preparing metal-oxide powders. A wide variety of metal oxides has been studied and is used in thick-film sensors. They include SnO_2, WO_3, ZnO, α-FeO_3, γ-FeO_3, TiO_2, ZrO_2, CeO_2, $BaTi_2O_3$, $MgFe_2O_4$, NaSiCON, YBCO. While some of these are semiconductors, others are solid electrolytes, metals or superconductors.

The most important aim of this thesis is the fabrication of SnO_2 and WO_3 active layers. Details of the fabrication processes used, can be found in chapters 4 and 5.

III.10.4 Glasses

Choosing the glass content for thick-film components is mainly dictated by the following requirements:

✓ The linear coefficient of thermal expansion (CTE) should be as close as possible to the CTE of the substrate (usually alumina with a CTE between 6.5 and 7.5 ppm/ºC in the range from 2500 to 3000ºC. A slightly lower CTE is tolerated, since the glass is put slightly in compression, i.e. in a condition safer than the opposite, which creates tensile strains.

✓ The softening point T_s should fall between 400ºC and 600ºC. In these circumstances, the viscosity of the glass will be low enough at the peak temperatures of the common firing cycles (850ºC to 1000ºC) for a continuous glassy matrix to form in a few minutes, and/or for there to be a liquid phase which assists the sintering of metal particles and the required reactions with the other components of the paste.

✓ No ions should be in motion under electric bias if mass transport and the degradation of the properties of the film are to be avoided. These conditions are prerequisites for the stability of the thick-film layers at relatively high temperatures.

Pure silica does not meet these requirements (mainly because the softening point is too high and the CTE is too low). Adding Bi_2O_3 decreases the T_s value and increases the CTE but makes the glass too "short" (namely the viscosity η changes too rapidly when the firing temperature is changed); moreover, Bi_2O_3 may induce devetrification. Alkaline or alkaline earth cations, widely used in the glass industry as a means for controlling the viscosity and workability of silicate glasses, cannot be used in large quantities because of their consistent ion mobilities. Lead is the added cation of choice in the composition of air-fireable thick-film materials. Ba and Ca are appropriate for nitrogen-fireable materials, and for dielectric air fireable pastes. PbO may be added to silica in large fractions without devetrification. Its cation exhibits low mobility in the glass and makes it very stable up to relatively high temperatures.
The crucial point here is that the specific composition of the glass (e.g. the relative amounts of SiO_2, Bi_2O_3, PbO) greatly affects the dissolution kinetics of Al and Be (from alumina and beryllia substrates), the reactions with the active ingredients of the ink, and the reproducibility of the glass batches because it affects the degree of volatilisation of Pb from the melted glass during the preparation of both the frit and the components.

Once the glass composition has been carefully chosen, the preparation of glass particles for the paste is a relatively simple process. In the traditional process the glass forming oxides, carbonates or hydroxides are weighed, mixed in a blender, placed in a ceramic or platinum crucible, fused at temperatures between 1000ºC and 1500ºC, and then poured into cold water. This quenches the molten glass and shatters it into a coarse powder. The process is known as

fritting, and the glass powder is known as the frit. The frit is then ball milled to a mean particle size of a few micrometers.

The paste preparation stays in the complexity of the systems, a complexity which resides not only on the multi-component nature of the pastes and the fired films but also on the inevitable number of phenomena required to transform the deposited layers in the functional layers. The preparation of thick-film pastes is a process that requires the ingredients (organic vehicle, functional components and additives) and their original sources to be carefully chosen on the basis of basic knowledge and expertise of the physical-chemical reactions, if appropriate thick-film sensors are to be obtained.

III.11 Bonding

Once the sensor chip is firmly in position, it is ready for wire bonding. The three most common methods are:

- ✓ Thermo-compression wire bonding
- ✓ Thermo-sonic wire bonding
- ✓ Ultrasonic wire bonding

It is important to select the appropriate conductor ink for the bond pads as not all inks are compatible with each wire bonding method. Essentially, there are three main types of wire bond: the ball, stitch and wedge.

Thermo-compression wire bonding, as its name suggests, forms the bond by a combination of heat and pressure. The interconnection is usually gold wire with a diameter of around 25 microns. Gold or palladium/gold bonding pads are the conductor inks of choice for this method. The wire is fed through a ceramic capillary and a ball is formed on the end of the wire by heating with a hydrogen flame, or sometimes by means of spark discharge from an electrode near the wire. A temperature of up to 350ºC is required to make the bond and this can be achieved by either heating the substrate or the capillary. With the former, epoxy bonding cannot be used, as the excessive substrate temperature would soften the epoxy bond. The first wire bond is usually made on the aluminium pad on the die, the capillary is lowered onto the pad and a pre-determined force is applied to form a ball bond. The wire feeds out through the capillary as the bonding tool is raised. The substrate is then moved so that the capillary is located directly above the bond pad on the substrate. The capillary is lowered and

the combination of pressure and heat forms a stitch bond. The wire can be clamped and broken and the process of forming a ball is repeated in order to enable further connections to be made.

The thermo-sonic bonding technique is a combination of thermo-compression and ultrasonic methods. The substrate is heated to a temperature of around 150ºC and the bond is made using ultrasound vibrations. Thermosonic bonding with gold wire is generally considered to be a very favourable method for thick-film circuits as it is amenable to multi-level and multi-direction bonding.

In ultrasonic wire bonding, force and friction play a critical role in the joining process. Ultrasonic energy is introduced into the contact region of the joining partners by a sonotrode. The oscillation amplitude is kept tangential to the direction of force (and therefore tangential to the substrate surface). The frequency range is between 15 and 60 kHz depending on the material, the thickness of the wire, and the type of bonder. The oxide skin of the surfaces of the joined partners is disrupted by ultrasonic oscillation and the clean surfaces to be joined are brought within atomic distance of each other. The oxide layers are broken down, but remain in the joining region. Therefore, it is important that these remnants be only a small fraction of the contact area. The power introduced by the sonotrode deforms the wire and brings the joining partners to within atomic distances of each other. A typical wire bonding machine is shown in figure III.13.

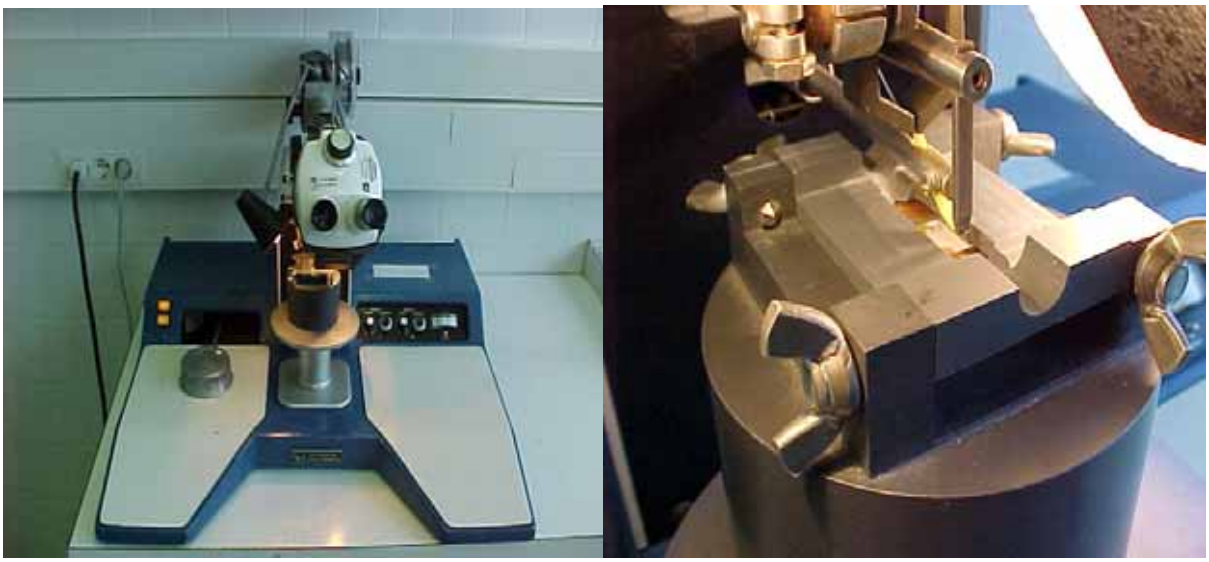

Figure III.13. Wire bonding machine (left) and sensor soldering (right)

The bonding parameters (ultrasonic energy, time, pressure) must be controlled very carefully if the results are to be repeatable. A good contact between the sonotrode and the joining partners is essential if there is to be no loss in ultrasonic power in the bond area. In addition, the substrate (thickness) and the ductility of the materials involved play an important role. Sonotrodes with rough surfaces can improve the effectiveness of the ultrasonic transfer. If the contact pressure is too high, the bond may be weakened; if it is too low, the surface of the sonotrode and the contact area may be damaged by the dissipation of frictional heat.

Ultrasonic bonding is predominantly used with aluminium wires. Normal diameters vary between 17 and 500 μm. Very thin wires from pure aluminium are too soft, so alloys with about 1 % silicon are generally used. Pure aluminium (Al 99.999) is used with wires of 100 μm diameter or more, because higher conductivity is preferable to mechanical strength. Process automation, however, is more expensive.

III.12 Packaging and testing

The objective of the package is to protect the circuit from harsh environmental conditions, mechanical damage and the ingress of water vapour pressure within the package itself. Ultimately this will affect the reliability, repair capability and cost of the sensor. The final stage of the thick-film process also involves assessing the quality of the circuit and comparing the performance with the initial specifications. The sensors are also electrically tested.

Testing the performance over a wide range of temperatures is usually an important consideration. Humidity and vibration are other types of environmental test, which various standards insist upon. Sensor applications of thick-film technology require considerable testing in relation to the measurand, which is being detected. Other forms of cross-sensitivity like electro-magnetic interference, noise, vibration, temperature, environmental pollutants etc. may have been designed to be rejected by the sensor and its associated electronic circuitry. Finally, the thermal characterization of the sensor was performed.

III.13 Conclusions

This chapter discusses the fabrication of thick-film gas sensors. It begins with a detailed review of thick-film technology and presents the whole substrate fabrication process. Particular emphasis is placed on the preparation of the active phase, and the calcination and firing process. Finally, the wire bonding, packaging and testing of the sensors is reviewed.

IV. FABRICATION OF THICK FILM GAS SENSORS ON Al_2O_3 SUBSTRATE

In recent years there have been many new developments in the sensor substrate technology. The selection of the substrate material is of major importance. In particular, the substrate must have low electrical conductivity, considerable thermal and chemical stability and guaranteed adhesion of the layer. At the same time, there must not be any undesirable reactions between the substrate and the gas-sensitive metal oxide layer while the sensor is being fabricated or during subsequent operation. For huge amount of sensor applications Al_2O_3 substrates have been used. For this substrate, to avoid reactions in all circumstances, the use of substrates equipped with a diffusion barrier can be considered. This diffusion barrier consists of a thin film of high-temperature stable SiO_2, which is sputter deposited with a typical thickness of 1 μm on the substrate prior to the deposition of the sensor substrates. This cheap pre-treatment of the substrate is recommended also for other thick-film metal oxide sensors because besides its inhibition of the formation of any mixed oxide phase, it also ensures that no doping effect of the sensors films due to metal ions (also impurities) from the substrate may occur.

The active layer has a crucial importance for the gas sensors performance. Nowadays, tin and tungsten oxides are the most commonly used materials for fabrication of the active phases. Due to the lack of selectivity of the pure active layers, noble metal doping and catalytic filters

are commonly used to improve the sensor response. To obtain high sensitive and selective sensors we synthesized a big variety of active phases. We studied carefully the influence of the grain size and the annealing temperature to the sensor response.

IV.1 Sensor fabrication

This chapter discusses the design and fabrication of sensors on Al_2O_3 substrate. These sensors are fabricated completely in University Rovira i Virgili. The fabrication procedure is explained in details beginning with the measurement electrodes, heater and temperature measurement resistance deposition on the substrate and discussion of the pastes used for active layer. After the sensor encapsulation and electrical measurements, the physical and chemical test performed with the above mentioned sensors are exhaustively described.

Thick films are generally deposited on plane substrates, which contain measurement electrodes, temperature measurement resistance and a heating resistance. This resistance can be placed on the substrate opposite the active layer (Figure IV.1a) or on the same side (Figure IV.1b). In the first case, the temperature gradient on the substrate means that the power consumption is greater, but that the fabrication process is easier.

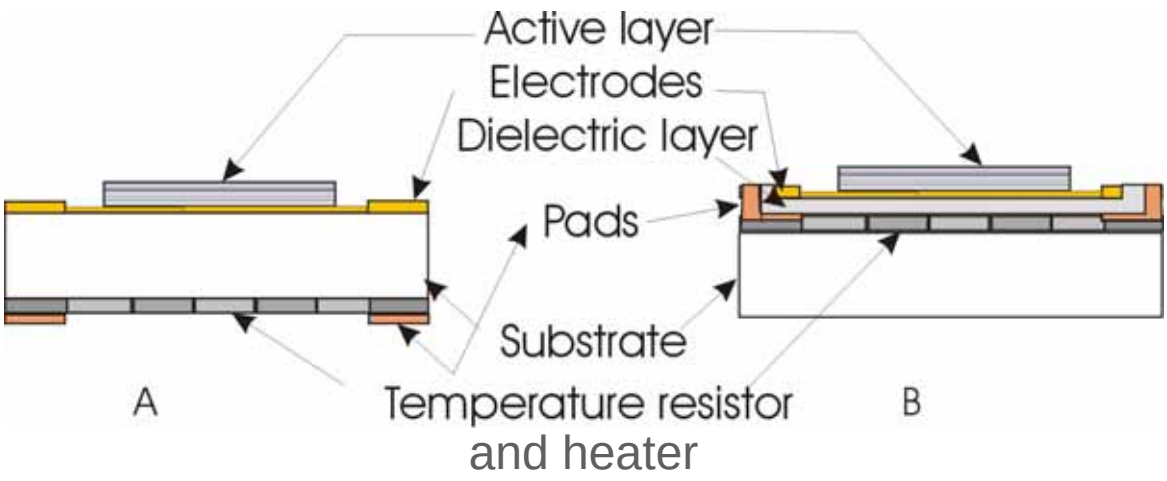

Figure IV.1. Cross-section of two geometries for plane sensors

In the second case, the sensor can be considerably smaller and this makes it possible to work with less power. Its fabrication, however, is more complicated. As we aim to make only the initial tests with this substrate, we choose the simplest configuration. Table IV.1 presents the individual steps followed and the most important information for successful results in thick-film fabrication.

Screen selection & design rules	Screen and mesh chosen according to the datasheet of the paste: Conductors and resistors - steel screen Dielectrics – polyamide / polyester screen Pads for pins 1.5x2 mm, for bonding (3 times bigger area than the diameter of a bond wire) 0.3 mm a minimum distance of a pattern from the substrate or from another pattern The minimum width of a path is 0.3 mm 0.3 mm a overprint of a connection of two different patterns
Screen printing	Squeegee pressure 30-40 psi Speed depends on paste viscosity (higher viscosity, higher speed) Screen-substrate space usually 0.3-0.6 mm (For large area of a pattern a bigger space must be set)
Levelling time (25ºC)	Determined by the datasheets of a paste – usually 10 to 20 min
Drying time	Determined by the datasheets of a paste: Usually 10 to 15 min at 120-150 ºC. The structure obtained should be without dark and light shades. If it is not, the levelling time should be extended.
Firing process	***Firing profile must fulfil the datasheet parameters for time in peak and ascent/descent slope*** The air-flow conditions should be set so that chamber does not take air in from the outside through the entry or exit. Dry air should be used.

Table IV.1. Technological steps

Since oxide sensors only work at high temperatures, a heating element must be built into the sensor. This heating element is often made of platinum. It is optimized for the temperature distribution (as homogeneous as possible) and stable and reproducibly set temperature dependence of the electrical resistance, in order to set the working temperature of the sensor as precisely and reproducibly as possible. The heater must ensure that the semiconductor oxide is uniformly heated with the minor energy loss. In some cases, the heater can also be used as a temperature sensor. In addition to the substrate, gas sensors require metal electrodes for electrical contacts. Because the temperatures during backing and tempering are high, gold contact electrodes are most commonly used. A simple interdigitated structure is used for the

electrode shape. Since the specific conductivity of many metal oxides is low, the relationship of length to width should be adjusted so that the conditioning circuitry can easily measure the resistance of the sensor layer. A temperature sensor must be added to complete the substrate. The aim of this sensor is to measure the substrate temperature during sensor operation. For the electrodes and temperature sensors, noble metals are usually used. The selection of these materials is conditioned by the fact that they must not oxidise or react with the substance to be detected.

IV.1.1 Sensor substrate fabrication

The thick-film sensors were prepared in the basic phases described as follows. In the first stage, the heater was deposited onto an alumina substrate using a commercial platinum paste and, after drying, a temperature sensor was deposited using a platinum paste with a stable temperature coefficient. After firing, pads were printed by using a commercial conductive gold paste and fired. Then, on the other side of the substrate, interdigitated gold electrodes were deposited and fired. All layers were fired in a belt furnace at 950ºC. The typical value of the temperature-measuring resistor was approximately 1.1 kΩ ± 5% with a temperature coefficient (TCR) of 3.00×10^{-3}°C^{-1}. The value of the heating resistor was 10 Ω ± 3% with a low temperature coefficient of approximately 3.45×10^{-6}°C^{-1}, for temperatures ranging between 25ºC and 350ºC.

IV.1.1.1 Fabrication of the heater/temperature sensor

The heater was fabricated using a Heraeus C3657 platinum paste and the temperature sensor was made with DuPont 5091D paste. The printing was carried out with a screen with the following characteristics:

- ✓ Mesh 280/25 μm
- ✓ Squeegee pressure=35 psi
- ✓ Fast print speed, because of the very low paste viscosity
- ✓ Snap-off=0.5 mm
- ✓ Levelling between 10 and 20 minutes, to eliminate any bad structures after the firing
- ✓ Drying in the oven for 10-20 minutes at 150ºC
- ✓ Firing in the furnace at 900ºC for 8 minutes (peak temperature/time)
- ✓ Rate of ascent/descent must be in the range 60-100ºC/min

Furnace settings for a firing profile with the following parameters: **900ºC/8 min at peak temperature**

Temperature [ºC]		Air flow [l/min]	
Zone I	425	Q_1	20
Zone II	889	Q_2	20
Zone III	883	Q_3	10
Zone IV	892	Q_4	16
		Q_{out}	4.62

Note: Q_{out} was established following equation $Q_{out}=0.07*sum(Q_i)$

IV.1.1.2 Fabrication of the pads

The pads were fabricated using an ESL 8884 gold paste. The gold is used, because of its excellent bonding properties and high temperature resistance. The printing was carried out with a screen with the following characteristics:

- ✓ Mesh 325/25 μm
- ✓ The print speed must be slow. The pattern must be covered with paste before printing.
- ✓ Squeegee pressure=40 psi
- ✓ Snap-off=0.5 mm
- ✓ Levelling for approximately 5-10 minutes at 25 ºC
- ✓ Drying in the oven for 10-15 minutes at 125 ºC
- ✓ Firing in the furnace at 875ºC for 10 minutes (peak-temperature/time)
- ✓ Rate of ascent/descent must be in the range 70-100 ºC/min

*Furnace settings for a firing profile with the following parameters***: 875ºC/10 min at peak temperature**

Temperature [ºC]		Air flow [l/min]	
Zone I	525	Q1	28
Zone II	860	Q2	14
Zone III	850	Q3	10
Zone IV	861	Q4	16
		Qout	4.76

IV.1.1.3 Fabrication of the electrodes

The electrodes were fabricated using an ESL 8884 gold paste. The printing was carried out with a screen with the following characteristics:

- ✓ Mesh 325/25 μm
- ✓ The print speed must be slow. The pattern must be covered with paste before printing.
- ✓ Squeegee pressure=45 psi
- ✓ Snap-off = 0.5 mm
- ✓ Levelling at room temperature for approximately 5-10 minutes at 25 ºC
- ✓ Drying in the oven for 10-15 minutes at 125 ºC
- ✓ Firing in the furnace at 950ºC for 10 minutes (peak temperature/time)
- ✓ Rate of ascent/descent must be in the range 60-100 ºC/min

Furnace settings for a firing profile with the following parameters: **950ºC/10 min at peak temperature**

Temperature [ºC]		Air flow [l/min]	
Zone I	465	Q_1	20
Zone II	942	Q_2	20
Zone III	934	Q_3	10
Zone IV	945	Q_4	15
		Q_{out}	4.55

The various steps which are composing the fabrication process of the sensor substrate can be observed in Figure IV.2. The whole fabrication process includes four printing stages: electrodes, heater, temperature sensor and bonding pads. For the firing processes only three stages are required: sensor electrodes, the heater and the temperature sensor which could be fired during the same firing process, and finally the bonding pads.

a) Top side

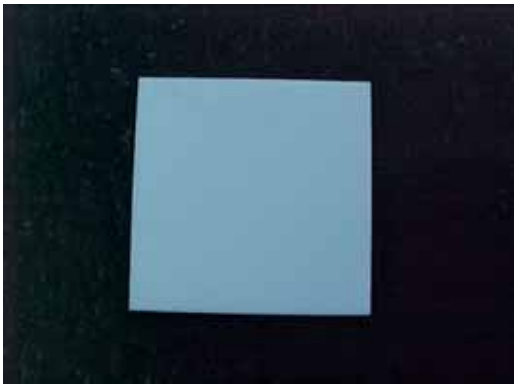

b) Top side

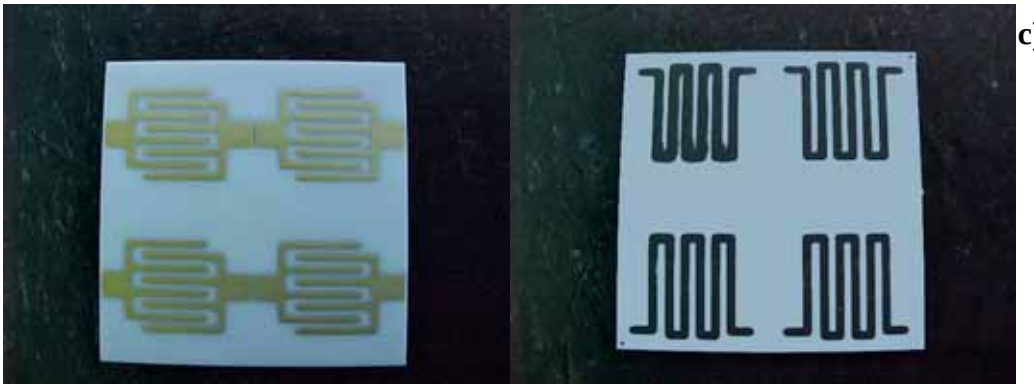

c) Bottom side

d) Bottom side

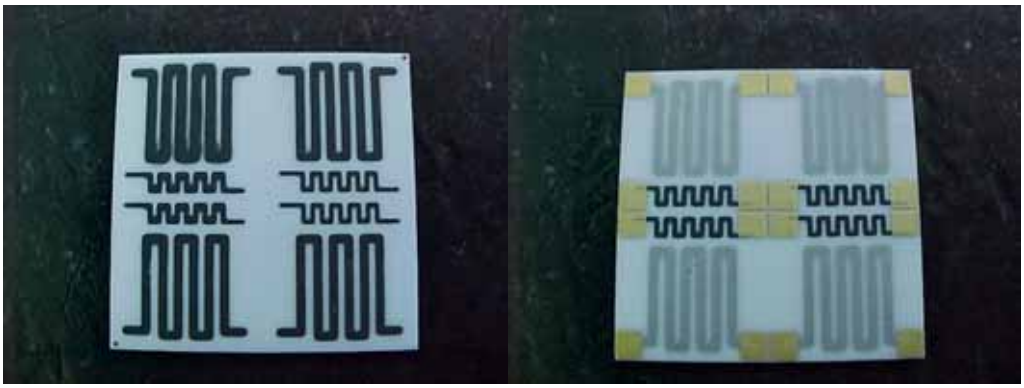

e) Bottom side

Figure IV.2. The steps in the fabrication process (a) Al_2O_3 substrate, b) gold sensor electrodes c) platinum heater, d) TCR temperature sensor, e) gold pads)

IV.1.2 Active phases

Pastes for active layers are prepared in two steps: first the organic matrix is prepared and then it is mixed with the powder of the active layer (filling of the paste). Optionally, when the powder is not fine enough, it can be milled previously.

IV.1.2.1 Preparation of lack matrix

We put an appropriate quantity of Heraeus HVS 100 thinner into a plastic beaker. Three or four glass balls and a magnetic stirrer were then added for mixing. A big glass beaker partly filled with water was put onto the magnetic stirring and heating plate. The plastic beaker was put into this glass beaker to make a water heating bath. The lid of the plastic beaker was on during heating. Then it was heated on the heating and magnetic stirrer plate to 45ºC. This temperature was maintained throughout the mixing process. In the next stage, an appropriate quantity of Texaphore 936 was added and stirred until dissolution. Then ethylcelullose was added and stirred until complete dissolution (tens of minutes). Finally, the magnetic stirrer

was removed and the desired quantity of Rilanit added. This was dissolved using a hand mixer at turbo speed for several minutes.

Two different lack matrices were developed for the sensors prepared on the ceramic substrate. The reason for preparation of two matrices is the different grain-size of the powders used. The matrix composition ensures homogeneity and very good adhesion of the active layer to the ceramic substrate. The first one was used mainly for powder with micrometric grain size, while the second was developed basically for nanopowders. The composition is detailed in Table IV.2.

Lack Matrix 1 – developed for micrometric powder and screen printing on a ceramic substrate	
Terpineol HVS100	*89.3 wt%*
Ethylcelulose	*1.2 wt%*
Texaphor 963	*6 wt%*
Rilanit spez. micro W	*3.5 wt%*
Lack Matrix 2 - developed for nanopowder and screen printing on a ceramic substrate	
Terpineol	*85.5 wt%*
Ethylcellulose	*1.1 wt%*
Texaphor 963	*5.7 wt%*
Rilanit spez. micro W	*3.4 wt%*
Disponil O5	*4.3 wt%*

Table IV.2. Lack matrix composition

If the matrix contains particles that have not fully dissolved, it can be filtered under vacuum. The prepared lack matrix has to be transferred from the beaker to the vessel and must be stored at temperatures between 0-5°C.

IV.1.2.2 Powder preparation

The size of the particles and their distribution through the layer (paste), especially in mixtures of different powders, is extremely important for the properties of the active layer. Some of the powders prepared during our investigation are listed in table IV.3.

SnO_2 powder	**WO_3 powder**
Commercial powder Merk K27783018.033 was milled in planetary mills: *35.11 g SnO_2 (65 mL) dried at 150ºC/15 min* *30 mL Xylene* *10 balls; 200 rpm/40 hours* *(1 hour/20 min pause, reverse)* Xylene was evaporated by heating at 80ºC. The milling was repeated: *60 mL SnO_2 dried at 150ºC/15 min* *35 mL xylene +0.253g disponil O5* *10 balls; 240 rpm/50 hours* *(1 hour/20 min pause, reverse)* The xylene was evaportaed by heating at 80ºC.	Commercial powder Prolabo 20739.188 was milled in planetary mills: *50 g WO_3 30 mL Xylene + 0.1% surfactant* *15 balls; 240 rpm/180 hours* *(1 hour/30 min pause, reverse)* After milling, the mixture was heated (80ºC) to evaporate the xylene. After that the powder was calcinated at 850ºC for 2h in air atmosphere. Then the powder was milled: *38 g WO_3 and 25 mL xylene* *10 balls;200 rpm/31 h* *(1 hour/30 min pause, reverse)* The xylene evaporated at 80ºC.
Bi_2O_3 powder	**Cu_2O powder**
Commercial powder Aldrich 22,398-1was milled in planetary mills: *100 g Bi_2O_3* *30 mL xylene* *10 balls; 280 rpm/100 hours* *(1 hour/20 min pause, reverse)* The xylene was evaporated by heating at 80ºC.	Commercial powder Aldrich 20882-5 was milled in planetary mills: 25 g Cu_2O 20 mL xylene 10 balls; 240 rpm/209 hours (1 hour/20 min pause, reverse) 0.33g of texaphor 963 was added and the xylene was evaporated by heating at 80ºC
Glass frit powder Commercial powder was milled in planetary mills: *189.7 g glass frit ($Pb0_2$, SiO_2, B_20_3, Al_2O_3, and Y_2O_3)* *60 mL xylene + 0189 g calcium stearate* *14 balls 1 cm + 5 balls 0.5 cm* *300 rpm/40 hours (1 hour/10 min pause, reverse)* The xylene was evaporated by heating at 80ºC.	

Table IV.3. Powder preparation

The size affects the sensitivity of the printed layer. Smaller sizes should improve sensitivity (see [136] and [137]). The nanopowder is used with very good results, but it is expensive to prepare and difficult to use to make rheologic paste, as our results show. The nanopowder

layer has very porous structure as can be seen in [138]. Porosity strongly depends on the rheology of the paste, the thickness of the film and the firing temperature.

IV.1.2.3 Additives

Oxides such as glass frits are used to ensure good adhesion. This affects the sensitivity of the film as is described in [139], where Bi_2O_3 is added. These materials usually increase the resistance of the film, because they fit active grains together to form a compact adhesive film on the substrate, but they have no catalytic properties. In the case of Bi_2O_3, the gas sensitivity was observed [140] and the results of [139] were confirmed: this material can work as a catalyst for NO. The quantity of the additives determines sensitivity by isolation of active grains boundary or as catalyser between boundaries. In this way, the porosity of the film can also be increased. As reference [141] shows, the quantity decreasing of the glass frits increase the porosity of the film.

The powders should be very well homogenised with small quantities of organic vehicle (17-26 wt%). If the paste is more viscose, the layer does not flow after printing and the trace of the mesh stays on the surface. The cross-sectional area may increase, but only in macro-view. For this reason, it is preferred to increase the porosity. The porosity can also be improved by decreasing the layer thickness. This can be done by putting a thinner mask on a screen.

IV.1.2.4 Calcination and firing process

The calcination of the powder before the paste preparation and the firing process of the printed film can determine the sensitivity of the active layer. With calcinations, grain boundaries are developed and the powder sinters to bigger agglomerates. This causes a higher surface area after firing and by this way higher sensitivity of the layer. The powder has to be milled after calcination. In paper [136] is shown that an increase in the firing temperature increases the grain size and the macro pores. But the sensitivity decreases if the firing temperature goes over 700ºC, because the specific surface area of the grain decreases. The crystalline size inside the grain does not change significantly in various firing conditions. The influence of the firing process is more significant when the nanopowder is used [142]. The homogenous uniform grain structure cracks to form two distinct grains: one is the original uniform grain (40 nm) and the other is a bigger rectangular grain (>200 nm – 1 μm), the size

of which increases as the temperature increases above 600ºC. The amorphous structure starts to make polycrystals in the triclinic phase between 400ºC and 600ºC. Cracking above this temperature depends on the thermal expansion coefficient of the substrate. The firing temperature of the printed nanopowder paste is set at 600ºC (see [143], [144] and [145]). The calcination takes from 1 hour to 10 hours, and the firing process from 10 min to 1 hour.

IV.1.2.5 Paste

When the filling consists of more substances, it has to be mixed previously. Appropriate quantities of powders are pre-weighed in a glass bottle and shaken in an ultrasound bath until homogenised. The lack matrix is renovated to prevent settled agglomerates from appearing in the solution. After levelling at ambient temperature, it can be moved into a beaker with a magnetic stirrer and renovated at 45ºC for a few minutes until the matrix becomes clear. Then it can be moved back to the vessel and returned to room temperature before use.

The appropriate quantity of the lack matrix should be put into the agate mortar. The paste filling is added in drops or small quantities, and then the paste is ground in the agate mortar until it is completely homogeneous. This is repeated until the desired composition is reached or until the rheology of the paste is suitable. The rheological properties of the paste determine how it behaves during viscosity measurements. Solvents can be divided into two groups: Newtonian fluids, whose properties do not change over time or at different spindle speeds, and Non-newtonian fluids, which are divided into the following more usual fluids (Fig. IV.3).

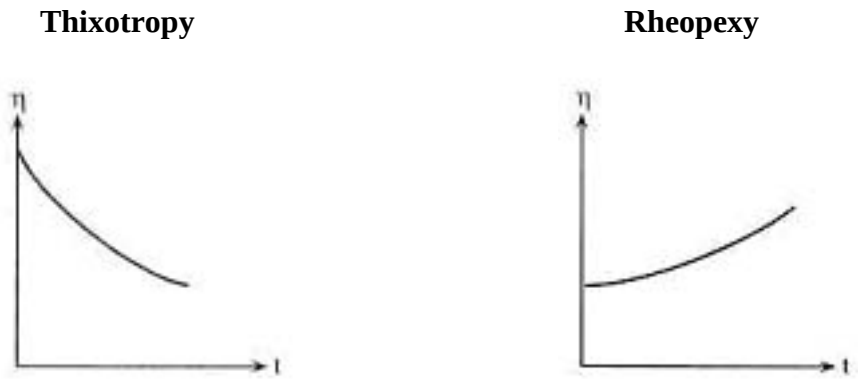

Figure IV.3. Rheology properties of the paste (left: The viscosity of a thixotropic fluid decreases over time, if the spindle speed is constant; right: The viscosity of a rheopeicy fluid increases over time, if the spindle speed is constant.)

Table IV.4 lists some of the prepared pastes and explains the fabrication method and composition. Two examples of tin and tungsten paste are described. The difference in the

paste composition between the pastes made from the same active material consists in the introduction of adhesion promoters.

Paste composition	Fabrication process
Type 1 SnO_2 Paste: **77.5 % (SnO_2 + 5 % Bi_2O_3) + 22.5 % LM1** **Properties:** • **good rheology for printing** • **dried 150°C/10min** • **fired 850°C/10min** **Excellent adhesion on ceramic: 49 sq.**	The 1.895 g of the prepared SnO_2 powder was mixed in a mortar with 0.125 g of Bi_2O_3. The powders were dried at 125ºC before weighing. Drops from Lack Matrix 1 (LM1) were added and homogenised sequentially until the viscosity was good.
Type 2 SnO_2 Paste: **79.4 % (SnO_2 + 5 % (Bi_2O_3 + Cu_2O)) + 20.6 % LM1** **Properties:** • **good rheology for printing** • **dried 120°C/10min** • **fired 850°C/10min** **Excellent adhesion on ceramic: 49 sq.**	The 1.887 g of the prepared SnO_2 powder was mixed in a mortar with 0.110 g of Bi_2O_3 and 0.020 g of Cu_2O. The powders were dried at 125ºC before weighing. Drops from LM2 were added and homogenised until the viscosity was good.
Type 1 WO_3 Paste: **73.2 % (WO_3 + 5 % Bi_2O_3) + 26.8 % LM1** **Properties:** • **good rheology for printing** • **dried 150°C/10min** • **fired 850°C/10min** **Excellent adhesion on ceramic: 49 sq.**	The 1.912 g of the prepared WO_3 powder was mixed in a mortar with 0.125 g of Bi_2O_3. The powders were dried at 125ºC before weighing. Drops from LM1 were added and homogenised sequentially until the viscosity was good.
Type 2 WO_3 Paste: **73.8 % (WO_3 + 5 % (Bi_2O_3 + Cu_2O)) + 26.2 % LM1** **Properties:** • **good rheology for printing** • **dried 120°C/10min** • **fired 850°C/10min** **Excellent adhesion on ceramic: 49 sq.**	The 1.914 g of the prepared WO_3 powder was mixed in a mortar with 0.116 g of Bi_2O_3 and 0.019 g of Cu_2O. The powders were dried at 125ºC before weighing. Drops from LM2 were added and homogenised until the viscosity was good.

Table IV.4. Pastes for active layers

The last step in the fabrication of the sensor is the firing of the active layer. Some of the furnace profiles used in our studies are summarized in table IV.5.

Zone	Temperature [ºC]	Air	L/min	Speed [mm/min]	Total time [min]
		Q1	34	34.3 (Pr.1)	53.6 (Pr.1)
1	405	Q2	24	27.5 (Pr.2)	66.6 (Pr.2)
2	880	Q3	12	21.2 (Pr.3)	86.1 (Pr.3)
3	850	Q4	22		
4	861	Qout	6.44		

Table IV.5. Profiles 850ºC/10 min; 850ºC/15 min; 850ºC/30 min

The high-temperature firing profiles (850ºC) are usually used to fabricate thick-film gas sensors on alumina substrates.

IV.1.2.6 Doping

The metal-oxide gas sensors, based on SnO_2 and WO_3 have a lot of promising properties such as high sensitivity, low cost and fast response. Commercially available sensors normally contain a small quantity of noble metals such as Ag, Ti, Pd and Pt, which are dispersed on the oxide as activators or sensitizers to improve the gas selectivity and lower the operating temperature. They enhance the selectivity to some gases of active layer activity. They also make the basic material active for particular reactions, thus making the layer more sensitive. For example, in [146] Pd doping in SnO_2 was tested. They increase the selectivity to organic substances and CO. The quantity of the doping can also modulate sensitivity (see [147]). In the case of WO_3, for example, the Au content was observed to improve the sensitivity to NO_2. Some metal oxides are very good catalysts. We have also used Bi_2O_3 and CuO in our experiments. Semiconductor metal oxides used in gas detection have catalytic properties and, with suitable doping, the catalytic reaction can be accelerated and directed to high selectivity for some gases. Some of the powders used in noble-metal doping are described in table IV.6.

Pt powder	**Commercial powder Aldrich 32,744-1**
Pd powder	**Commercial powder Aldrich 32,666-6**
Ag powder	**Commercial powder Aldrich 32,708-5**
Au powder	**Dried commercial Au paste ESL 8884**

Table IV.6. Powders used in noble metal doping

IV.1.2.7 Catalytic filters

The metal oxide-based sensors react to a wide range of gases with similar chemical properties. Catalytic filters can be applied to some of them so that selectivity is high. Recently some catalytic filters have been used in the construction of gas sensors (see chapter II). They prevent any reactions with some gases by removing these gases by combustion or some other reaction before they reach the active layer. A Pt catalytic layer is very common now. Platinum and palladium filters have been used for SnO_2 thick-film sensors in hydrocarbon gas detection. Pt supported on Al_2O_3 can be successfully used to decompose NO to NO_2. Then subtraction and sum of both tested gases can be detected and the concentration could be determined. A CuO filter was used to increase the selectivity of the SnO_2-based sensor for CO gases and decrease its selectivity to ethanol. In this case, the Al_2O_3 sputtered layer isolated the active layer from the sputtered catalytic filter. Table IV.7 presents two samples of our catalytic filters.

Catalytic Pt filter composition: Active layer + dielectric layer (Al_2O_3 paste) + Pt paste Heraeus C3657	**1.** Dielectric layer (Al_2O_3 paste) printed over the active layer and dried. Then Pt paste Heraeus C3657 was printed over the dielectric layer, dried and fired at 850ºC/10 min.
	2. Dielectric layer printed with paste prepared from 66.7 wt% of Al_2O_3 powder and 33.3 wt% of Pt paste Heraeus C3657, and a small quantity of Lack Matrix 1 to obtain printable viscosity. The paste was printed over the active layer and dried, and then fired at 850ºC/10 min.

Table IV.7. Pt catalytic filters

Catalytic materials have a particular selectivity, which cannot be increased. Some compositions of active layer with catalytic dopants have been found to increase the selectivity of sensors. Another way to increase the selectivity is to use a porous ceramic layer to decompose the rejected gases at high temperatures into non-interfering gases. Such sensors in a sensor array can determine the concentration of gases.

IV.1.3 Bonding, packaging and testing

Once the fabrication is completed the sensors are cut with diamond, wire-bonded and ready to use. The sensors are fabricated in groups of four in order to simplify the fabrication procedure. Figure IV.4 shows some ready-to-use sensors.

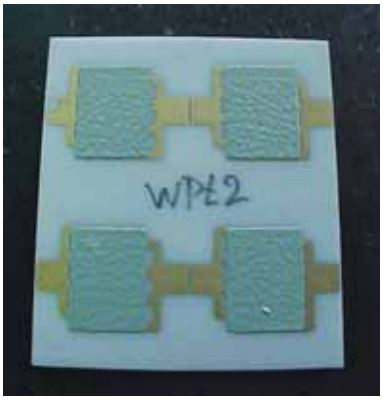

Figure IV.4. Sensors on Al_2O_3 substrates

Figure IV.5 show a detailed view of a single sensor fabricated on Al_2O_3 substrate with its principal components. The sensor chip is 1 cm^2 with active area of approximately 0,3 cm^2. These dimensions affect dramatically its power consumption.

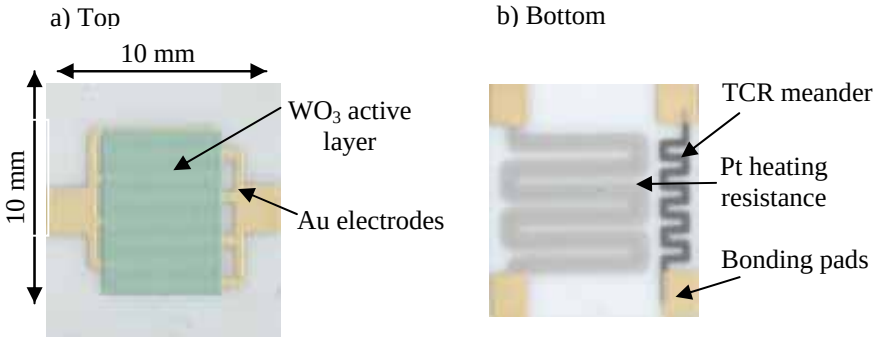

Figure IV.5. Structure of Al_2O_3 sensors

Once the sensor chip is firmly in position, it is ready for wire bonding. In our case the wire used to solder fabricated on Al_2O_3 was 380 μm and it was made of 99.999 Al. Figure IV.6 shows pictures of various encapsulates and wire bonded sensors.

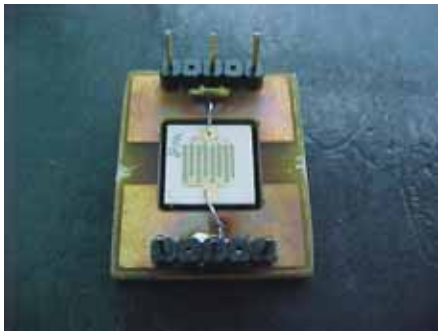

Figure IV.6. Sensors bonded PCB

Figure IV.7 shows the power consumption for the sensor studied. The graphic represent the electrical power that has to be applied to the heater if we want to obtain the desired working temperature.

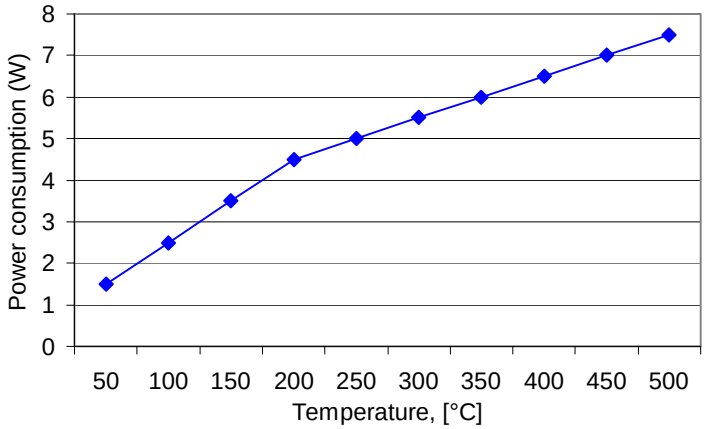

Figure IV.7. Power that has to be supplied to the heating element in order to reach the desired working temperature

It is obvious that the power consumption of the sensors produced on alumina substrate is too high. This is the reason why an alternative substrate that consumes less power must be used.

IV.2 Physical characterization

Various techniques were applied to physically characterize the sensors active layer. SEM analysis is used to obtain information about the active phase structure and the grain size. EDS provided us with the spectrum of the elements that made up our active layers and permitted us to make quantitative and qualitative analyses. The electronic structure of the layers was investigated by XPS and Raman spectroscopy (by C.Bittencourt, LISE-Belgium). These techniques confirmed the doping distribution in the active surface and provided a possible explanation for the chemical reactions that can take place on the oxide surface when the sensor is exposed to gases. More information about the techniques used can be found in Appendix A.

IV.2.1 SnO_2 sensors

a) ***Non doped SnO_2 sensor (set I)***
b) ***SnO_2 doped with Pt (sputtering) (set II)***
c) ***SnO_2 doped with Pt (Pt paste was introduced directly in the active layer*** (***set III)***

We study how the doping method affects the sensitivity of Pt-doped SnO_2 sensors to traces of ethanol. The tin oxide films were obtained by a screen-printing process. Two different methods were used to obtain Pt-doped films. In the first method, the screen-printed tin-oxide layer was doped with Pt by using R.F. magnetron sputtering and a subsequent thermal

treatment. The second method consisted of mixing a SnO_2 paste with a Pt paste before the screen-printing process. The different active layers had different chemical properties. XPS and SEM measurements showed that this behaviour could be associated with the spatial distribution of the doping elements within the tin oxide film. Although in Pt-sputtered sensors, most of the Pt atoms were found on the surface of the active layer, in the sensors made by mixing Pt and SnO_2 pastes, the distribution of the doping Pt atoms was homogeneous.

The samples were coated previously with a thin gold layer, which was sputtered to avoid charging effects. We investigated how the different doping techniques affected the grain size of the SnO_2. To do so we performed SEM analyses of different samples. One of these samples was non-doped SnO_2 and the others were from samples doped with Pt (sputtering or mixing with the paste). Table IV. 8 summarises the conditions in which the pictures were taken.

Active layers tested	1. Non-doped 2. Doped via sputtering 3. Doped via paste
Working distance	15 mm
Acceleration voltage	25 kV
Magnification	7000/20000

Table IV.8. Working conditions under which the photos were taken

IV.2.1.1 SEM and EDS analysis

To understand how doping affects the morphology of the SnO_2 active layers, a structural characterisation based on scanning electron microscopy analysis was performed. The micrographs recorded for the different sensors showed that the films are essentially inhomogeneous, and made up of grains (of about 60 nm) and voids (see figure IV.8). The voids within the film structure provide direct conduits for gas molecules to flow in from the environment. An EDS analysis showed that the grains and the bottom of the voids contained tin (the equipment used was not suitable for detecting the presence of oxygen).

Figure IV.8 *a*, *b* and *c* shows the surface of Pt-doped (by sputtering), Pt-doped (by paste mixing) and non-doped tin oxide, respectively. The SEM micrographs clearly show that there are no significant changes in the morphology of the samples. Therefore, the two different

procedures used to obtain Pt-doped tin-oxide films did not significantly alter the morphology at the surface.

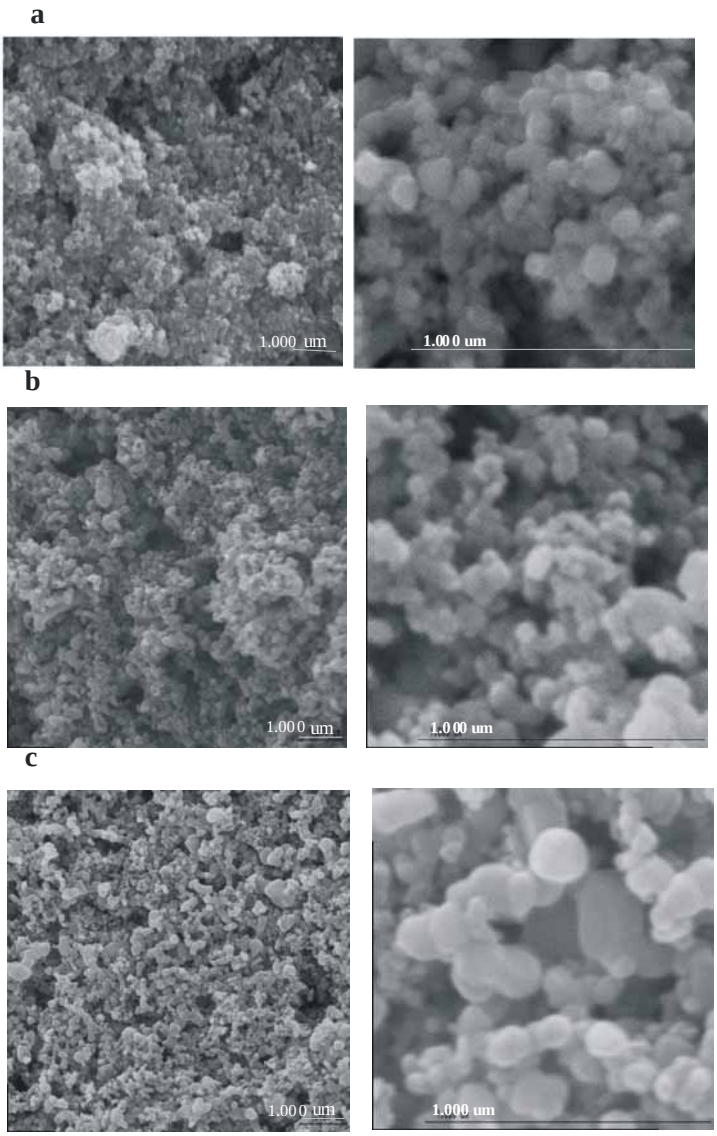

Figure IV.8. SEM analysis of the samples. a) Pt-doped tin oxide from set I, b) Pt-doped tin oxide from set II, c) non-doped tin oxide from set III

Images using backscattering electrons were used to analyse the homogeneity of the Pt distribution within the doped films. The samples analysed were cut and their in-depth morphology was studied. Film thickness varied between 20 and 25 μm. In backscattering electron imaging, greyscale intensity is characteristic of atomic number, and the distribution of Pt in the oxide layer is revealed. These results are shown in figure IV.9. The homogeneous aspect of the image that corresponds to films doped by adding a Pt paste to the tin oxide paste (set II) indicates that the Pt is homogeneously distributed within the tin-oxide layer. On the other hand, the films that were doped by Pt sputtering (set I) have a sharp contrast in intensity,

which shows that Pt is mainly concentrated in a layer (around 3 μm thick) on the surface of the tin-oxide film.

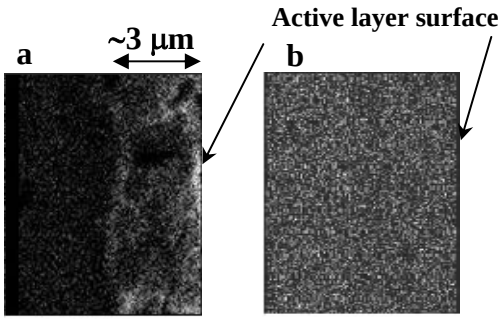

Figure IV.9. SEM analysis (backscattering electron image) of a section of Pt-doped samples. a) Sample from set I where the layer near the surface containing Pt is clearly visible; b) Sample from set II

Figure IV.10 shows the spectrums of the Pt-doped (paste) active layer. It is clear that the active layer consists of tin, oxygen and platinum.

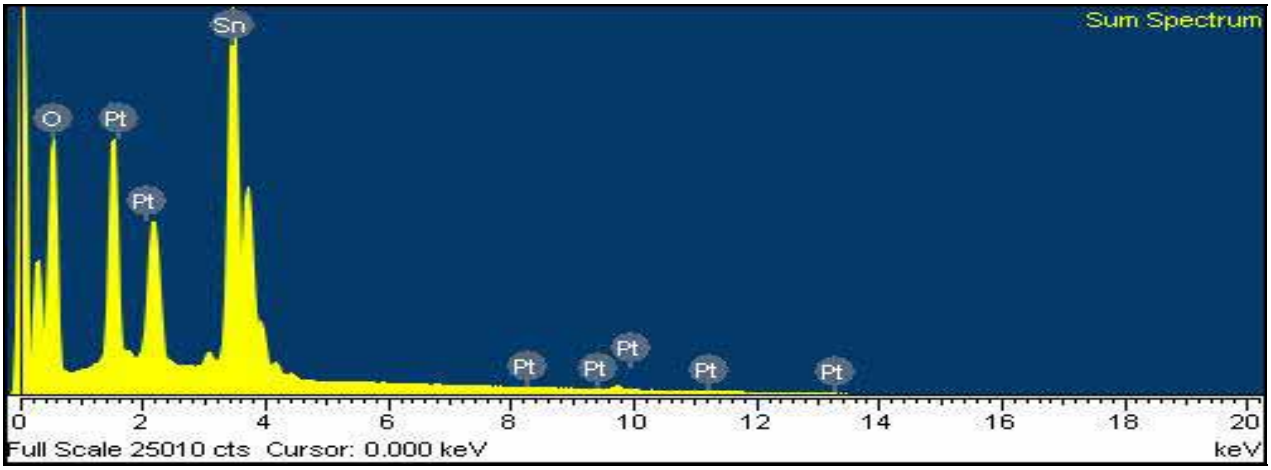

Figure IV.10. Spectrum of the active layer

Taking the spectrum from the different samples, we made a quantitative analysis, the results of which are shown in Table IV.9. The Co spectrum was used as a reference.

Spectrum	Sn (%)	O (%)	Pt (%)	Total (%)
Non-doped	83.75	16.25	0.00	100.00
SnO_3 (Pt sputtering)	81.94	16.94	1.12	100.00
SnO_3 (Pt paste)	82.16	16.48	1.36	100.00

Table IV.9. Results of the quantitative analysis (all results are in weight percent)

From these results we can observe that the Pt concentration varies between 1.12 and 1.36 %, while the variation in the tin and oxygen quantities is insignificant. The results are in good agreement with the following XPS analysis.

IV.2.1.2 XPS analysis

The first step when working with tin oxides is to determine the type of oxide under analysis, i.e. to distinguish between SnO and SnO_2. This can be done by analysing the valence-band (VB) region. The energy difference between the Sn 4*d* peak and the first peak in the VB toward low E_B has to be determined. In order to do so, XPS spectra were recorded on the samples. Figure IV.11 shows the typical XPS spectra used in the identification. The energy difference between the Sn 4*d* peak and the O 2p – derived structure near E_B = 4.5 eV measured on all the analysed samples ranged from 21.23 to 21.3 eV. This result is in close agreement with the reported value for SnO_2. It indicates that the doping procedures used did not modify the type of tin oxide.

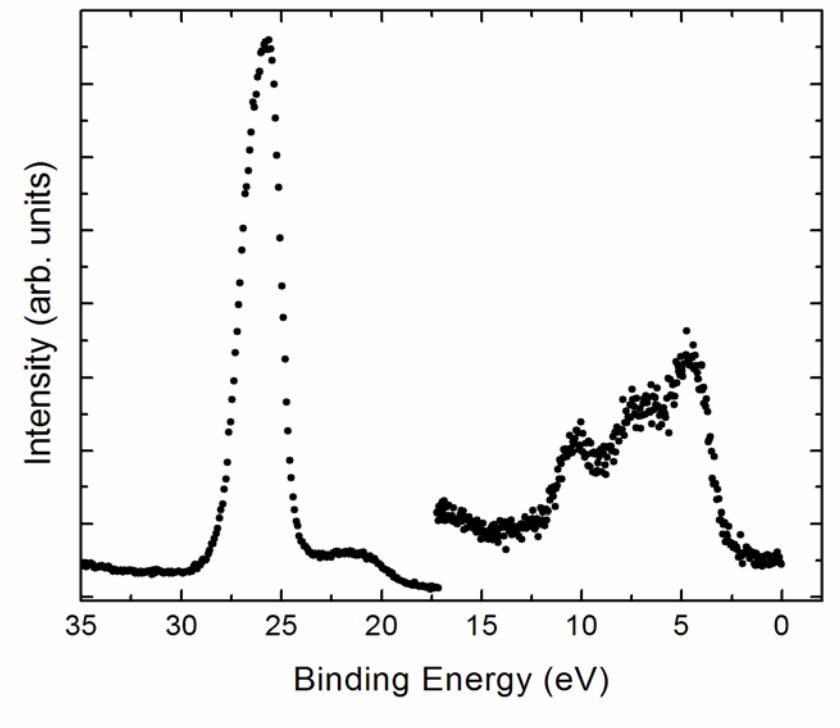

Figure IV.11. Typical XPS spectrum of valence-band and near-core region recorded on the studied samples. The binding energy scale refers to the Fermi level. The VB region has been magnified with respect to the Sn* 4d *region.

The Sn 3d core level spectra recorded on the samples showed two components associated with the Sn $3d_{5/2}$ e Sn $3d_{3/2}$ spin-orbit doublet separated 8.41 eV, in good agreement with the

tabulated value. A close inspection of the Sn 3d core level spectra recorded on the samples showed that the spectra could be fitted using a single Voigt profile per component centred near 486 eV and 494.5 eV, respectively. This suggests that the films are mainly formed by Sn^{4+} species; Sn^{2+} species is more likely to be found in SnO.

The presence of +2 and +4 metallic oxide states of the Pt atom was inferred by XPS. The spectra indicated that +2 and +4 metallic oxide states were present on samples of both sets I and II. It was reported that metal atoms fixed at the surface and surrounded by absorbed O atoms are the origin of the +4 chemical state of the noble metal additive and the +2 chemical states correspond to metal atoms surrounded by Sn and O atoms inside of the SnO_2 grains.

In order to verify the homogeneity of the in-depth Pt concentration, XPS analysis of set I and set II was carried out in two steps. In the first step, the samples were analysed as they were deposited. In the second step, samples were analysed after thin layers had been mechanically removed. By analysing the XPS spectra recorded on the samples after the surface thin layer had been removed, it can be said that the doping of the active layer of set II samples did not change, i.e., the procedure used to dope this set led to homogeneous doping of the base material. On the other hand, for samples in set I, it was observed that the concentration of the dopants (the proportion of dopant atoms to tin atoms) changed while the layers were removed, i.e., this procedure led to a non-homogeneously doped active layer. The concentration of Pt on the top layers was found to be nearly 10 times higher than on the bottom layers. Furthermore, the surface concentration of Pt in samples from set I was higher than in samples from set II.

IV.2.2 WO_3 sensors with catalytic filters

a) **Sensor W1: WO_3 sensor with no catalytic filter**
b) **Sensor W1CF: WO_3 sensor prepared by printing an insulating alumina paste that covered the tungsten-oxide layer. After drying this alumina layer, a Pt layer was printed on top. This resulted in the surface loading of the alumina film.**
c) **Sensor W1CFD: WO_3 sensor made by printing a dielectric layer of Al_20_3 and Pt**

IV.2.2.1 SEM analysis

We investigated the catalytic filter (Pt-Al_2O_3) printed on a tungsten-oxide active layer. Catalytic filters are used to burn off interfering gases before they can reach the active layer.

Therefore, only the target gases are able to reach the sensing layer and alter its conductance. Catalytic filters consist of an insulating layer (Al_2O_3), which is loaded with noble-metal catalysts (Pt). The catalyst can be either homogeneously distributed throughout the insulating layer (bulk loading) or spilt over the surface of the insulating layer (superficial loading), which results in significant differences in their filtering properties. The screen-printing technique leads to more porous active layers than other deposition techniques such as physical or chemical vapour deposition. The films obtained had very high surface-to-volume ratios.

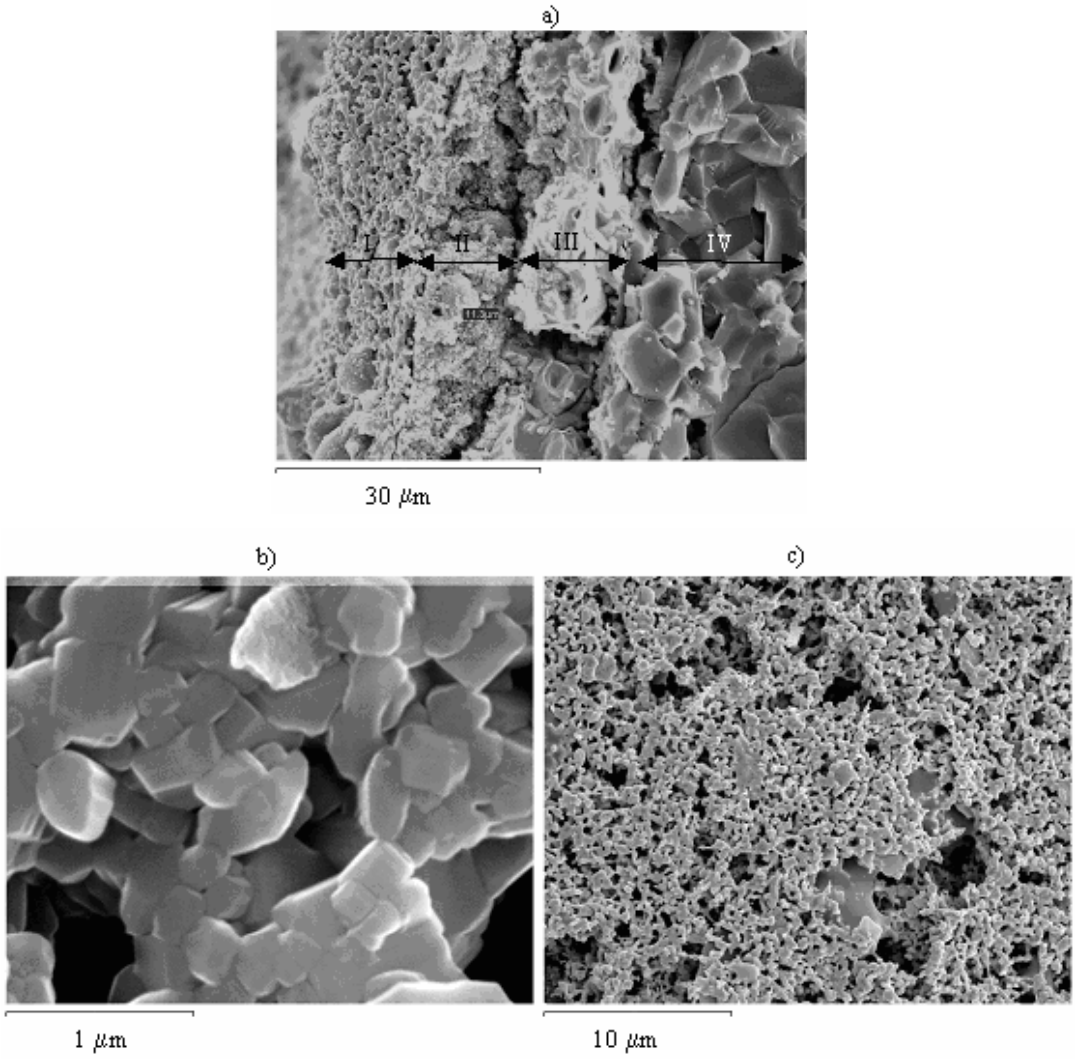

Figure IV.12 SEM images: a) Image of a section of a WO_3 sensor coated with catalytic filter, b) Image of the WO_3 surface, c) Image of the catalytic filter surface

The morphology of the active films and catalytic filters was investigated by SEM. Figure IV.12 *a* shows the SEM image of a cross-sectional cut of a W1CF sensor (with surface Pt-loaded catalytic filter). From the surface towards the substrate (left to right), the different regions labelled on the picture correspond to: I) platinum layer, II) insulating alumina,

III) gold electrode and tungsten-oxide layer, IV) alumina substrate. The tungsten polycrystalline oxide layers were nano-particular with a particle size of nearly 150 nm, as can be seen in Figure IV.12 *b* which shows a picture taken from a W1 sensor (without catalytic filter). Finally, Figure IV.12 *c* shows a picture of the surface of a W1CF sensor. It can be derived that the platinum layer is very porous.

IV.2.3 WO_3 sensors doped with Ag

- **Non doped WO_3 sensor**
- **WO_3 sensor mixed with 0.5% (in weight) of Ag**
- **WO_3 sensor mixed with 1% (in weight) of Ag**
- **WO_3 sensor mixed with 1.5% (in weight) of Ag**
- **WO_3 sensor mixed with 3% (in weight) of Ag**

IV.2.3.1 AFM results

The surface morphology and homogeneity of the samples were investigated with an AFM in a Nanoscope III (Digital Instruments) and using a triangular shaped (0.06 N/m) Si_3N_4 cantilever tip operated in the contact mode. To understand how the loading affects the morphology of the WO_3 samples, AFM micrographs were recorded. Because of the powder nature of the films the AFM measurements were very hard to perform. The AFM measurement on the non-loaded sample could not be made due to the strong interaction between tip and surface. For the sample loaded with 0.5% of Ag only small regions could be scanned and recorded. Figure IV.13 shows AFM micrographs recorded on the samples loaded with different levels of Ag (1%, 1.5% and 3% from left to right).

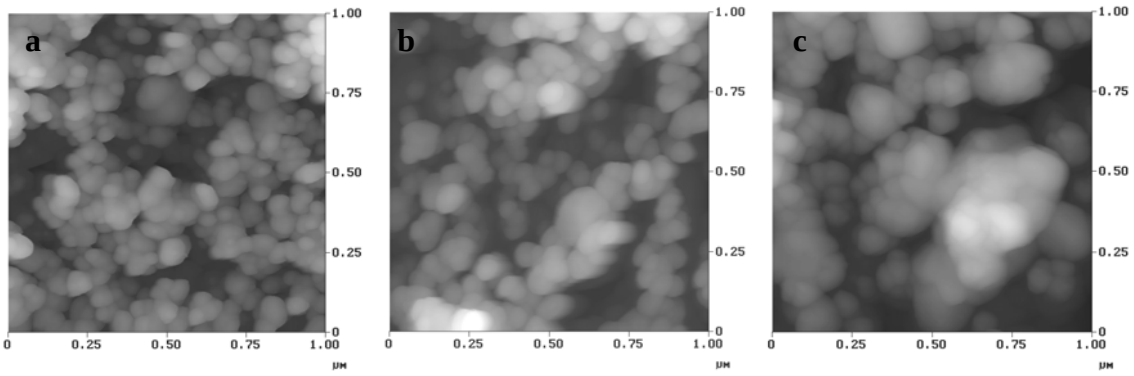

Figure IV.13. AFM micrographs recorded on the samples loaded with different levels of Ag: a) 1% wt. doped, b) 1.5% wt. doped c) 3% wt doped

The surface of the films is essentially inhomogeneous, and made up of grains and voids. The voids within the film structure provide direct conduits for oxygen and gas molecules to flow in from the environment. The average size of the grains increases as the level of Ag loading is increased. It is important to emphasize that the only parameter that changed between the different samples analysed was the Ag content. Given the tendency of noble metals to form clusters at the surface of the metal-oxide grains, the increase observed in the average size of the grains may be due to the increase in the size of Ag clusters formed at the surface of the WO_3 film.

IV.2.3.2 Raman measurements

Raman scattering measurements were carried out to identify the nano-crystallization of the WO_3 films and the evolution of the bonds upon Ag loading. The Raman spectra were recorded at room temperature with a Spex 1403 1 m double pass spectrometer equipped with a cooled photo-multiplier tube and the 330 laser line of an Ar laser. The laser power focused onto the sample was 0.26 mW. The resolution of the Raman spectrometer was 5 cm^{-1}. The Si band at 500 cm^{-1} was used for calibration.

The Raman spectra recorded on the films are shown in figure IV.14.

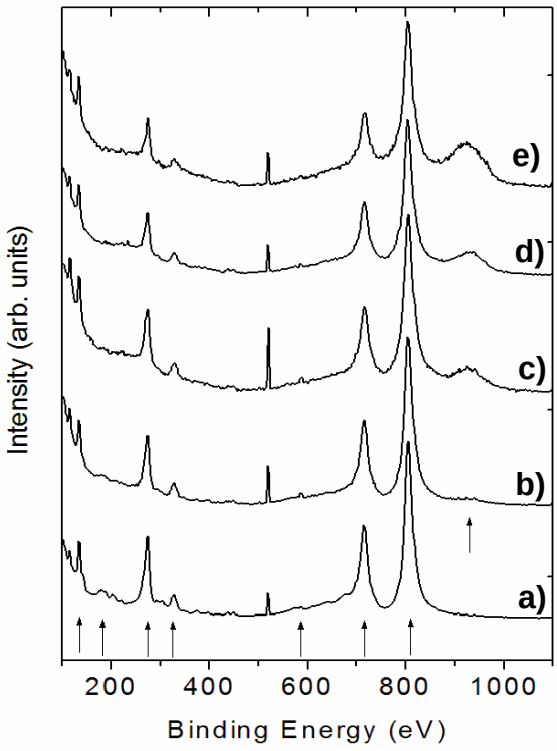

Figure IV.14. Raman spectra recorded on screen-printed WO_3 films with different levels of Ag loading: a) Non doped, b) 0.5% wt, c) 1.0% wt, d) 1.5% wt and e) 3.0% wt

The spectrum of the pure WO_3 film (see figure IV.14 a) has bands at 810, 720 and 580 cm^{-1} corresponding to the stretching vibrations (ν) of WO_3. The bending vibration (δ) bands are observed at 276 and 330 cm^{-1} and the lattice modes are near 190 and 138 cm^{-1}. By comparing the spectrum recorded with the ones reported for several WO_3 structures, it can be suggested that the symmetry of the WO_3 films is tetragonal. In addition to the bands observed for the pure film, the film loaded with 0.5 % of Ag (see figure IV.14 b) shows a new band peaking at 930 cm^{-1}. The intensity of this band increases as the Ag content increases (see figure IV.14 c). Therefore, the new band can be associated to modifications induced by the Ag atoms in the WO_3 lattice. The band at 930 cm^{-1} is associated to the vibrational modes of silver tungstanates, which suggests that an Ag_xWO_3 bronze has appeared by silver becoming intercalated in the WO_3 tunnels.

Tungsten trioxide has a cubic perovskite-like structure based on the corner sharing of WO_6 regular octahedral, with the O atoms (W atoms) at the corner (center) of each octahedron. However, distortions (corresponding to antiferroelectric displacements of W atoms) and mutual rotations of the octahedral units, cause deviations from the ideal cubic perovskite type (like ReO_3) structure, which gives rise to a series of lower symmetry structures.

IV.3 Electrical characterization

We tested a wide variety of sensors fabricated on alumina substrates with numerous simple volatile compounds and gases. The properties of the sensor substrate are detailed in Table IV.10.

Parameters	Values
Substrate dimension	1 cm x 1 cm
Dimension of the active layer	5 mm x 6 mm
Heater resistance (at room temperature)	R_H=10 Ω ± 3%
Temperature sensor resistance	R_0=1.1 kΩ ± 5%
Temperature coefficient of resistivity	3.45×10^{-6}°C^{-1}

Table IV.10. Properties of the Al_2O_3 substrate

The effect of relative humidity was also studied. This section includes all the gas measurements and there are various subsections depending on the measurement system used. Each system measured the response to different gases. Every section describes the measurement system, the gases that were measured, the type of the sensors used and the results.

These sensors were tested using the "**Injection**" measurement system. To investigate the gas sensing properties, we placed groups of eight sensors, with the same active layer, into a thermally controlled test chamber. The operating temperature of the sensors was adjusted successively for the different series of measurements to 250ºC, 300ºC and 350ºC. The control of the temperature was realized via software and IR thermometer (figure IV.15a). We checked the sensor selectivity by placing different contaminants in the test chamber with high precision chromatographic syringes (figure IV.15b).

Figure IV.15. Devices used during the measurement: a) IR thermometer, b) High precision chromatographic syringe

Dry air was used as the reference gas. We consecutively injected into the test chamber the liquid or the gas quantities required to create the desired concentrations of the measured species. The first injection took place 50 seconds after data acquisition started and the remaining ones were made every 100 seconds. After the last one we waited two minutes and then cleaned the test chamber with dry air. Between every two measurements there was a pause of 30 minutes. A commercially available Figaro TGS 822 sensor was used as a reference [148]. The TGS 822 is highly sensitive to the vapours of organic solvents as well as other volatile vapours. It is also sensitive to a variety of combustible gases such as carbon monoxide.

The electrical resistance of the sensors was acquired and stored in a PC by means of HP 34970A multi-meter and written-in-house control software (figure IV.16).

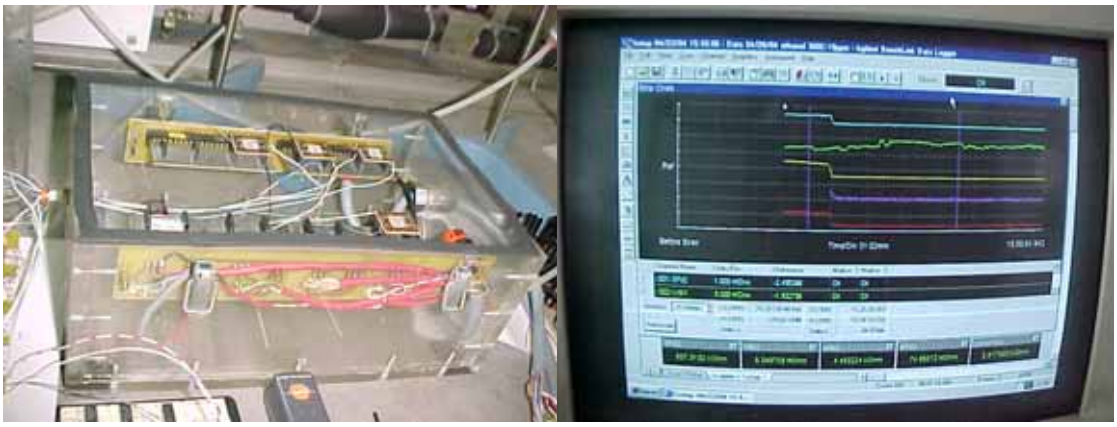

Figure IV.16. Measurement system: a) Test chamber, b)Acquisition software

The baseline resistance of the thick-film sensors was stabilized in dry air at the selected operating temperature before the test gases were injected. Figure IV.17 shows the experimental set-up.

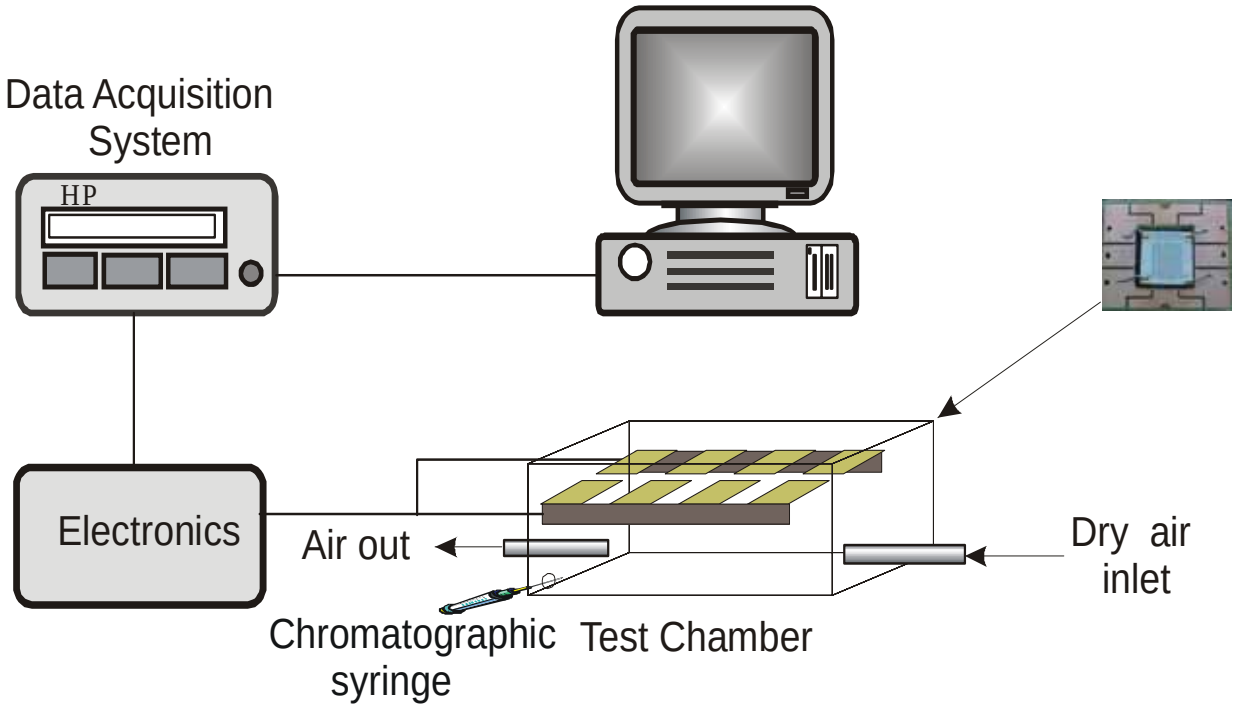

Figure IV.17. Experimental set-up for "Injection" system

The gas sensing properties of the fabricated thick-film gas sensors were investigated. During the measurements, the moisture level inside the sensor chamber was kept to 10% R.H. (measured at 30^{o}C). The sensor response (sensitivity) was defined as follows:

$$\begin{cases} S = \dfrac{R_g}{R_a} & \text{if } R_g > R_a \\ S = \dfrac{R_a}{R_g} & \text{if } R_g < R_a \end{cases} \qquad \text{(IV.1)}$$

where R_a is the sensor resistance in air (i.e. baseline) and R_g is the sensor resistance in the presence of the gas measured. Given that tin and tungsten oxides behave as n-type semiconductors, their resistance decreases (increases) when exposed to reducing (oxidising) gases.

Another important parameter, when characterizing gas sensors is the selectivity. The selectivity S_i for a given sensor to an *i* species, considering a set of *n* species, can be defined with the following equation:

$$Si = \frac{(R_a / R_{1_i} - 1)}{\sum_{j=1}^{n} (R_a / R_{1j} - 1)} \qquad \text{(IV.2)}$$

where R_a is the resistance value in air, and R_{1i} is the resistance of the sensor when there is 1 ppm of the contaminant. The selectivity value, as defined in the equation above, is always between 0 and 1.

IV.3.1 SnO_2 sensors

In this subchapter we will discuss all the results obtained with the following thick-film gas sensors:

a) **Non Doped SnO_2 sensor**
b) **SnO_2 doped with Ag (sputtering)**
c) **SnO_2 doped with Ti (sputtering)**
d) **SnO_2 doped with Pt (sputtering)**
e) **SnO_2 doped with Pt (Pt paste was introduced directly in the active layer)**

The gases measured are ethanol, ammonia, benzene, methane and relative humidity in the range 10-85%. The following figures (IV.18- IV.22) present all the results obtained from the measurements. The results expressed in numeric values could be found in tables B.1, B.2 and B.3 presented in Appendix B. Methane is not included in the graphics, because no reaction was detected.

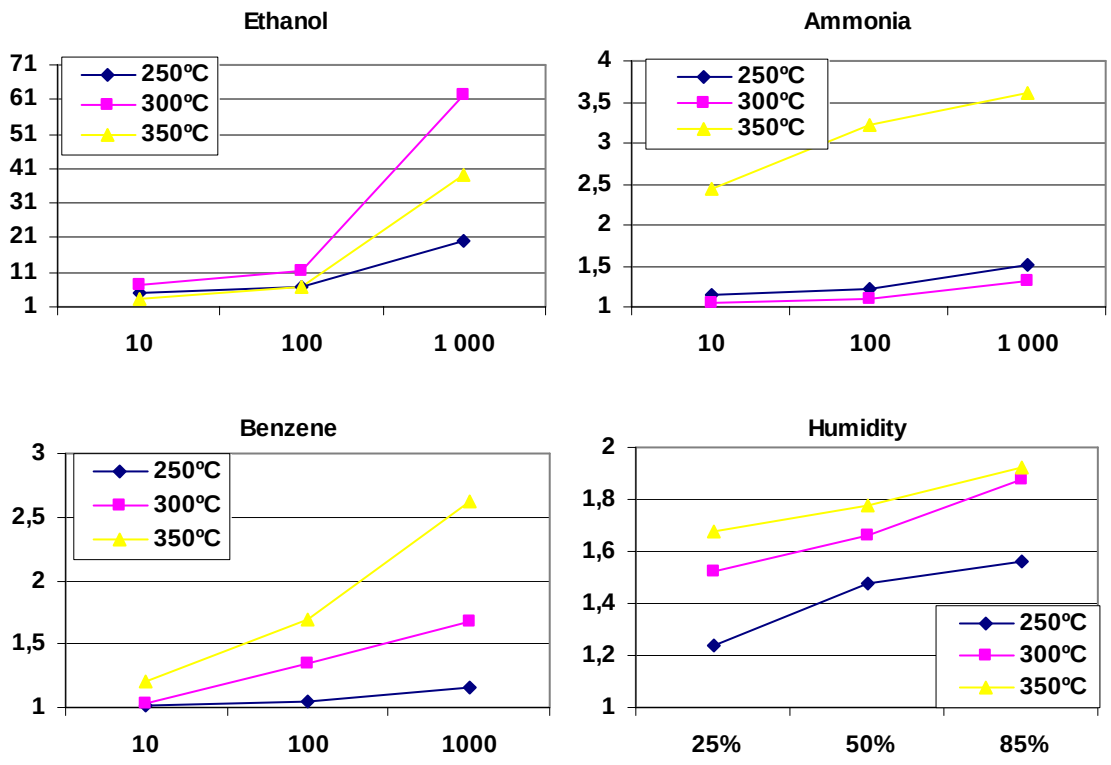

Figure IV.18. Results of the measurements of non doped SnO_2

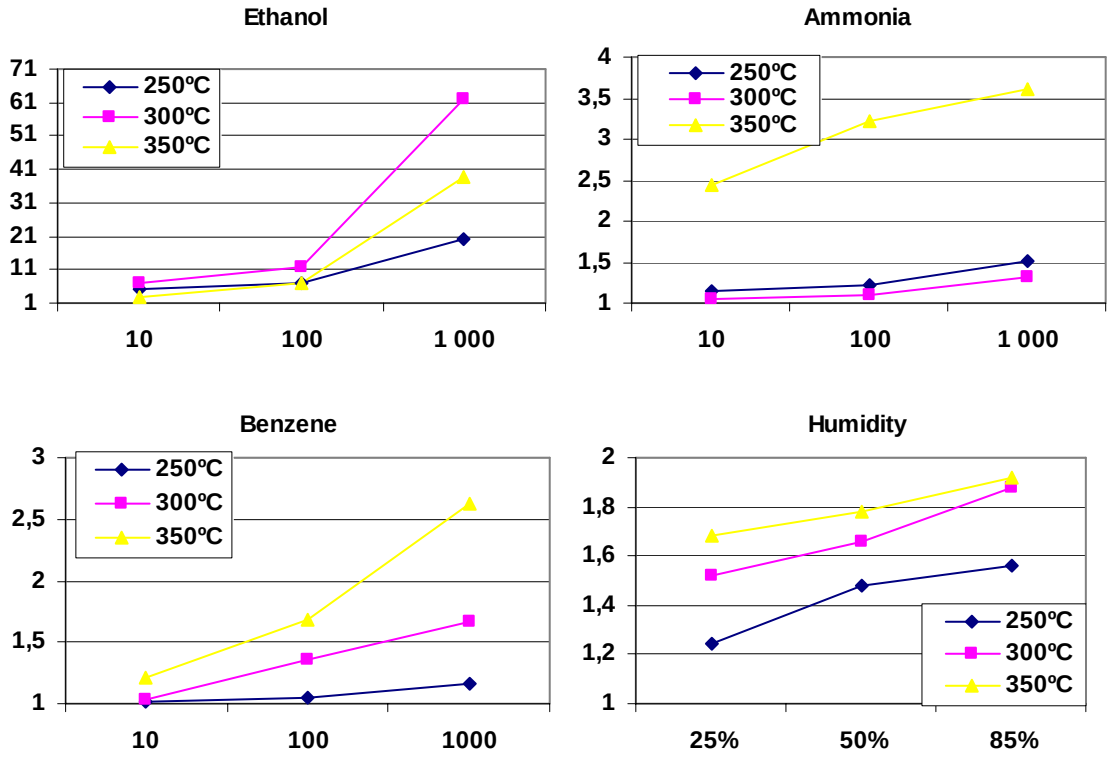

Figure IV.19. Results of the measurements of Ag SnO_2

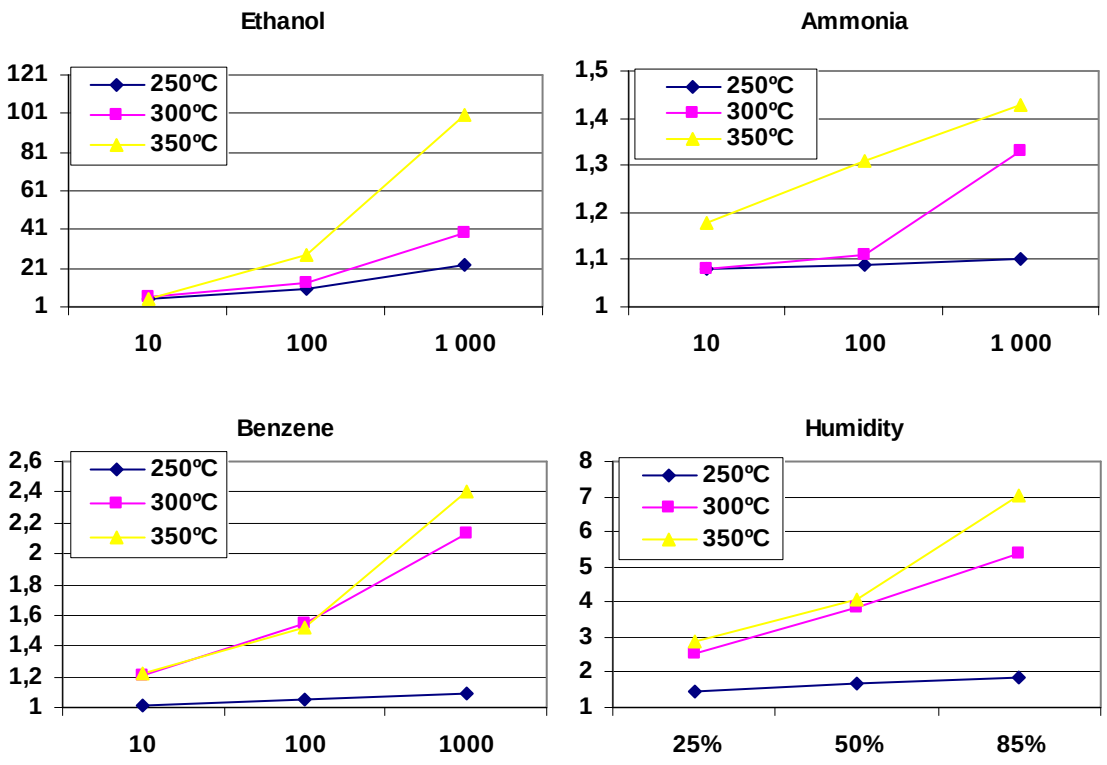

Figure IV.20. Results of the measurements of Ti doped SnO_2

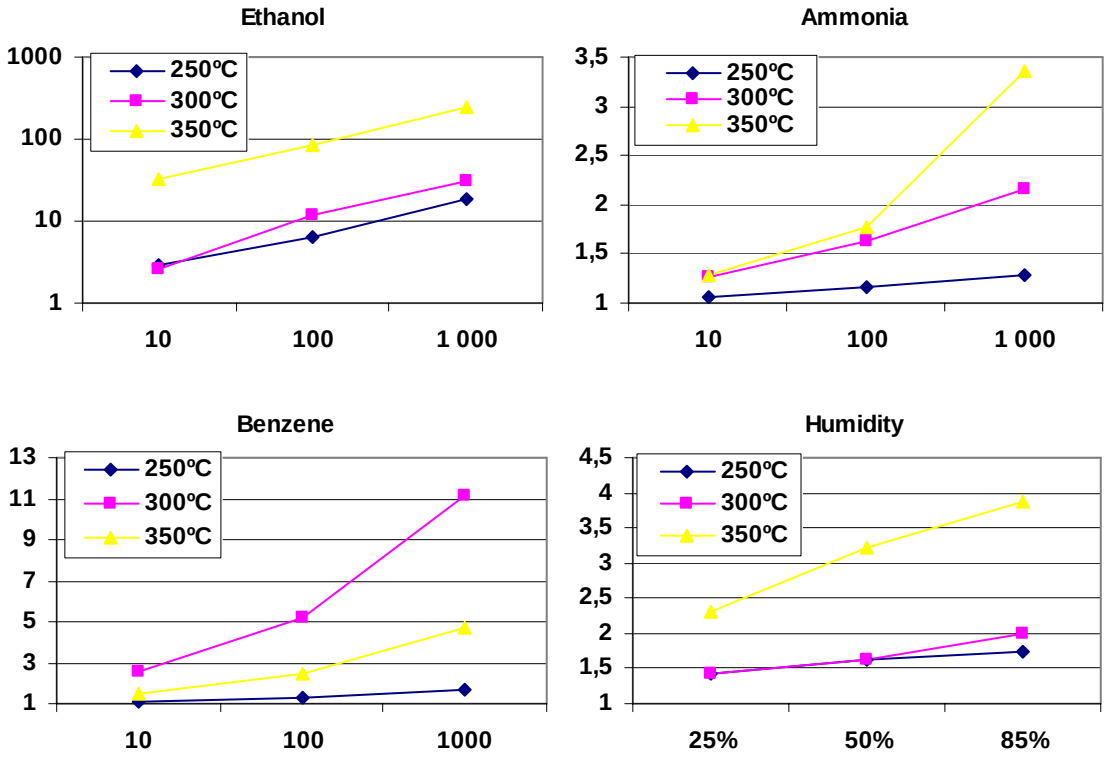

Figure IV.21. Results of the measurements of Pt doped (via sputtering) SnO_2

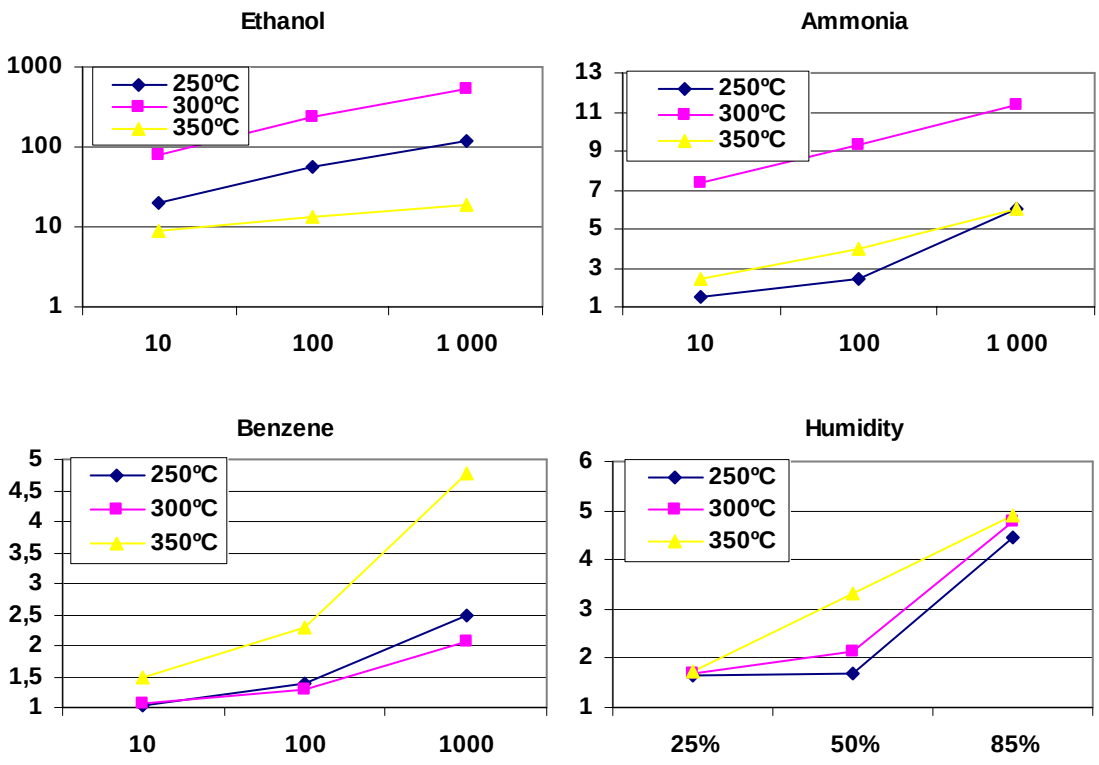

Figure IV.22. Results of the measurements of Pt doped (via paste) SnO_2

IV.3.1.1 Response to ethanol

Detailed measurements were made for the five sensor groups. The Pt-doped sensors showed an extremely high response to ethanol, which is why additional measurements for ethanol from 1ppb to 100ppb were made. A typical sensor response can be observed in Figure IV.23.

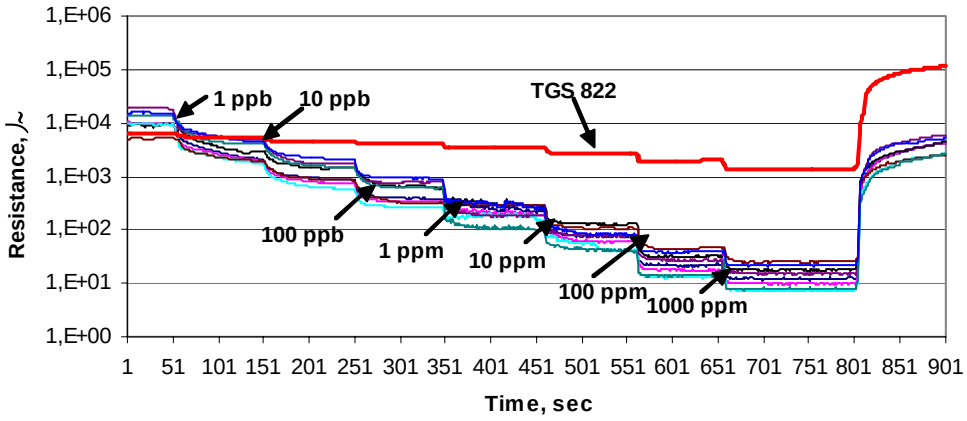

Figure IV.23. Response of the 8 Pt (paste)-doped SnO_2 sensors working at 300ºC to successive injections of ethanol

Comparison between the differently doped sensors showed that sensitivity to ethanol was maximum for the sensors doped with Pt, particularly for the ones prepared by mixing the SnO_2 paste with Pt. The sensitivity was 560 for 1000 ppm, which is more than 55 times that of the commercial TGS 822 (Figure IV.24). For the lowest studied concentration of 1 ppb, the sensitivity of the Pt-doped sensor (via mixing SnO_2 with Pt paste) is nearly twice that of the commercial sensor. The sensors doped with Pt (by rf-sputtering) had the second highest sensitivity to ethanol, which goes beyond the commercial sensor for concentrations between 100 ppb to 1000 ppm. The other sensors performed best at concentrations between 10 and 1000 ppm.

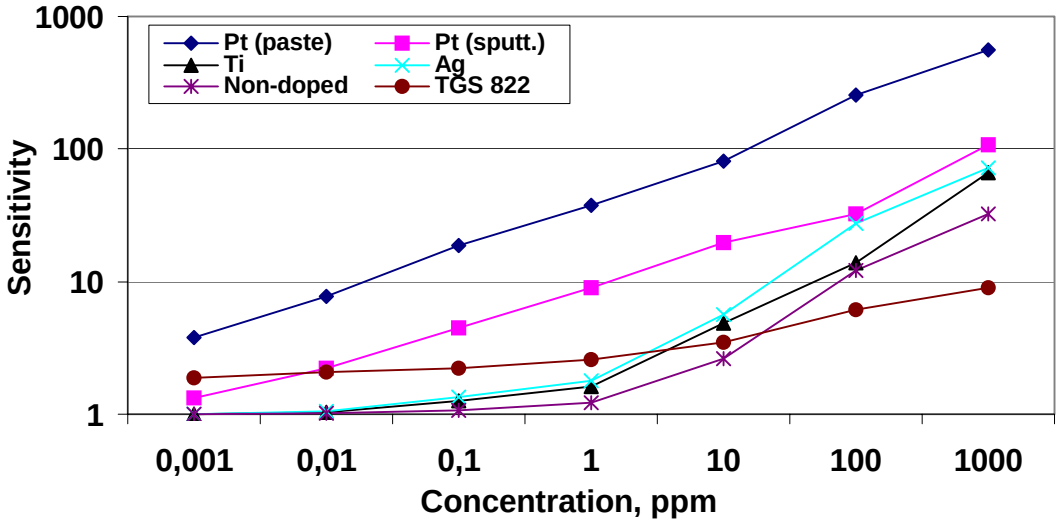

Figure IV.24. Sensitivity to ethanol of all types of SnO_2 sensors at 300 ℃

Another advantage is that for concentrations between 1 ppb and 1 ppm the selectivity of the Pt-doped sensors (via mixing Pt with the SnO_2 paste) for ethanol is equal to 1 (since they are not sensitive to the other gases studied in those concentrations). The linearity of this sensor was also better (in the ppb range) than all the other sensors studied (Figure IV.24).

Once it had been determined that the Pt-doped sensors gave the best results for ethanol detection, we studied how the operating temperature affected the sensitivity to ethanol. Figure IV.25 shows the sensitivity of the Pt-doped sensors working at 250ºC, 300ºC and 350ºC. Independently of the doping method, the sensitivities to ethanol were best when the sensors operated at 300ºC. Increasing or decreasing this operating temperature decreased sensitivity. Even so, the sensors operating at 350ºC gave better results than those operating at 250ºC.

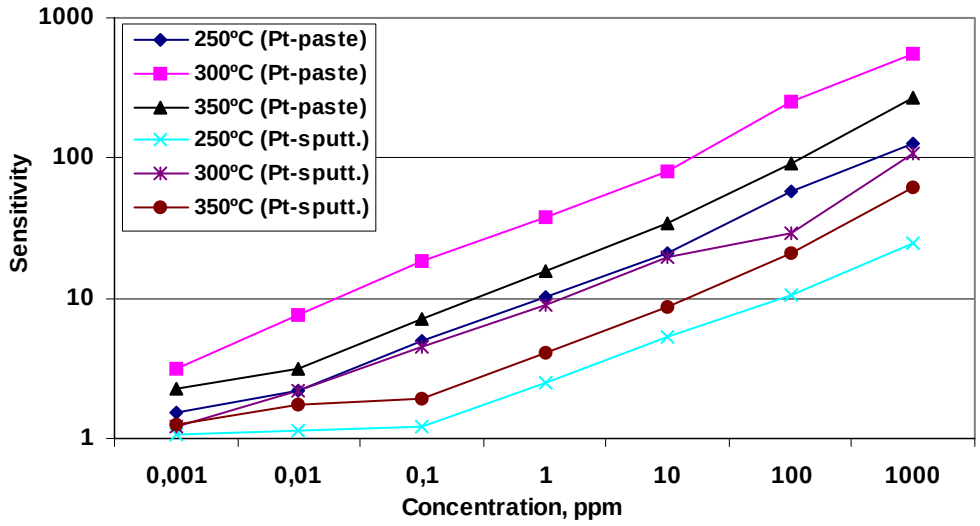

Figure IV.25. Sensitivity to ethanol of the SnO_2 Pt-doped sensors at the following temperatures: 250 ℃, 300 ℃ and 350 ℃

The selectivity results for all of the sensors studied are presented in Table IV.11.

Type T [ºC]	Pt (paste)	Pt (sputtering)	Ag	Ti	Intrinsic sensors
Concentration 10-1000 ppm					
250 ºC	0.667	0.554	0.932	0.984	0.995
300 ºC	0.828	0.799	0.862	0.827	0.991
350 ºC	0.528	0.478	0.639	0.797	0.583

Table IV.11. Selectivity of the fabricated SnO_2 sensors to ethanol

To sum up, this study used two different methods of doping the SnO_2 active layer. In the first method, the active layer was doped with Pt using RF Magnetron Sputtering and in the second by mixing the SnO_2 paste with a Pt paste before the firing. The sensitivity to ethanol of the sensors prepared with the second method was five times higher than that of the sensors prepared with the first method. The doping with Pt considerably improved the sensitivities of SnO_2 to ethanol in air, which showed that increasing the doping quantity leads to better sensitivity. The 3% Pt-doped sample is extremely sensitive to ethanol vapour and its response is linear almost in all concentrations range. Its detection limit is below several ppb for the optimal operation temperature of 300ºC. The sensitivity of the sensor is one of the highest reported [149] and [150].

On the whole, the Pt-doped SnO_2 material has low resistance, high sensitivity and fast response to ethanol compared with pure SnO_2. The fabricated sensors can be used determining alcohol on the breath, for controlling food degradation and for monitoring and controlling small concentrations of ethanol instantaneously [151-152].

IV.3.1.2 Response to ammonia

The Pt-doped sensors also showed a specific response to ammonia. Figure IV.26 shows the response of pure-SnO_2 sensors to ammonia at 250, 300 and 350ºC. As we can see, the resistance of the sensor decreases throughout the temperature range studied and, as stated in the tables above, sensitivity is very low at 250 and 300ºC and only moderate for the operating temperature of 350ºC.

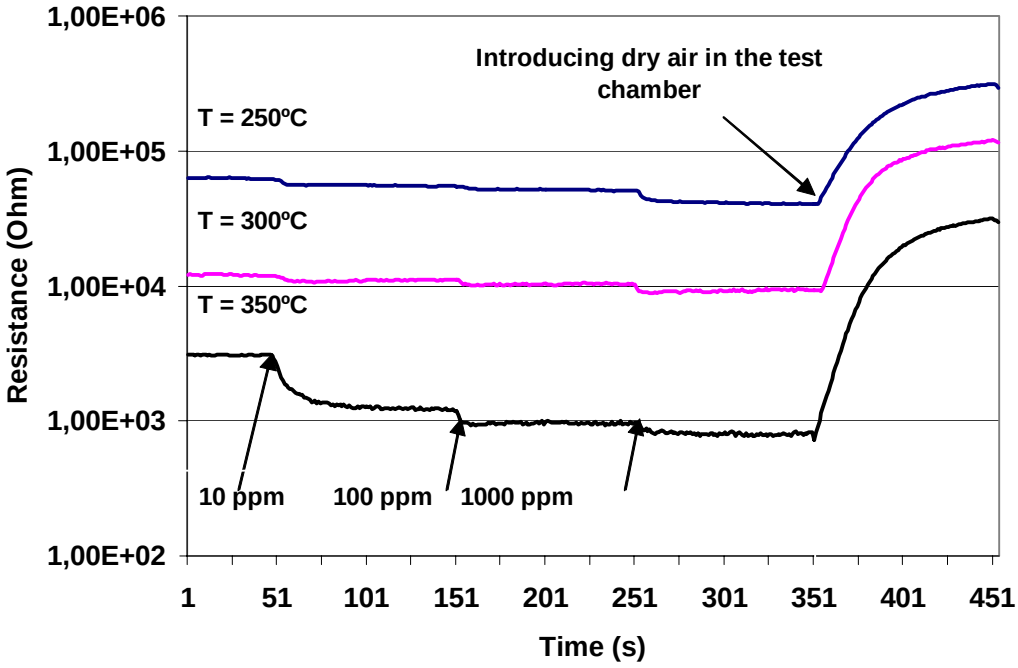

Figure IV.26. Sensor response of pure tin dioxide sensors to ammonia at the following temperatures: 250 ℃, 300 ℃ and 350 ℃

When the Pt-doped sensors were measured against ammonia, the results were complex. They will be described later in this section.

To obtain more information, measurements were made at 50ºC steps between 200ºC and 400ºC. Results show that this type of material increases or decreases resistance depending on the working temperature and ammonia concentration. Figure IV.27 indicates that NH_3 can interact with the tin-oxide surface in numerous ways.

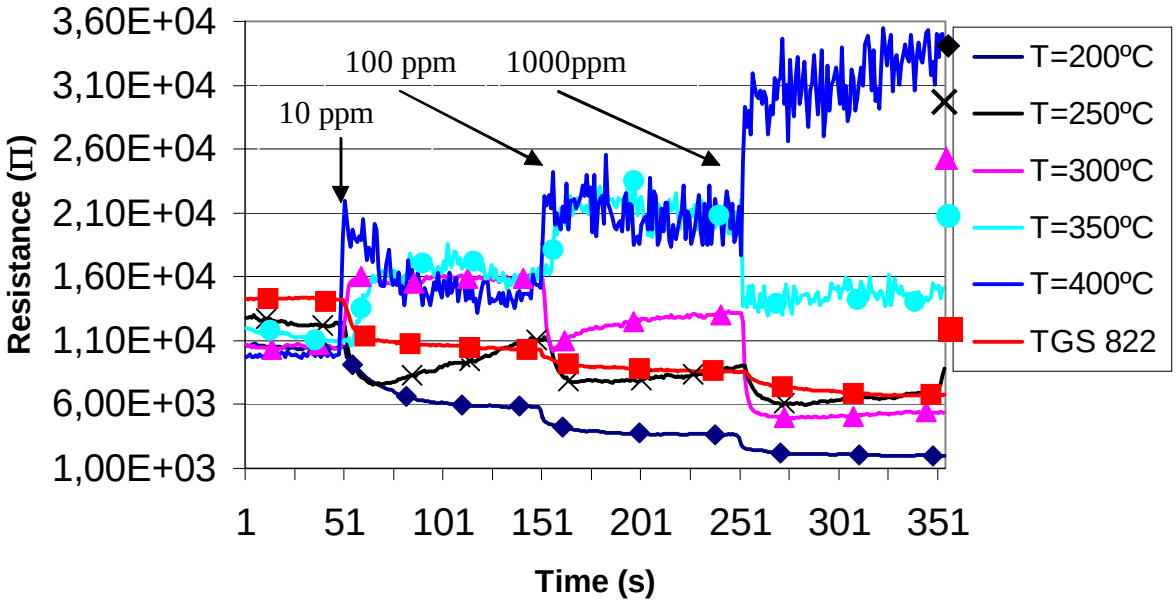

FigureIV.27. Sensor response of Pt-doped sensors to ammonia at 200 ℃, 250 ℃, 300 ℃, 350 ℃ and 400 ℃

Several of the surface temperature regimes are particularly significant:

- ✓ Below 250ºC the expected reduction process was observed and the semiconductor showed a decrease in resistance.
- ✓ Between 300ºC and 350ºC the resistance increases or decreases, depending on the ammonia concentration. At low ammonia concentrations (e.g. 10 ppm), the resistance increases, indicating that an oxidizing process takes place. At high concentrations (e.g. 1000 ppm), the resistance decreases at all temperatures. At an intermediate concentration of 100 ppm, resistance increases at 350ºC and decreases at 300ºC.
- ✓ At 400ºC resistance increases at all concentrations, thus indicating that an oxidizing process takes place.

The measurements show that the oxidising behaviour is enhanced at high working temperatures and low ammonia concentrations.

The sensing layer used in these sensors consisted of a Pt (3 wt.%)-SnO_2 oxide semiconductor. Figure IV. 27 shows that additive material such as platinum acts as a catalyst, enhancing the sensitivity, accelerating the formation of the oxidizing species and, therefore, leading to an oxidizing reaction in certain cases. In the next section, we will make some basic hypotheses,

from the chemical point of view, about the role of the Pt catalyst in the ammonia sensing properties of SnO_2 layers.

IV.3.1.3 Gas-kinetic interaction of NH_3 with Pt-doped SnO_2 surfaces

Ammonia burns in air with difficulty in the absence of a catalyst. Generally speaking, normal combustion of ammonia yields nitrogen but, in the presence of a Pt catalyst at 750ºC, the reaction proceeds further to give the thermodynamically less-favoured products NO and NO_2. The reactions that occur and the enthalpy changes per mole of N atoms at 25°C are:

$$4NH_3 + 3O_2 \longrightarrow 2N_2 + 6H_2O \qquad \Delta H = -1268 \text{ kJ/mol} \qquad \text{(IV.3)}$$

$$4NH_3 + 4O_2 \longrightarrow 2N_2O + 6H_2O \qquad \Delta H = -1105 \text{ kJ/mol} \qquad \text{(IV.4)}$$

$$4NH_3 + 5O_2 \longrightarrow 4NO + 6H_2O \qquad \Delta H = -292.5 \text{ kJ/mol} \qquad \text{(IV.5)}$$

$$2NO + O_2 \longrightarrow 2NO_2 \qquad \Delta H = -56.8 \text{ kJ/mol} \qquad \text{(IV.6)}$$

Actually, NO oxidizes to NO_2 quickly in contact with air. The thermodynamics of other related reactions are as follows:

$$3NO_2 + H_2O \longrightarrow 2HNO_3 + NO \qquad \Delta H = -23.3 \text{ kJ/mol} \qquad \text{(IV.7)}$$

meaning that they are all thermodynamically favourable.

In the paragraphs below we will review the possible reactions of NH_3 with Pt-doped SnO_2 surfaces in the presence of oxygen [153-155].

Platinum is a well-known oxidation catalyst, which reduces the activation energy, and then increases the rate of dissociation of the O_2 molecule into oxygen atoms, where temperatures between 350°-800° C are needed depending on the surface properties of the manufactured catalyst. On an n-type semiconductor such as SnO_2, the adsorption of oxygen leads to the transfer of electrons from electron donor sites toward adsorbed oxygen through the appearance of surface species such as O_2^-, O^- and O^{2-}, which make SnO_2 highly sensitive to combustion products in sensor devices. Doping SnO_2 with platinum significantly increases the amount of atomic oxygen available and particularly the rate of replacement of the surface species responsible for the reactivity and sensitive behaviour in oxidation reactions.

The experimental results described above suggest that the following surface reactions might help to deal with the more applied aspects of the engineering of gas sensor devices. If we compare the Pt-doped and the un-doped SnO_2, in the range of temperatures below 300°C, the sensitivities on Pt-doped surfaces are higher, probably because the concentration of adsorbed ionic-type species on the doped surface is higher [156-157].

$$4NH_3(gas) + 3O_2^-(surf) \rightarrow 2N_2 + 6H_2O + 3e^-(cond.\ band) \quad (IV.8)$$

$$4NH_3(gas) + 4O_2^-(surf) \rightarrow 2N_2O + 6H_2O + 4e^-(cond.\ band) \quad (IV.9)$$

If we postulate the O_2^- (surf) as the predominant surface species at temperatures lower than 250°C and consider the above chemical equations to be thermodynamically and kinetically favourable reactions below 250°C [158-159] (even though the reaction, $4NH_3(gas) + 5O_2 \rightarrow 4NO + 6H_2O$ is thermodynamically favourable it is kinetically limited at temperatures below 350° C) then the decrease in resistance of the tin oxide sensors is accounted for, as the surface Fermi energy level of SnO_2 is raised and the height of the surface potential barriers is reduced.

For 350°C and above, the platinum catalyst becomes active and the kinetically relevant reaction is as follows [160-163],

$$4NH_3 + 5O_2 \rightarrow 4NO + 6H_2O \quad (IV.10)$$

becoming, in turn, kinetically limited the formation of N_2 and N_2O. Almost at the same time, two new consecutive reactions appear that are thermodynamically and kinetically favourable:

$$2NO + O_2 \rightarrow 2NO_2 \quad (IV.11)$$

$$3NO_2 + H_2O \rightarrow 2HNO_3 + NO \quad (IV.12)$$

The following reactions on the surface of the Pt sensor are assumed to take place:

$$2NH_3 + 5\,O\ (Pt\ surf.) \rightarrow 2NO + 3H_2O \quad (IV.13)$$

$$NO + O\ (Pt\ surf) \rightarrow NO_2 \quad (IV.14)$$

Because NH_3 and NO behave as reducers they are oxidized very quickly by the atomic oxygen that is chemisorbed on the platinum surface at low concentrations of NH_3 (reaction time for

$NH_3 \rightarrow NO$ in the presence of platinum at 800°C is about 10^{-11} sec, and $NO \rightarrow NO_2$ takes place spontaneously with no catalyst). So, the reaction of NO_2 with the surface is as follows,

$$NO_2 + 1e^- (surf) \rightarrow NO_2^- (surf) \quad (IV.15)$$

$$NO_2^- (surf) \rightarrow NO(gas) + O^- (surf) \quad (IV.16)$$

As NH_3 cannot be oxidized into NO_2^- in a single step (the consecutive reactions $NH_3 \rightarrow NO \rightarrow NO_2 \rightarrow NO_2^-$ are required), we postulate that reactions (IV.13) and (IV.14) take place mainly on the platinum surface and reactions (IV.15) and (IV.16) take place on the SnO_2 surface, giving rise to a net decrease in conductivity at temperatures higher than 350°C.

In the presence of high concentrations of NH_3 or insufficient concentrations of oxygen, the reactions $NH_3 \rightarrow N_2$ and $NH_3 \rightarrow N_2O$ become significantly important and give rise to the reductive behaviour shown before with a corresponding increase in the conductivity of the n-type SnO_2 system.

In general, we observe that the Pt-SnO_2 sensors are more sensitive than the pure ones. This is probably due to the higher concentration of adsorbed ionic-oxygen species in the catalyzed layers.

At the same time, and at low-medium temperatures, we observed that the resistance of Pt-doped sensors decreased when sensors are exposed to ammonia vapours, whereas at high temperatures (> 300ºC), their resistance increased, because Pt at this temperature leads to the formation of NO_2 oxidizing species.

IV.3.2 WO_3 sensors

In this subchapter we will present all the results obtained with the following sensors:

a) **Non doped WO_3 sensor**
b) **WO_3 doped with Ag (15 nm Ag sputtered layer)**
c) **WO_3 doped with Pt (Pt was introduced directly in the active layer**)
d) **WO_3 doped with Pd (Pd was introduced directly in the active layer)**
e) **WO_3 doped with Au (Au was introduced directly in the active layer)**
f) **WO_3 doped with Au (15 nm Au sputtered layer)**
g) **WO_3 doped with Au (25 nm Au sputtered layer)**

The objective of this sensor set is to discover which doping technique provides better results with the screen printed sensors: the superficial doping via sputtering or the bulk doping via previously doped paste. The results clearly show that the second method has better effect to the fabricated sensors. As the WO_3 active layer is usually used to detect ammonia and nitrogen dioxide, we tested the fabricated sensors with these gases. We also made additional tests with ethanol and humidity, which can interfere in the NH_3 and NO_2 detection. The following figures (IV.28-IV.34) present all the results obtained from the measurements. The results expressed in numeric values could be found in tables B.4, B.5, B.6 and B.7 presented in Appendix B.

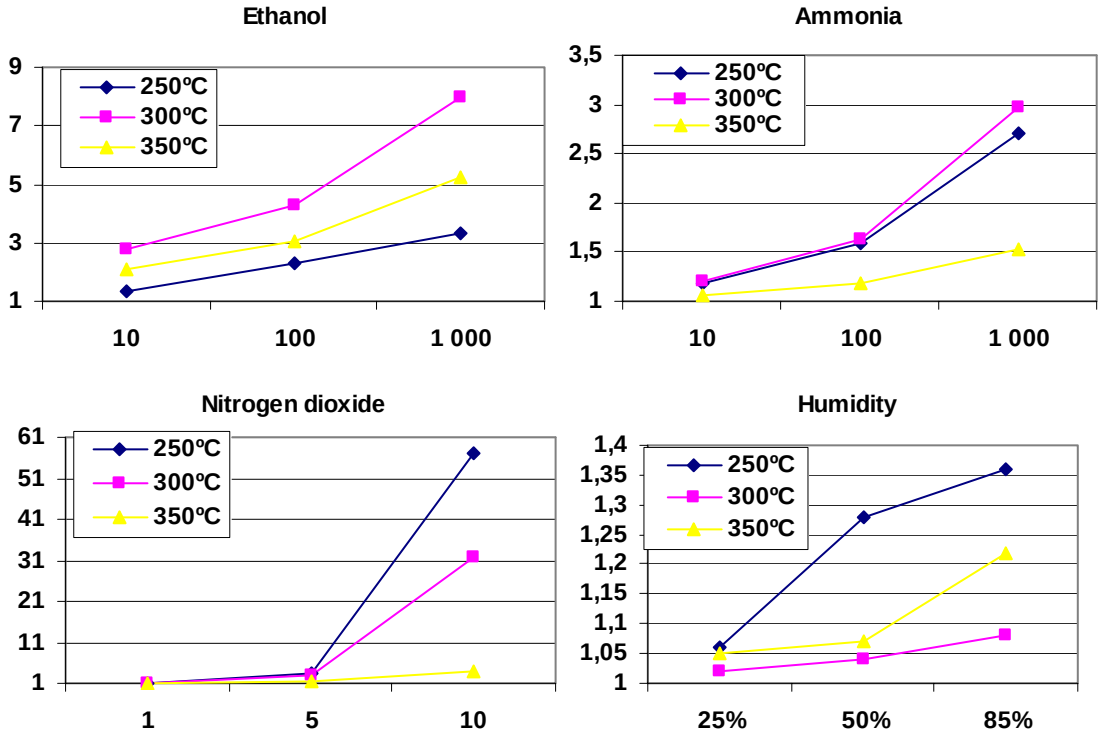

Figure IV.28. Results of the non- doped WO_3 measurements

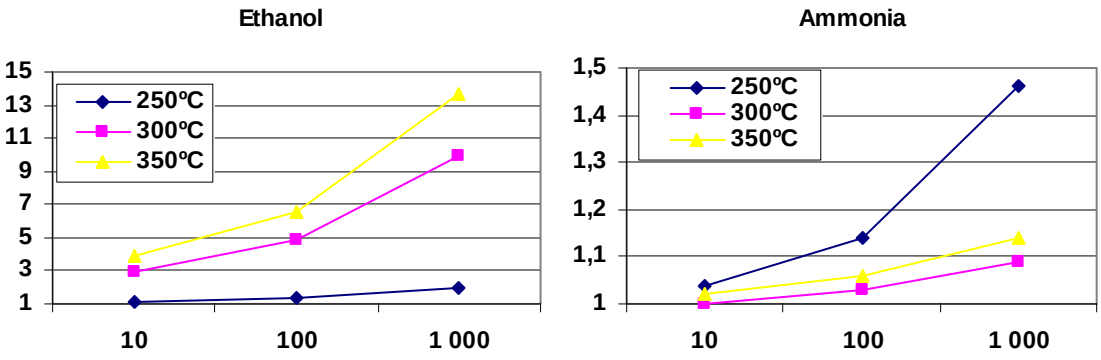

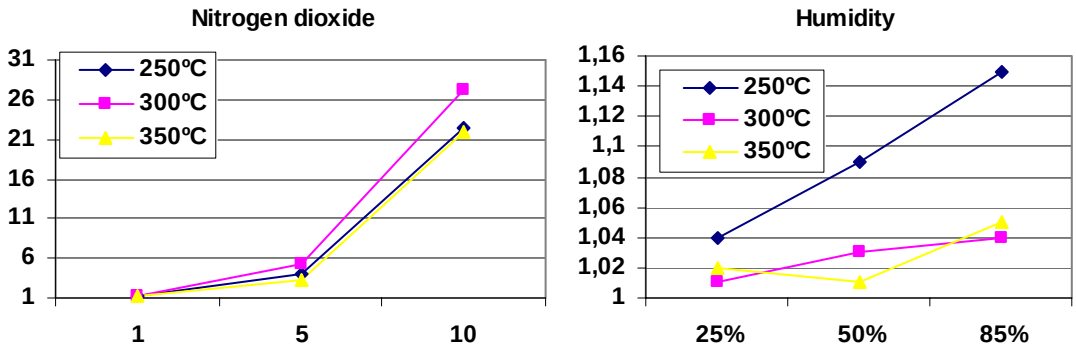

Figure IV.29. Results of the Ag-doped WO_3 measurements

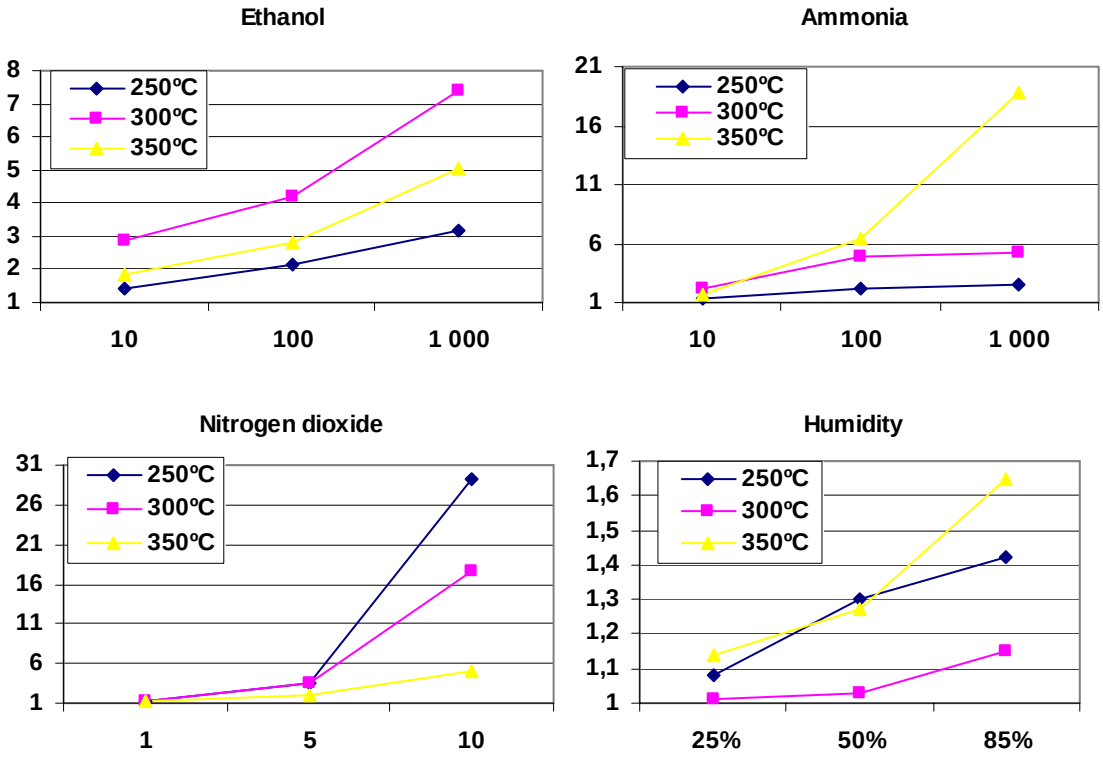

Figure IV.30. Results of the Pt-doped WO_3 measurements

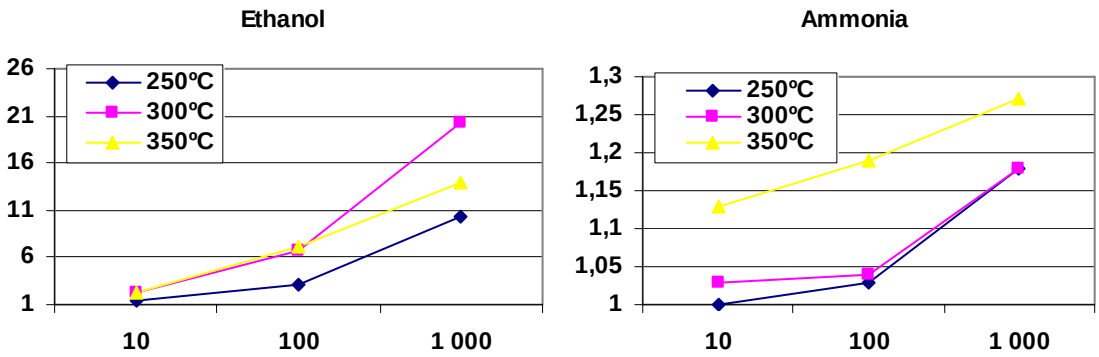

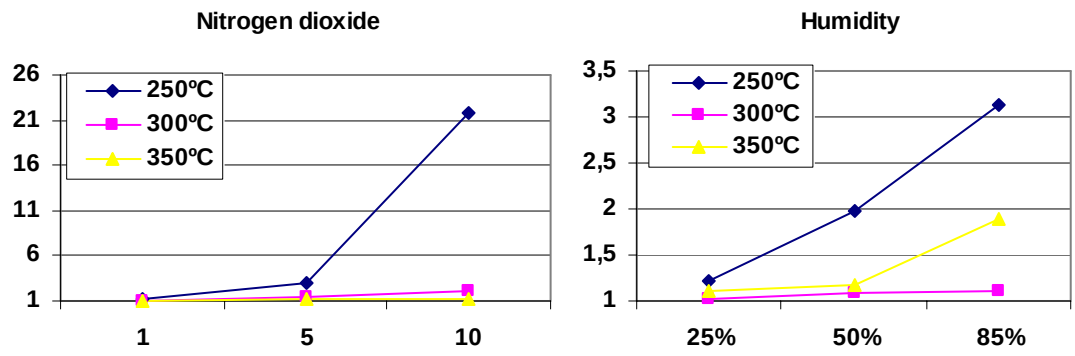

Figure IV.31. Results of the Pd-doped WO_3 measurements

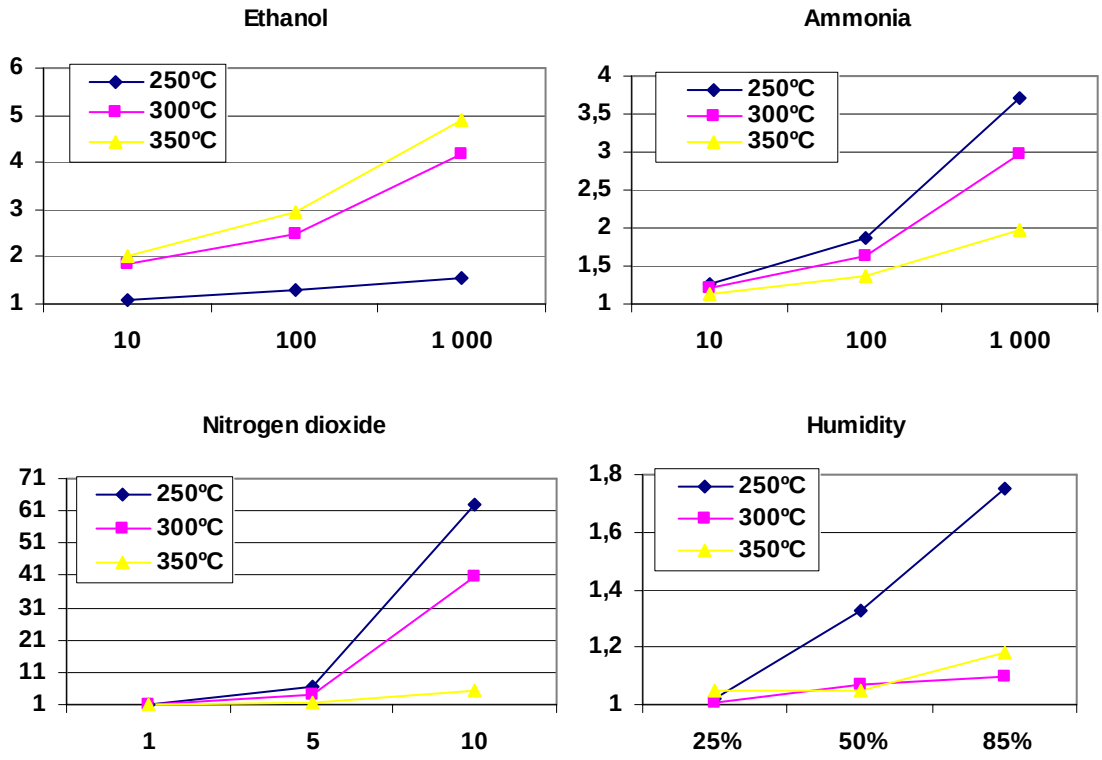

Figure IV.32. Results of the Au-doped (via paste) WO_3 measurements

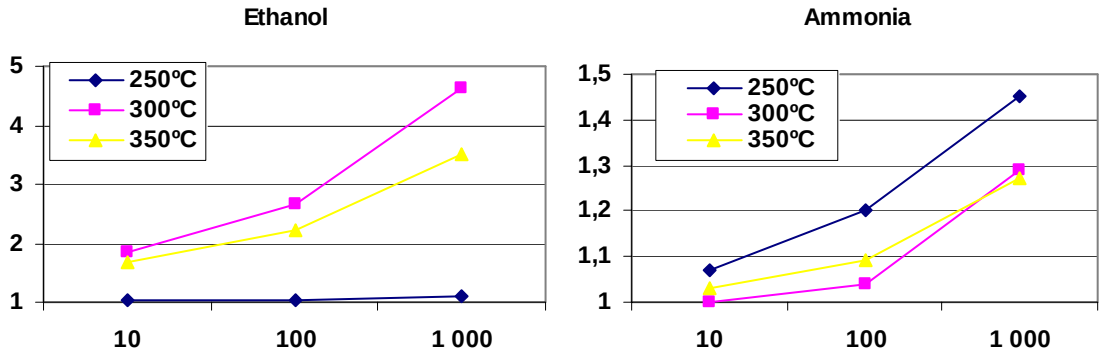

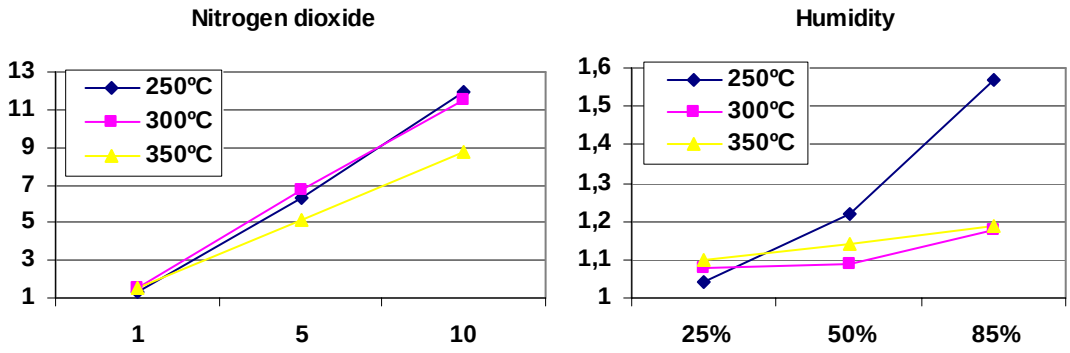

Figure IV.33. Results of the Au-doped (15nm via sputtering) WO_3 measurements

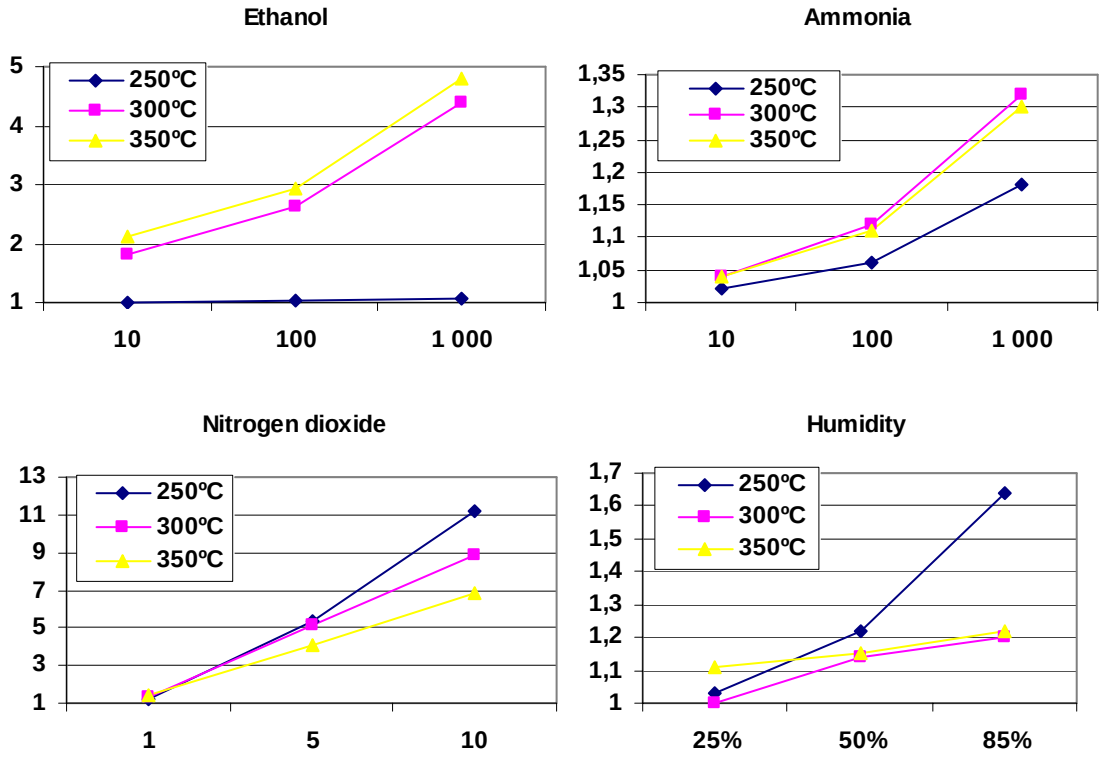

Figure IV.34. Results of the Au-doped (25nm via sputtering) WO_3 measurements

The results show that the response of the pure WO_3 sensor is good to NH_3 and excellent to NO_2. This response is slightly better when gold is introduced in the paste. The sensitivity of the sensors doped with gold by sputtering is very poor. Their sensitivity to NO_2 of approximately 11 is much below in comparison with the sensors fabricated with paste doped directly with gold. This conclusion is used in the future experiments in order to obtain better results for the doped sensors. The Ag and the Pd doping catalyze the reaction to ethanol, while the response of Pt-doped sensors to ammonia is excellent. The response of the fabricated

tungsten trioxide sensors to humidity is very low. Increase of this sensitivity could be observed in the case of the Pd doping.

IV.3.3 WO_3 and SnO_2 sensors with surface adhesion promoters

In this subchapter we will discuss all the results obtained with the following set of gas sensors:

a) **Sensor W1:73.2 % (WO_3 + 5 % Bi_2O_3) + 26.8 % lack matrix**
b) **Sensor W2:73.8 % (WO_3 + 5 % (Bi_2O_3 + Cu_2O)) + 26.2 % lack matrix**
c) **Sensor S1:77.5 % (SnO_2 + 5 % Bi_2O_3) + 22.5 % lack matrix**
d) **Sensor S2:79.4 % (SnO_2 + 5 % (Bi_2O_3 + Cu_2O)) + 20.6 % lack matrix**

The adhesion of the active layer to the substrate is very important for the sensors performance and lifetime stability. In some cases after long period of use, parts of the active layer wear away, which leads to an increase of the sensor resistance and reduction of the sensor sensitivity and selectivity. The objective of this sensor set is to find out how the adhesion promoters affect the sensor response. The gases measured in this study are ethanol, ammonia, benzene, nitrogen dioxide, carbon monoxide, methane and relative humidity in the range between 10 and 85%.

We studied the effect of adhesion promoters (bismuth and copper oxides) on the gas-sensing properties of screen-printed tin and tungsten oxide sensors. The gas-sensitive pastes were prepared by mixing either tin or tungsten oxide powders with an organic vehicle based on terpineol. The paste composition included two different additives to enhance the adhesion of the active films to the substrate (Bi_2O_3 or Bi_2O_3 + Cu_2O). After printing and firing, the films had high porosity and excellent adherence. Morphology studies showed that the films have a well-defined microstructure and gas sensitivity studies showed that additives not only help to promote film adhesion, but also to modify the response of the sensors. Their sensitivity at different operating temperatures was evaluated for ammonia, nitrogen dioxide, ethanol, benzene, carbon monoxide, methane and water vapour.

We investigated the gas-sensing properties of the fabricated thick-film SnO_2 and WO_3 gas sensors. Figure IV.35 shows the response of the different sensors at 250, 300 and 350^oC to ethanol, ammonia, nitrogen dioxide and benzene.

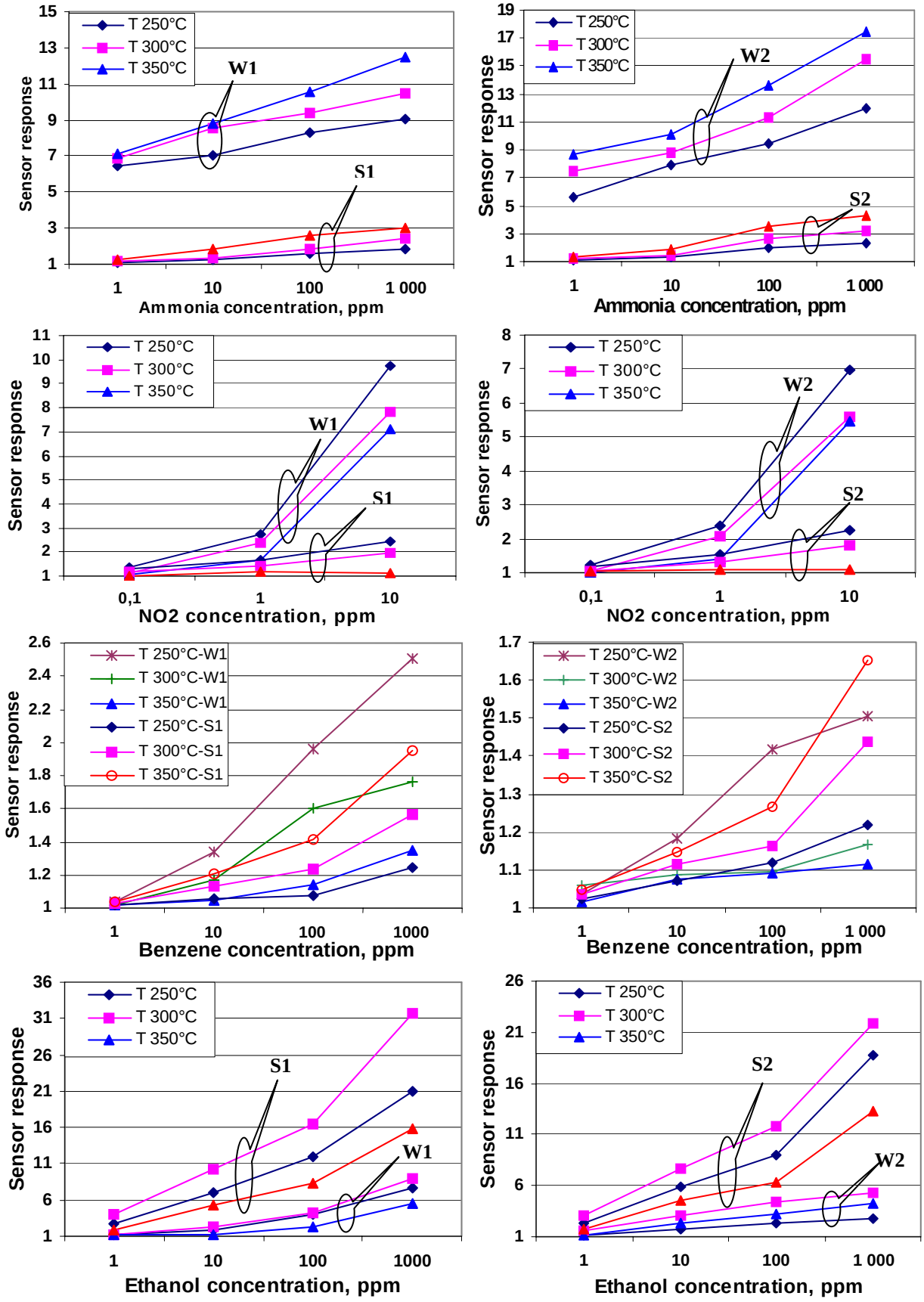

Figure IV.35. Sensor responses to ethanol, ammonia, NO_2 and benzene. Sensors operated at 250 ℃, 300 ℃ and 350 ℃ (S-tin oxide; W-tungsten oxide)

Figure IV.35 shows that the SnO_2-based sensors are more sensitive to ethanol, while WO_3 sensors are more sensitive to NH_3 and NO_2. None of the sensors tested were sensitive to carbon monoxide and methane.

IV.3.3.1 Response of WO_3 –based sensors to gases

WO_3–based sensors are highly responsive to NH_3 and NO_2. Their response to ammonia vapours is highest when they are operated at 350°C and their response to NO_2 is highest when they are operated at 250°C. While the sensitivity to ammonia increases when the operating temperature is raised, sensitivity to NO_2 increases when the operating temperature is decreased. The response of W2 sensors (WO_3 with Bi_2O_3 and Cu_2O) to ammonia was slightly higher than that of W1 sensors (WO_3 with Bi_2O_3). On the other hand, W1 sensors were slightly more responsive to NO_2 than W2 sensors. The sensors were also sensitive to benzene and ethanol vapours but their sensitivity was much lower (by a factor of at least 6 or 2 for benzene or ethanol, respectively) than their sensitivity to NH_3 and NO_2.

Figure IV.36 shows the selectivities at 1 and 10 ppm of the tin and tungsten oxide based sensors. Tungsten oxide sensors are very selective for ammonia at low concentrations of the gases tested. For example, their selectivity (at 1ppm) is higher than 0.72 and peaks at 0.9 when they are operated at 350^{o}C. On the other hand, at higher concentrations of ammonia and nitrogen dioxide, W1 and W2 sensors show slightly different behaviour. While W2 sensors are more sensitive to ammonia at all of the three operating temperature tested, W1 sensors are more sensitive to nitrogen dioxide than to ammonia when operated at 250^{o}C.

IV.3.3.2 Response of SnO_2 –based sensors to gases

SnO_2 sensors show high sensitivity to ethanol. The response to ethanol is highest when the sensors are operated at 300°C. Sensors also respond to NO_2, NH_3, and benzene, but the response to these species is around 6 times lower than the response to ethanol. Like the tungsten oxide based sensors, tin oxide sensors containing Bi_2O_3 only (S1) are slightly more sensitive to the species measured, except for ammonia. SnO_2 sensors containing Bi_2O_3 and Cu_2O (S2) are more sensitive to ammonia.

Figure IV.36 shows also the selectivity of the SnO_2 sensors for the different species studied. This figure shows that S1 sensors are highly selective to ethanol (selectivity for ethanol is higher than 0.81 when the tested sensors are operated at 350°C).

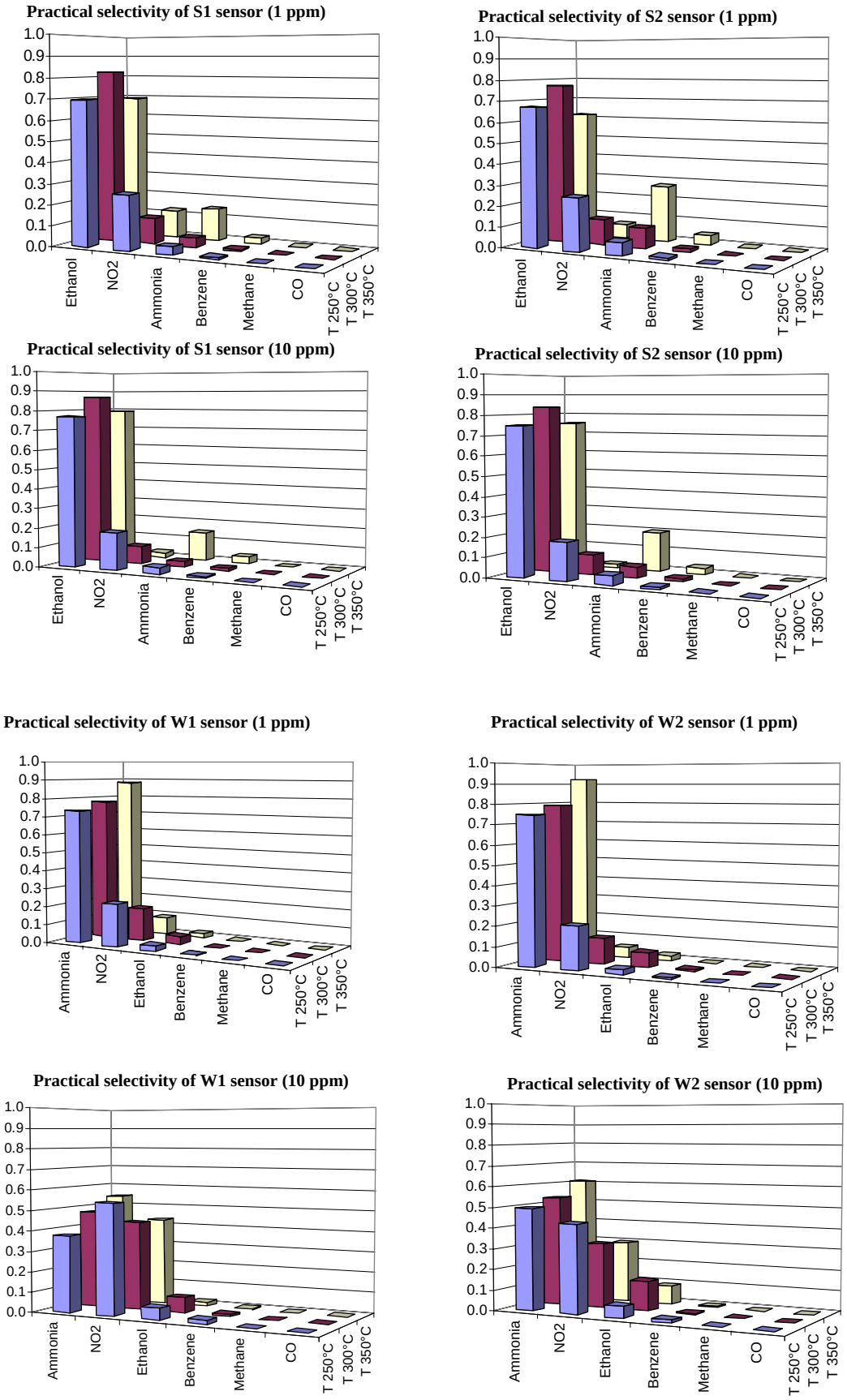

Figure IV.36. Practical selectivity of the sensors for the different gases and vapours studied

IV.3.3.3 Response to humidity

We studied the responses of the sensors to air with three levels of moisture (25, 50 and 85% R.H., measured at 30°C). The reference level of water vapour inside the sensor chamber was equal to 10% R.H. The sensor responses to a humidity change from 10 to 85% R.H. are summarised in Figure IV.37. While the sensitivity of tungsten oxide based sensors to humidity is very low, the response of tin-oxide sensors is higher,. Figures IV.35 and IV.37 show that humidity will have little effect on the detection of ammonia and ethanol using sensors W2 and S1, respectively. However, moisture can significantly influence the detection of low concentrations of nitrogen dioxide (1 ppm) and hinder the detection of benzene. The inclusion of Cu_2O during paste preparation (sensors W2 and S2) increases the response to water vapour, especially in the case of tin oxide sensors. Cu_2O possibly acts as a catalyst at the solid-gas interface for water vapour, thus increasing the sensitivity of W2 and S2 to humidity.

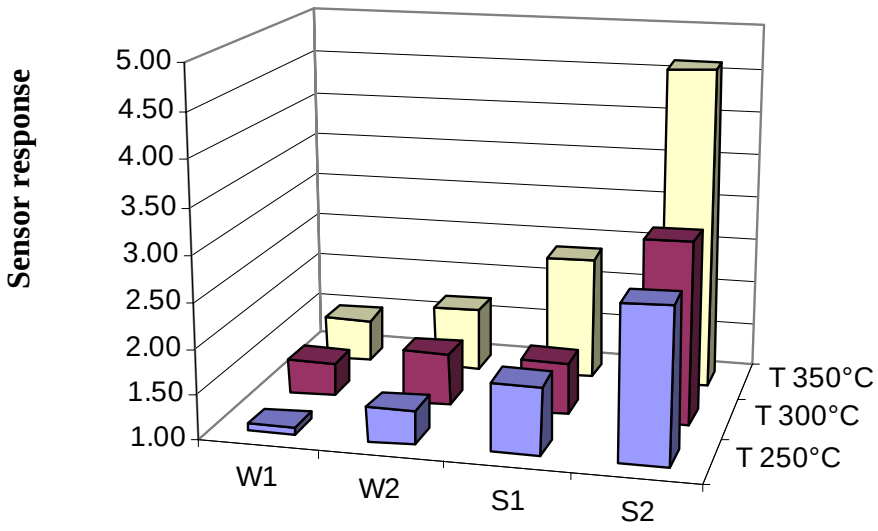

Figure IV.37. Sensitivity to humidity (change from 10 to 85% R.H.) of all the sensors operated at 250 °C, 300 °C and 350 °C

Tin oxide sensors containing only Bi_2O_3 were found to be sensitive and very selective to ethanol vapours (i.e. they show little interference from the other species tested). Tungsten oxide sensors with Bi_2O_3 and Cu_2O were found to be very sensitive to ammonia. However they show important cross-sensitivity with nitrogen dioxide. Their selectivity to ammonia can be improved by selecting a high operating temperature (e.g. 350°C) and also by increasing the

amount of Cu_2O within the active film (since Cu_2O enhances ammonia sensitivity). Tungsten oxide sensors containing Bi_2O_3 are only more sensitive to nitrogen dioxide than to ammonia when they are operated at low temperatures (e.g. 250^oC). Since it has been reported that Bi_2O_3 increases the sensitivity of tungsten oxide films to nitrogen oxides, further work is in progress to asses whether the amount of Bi_2O_3 incorporated into the tungsten oxide film can lead to highly selective nitrogen dioxide sensors.

IV.3.4 WO_3 sensors with catalytic filters

In this subchapter we will present all the results obtained with the following sensors:

a) **Sensor W1: WO_3 sensor without catalytic filter**
b) **Sensor W1CF: WO_3 sensor prepared by printing an insulating alumina paste that covered the tungsten oxide layer. After drying this alumina layer, a Pt layer was printed on top. This resulted in the surface loading of the alumina film.**
c) **Sensor W1CFD: WO_3 sensor prepared by printing a single dielectric layer prepared by mixing Al_2O_3 and Pt pastes. This resulted in a homogeneous bulk loading of the alumina film.**

We present the results of using a catalytic filter (Pt-Al_2O_3) printed on a tungsten oxide active layer to selectively detect benzene. The effect of the catalytic layer is twofold: first, it dramatically increases the sensitivity of the tungsten oxide film to benzene vapours and second, it de-sensitises the film to ethanol. We also studied the response of the sensors with both types of catalytic filter to other gases such as carbon monoxide, methane, ammonia and nitrogen dioxide. Particular attention is paid to the sensor response to humidity.

Neither the sensors with catalytic filters nor those without filters were sensitive to CO and CH_4 at the operating temperatures studied. Both types of sensors were responsive to ethanol. However, the sensitivity of the sensors with catalytic filters was slightly lower than the sensitivity of the bare tungsten oxide sensors. On the other hand, while the sensors without catalytic filters were almost insensitive to benzene, the response of the sensors with catalytic filters was significant.

Figure IV.38 shows the responsiveness to benzene of a tungsten oxide sensor without a catalytic filter (W1). W1 sensors are characterised by a low sensitivity to benzene. The response is very weak at low benzene concentrations (e.g. 1 ppm). Furthermore, their

sensitivity to benzene decreases when their operating temperature is raised. Figures IV.39 and IV.40 show the responsiveness to benzene of sensors coated with catalytic filters: W1CF sensors (alumina with platinum layer on top) and W1CFD sensors (alumina with homogeneous platinum loading), respectively.

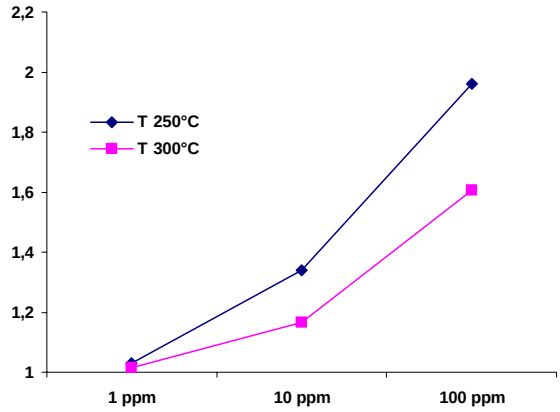

Figure IV.38. Sensitivity to benzene of the W1 at 250 ℃ and 300 ℃

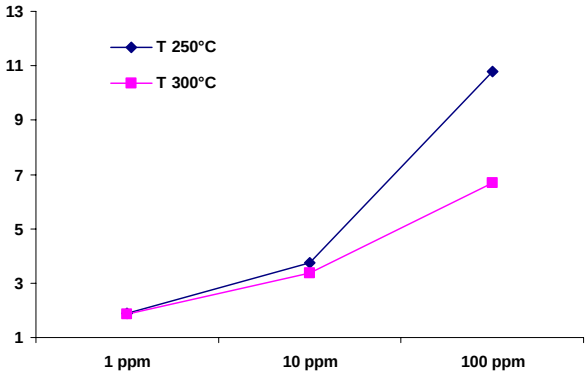

Figure IV.39. Sensitivity to benzene of the W1CF at 250 ℃ and 300 ℃

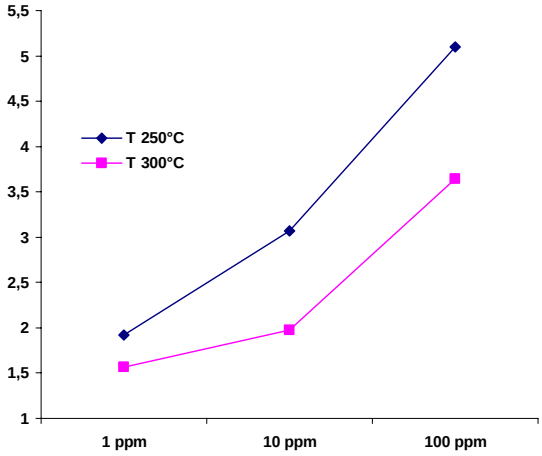

Figure IV.40. Sensitivity to benzene of the W1CFD at 250 ℃ and 300 ℃

The catalytic filter increases the sensitivity to benzene by a factor of 5 (W1CF) or by a factor of 2.5 (W1CFD). Once again, the sensitivity to benzene decreases when the operating temperature of the sensor increases. The platinum catalyst promotes the decomposition of benzene. Benzene by-products reach the surface of the tungsten oxide film and react with the active layer, which changes the sensor resistance.

The fact that W1CF sensors are more responsive than W1CFD sensors may be because the homogeneous Pt-loaded alumina layer (W1CFD) is more efficient at burning out benzene than the alumina layer with a Pt layer on its surface (W1CF). In other words, the concentration of by-products resulting from the incomplete catalytic combustion of benzene, which can then interact with the WO_3 film, is higher for W1CF sensors than for W1CFD sensors. This may explain why W1CF sensors are more sensitive to benzene.

Table IV.12 summarises the sensitivities of the tungsten oxide sensors to the different gases studied and shows the effects of the catalytic filters. For all the species tested, the results are for concentrations of 10 ppm except for the nitrogen dioxide, where the results are for concentrations of 1 ppm.

While the catalytic filters have a considerable influence on the sensitivity to benzene, the effects on the sensitivity to the other vapours studied is mild. This property can be used to design a sensor with a high specificity for benzene. In fact, the specific sensor would consist of two tungsten oxide sensors: one of type W1 and one of type W1CF. The response of the selective sensor would be the differential responsiveness defined as:

$$\Delta S_i = \frac{R_{air,W1CF}}{R_{i,W1CF}} - \frac{R_{air,W1}}{R_{i,W1}} \qquad \text{(IV.17)}$$

where $R_{air,W1CF}$ is the resistance in air of sensor W1CF and $R_{i,W1CF}$ is the resistance of the same sensor in the presence of species *i* diluted in air.

Under these conditions, the selectivity of the sensor for a species *i* could be defined as:

$$Sel_i = \frac{\Delta S_i}{\sum_{j=1}^{k} \Delta S_j} \qquad \text{(IV.18)}$$

where *k* is the number of species considered. The higher the selectivity for a given species is, the more specific is the sensor for this species.

Measured vapour	W1CF	W1CFD	W1
C_2H_5OH (250ºC)	1.37	1.50	1.93
C_2H_5OH (300ºC)	**2.06**	**2.46**	**2.19**
C_2H_5OH (350ºC)	1.22	1.44	1.28
C_6H_6 (250ºC)	**3.74**	**3.07**	**1.34**
C_6H_6 (300ºC)	3.37	2.00	1.17
C_6H_6 (350ºC)	2.79	1.63	1.05
NH_3 (250ºC)	6.95	7.03	7.07
NH_3 (300ºC)	8.49	8.46	8.51
NH_3 (350ºC)	**9.56**	**10.06**	**8.78**
NO_2 (250ºC)	**3.65**	**1.43**	**2.71**
NO_2 (300ºC)	2.23	1.18	2.36
NO_2 (350ºC)	1.47	1.16	1.65

Table IV.12. Sensitivity at different operating temperatures for sensors with (W1CF), (W1CFD) and without (W1) catalytic filter

Figure IV.41 shows the selectivity of a sample differential sensor defined by equations (IV.17) and (IV.18).

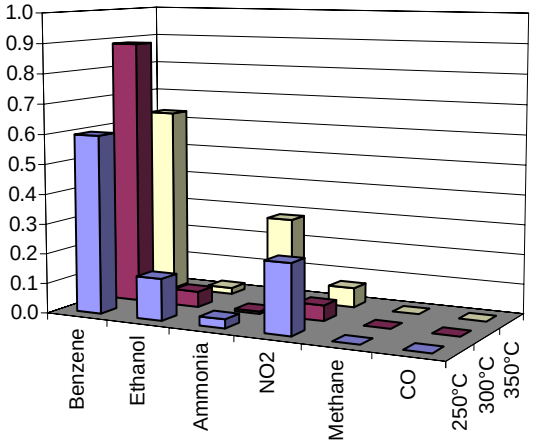

Figure IV.41. Selectivity of the differential W1CF - W1 at 250 ℃, 300 ℃ and 350 ℃ for 10 ppm of gases, 1ppm of NO_2

It can seen that a very selective benzene sensor can be made by combining sensors W1CF and W1 working at 300°C (e.g. selectivity for benzene is near 0.9). However, this strategy to enhance selectivity is only of use for low concentrations of the interfering species, where the sensors show a quasi-linear response (up to 10 ppm of ethanol and ammonia vapours and 1 ppm of NO_2). At higher concentrations, the excellent selectivity figures would start to degrade due to the increasing importance of the non-linear sensor response.

Finally, the effect of changing the humidity level on the different sensors was also investigated. Figure IV.42 shows the responsiveness of the different sensors to a sudden change from 10 to 85% in the humidity level, as a function of the working temperature. The responsiveness to humidity of sensors W1CF and W1 is moderate and very similar. Therefore, humidity effects would almost be cancelled out if the differential response defined in equation (IV.18) is used.

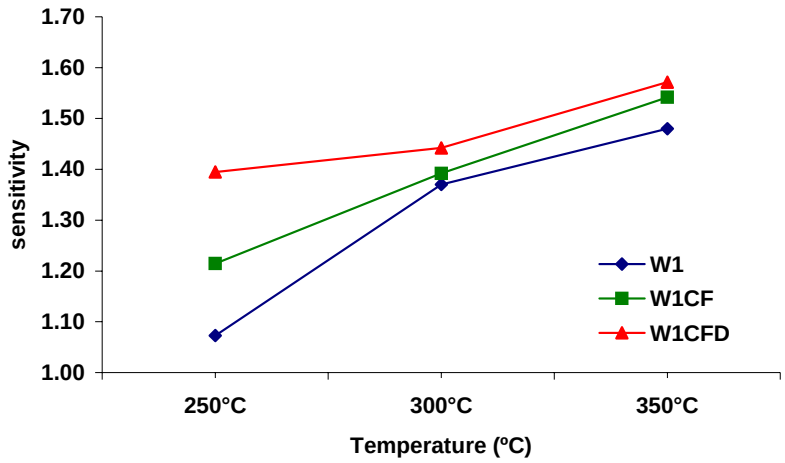

Figure IV.42. Sensitivity of the sensors to 85% humidity vapours at the following temperatures: 250 ℃, 300 ℃ and 350 ℃

Placing a Pt catalytic filter on top of a WO_3 gas sensor makes it possible to selectively detect benzene in the ppm range at moderate temperatures (250°C). The CF type filter proved to be the best for benzene detection: the WO_3 layer detects gases only after combustion in the catalytic filter. The benzene response of the CF filter is higher than that of the CFD filter. The CF filter reduces sensor sensitivity to ethanol at 250°C and increases sensor response to benzene. Loading Pt into the active layer is the most efficient way of increasing sensitivity to ethanol. The catalytic filter also affects NH_3 detection. A chemical reaction takes place on its surface and produces nitrogen oxides, which oxidises the WO_3 surface.

On the other hand, the Pt catalytic filter does not alter the NO_2 sensing capability of WO_3. Besides, the filter does not improve the WO_3 sensor response to methane nor carbon monoxide.

IV.4 Conclusions

This chapter discusses the fabrication of thick-film gas sensors on Al_2O_3 substrates. It presents the whole substrate fabrication process, starting with the fabrication of the heater/temperature sensor, the pads and the electrodes. Particular emphasis is placed on the preparation of the active phase, the additives, and the calcination and firing process. The wire bonding, packaging and testing of the fabricated sensors is reviewed. Various sensors with active layers based on pure and doped SnO_2 and WO_3 are fabricated. The influence of the adhesion promoters and catalytic filters is also studied. The complete results from the physical and chemical studies performed are presented and discussed.

Summarizing, this chapter explains the proceeding of our study, which begins with the sensor design and fabrication. For the initial tests we used active layer based on the most widely used metal oxide – SnO_2. Once we have learned to deposit active layer based on tin dioxide we proceeded to experiments with WO_3. The fabricated pastes had good adhesion, morphological and electrical properties. To improve the active layer properties we incorporated various surface promoters. We discovered the effects of the different doping and found out the most favourable doping for the different gases studied. The produced SnO_2 sensors showed excellent response to ethanol, while the developed WO_3 gas sensors showed good results in detection of ammonia and nitrogen dioxide, which were some of the target gases in our study. To improve the sensor selectivity, different catalytic layers were deposit. These layers permitted us to obtain sensors for selective benzene detection.

V. FABRICATION OF THICK FILM GAS SENSORS ON MICROHOTPLATE AND SILICON ON INSULATOR SUBSTRATE

In recent years substrates such silicon or sapphire have been exhaustively investigated. Nowadays, the silicon substrate is one of the most commonly used in sensor technology, because of its low cost and compatibility with IC fabrication. Silicon's excellent semiconductor properties have made it the basic building material in the electronics industry. Silicon also has excellent physical properties that make it an ideal building material for mechanical devices. Its tensile strength is greater than that of steel and it is almost perfectly elastic, making it a wonderful material for use in MEMS products. It is free of hysteresis, and its crystalline structure is well suited to the fabrication of miniature precision products. These devices have several advantages: they are small; their performance is high due to the precise dimensional control in the fabrication, and they are cheap. Gas-sensitive metal oxide layers have been integrated in standard microelectronic processing and, together with the use of micromachining steps, led to micro-machined metal oxide gas sensors [164]. This technology is very promising. The sensitive layer of micro-machined metal oxide gas sensors is deposited onto a thin dielectric membrane with low thermal conductivity, which provides good thermal

isolation between substrate and the gas-sensitive heated area on the membrane. In this way the power consumption can be kept very low (typical values lie between 30 and 150 mW [165-167] and the substrate itself stays nearly at ambient temperature. The sensor elements are easier to mount, and control and signal-processing electronics can be integrated on the same substrate if desired. Sensor arrays, which are often needed to overcome the bad selectivity of single-sensor elements, can be easily implemented in this technology.

Chapter IV showed us that no matter the good results obtained with the sensors fabricated on alumina substrate the power consumption of these sensors is too high. This is the reason why an alternative substrate that consumes less power is needed. In this chapter, we introduce the microhotplate and the silicon-on-insulator microhotplate as one of the promising sensor substrates. The active layer was deposited on the substrates by screen printing. For this type of substrates, the above mentioned technique was used from a very few groups of investigation and represent a special novelty in the sensor fabrication. We begin our test with non-doped SnO_2 and WO_3 active layers. We study the influence of the grain size and once the optimal grain size is determined we proceed to doping of the active layers. Various noble metals (Au, Pd and Pt) and various doping quantities were tested. Subsequently we proceed to data processing of the obtained data with a set of pattern recognition techniques. The results of the analysis permit us to identify and quantify the studied organic compounds.

V.1 Substrate fabrication

The surface-micro-machined microhotplate structure that is common to the various platforms was designed for fabricating conductometric gas micro-sensor prototypes. Microhotplate elements include functionality for measuring and controlling temperature, and measuring the electrical properties of deposited films. As their name implies, they are of particular interest because of their ability to examine temperature-dependent phenomena on a micro-scale, and their rapid heating/cooling characteristics have led to the development of low power sensors that can be operated in dynamic temperature programmed modes. Tens or hundreds of the microhotplates can be integrated within arrays that serve as platforms for efficiently producing processing/performance correlations for sensor materials. The micro-devices also provide a basis for developing new types of sensing prototypes and can be used to investigate proximity effects and surface transient phenomena. The evolution of micromachining as a fabrication technology for chemical sensing has allowed miniaturization to progress with improved fabrication methods. Micromachining of silicon to produce sensor platforms also

makes it possible to include on-chip circuitry, and it is straightforward to replicate device structures into integrated arrays. Beginning in the early 1990s, the opportunities of silicon micromachining led to the fabrication of new types of microhotplate devices and arrays for gas sensing. These devices have been produced both by surface [168] and bulk [169, 170] etching of silicon, and have been used to develop gas micro-sensor prototypes [171]. The ability to locally heat miniature elements has been used both to fabricate gas micro-sensor films and operate devices in the rapid temperature-programmed mode [172]. Recently, the advantages of microhotplates as gas sensor platforms have been amply demonstrated [173, 174]. The Process Sensing Group at NIST (National Institute of Standards and Technology) is investigating generic technology issues related to next-generation chemical measurements with solid-state devices. The technology developed by this group is discussed here in considerable detail because of its importance for micro-machined devices. The microhotplate contains a built-in heater, thermometer, and sensing film. The device uses conductance changes in the sensing film to detect the presence of adsorbed gas species. Temperature changes may be used to alter the reaction kinetics between the gas and sensor surface. A single element is illustrated in figure V.I (left) [175].

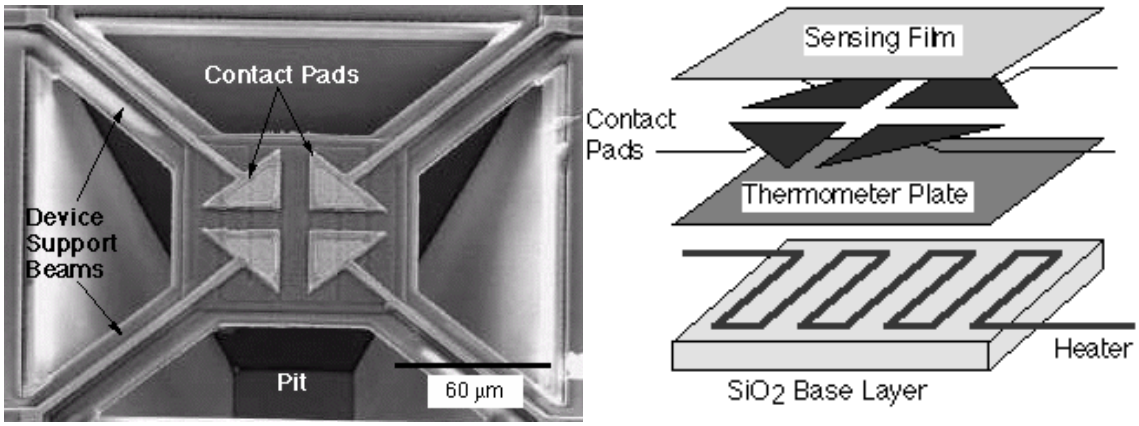

Figure V.I. Micrograph of single microhotplate with four arrow-shaped electrodes

The microhotplate is a multi-layer structure, which has three functional layers: a polysilicon heater, a metal (for example Al or W) thermometer/heat distribution plate, and sensing film electrical contacts (figure V.I, right). These layers are separated by insulating layers of SiO_2. In order to measure the electrical characteristics of the sensing films, the surface electrodes are in direct contact with the sensing film but isolated from the heat distribution layer by a SiO_2 layer. Maximum device temperatures are largely governed by the types of metallization available at a given foundry. For Al metallization, the maximum temperature is approximately 500°C, and metal post processing is needed to produce more acceptable sensing film contact

composition. When other metallizations, such as W or Ti-W, are available at the foundry, devices can be heated to as high as 750°C.

V.1.1 Micro-hot-plates fabricated at National Centre of Microelectronics

The integrated micro-hotplates with arrays of four microsensors were fabricated on double-side polished p-type <1 0 0> Si substrates, 300 μm thick (4-40 Ω·cm). The structure of the device basically consists of a gas sensing layer, the electrodes, insulating layers and a polysilicon heater. The technological process needed to fabricate the sensors had the following steps [176, 177]: (1) Deposition of the membrane layer. The dielectric membranes consisted of a 0.3 μm thick Si_3N_4 layer grown by LPCVD. Each chip had 4 membranes, the size of which was 900 × 900 μm^2. (2) Deposition and patterning of a $POCl_3$-doped polysilicon heating meander with a resistance of 6 Ω/sq. The temperature coefficient of resistivity (TCR) of polysilicon depends on the doping level which, for our devices, was 6.79×10^{-4}. The heater was also used as a temperature sensor. (3) Deposition of a 0.8 μm-thick SiO_2 layer to insulate the heater from the electrodes and the sensing film. (4) Opening of contacts for the heater bonding pads to be accessible. (5) Deposition of either parallel or interdigited 0.2 μm-thick Pt electrodes, patterned by lift-off. A thin layer (20 nm) of Ti was deposited prior to Pt to promote electrode adhesion. The electrode area was 400 × 400 μm^2. Figure V.2 shows a planar view of the membrane with heater and electrode configuration (6) Patterning of the backside etch mask. (7) Deposition of the sensing layer onto the electrode area. (8) Backside silicon etching with KOH at 70^oC (40% wt.) to create the thermally-insulated membranes. (9) Wire bonding and packaging. Each chip was mounted on a TO-8 package. Gold wires with a diameter of 25 μm were used for standard ultrasonic wire bonding. To prevent the membranes from breaking due to air expansion in the cavity below the membranes when the device is heated, the chips were not glued directly to the surface of the metallic package but kept elevated by using two lateral silicon spacers.

The sensing films of interest include oxides, metals and polymers that can be produced and tailored by a wide variety of techniques. Typically, the films are deposited after silicon has been etched away to produce the thermally-isolated structures. Etching chemicals are usually too aggressive to properly maintain the integrity of pre-deposited films. The etch pits can be problematic, for example, when spin-on methods or certain types of lift-off processing are used. Unlike previous studies, the technological procedure reported in [178] enables the

sensing layers to be deposited before the membranes have been etched. This prevents themembranes from being damaged during film deposition, which leads to gas sensor microsystems with an excellent fabrication yield. The deposition method overcomes disadvantages such as low porosity and low surface area, generally associated to chemical vapour deposition or sputtering methods, and keeps power consumption low (80 mW for a working temperature of 480^{o}C).

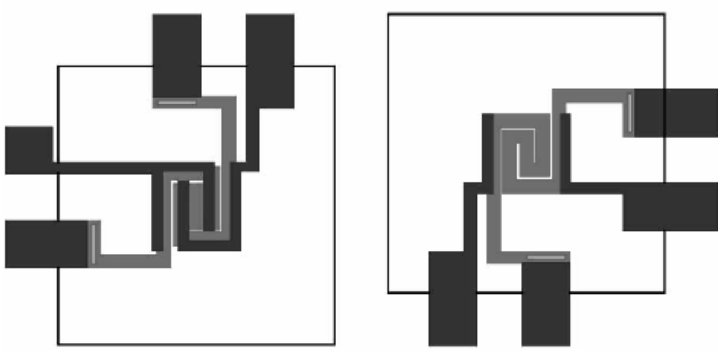

Figure V.2. Planar view of the micromachined gas sensor membrane; left: interdigited electrodes; right: parallel electrodes

V.1.2 SOI Micro-hot-plates fabricated at Catholic University of Louvain

Another way to further minimize the power consumption is the silicon-on-insulator technology. Figure V.3 shows a SOI solid-state gas-sensor with an original design of a polysilicon loop-shaped microheater fabricated on a thin-stacked dielectric membrane [179]. The microheater ensures high thermal uniformity and very low power consumption (20 mW for heating at 400°C). The use of completely CMOS-compatible TMAH-based bulk micro-machining techniques during the fabrication process means that it is straightforward to integrate smart gas sensors in SOI-CMOS technology.

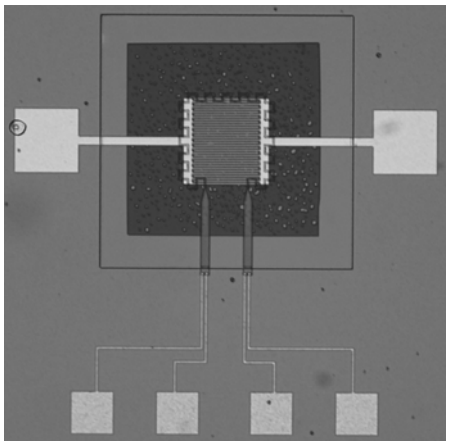

Figure V.3. Picture of a 600x500 µm² gas sensor in SOI technology

The gas-sensor has high thermal uniformity, low-power consumption, low cost and is compatible with standard IC processes. Because it is fabricated on SOI substrate, it can be used to build a fully integrated smart gas sensor in SOI-CMOS technology by integrating both the sensing device and the control electronics on the same chip. In this case, the 400nm-thick SOI buried oxide can be advantageously used as a part of the membrane and the upper monocrystalline silicon film can be used to integrate reliable electronics close to the sensor (Figure V.4). SOI technology is uniquely suited to such harsh environments as high temperatures or radiation and has unique advantages in microsystem applications.

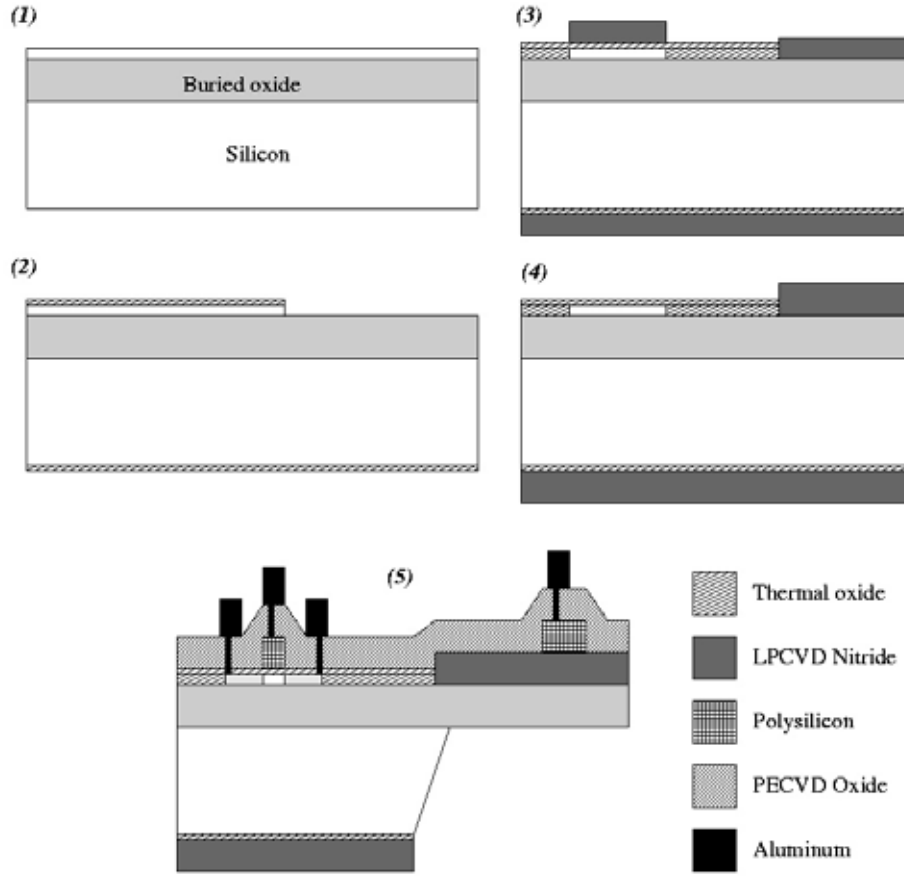

Figure V.4. Schematic process flow of integrated SOI-CMOS microheater. A SOI transistor is grown (left) in same time as the microheater on membrane (right).

The thin-film membrane is one of the most important parts of the whole integrated structure, since it is the mechanical support for the microheater and the sensing film and it is responsible for good thermal isolation and temperature uniformity, and therefore low-power consumption. The original loop-shaped design for the phosphorus-doped polysilicon heater was defined using electro-thermal simulations (ANSYS^{TM}) to optimize the size of the heater and the thermal uniformity on the membrane area.

The membrane consists of three stacked dielectric layers: SiO_2 (400nm LPCVD), Si_3N_4 (300nm LPCVD) and SiO_2 (290nm PECVD). The thickness and deposition parameters are chosen carefully to compensate for the high residual stresses of the deposited films. Strain-free membranes with areas larger than $1mm^2$ were successfully produced. The small total thickness of the membrane (approximately 1 µm) also leads to extremely high thermal insulation (about 15°C/mW) from the bulk and a thermal response as low as 16 ms to reach the temperature of 400°C.

The membrane is released in a single post-processing step, consisting of a backside bulk micromachining with a TMAH-based etching solution. TMAH is used because of its excellent clean room compatibility and excellent selectivity to silicon oxide and nitride. In order to use aluminium as the low-cost metallic layer, aluminium was classically passified with additives in the etching solution since pure TMAH attacks aluminium interconnections. A TMAH 5% solution was used at a working temperature of 90°C. For aluminium passivation, the etching solution was saturated with Si powder. To reduce surface roughness, ammonium persulfate powder was added. No deterioration of the aluminium interconnections was observed after completely etching the 200µm deep cavity (~3 hours) to release the membrane. The sensitivity and selectivity of the fabricated sensor can be significantly modified by treating surfaces with additives such as Pt, Pd and Ru [180, 181].

V.2 Active layers deposition

As we already mentioned, we used two different substrates for the sensor fabrication:, silicon microhotplates and SOI-MHP. The microhotplates were developed by the National Center of Microelectronics and the SOI-MHP by UCL (Belgium). Once the technology had been set up, the microhotplates were used to make detailed studies of the method for depositing the active layers. Finally active layers were deposited on the SOI-MHP substrate to reduce the power consumption even more. Two types of metal oxides were studied: tin dioxide and tungsten trioxide. We also describe the use of various dopants for improving the sensitivity of the devices.

For the sensors fabricated on the above mentioned substrates a special lack matrix (Table V.1) with improved adhesion properties was developed. This matrix provides better adhesion at lower firing temperatures.

Lack Matrix 3 - developed for screen printing of nanopowder on silicon substrates	
Terpineol	*91.6 wt%*
Cellulose	*0.4 wt%*
Texaphor 963	*6.2 wt%*
Rilanit spez. micro W	*1.8 wt%*
Terpineol	*91.6 wt%*

Table V.1. Lack matrix composition

The pastes for the sensors were similar to the pastes used for the alumina sensors. The major difference consists in the powders used. For these sensors commercial nanograin powders were used. Another important difference with the alumina sensors was the doping method. The active layer was not doped using shadow mask, sputtering or direct mixture between the powder and metal pastes. In order to obtain high precision in the doping and homogeneous distribution of the doping particles, we used chlorides of Pt, Pd and Au. HCl and HNO_3 was used to dissolve the chlorides. After that the solution was neutralized with HN_4. From the concentration obtained was calculated the volume of the doping to impregnate the metal oxide powder SnO_2/WO_3. Subsequently we evaporated the solution and annealed the powder at 350º for 20 minutes. Then the powder was milled in mortar and then used directly for pastes preparation.

As the MHP and SOI sensors could not support the firing profiles used for the alumina sensors, another profiles have been used. For the standard silicon substrate temperatures of 600ºC could be used, while for the microhotplates or SOI substrates, firing profiles with lower peak temperatures (500ºC) were used. Detailed information about the firing profiles used is presented in table V.2.

Zone	**Temperature [ºC]**	**Air**	**L/min**	**Total time [min]**	**Speed [mm/min]**
		Q1	14	52.6	34.7
1	560 (470)	Q2	22		
2	605 (505)	Q3	10		
3	600 (500)	Q4	20		
4	590 (500)	Qout	4.62		

Table V.2. Profiles 600ºC/20 min; 500ºC/20 min

Figure V.5 shows some ready-to-use sensors and their electrode/heater configuration. The sensors are fabricated in groups of four in order to simplify the fabrication procedure. Once the fabrication is completed the sensors are cut with a diamond saw, wire-bonded and ready to use.

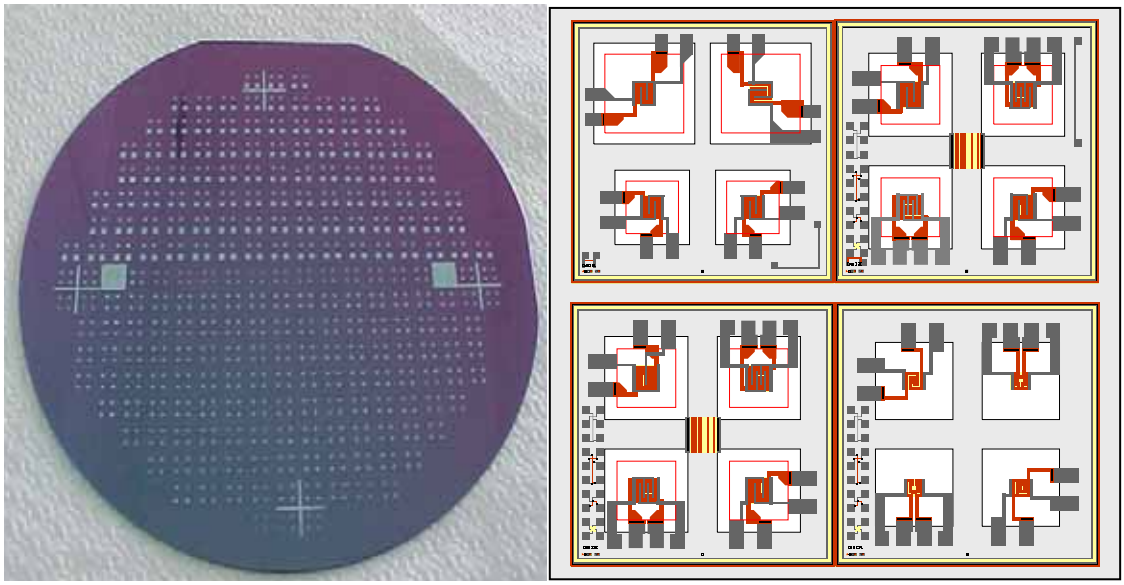

Figure V. 5. Sensors on MHP substrate (left) and electrode/heater configuration (right)

Figure V.6 show a schematic view of the sensor fabricated on MHP substrate with its principal components and active layer of tin dioxide.

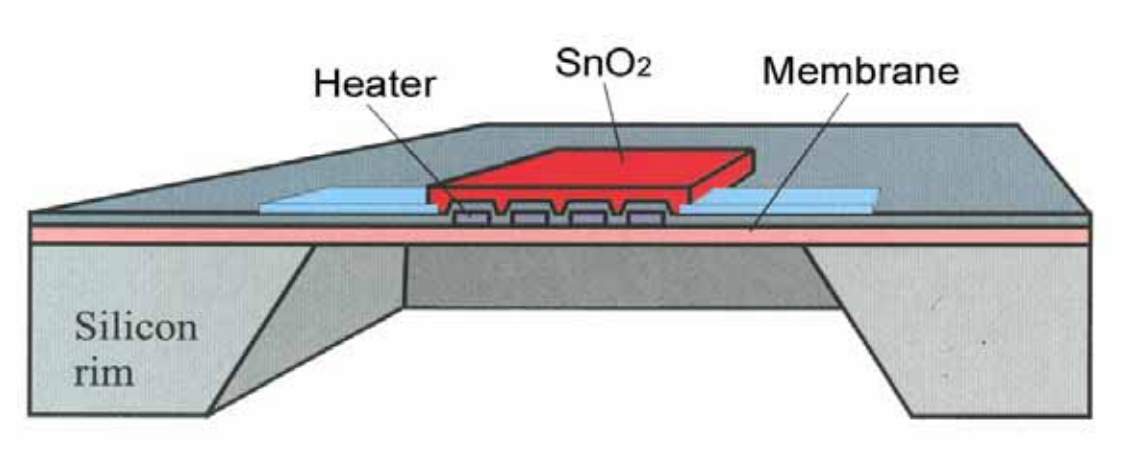

Figure V.6. Structure of microhotplate gas sensors

Once the sensor chip is firmly in position, it is ready for wire bonding. In the case of micro-machined sensors, each chip was mounted on standard TO-8 packages to characterize the sensor. Gold wires 25 μm in diameter were used for standard chip bonding by ultrasounds. The standard silicon sensors were bonded with Al wire. Figure V.7 shows pictures of various encapsulates and wire bonded sensors.

Figure V.7. Sensors bonded on different packages (from left to right: MHP, SOI)

Figure V.8 shows the power consumption curve for the sensors studied in this chapter; that is to say, the electrical power that has to be applied to the heater to obtain the desired working temperature.

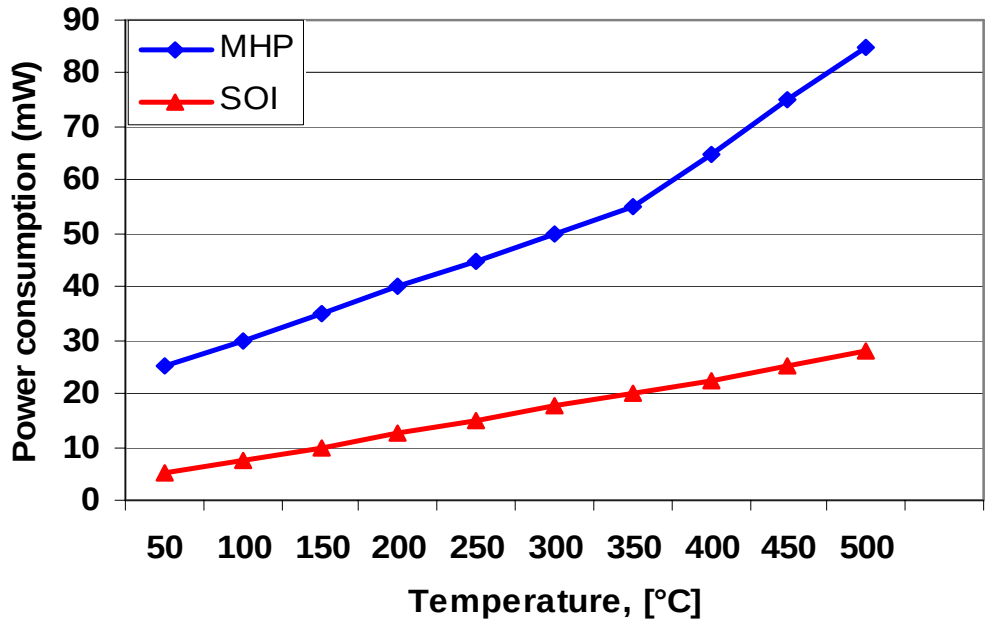

Figure V.8. Power that has to be supplied to the heating element in order to reach the desired working temperature

Figure V.8 shows the power consumption of the sensor fabricated on the microhotplate and the one fabricated on the SOI substrate. The power consumption of these substrates is minimal (approximately 80 mW and 25 mW for sensors working at 500°C, respectively). It is obvious that these substrates are the future of gas sensors. Nevertheless, exhaustive testing is still required to assess the effectiveness of the fabrication techniques that have been used.

V.3 Physical characterization

For the different sensors fabricated SEM and EDS analysis was performed. EDS provided us with the spectrum of the elements that made up our active layers and permitted us to make quantitative and qualitative analyses. The influence of the doping on the grain size and the morphology of the film was studied by SEM. The results below showed that introducing Au into the active layer increases the grain size and forms conglomerates. We concluded that for WO_3 doped with gold, micro-cracks would be produced.

V.3.1 SnO_2 layer based on nano-metric grains

We used a standard screen-printing technique (with a high-resolution mask alignment system), which is a good alternative for fabricating micro-machined gas sensors based on stabilised metal oxide nano-powders. The fact that, for the first time, the active pastes had been printed and fired before the silicon substrates were back etched to create the membranes, led to an excellent yield after the micro-sensors had been etched, diced and packaged. The method made it possible to vary the thickness of the deposited layer (after firing) between 2 and 20 μm, depending on the settings chosen for the process parameters. The morphology of the screen-printed films was investigated by scanning electron microscopy and energy-dispersive X-ray spectroscopy.

V.3.1.1 SEM and EDS analysis

Figure V.9 shows the micrograph of a membrane coated with a screen-printed tin oxide layer. The picture shows an MHP chip with four sensors (left) and a zoomed picture of two of the sensors (centre and right) in the chip. It is clear that the active film is well defined in a central area of about 400 × 400 μm^2 on top of the 900 × 900 μm^2 membrane. This proves that our method makes it possible to control the deposition on the membrane with high accuracy.

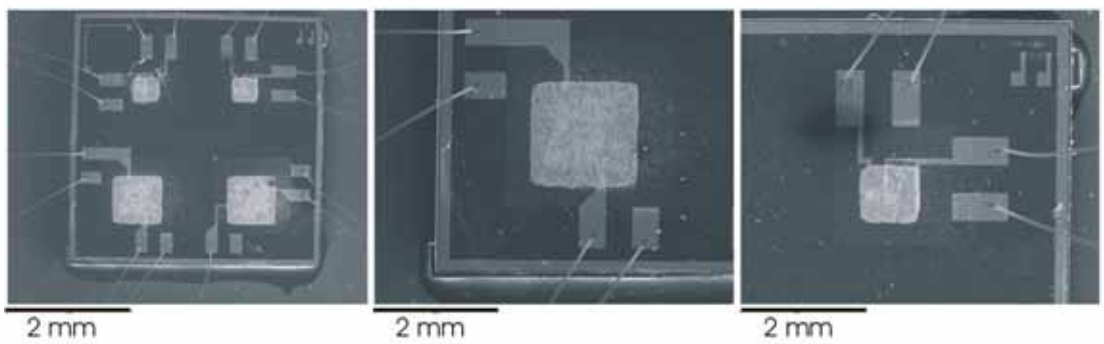

Figure V.9. Micrograph of a MHP chip (left) and two membranes coated with a screen-printed tin oxide (centre and right)

Figure V.10 shows two detailed views of the surface of a sensitive layer. The accelerating voltage was 15 kV. Figure V.10a (magnification 17000) shows a general view of an active coating, which appears not to be cracked and to be made up of homogenously-sized grains. Figure V.10b (magnification 110000) shows a more detailed view of the sensitive layer. As can be seen, the grain size is below 40 nm and the grains form agglomerates, which create a porous layer. The thickness of the sensitive films was determined by a SEM analysis and it was found to be 5 μm. The sensitive layer is thicker than usual in micro-machined gas sensors, although it is hin enough to maintain the good properties of the membrane in terms of power consumption and thermal inertia.

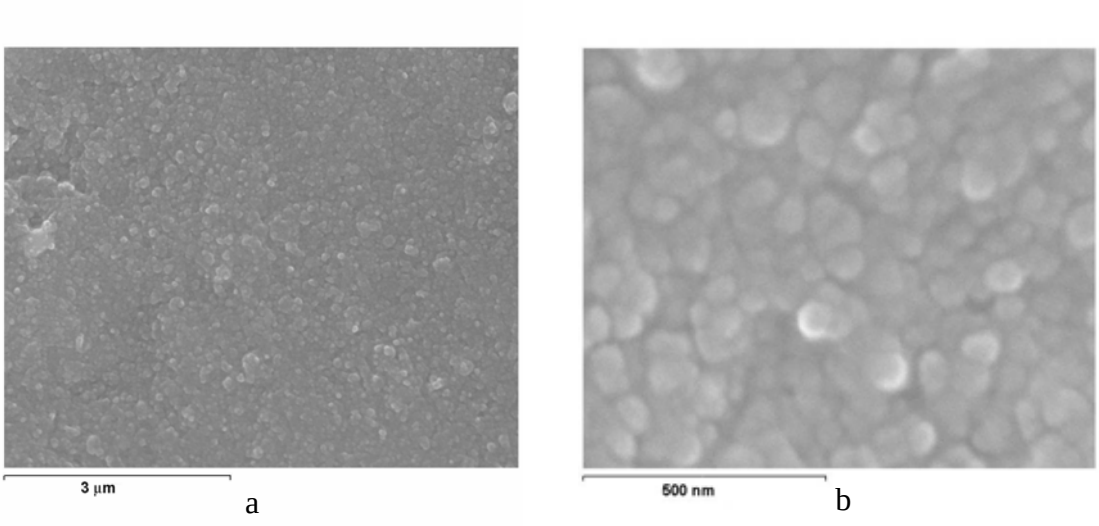

Figure V.10. SEM analysis of the surface of a sensitive layer

Tin-oxide films have the typical microstructure of screen-printed sensing layers. Films are made of grains and voids. EDS analysis showed that the grains and the bottom of the voids contained tin. Thus, SEM and EDS results showed that the samples were porous. Because the surface area exposed to gases is greater, these sensors are expected to be more sensitive than those obtained by sputtering or CVD, where layers are very compact and the interaction between the gases and the sensitive layer is limited to the surface itself [182].

V.3.2 Doped SnO_2 / WO_3 active layers deposited on MHP

Detailed analyses were performed with the doped layers deposited on MHP. Due to the specific active layer deposition technique (for the fabrication of each chip, four different masks and four consecutive alignments/depositions were performed), general pictures of the chips were made. These pictures showed that the active layers were perfectly defined on the membrane area (figure V.11).

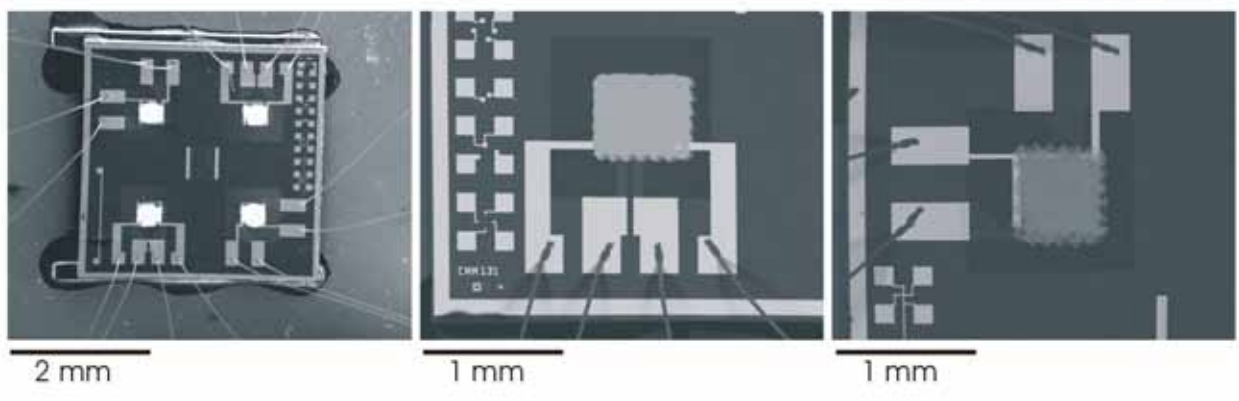

Figure V.11. Micrograph of a MHP chip and two membranes

Figure V.11 show that for the doped active layer sensor chips with four equal membranes were used. It permits to obtain comparable results from the different sensors on the chip and give us information about the repeatability of the method.

V.3.2.1 SEM and EDS analysis

To study the structure of the active layer (surface scratches, structural composition, grain size/shape and porosity) we took a set of photos for each sample. In table V.3 the working conditions under which the different photos were taken can be observed.

Parameters	Picture 1	Picture 2	Picture 3	Picture 4
Working distance	15 mm	15 mm	7 mm	7 mm
Acceleration voltage	20 kV	25 kV	25 kV	35 kV
Magnification	500/2'000	10'000	50'000	100'000

Table V.3. Working conditions under which the different photos were taken

A sample picture of the non-doped SnO_2 layer with 100'000 magnification is shown below (figure V.12). The excellent resolution of this picture allows us to see clearly the structure of the deposited active layer.

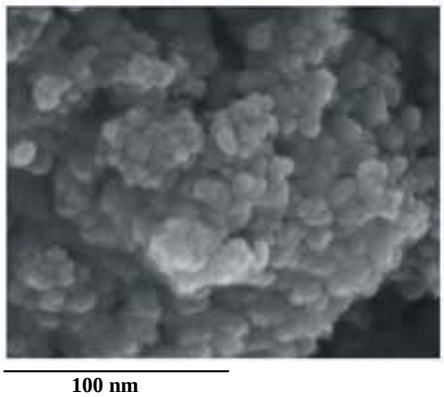

Figure V.12. SEM analysis of the surface of a sensitive layer with 100'000 magnification

As we found that the results from pictures with a magnification of 50'000 and 100'000 were similar and did not give additional information, the pictures shown below only the magnification of 50'000, because of the pictures are of better quality. The results from the SEM analysis are detailed in figures V.13, V.14 and V.15.

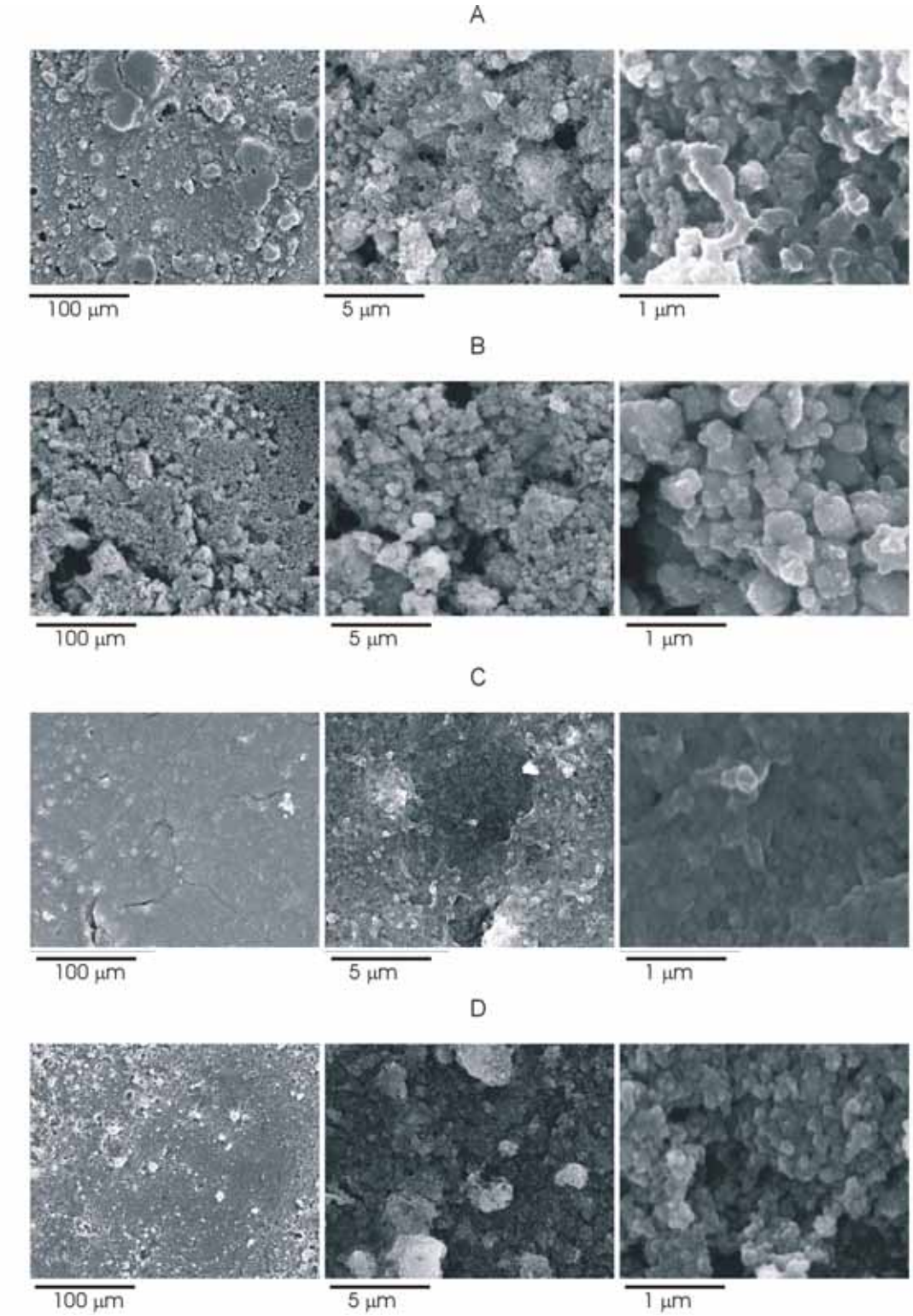

Figure V.13. SEM analysis of active layers A) Non doped SnO_2 B) SnO_2 doped with 1wt% Au C) SnO_2 doped with 1wt% Pd D) SnO_2 doped with 1wt% Pt

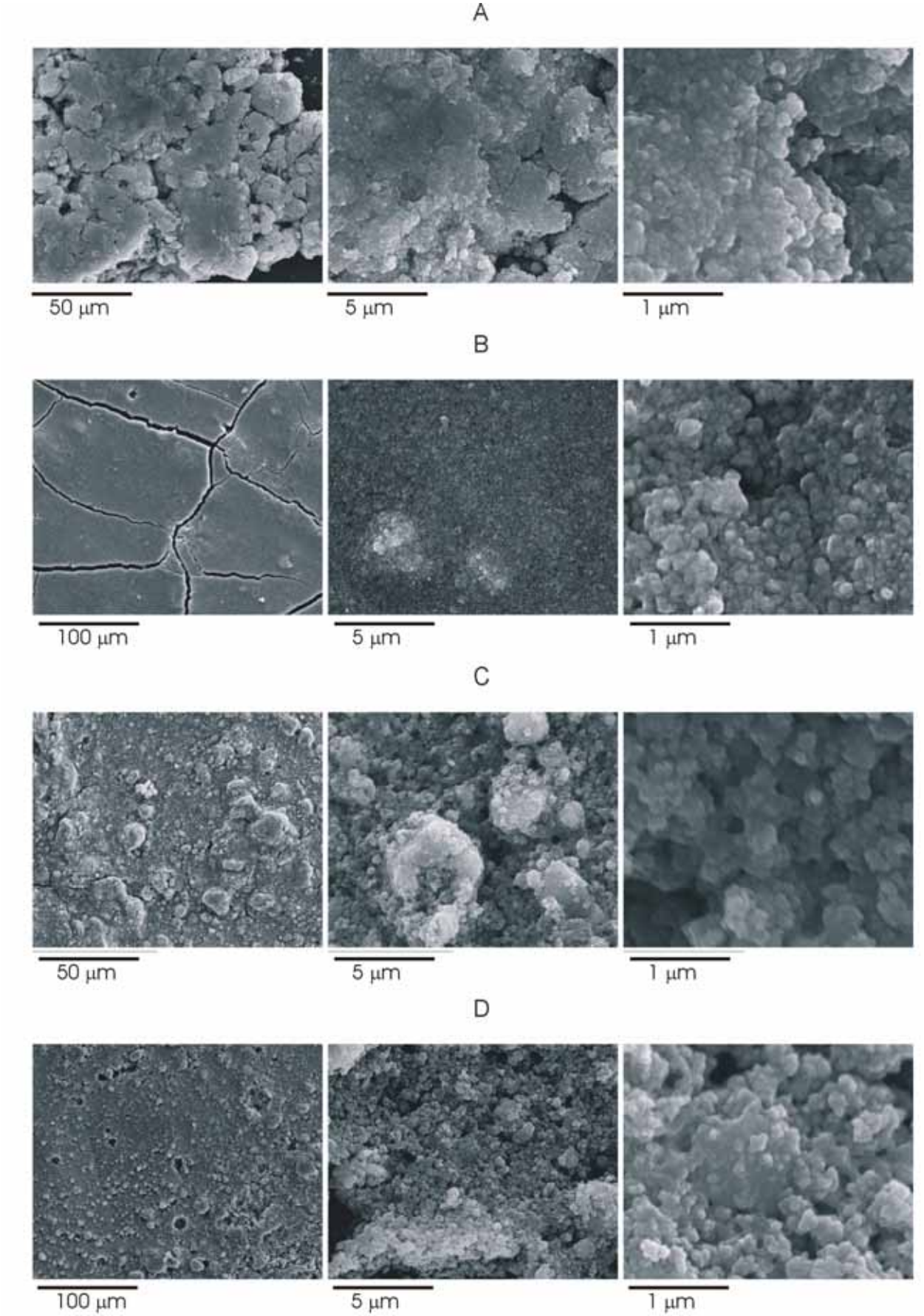

Figure V.14. SEM analysis of active layers A) Non doped WO_3 B) WO_3 doped with 1wt% Au C) WO_3 doped with 1wt% Pd D) WO_3 doped with 1wt% Pt

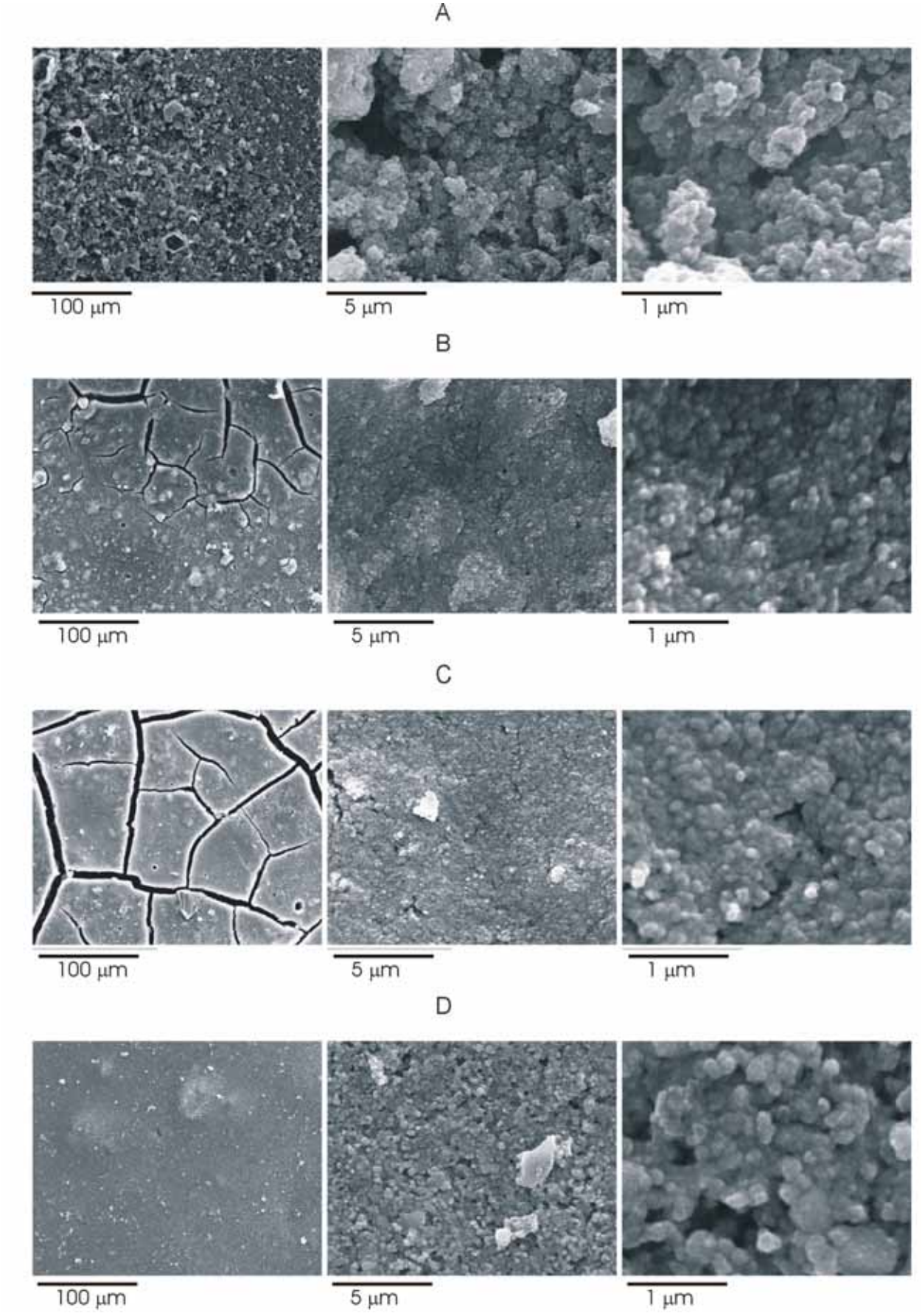

Figure V.15. SEM analysis of active layers A) Non doped WO_3 B) WO_3 doped with 1wt% Au C) WO_3 doped with 2wt% Au D) WO_3 doped with 4wt% Au

For each sample we searched for the best conditions; that is to say, the combination of acceleration voltage and working distance which provided the best-quality image.

The SnO_2 and WO_3 thick films are amorphous. The tin films had a very homogeneous surface. The pictures with small magnification showed that the Au-doped layer is more porous and that the grains are larger. The particles in the non-doped layer formed laminas, probably because of the organic vehicle used in the paste preparation. The Pt and the Pd did not affect the active layer properties.

A comparison of the WO_3 sensors deposited in the same conditions but with the only difference of the Au quantity shows that morphologies can be different for the same type of layer. Once again it can be seen that the Pt and Pd doping did not affect the morphologic properties of the active layers.

It was found that the optimal firing temperature for providing homogenous films was between 450 and 650°C. However, temperatures that were too high caused cracks in the film due to the mechanical stress induced at higher temperatures. For our samples, annealed at 600°C, some active layers appeared with cracks, probably due to film stress during the firing process. For the films studied the average grain size was about 40-60 nm.

We also made maps of the elements of the samples to obtain the doping distribution in the active layer. The conditions in which the maps of elements were made were as follows: the working distance was 34 mm and the acceleration voltage 15 kV. A map is presented in figure V.16. The first image is the real surface from which the map was taken.

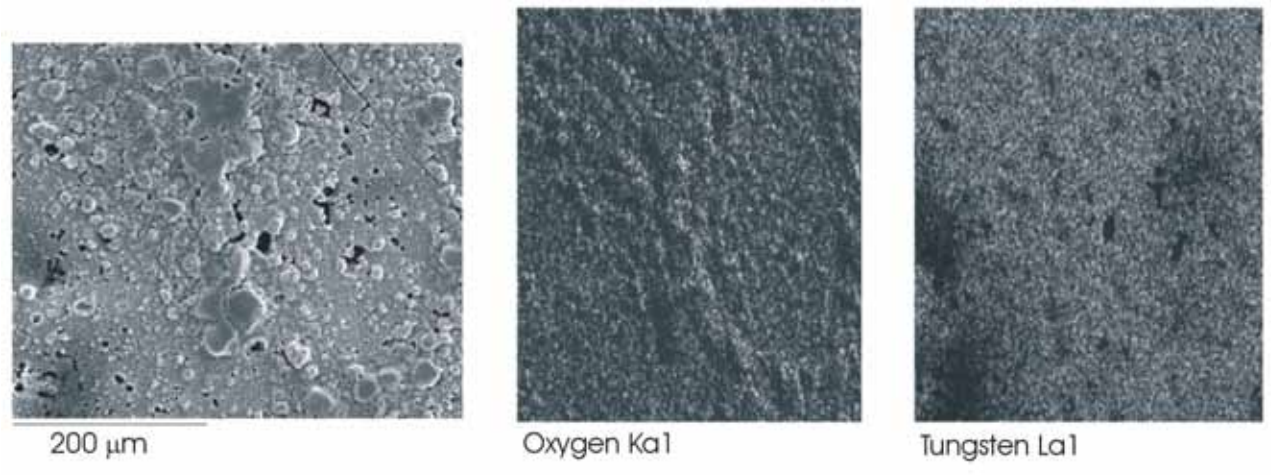

Figure V.16. Map of the elements of the non-doped WO_3 layer

Figure V.17 shows the map of the Pt-doped SnO_2 layer. It seems that some brilliant particles on the surface appeared which can be explained by the presence of Pt [183]. The mean grain size was of the order of 45 nm, which improves the sensing properties [184, 185]. This picture also shows the active area, which has been used lately to obtain the spectrum and to make the qualitative and quantitative analysis. We can see that the Pt atoms were distributed homogeneously in the tin layer (the pictures in the second row show the distribution of the tin, platinum and oxygen atoms). The agglomerates of atoms in the SEM picture (first row-left) could be explained by surface defects and superficial roughness.

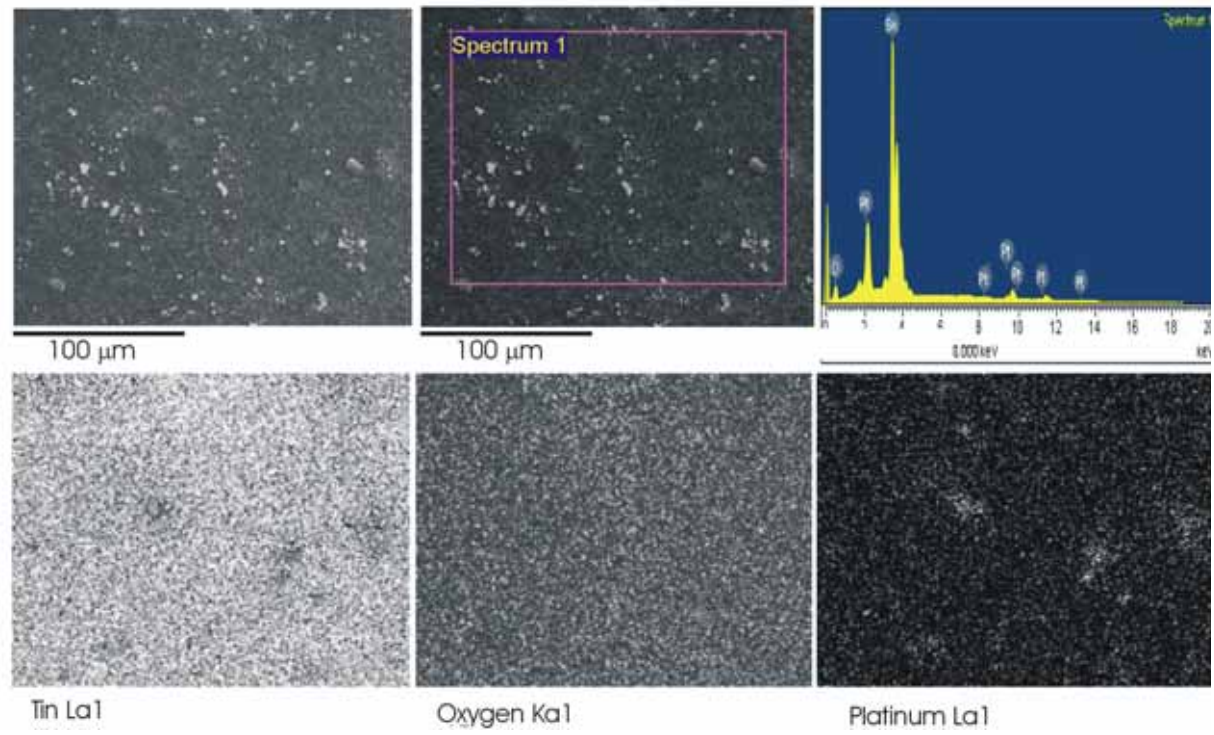

Figure V.17. Map of the elements of the Pt-doped SnO_2 layer

A quantitative analysis was made for each sample in order to define the exact quantity of the doping. For this purpose, doped active layers with no Au coating were investigated (the active layers were not covered with gold, because it was going to influence the quantitative measurements). The results shown in the table below confirm that the quantity detected in the material is very similar to the quantity introduced in the paste. The fabricated sensors were doped with 1wt.% of Pd and Pt and Au (for the SnO_2 sensors) and with 1 wt.% of Pd, 1wt.% of Pt and 1, 2 and 4 wt.% of Au (for the WO_3 sensors).

Table V.4 presents an exhaustive analysis of all the fabricated pastes. The variance between the paste doping and the real value maximum was maximum for 4% gold-doped tungsten-

oxide paste and palladium doping for both types of active layers. The difference between the expected and the real value is approximately 10% (for the Au) and 20% (for the Pd).

Obtained spectrum	Au	Co	Sn	O	Pd	Pt	W	Total (wt.%)
WO_3				17.46			82.54	100
WO_3 +1wt.%Au	1.12			18.01			80.87	100
WO_3 +2wt.%Au	2.08			18.53			79.39	100
WO_3 +4wt.%Au	4.37			20.32			75.31	100
WO_3 +1wt.%Pd				18.72	1.2		80.08	100
WO_3 +1wt.%Pt				23.19		1.17	75.64	100
SnO_2			74.34	25.66				100
SnO_2 +1wt.%Au	1.03		72.21	26.76				100
SnO_2 +1wt.% Pd			74.38	24.37	1.25			100
SnO_2 +1wt.% Pt			72.04	26.87		1.09		100
Reference		100						100
Minimum	1.03	100	72.04	17.46	1.2	1.09	75.31	100
Maximum	4.37	100	74.38	26.87	1.25	1.17	82.54	100

Table V.4. Results of the quantitative analysis (all results are in weight percent)

The use of cobalt sample as reference element ensures the validity of the measurements performed.

V.3.2.2 Surface porosity

We also studied the porosity of the active layers. Porosity, which is defined as the percent of voids in the surface, is a very important factor for the gas sensitivity. If the layer is highly compact, the gas molecules react only at the surface area. On the other hand, if the surface is porous, the gas can penetrate these holes and thus, expand the active surface. Figure V.18 shows a sample measurement of the porosity. The porosity measurements varied between 4 and 15% (values were higher for the doped active layers).

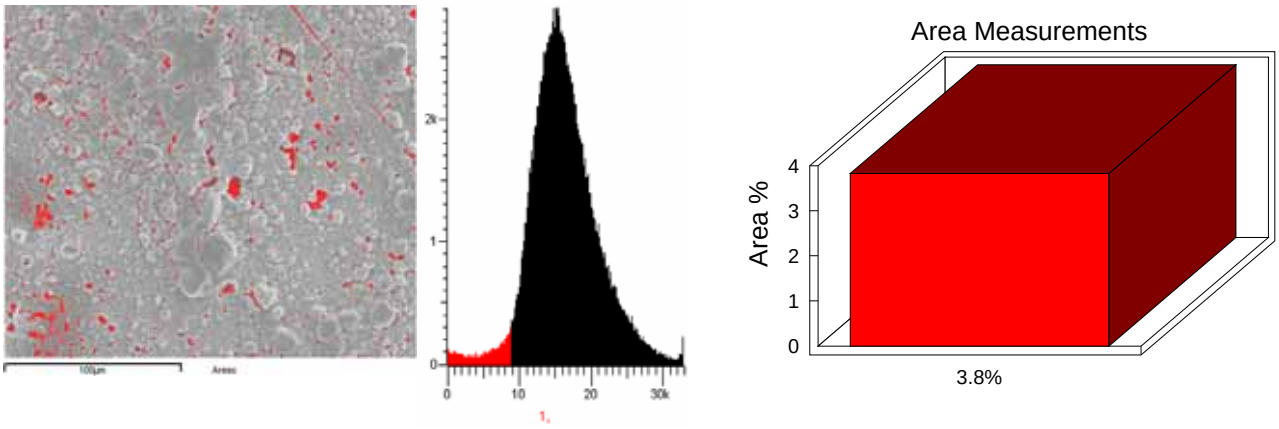

Figure V.18. Analysis of the porosity of the non-doped WO_3 layer

Another important question is whether these porous films adhere well to the substrate. To confirm the continuity of the active layer we took images of the sample cross-section, which proved that the adhesion to the substrate surface good.

V.4 Electrical characterization

The sensors fabricated on Al_2O_3 substrate showed promising results although the power consumption was rather high. In order to obtain sensors with lower power consumption we opted for micro-hotplates. Using integrated circuit technology, we can batch-fabricate thousands of electronic circuits simultaneously through a single processing sequence. By means of a screen-printing technique, sensitive layers of metal oxides (pure and doped tin dioxide and tungsten trioxide) were deposited on silicon micro-machined substrates. The thickness of the sensing layers was 5 μm. Each chip contained four thin silicon nitride membranes, on the centre of which were stacked a poly-silicon heating resistor, insulating layers, platinum electrodes and a sensitive layer. The technological procedure made it possible to deposit the sensing layers before the membranes had been etched. This prevents the membranes from being damaged during film deposition, which leads to gas sensor micro-systems with an excellent fabrication yield. The deposition method overcomes disadvantages such as low porosity and low surface area, generally associated to chemical vapour deposition or sputtering methods, and keeps power consumption low (approximately 80 mW for a working temperature of 480^{o}C).

Five different sets of sensors were created and tested with numerous simple volatile compounds and gases. The properties of the substrate are detailed in Table V.5. The effect of the relative humidity was also studied.

Parameters	Values
Active area size	400 x 400 μm^2
Active layer	Nano-grain SnO_2\WO_3
Active layer thickness	5 μm
Membrane size	900 x 900 μm^2
Inter-electrode distance	50 μm / 100 μm
Heater material	Poly-silicon (16 Ω/sq)
Heater resistance (room temperature)	700 Ω (for the 50 μm gap) 800 Ω (for the 100 μm gap)
Heater power consumption (at 300ºC)	≈ 30 mW
Response time (10-90%) (300ºC)	≈ 20 ms
Electrode material	Platinum

Table V.5. Properties of the MHP substrate

The sets A and B were tested using two different measurement systems —"**Headspace auto-sampler**" and "**Continuous flow system**"— and six temperatures. The binary mixtures were introduced additionally to determine whether one four-sensor chip is capable of discriminating between various gases and their combinations. For the measurements, two four-element integrated micro-arrays were connected in a thermally controlled test chamber. Each array consisted of two sensors with an inter-electrode gap of 50 μm and two with an inter-electrode gap of 100 μm. The temperature was kept constant during the measurement and the relative humidity was 15 %.

The first test system was "**Headspace auto-sampler**". It was used to inject the vapours of the tested species into the chamber. Repeatable concentrations of vapours and vapour mixtures were delivered to a10 ml test chamber at a fixed flow rate of 100 ml/min. Humidity was kept constant at 15% R.H during all the measurement process. Between the different measurements a pause of approximately half an hour was made. Figure V.19 shows the experimental set-up for this system.

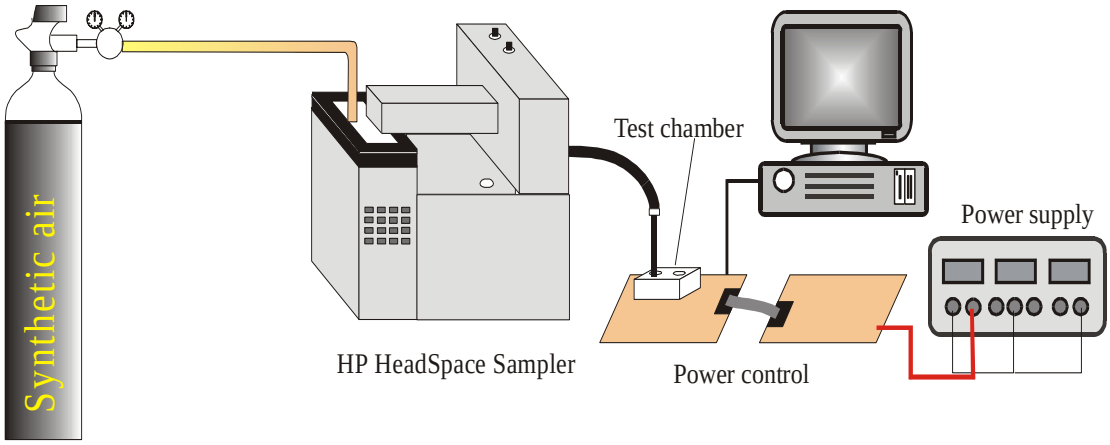

Figure V.19. Headspace auto-sampler system

Sensors were operated at a set of different temperatures between 110 and 480^{o}C. The operating temperature of the microsensors was set by applying a current to their polysilicon heating resistor. Standard A/D computer boards were used to acquire both the resistance of the metal oxide films (to compute sensitivity) and of the polysilicon heaters (to compute operating temperature). The system was controlled via in-house written software, which provides management in real time to all the measurement parameters (applied voltage, temperature of the sensor and resistance of the active layer). Table V.6 summarizes the headspace sampler parameters.

Parameters	Values
Oven temperature	70° C
Loop temperature	75° C
Tr. line temperature	80° C
Vial equilibration time	5 min
Pressurization time	1 min
Loop fill time	1 min
Loop equilibration time	0.05 min
Injection time	10 min
Whole cycle time	45 min
Time between the cycles	25 min

Table V.6. Headspace auto-sampler settings

The second test system was the "**Continuous flow system**", which made the measurements with a total gas flow of 200 ml/min of synthetic air flowing through a 10-ml volume test chamber (Figure V.20).

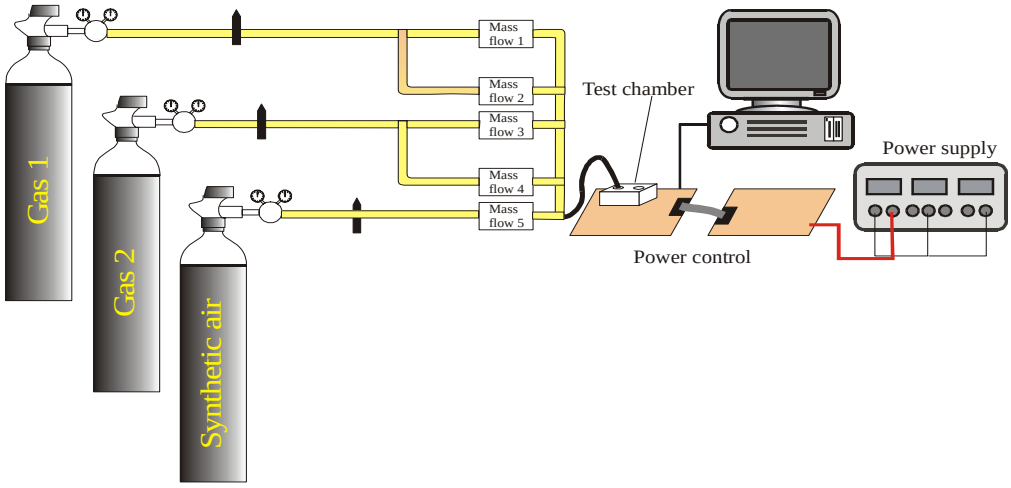

Figure V.20. Continuous flow experimental system

This chamber was connected to a continuous flow system that allowed us to obtain, with high reproducibility, different concentrations of pollutant gases diluted in dry air. Gas mixtures were obtained by computer-supervised mass-flow controllers (Figure V.21).

Figure V.21. Gas flow system: Gases stored in bottles under high pressure (left); Gas transport system (center); Mass-flow controllers (right)

Moisture level was 20% R.H (measured at 30^{o}C ±1^{o}C) during all the measurement process. A written-in-house MATLAB program running on a PC platform was in charge of controlling a data acquisition board. A digital output of the data acquisition board was used to input the signal to a set of Howland voltage-controlled current sources. Each current source injected a current signal to the polysilicon heating resistor of each micro-hotplate sensor (Figure V.22).

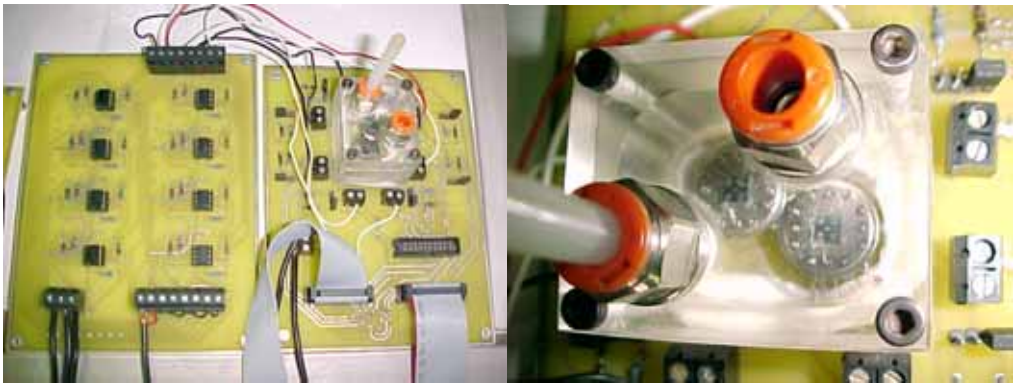

Figure V.22. Experimental system: Howland voltage-controlled current sources (left); Close view of the gas chamber (right)

We used synthetic air as both the reference and diluting gas to obtain the mixtures with different concentrations. During each measurement, the total flow was kept constant. The accuracy of each gas flow meter was ±1 % of its full scale.

V.4.1 Pure SnO_2/WO_3 micro-hotplate gas sensors

The first two sensor sets were fabricated in order to select which grain size is best for the active layer of the thick-film micro-hotplate gas sensors. The measurements clearly showed that the response of the active layers made of nano-particles was better than that of the ones made of micrometric grains. Details about the sensor composition could be found in table V.7.

Set A & Set B					
Metal oxide	**Grain size**	**Inter-electrode distance**	**Doping metal**	**Doping quantity**	**Reference code**
Tin dioxide	Micro-grain	50 μm	None	0 wt.%	Sn_μ_XX_0_50
Tin dioxide	Micro-grain	100 μm	None	0 wt.%	Sn_μ_XX_0_100
Tin dioxide	Nano-grain	50 μm	None	0 wt.%	Sn_n_XX_0_50
Tin dioxide	Nano-grain	100 μm	None	0 wt.%	Sn_n_XX_0_100
Tungsten trioxide	Micro-grain	50 μm	None	0 wt.%	W_μ_XX_0_50
Tungsten trioxide	Micro-grain	100 μm	None	0 wt.%	W_μ_XX_0_100
Tungsten trioxide	Nano-grain	50 μm	None	0 wt.%	W_n_XX_0_50
Tungsten trioxide	Nano-grain	100 μm	None	0 wt.%	W_n_XX_0_100

Table V.7. Non-doped sensors studied

The gases measured are detailed in Table V.8, which also specifies the measurement system used in the different experiments. For the liquid compounds (simple volatiles and binary mixtures), the experiments were performed with the headspace sampler, while for the gas measurements a continuous flow system was used.

Headspace auto-sampler		**Continuous flow**
Simple volatiles	**Binary mixtures**	**Gases**
Ethanol	*Acetone + Ethanol*	*Nitrogen dioxide*
Acetone	*Acetone + Ammonia*	*Carbon monoxide*
Ammonia	*Ammonia + Ethanol*	*Humidity*

Table V.8. Measured species

With these sensors, two different experiments were performed. In the first one, the sensitivity of the sensors to ammonia, ethanol and acetone vapours, and their binary mixtures was studied. For this purpose, different concentrations of the vapours were delivered to the 10 ml test chamber at a fixed flow rate of 100 ml/min. Humidity was kept constant at 15% R.H (measured at 30°C ±1°C) throughout the measurement process. The sensors were operated at three different temperatures between 110 and 480°C. Before the measurements were started, the sensors were kept at the maximum temperature for 8 hours. Data acquisition started 40 seconds before the volatiles were injected into the sensor chamber (initially clean air flowed through the chamber, so the baseline sensor resistance could be recorded). An automatic static headspace sampling system injected a sample of the volatiles in the airflow. A typical sensor response can be observed in Figure V.23. Similar sensors behave in the same way, which shows that reproducibility is good.

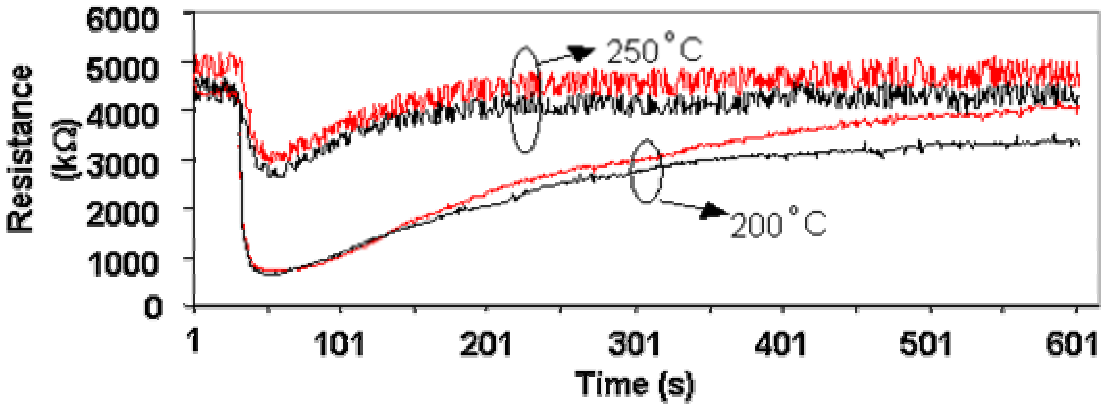

Figure V.23. Typical response of four SnO_2 sensors to NH_3 (two sensors with a 50μm interelectrode gap operated at 200℃ and two sensors with a 100μm gap operated at 250℃)

Every measurement took 10 minutes to complete and was replicated 5 times. The concentrations of the single gases and gas mixtures shown in Table V.9 were estimated by injecting the samples delivered by the headspace auto-sampler into a calibrated GC-MS system (Shimadzu, Inc.).

	Ethanol	Acetone	Ammonia		Ethanol	Acetone	Ammonia
Single vapour	1.0C	-	-	**Binary mixtures**	1.0C	2.5C	-
	2.8C	-	-		2.8C	5.5C	-
	7.3C	-	-		7.3C	11.0C	-
	-	2.5C	-		1.0C	-	25.0C
	-	5.5C	-		2.8C	-	37.5C
	-	11.0C	-		7.3C	-	75.0C
	-	-	25.0C		-	2.5C	25.0C
	-	-	37.5C		-	5.5C	37.5C
	-	-	75.0C		-	11.0C	75.0C

Table V.9. Concentrations used for the measurements performed with simple gases and binary mixtures (C=25 ppm)

Finally, the response of the sensors to different levels of moisture (between 10 and 70% R.H. at 30^{o}C) in air was also investigated. For this purpose, a computer-driven system was used to inject a continuous flow of humidified air into the sensor chamber.

In the second experiment, the sensor response to NO_2 and CO was also investigated. For these measurements, the sensor arrays from experiment one were tested in the same chamber using a continuous flow system. The temperature was kept constant during each measurement and the relative humidity was 10 %. The sensors were operated at the same working temperatures as in the other measurements. Each measurement was replicated five times.

The graphics below summarize the results of the sensitivity study. The values in the graphics are the averages of five replicate measurements and the optimal results are highlighted. The operating temperatures were 110, 200 and 380^{o}C for the sensor with the 50μm gap between

electrodes and 150, 250 and 480^{o}C for the sensors with the 100μm gap between the electrodes. The differences in operating temperatures are due to the fact that membranes with different gaps between the electrodes had different values of the heating poly-silicon resistors (i.e. 600 Ω and 700 Ω for the sensor with a gap between the electrodes of 50μm and 100μm, respectively) and the same heating current was injected into these resistors. The power consumption of the membranes operated at 480^{o}C was around 80 mW. Devices with a 50μm gap between electrodes have higher sensitivities at lower operating temperatures than those with a 100μm gap between electrodes. As we stated above, these results are in good agreement with the theory of porous active layers with a uniform distribution of active sites, which predicts that sensor response will increase if electrode spacing is reduced and film thickness and electrode length are unchanged. The response curves prove that the technological processes used lead to very sensitive metal oxide micro-sensor arrays with a very high yield (more than 95% of the micro-sensors work after dicing, wire bonding and packaging).

The sensors are very sensitive to ammonia and ethanol. They are much less sensitive to acetone than to ammonia. Accordingly, sensitivities were highest for binary mixtures containing ammonia. This explains why the sensitivity to the binary mixture of acetone and ethanol was lowest. The sensitivity to the volatiles studied increased significantly when the working temperature of the sensors was increased.

We examined the sensor response to NO_2 and CO. All sensors reacted to NO_2, but only the sensors with a SnO_2 active layer reacted to CO. Therefore, the sensors with a WO_3 active layer did not show cross sensitivity and were used for NO_2 detection in the presence of CO. Response to nitrogen dioxide was as high as 106 for the SnO_2 layer at 250ºC, while the best reaction for the tungsten active layer was 6 times lower. The sensor reaction to carbon monoxide was very low. For the highest operation temperature and concentration, the resistance only doubled.

In all cases, except for the binary mixture of ammonia and ethanol (WO_3 sensor with an inter-electrode gap of 50μm), the sensitivity of the SnO_2 sensors was greater than that of the WO_3 sensors. This may be because agglomerates form in the SnO_2 layers and make the film more porous. Thus, the response of the sensors to the tested species was better.

The repeatability of SnO_2 sensors was very good. For each vapour or mixture and concentration measured, the ratio between the standard deviation of the response and its mean value (over five replicate measurements) was below 1.3×10^{-1}. For the WO_3 sensors, the results for the repeatability were even better: 4.1×10^{-2}. The lower this ratio is, the better the repeatability is.

The response of the sensors to variations in the ambient moisture was also studied. It was observed that the sensor resistance decreased when the relative humidity was increased. Furthermore, when the sensors were operated at higher temperatures, the change in their resistance caused by a change in the moisture level was higher. The graphics below show the ratio between the resistance of the sensors at 10% R.H. (this humidity level is taken as a reference value) and different humidity levels up to 85% R.H. The minimum values are in blue. The response to moisture can be considered as moderate, when compared to the sensitivities found for the different vapours studied.

The results from the two non-doped sensor sets are presented below. The codification used is described in table V.7. A simple sensor code is composed by the following fields: Active layer, Grain size, Doping metal, Doping quantity, Inter-electrode distance).

A) The first set consisted of the following SnO_2 micro-hotplate gas sensors:

- ***SnO_2 based on micrometric grains (Sn_μ_XX_0_50, Sn_μ_XX_0_100)***
- ***SnO_2 based on nanometric grains (Sn_n_XX_0_50, Sn_n_XX_0_100)***

The three groups of graphics below (V.24, V.25 and V.26) describe the first set, consisting of the SnO_2 MHP gas sensors. The results are based on the measurements performed with four sensor chips. Each chip is composed by 4 individual sensors (two sensors with 50 μm interelectrode distance and two sensors with 100 μm interelectrode distance). In this set, two sensor chips have active layers based on micrometric grains, while the other two have active layers based on nanometric grains. In appendix B, detailed information about the results obtained can are summarized (the best results are highlighted in the tables; the minimum values, where minimum sensitivity is needed are in blue and the measured species, for which no result was detected, are marked in green).

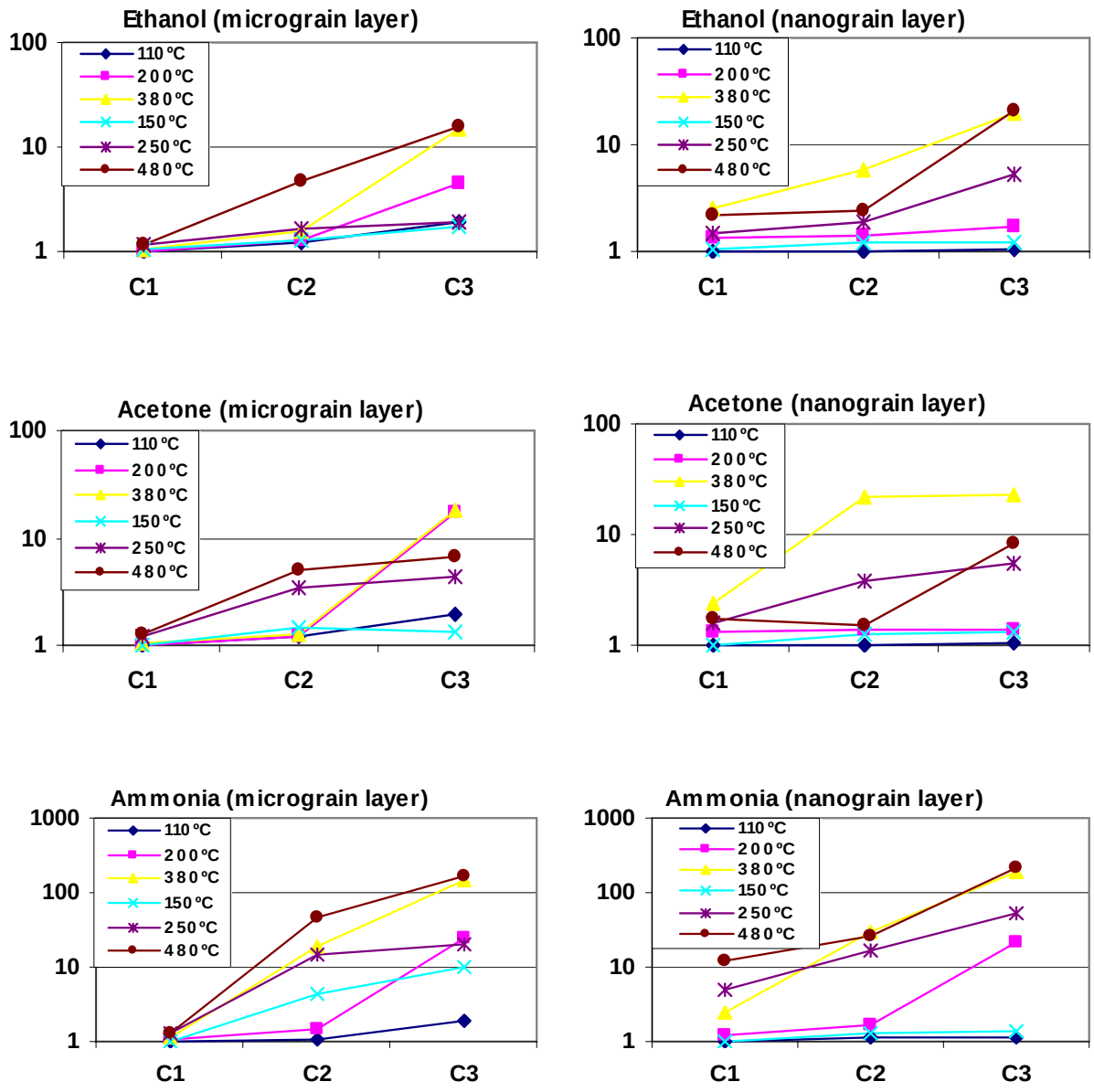

Figure V.24. Non-doped SnO_2 sensor responses to simple volatile: ethanol, acetone and ammonia (Sensors: Sn_μ_XX_0_50, Sn_μ_XX_0_100, Sn_n_XX_0_50, Sn_n_XX_0_100).

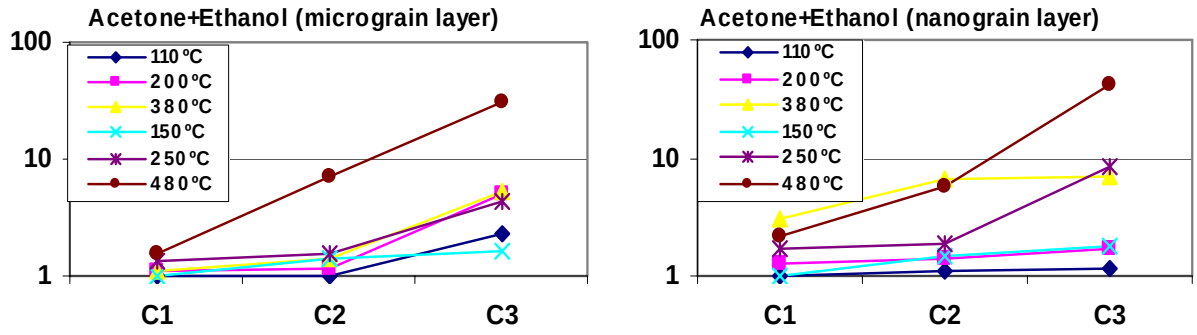

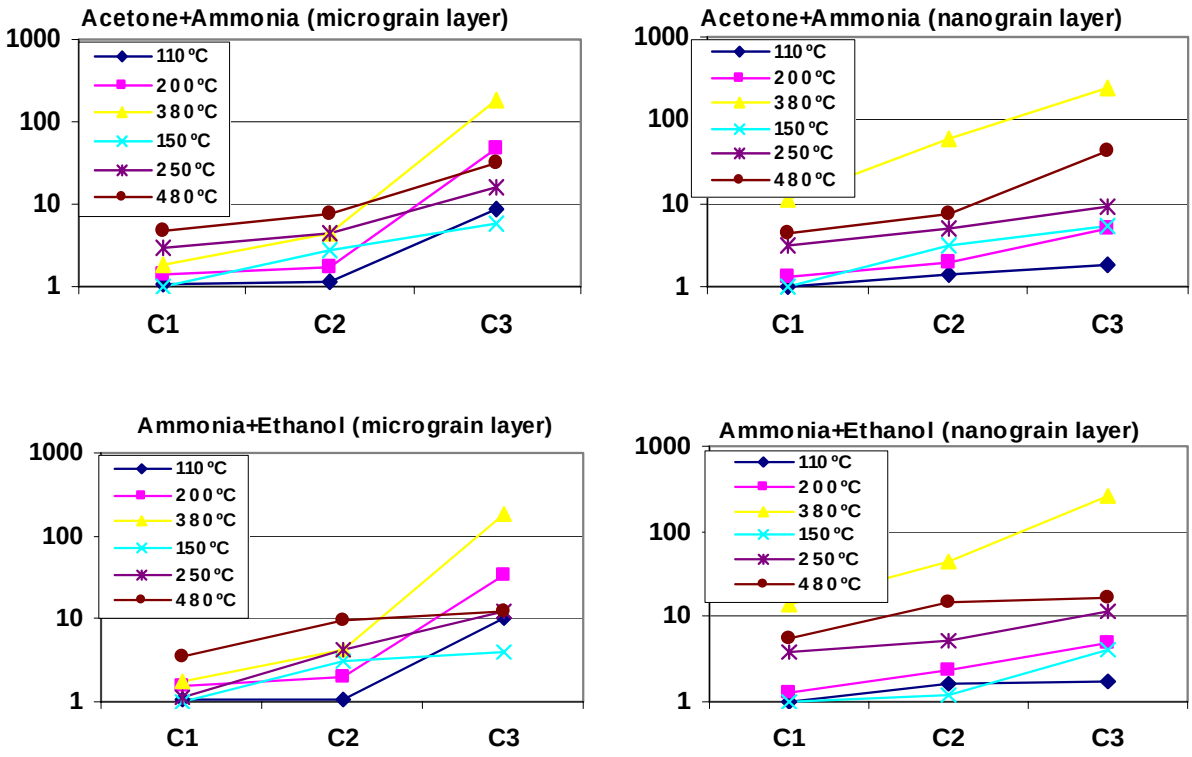

Figure V.25. Non-doped SnO_2 sensor responses to binary mixtures: acetone+ ethanol, acetone + ammonia and ammonia+ ethanol (Sensors: Sn_μ_XX_0_50, Sn_μ_XX_0_100, Sn_n_XX_0_50, Sn_n_XX_0_100).

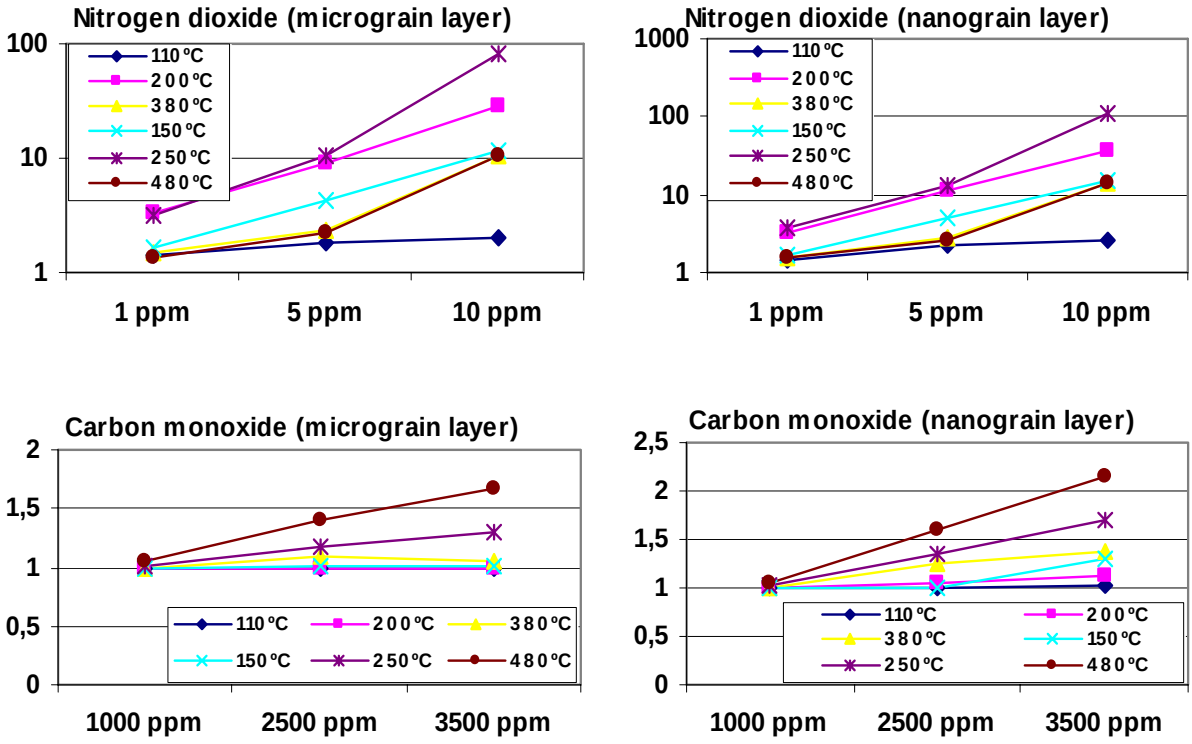

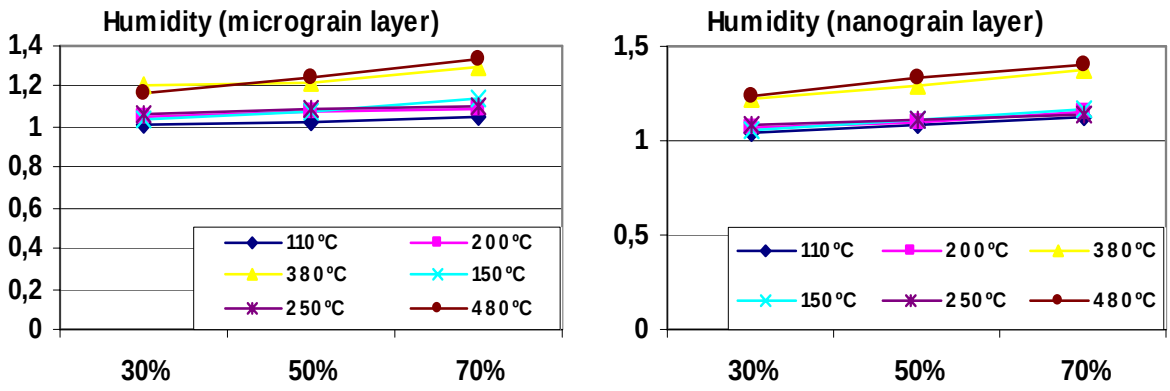

Figure V.26. Non-doped SnO_2 sensor responses to gases: nitrogen dioxide, carbon monoxide and humidity (Sensors: Sn_µ_XX_0_50, Sn_µ_XX_0_100, Sn_n_XX_0_50, Sn_n_XX_0_100).

B) The second set consisted of the following WO_3 micro-hotplate gas sensors:

- ***WO_3 based on micrometric grains (W_µ_XX_0_50, W_µ_XX_0_100)***
- ***WO_3 based on nanometric grains (W_n_XX_0_50, W_n_XX_0_100)***

The three groups of graphics below (V.27, V.28 and V.29) describe the second set, consisting of the WO_3 MHP gas sensors. No graphic was presented for carbon monoxide as no response was obtained during the measurements with this sensor set. The results are based no the measurements performed with four sensor chips. Each chip is composed by 4 individual sensors (two sensors with 50 µm interelectrode distance and two sensors with 100 µm interelectrode distance). In this set, two sensor chips have active layers based on micrometric grains, while the other two have active layers based on nanometric grains. As we stated before, in appendix B, detailed information about the results obtained can be achieved.

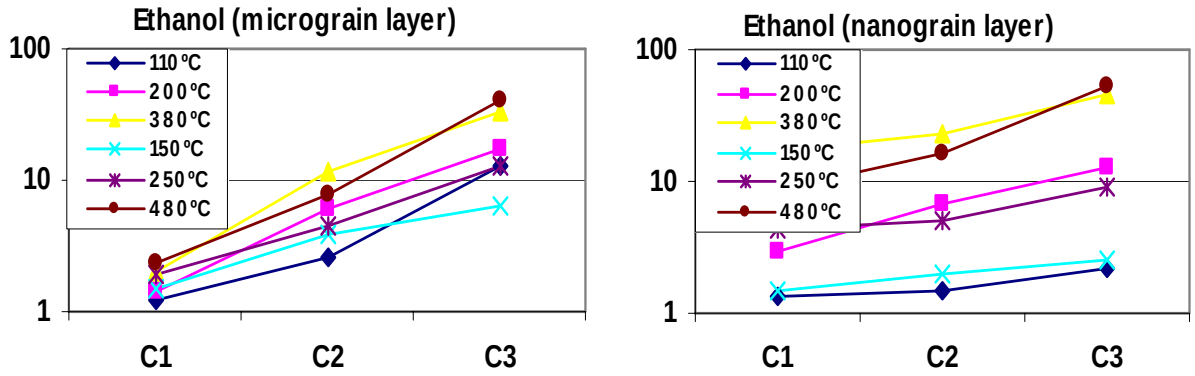

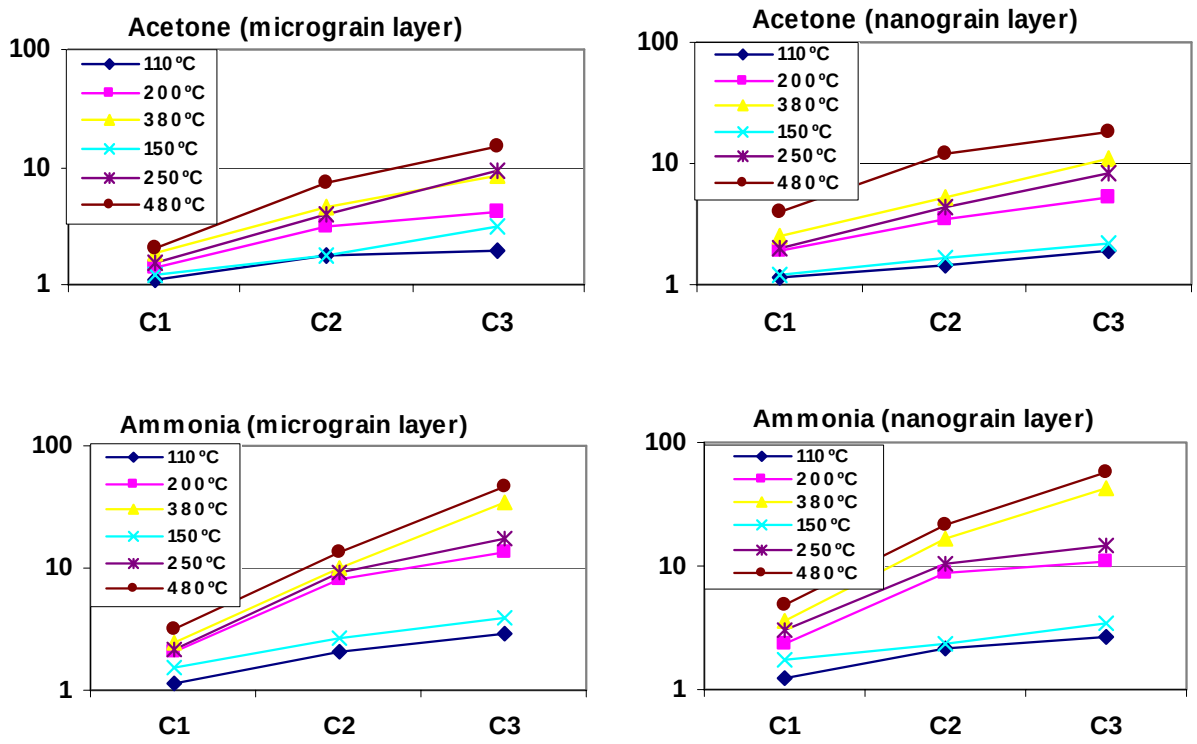

Figure V.27. Non-doped WO_3 sensor responses to simple volatile: ethanol, acetone and ammonia (Sensors: W_μ_XX_0_50, W_μ_XX_0_100, W_n_XX_0_50, W_n_XX_0_100).

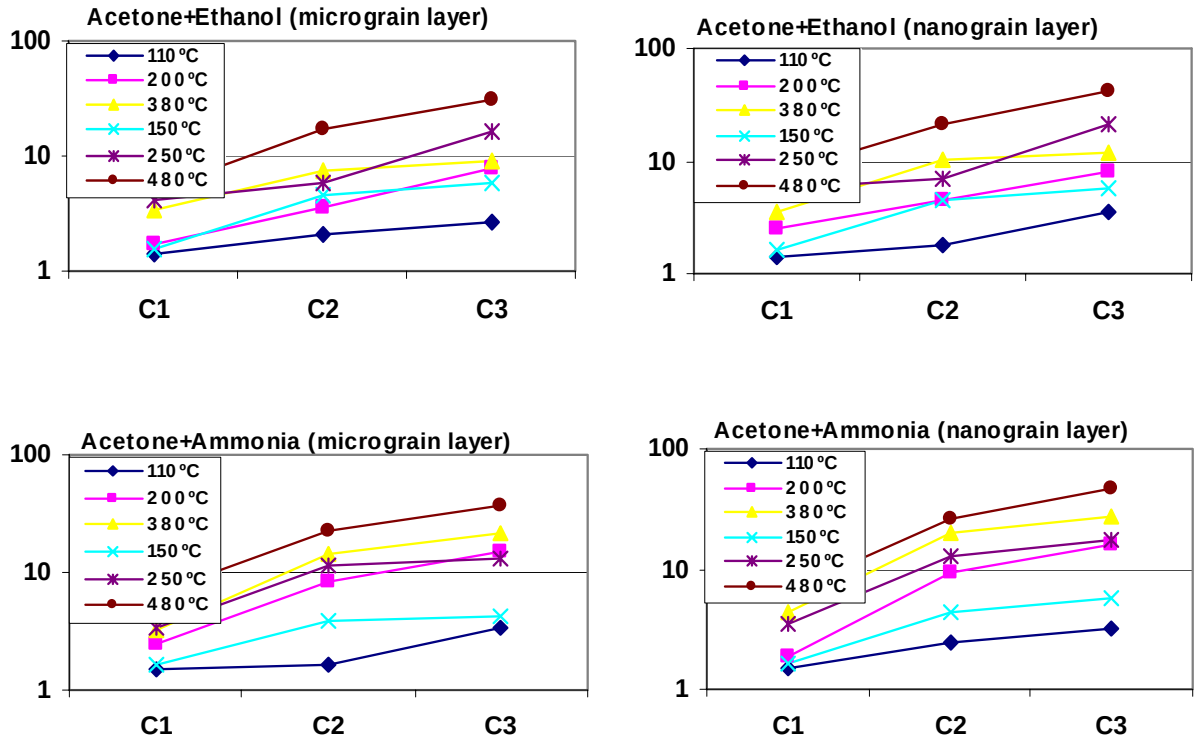

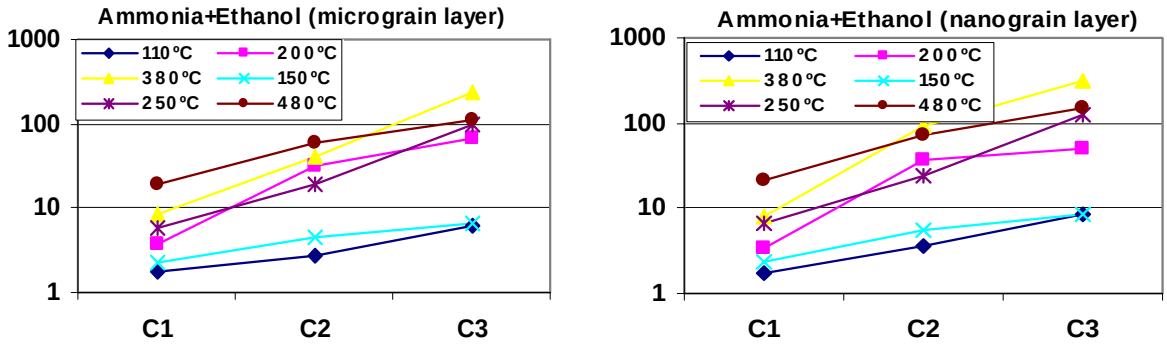

Figure V.28. Non-doped WO_3 sensor responses to binary mixtures: acetone + ethanol, acetone + ammonia and ammonia + ethanol (Sensors: W_μ_XX_0_50, W_μ_XX_0_100, W_n_XX_0_50, W_n_XX_0_100).

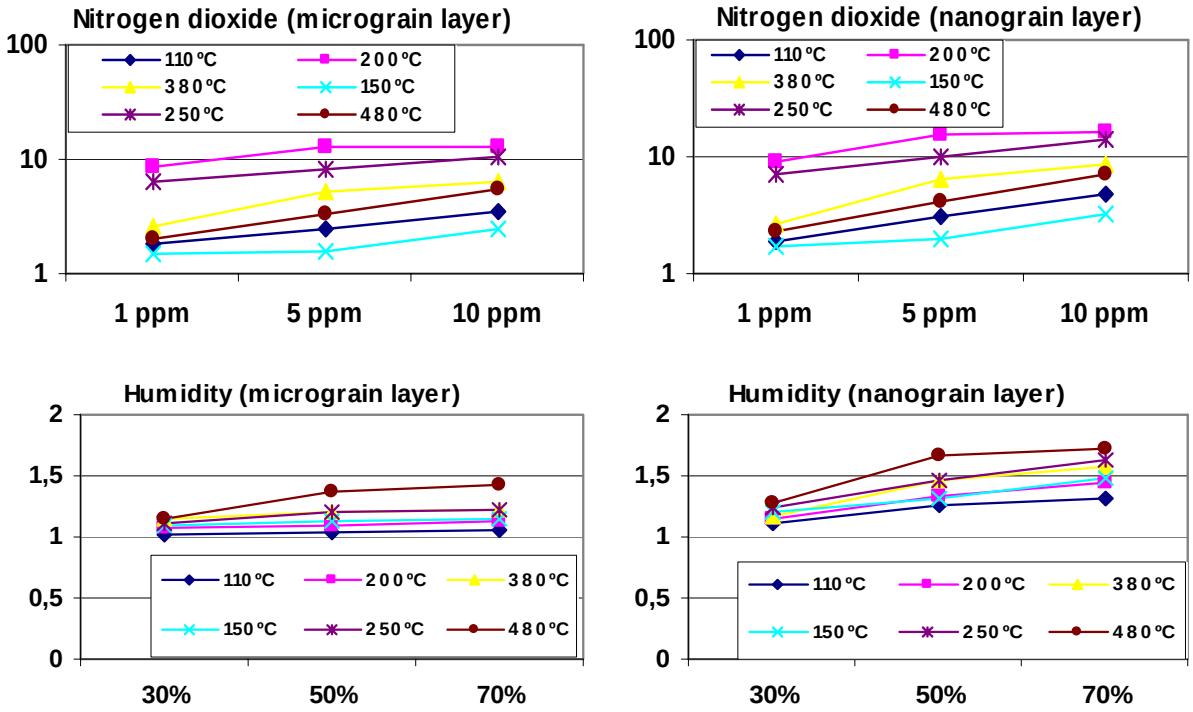

Figure V.29. Non-doped WO_3 sensor responses to gases: nitrogen dioxide and humidity.

To sum up, a new technological procedure for fabricating micro-machined gas sensors and gas-sensing micro-systems has been presented. It combines the advantages of micro-machined silicon structures and screen-printed tin and tungsten oxide sensing films. The techniques used to deposit the sensitive layers and the conventional microelectronic techniques used to fabricate the integrated micro-hotplates are shown to be completely compatible. Silicon micro-machined structures are of interest because they considerably reduce the power consumption of metal-oxide based gas sensors. Furthermore, the low thermal inertia of such structures enables the sensor operating temperature to be effectively cycled, which makes it

possible to analyse multi-component gas mixtures. Screen-printed active layers are of interest because the microstructure of the film is well defined. The porosity (and surface area) of screen-printed films is higher than that of the films deposited by CVD or sputtering techniques. Thicker and more porous films are also more resilient to aging than thin layers. The sensitivity of the fabricated sensors to various volatile organic compounds and their binary mixtures was investigated. The sensitivities to the species tested were good (as high as 250). Micro-sensors with smaller inter-electrode gaps were more sensitive at lower operating temperatures than micro-sensors with bigger inter-electrode gaps.

V.4.2 Doped SnO_2/ WO_3 micro-hotplate gas sensors

In order to obtain comparable results, only one measurement system (the "Continuous flow system") and three temperatures were used for sets C, D and E. This was possible because all the sensors tested had the same inter-electrode gap (50 μm) and the same heater resistance (≈700Ω). Because the results from sets A and B showed that the response of sensors fabricated from nano-powders was better than that of the ones fabricated with micro-powders, for sets C, D and E only nano-powders were used. Details about the sensor composition could be found in table V.10.

Set C & Set D & Set E					
Metal oxide	**Grain size**	**Inter-electrode distance**	**Doping metal**	**Doping quantity**	**Reference code**
Tin dioxide	Nano-grain	50 μm	None	0 wt.%	Sn_n_XX_0_50
Tin dioxide	Nano-grain	50 μm	Gold	1 wt.%	Sn_n_Au_1_50
Tin dioxide	Nano-grain	50 μm	Palladium	1 wt.%	Sn_n_Pd_1_50
Tin dioxide	Nano-grain	50 μm	Platinum	1 wt.%	Sn_n_Pt_1_50
Tungsten trioxide	Nano-grain	50 μm	None	0 wt.%	W_n_XX_0_50
Tungsten trioxide	Nano-grain	50 μm	Gold	1 wt.%	W_n_ Au_1_50
Tungsten trioxide	Nano-grain	50 μm	Gold	2 wt.%	W_n_ Au_2_50
Tungsten trioxide	Nano-grain	50 μm	Gold	4 wt.%	W_n_ Au_4_50
Tungsten trioxide	Nano-grain	50 μm	Palladium	1 wt.%	W_n_ Pd_1_50
Tungsten trioxide	Nano-grain	50 μm	Platinum	1 wt.%	W_n_ Pt_1_50

Table V.10. Doped sensors studied

The gases measured with these sensors were ammonia, ethanol, ethylene, nitrogen dioxide, carbon monoxide, hydrogen sulphide, methane and humidity. Special attention was dedicated to the ethylene. In the last few years, the monitoring of ethylene such as ripening agent has received a great deal of attention. Ethylene gas causes fruits to ripen and decay, vegetables and floral to wilt. Controlling ethylene gas after picking extend the life cycle of the fruit, allowing to be held for much longer period of time. While refrigeration and humidity slow decay, they do not halt the production of harmful ethylene gas. Ethylene gas is also used in ripening rooms to colour up the fruit, which then is moved to a regular cold storage room with other products. Some fruits gassed with ethylene are bananas, tomatoes and avocados. Ethylene gas and its removal are both important in giving the consumer the best possible product. While ethylene gas is used under controlled conditions as a ripening agent, even small amounts of ethylene gas during shipping and storage causes most fresh produce to deteriorate faster. Automotive emissions, plastics and smoke all increase ethylene gas levels.

The results from the three doped sensor sets are presented below. The codification used is described in table V.10. A simple sensor code is composed by the following fields: Active layer, Grain size, Doping metal, Doping quantity, Inter-electrode distance).

C) The third set consisted of the following 1%wt. doped SnO_2 MHP sensors

- ***SnO_2 based on nanometric grains (Sn_n_XX_0_50)***
- ***SnO_2 doped with 1wt% Au (Sn_n_Au_1_50)***
- ***SnO_2 doped with 1wt% Pd (Sn_n_Pd_1_50)***
- ***SnO_2 doped with 1wt% Pt (Sn_n_Pt_1_50)***

The two groups of graphics below (V.30 and V.31) present all the results obtained from the measurements of set C. The results are based no the measurements performed with two sensor chips. Each chip is composed by 4 individual sensors (one non-doped and tree doped). No graphic was presented for hydrogen sulphide and methane as no response was obtained during the measurements with this sensor set. In appendix B, detailed information about the results obtained can be achieved: the best doping for the measured specimen is highlighted and the best result is marked in red; the measured gases with no response are indicated in green; in some cases, where minimum sensitivity is desired (for example in the case of humidity) the optimal values are in blue.

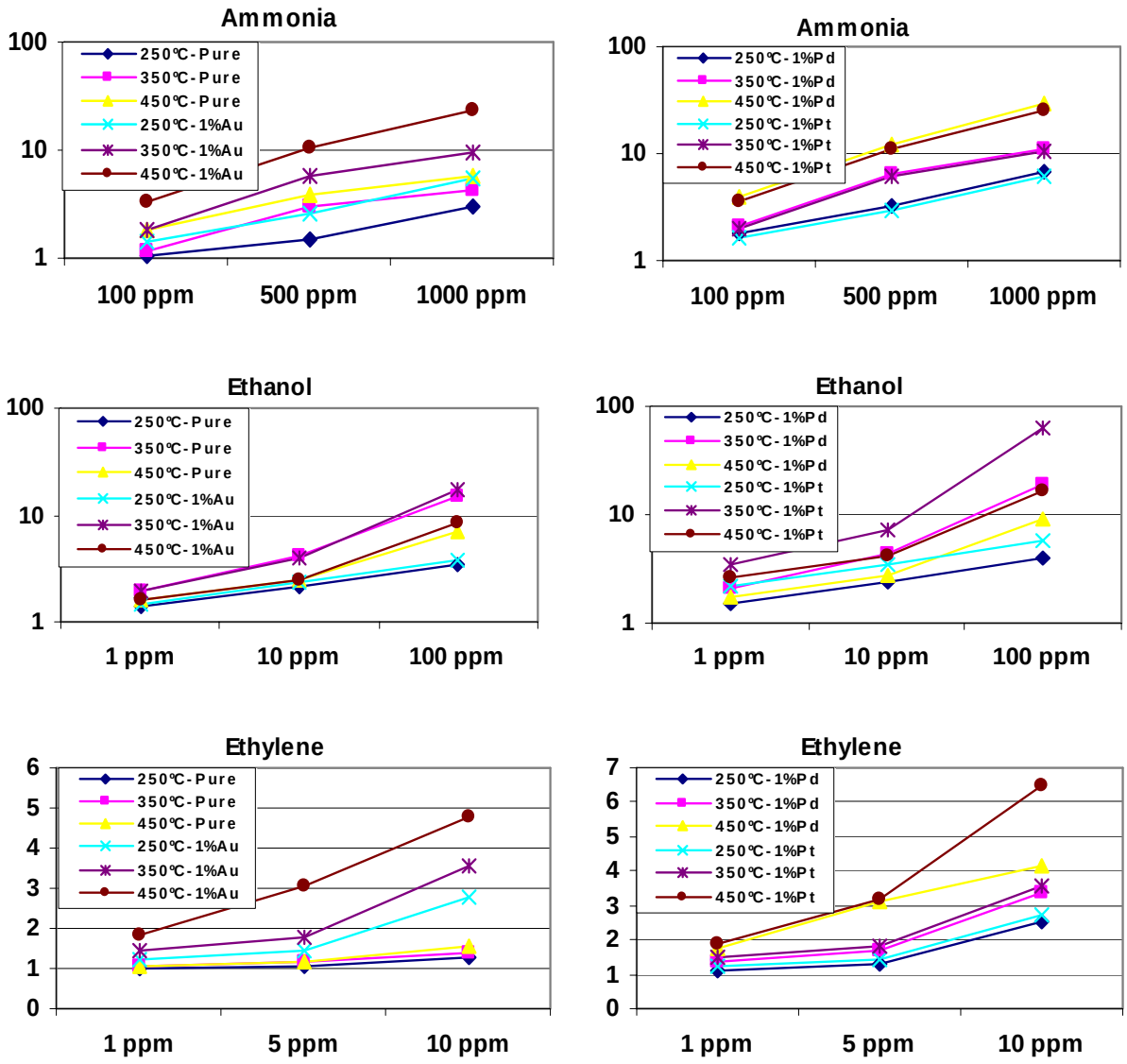

Figure V.30 Doped SnO_2 sensor responses to ammonia, ethanol and ethylene (Sensors: Sn_n_XX_0_50, Sn_n_Au_1_50, Sn_n_Pd_1_50, Sn_n_Pt_1_50).

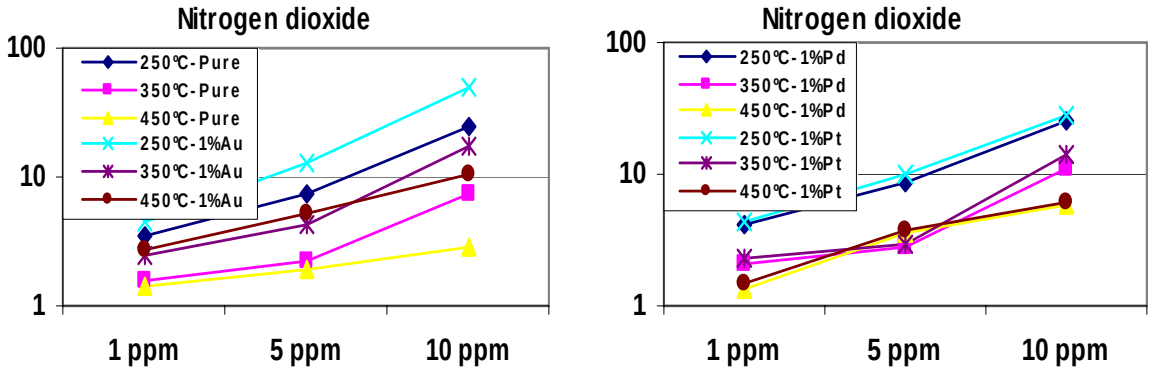

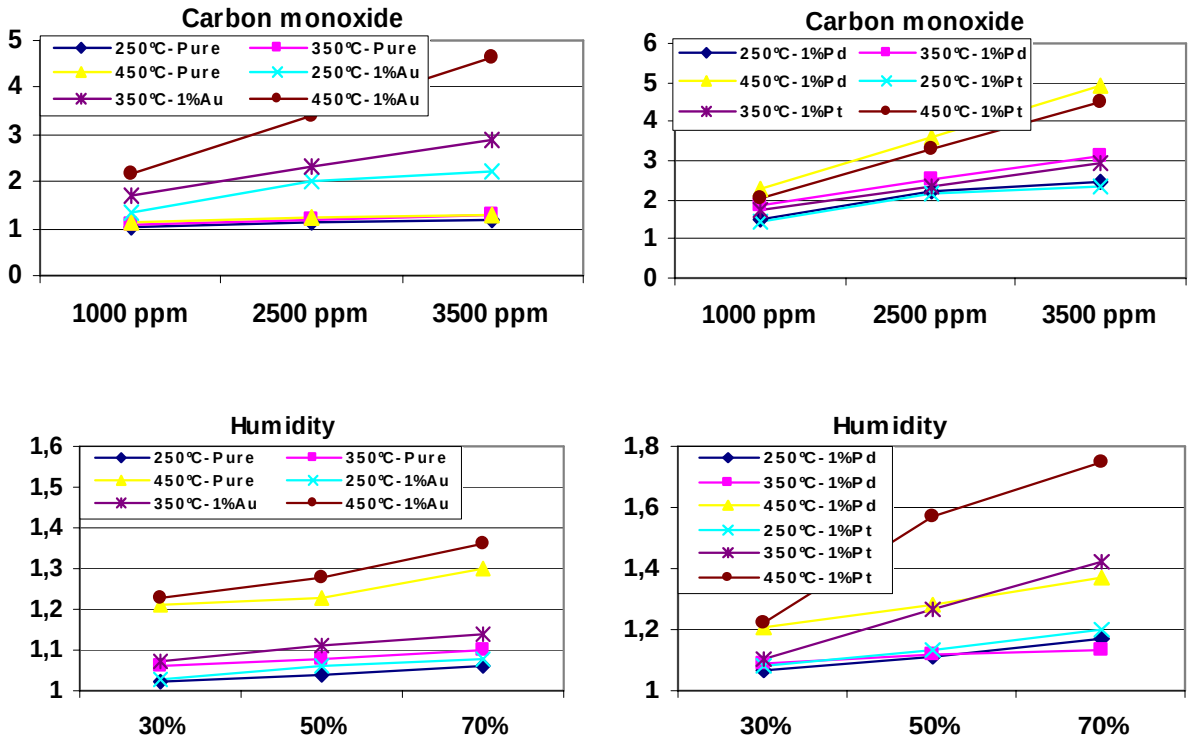

Figure V.31 Doped SnO_2 sensor responses to nitrogen dioxide, carbon monoxide and humidity (Sensors: Sn_n_XX_0_50, Sn_n_Au_1_50, Sn_n_Pd_1_50, Sn_n_Pt_1_50)

The Pd-doped sensors showed the best response to ammonia. It was up to 6 times higher than that of the undoped SnO_2 sensors. The graphics clearly show that the Pt-doped sensors had the best reaction to ethanol (10 times higher than the un-doped ones). The Pt doping also promotes the detection of ethylene. If our aim is to detect toxic gases, the best doping for NO_2 is gold, while for CO the best is Pd. No SnO_2 sensors responded to methane or H_2S. Nevertheless, in the humidity tests, the doping does not considerably affect the sensor performance. Response was minimum for the non-doped layers, while the Pt doping catalyzes this reaction well.

D) The fourth set consisted of the following 1%wt. doped WO_3 MHP sensors

- ***WO_3 based on nano-metric grains (W_n_XX_0_50)***
- ***WO_3 doped with 1wt% Au (W_n_Au_1_50)***
- ***WO_3 doped with 1wt% Pd (W_n_Pd_1_50)***
- ***WO_3 doped with 1wt% Pt (W_n_Pt_1_50)***

The two groups of graphics below (V.32 and V.33) present all the results obtained from the measurements of set D. The results are based on the measurements performed with two sensor chips. Each chip is composed by 4 individual sensors (one non-doped and tree doped). No graphic was presented for ethylene, carbon monoxide and methane as no response was obtained during the measurements with this sensor set.

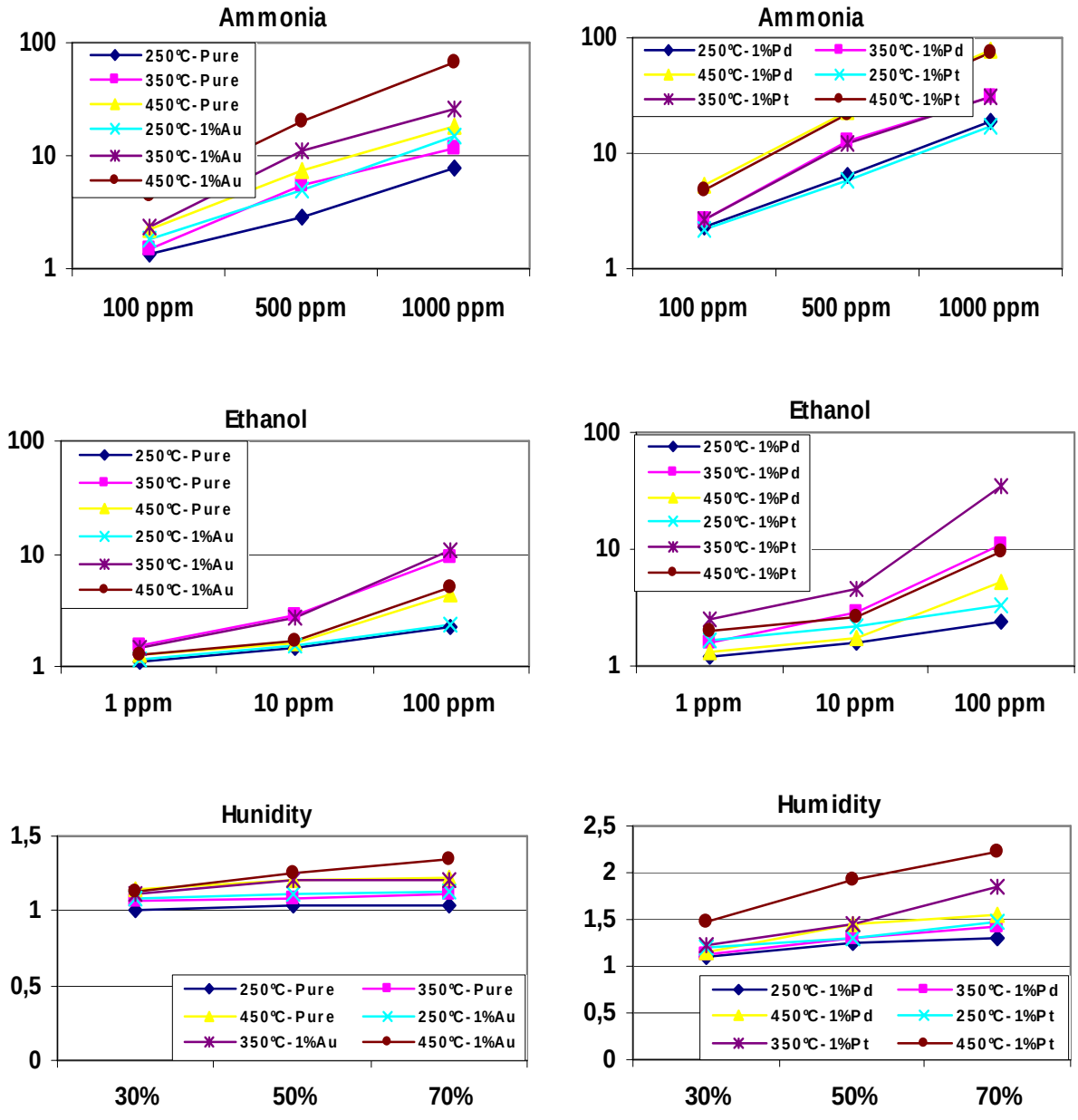

Figure V.32 Doped WO_3 sensor responses to ammonia, ethanol and humidity (Sensors: W_n_XX_0_50, W_n_Au_1_50, W_n_Pd_1_50, W_n_Pt_1_50).

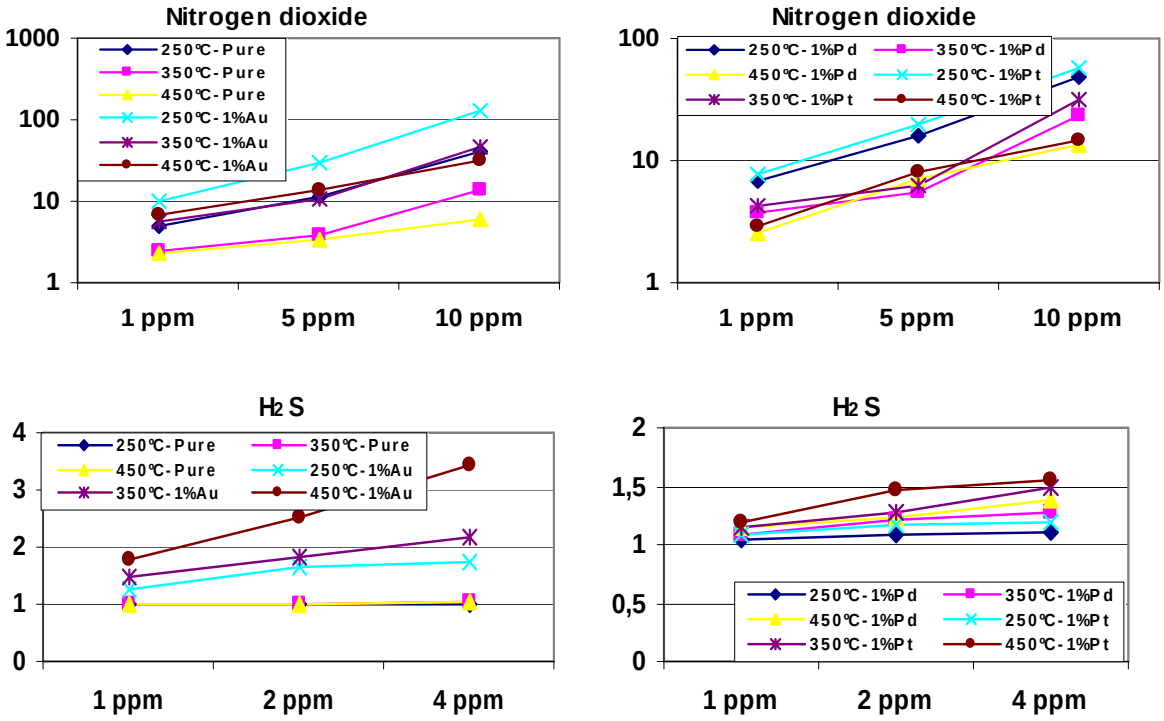

Figure V.33 Doped WO_3 sensor responses to nitrogen dioxide and hydrogen sulphide (Sensors: W_n_XX_0_50, W_n_Au_1_50, W_n_Pd_1_50, W_n_Pt_1_50).

The WO_3 layer showed excellent response to ammonia and NO_2. The change in the sensor resistance is more than 78 for the Pd-doped sensor when sensing ammonia and 127 times for the Au doped sensor, when sensing NO_2. The response to ethanol decreases twice if comparing with the SnO_2 layer. The sensors reacted to H_2S, for which the best doping was Au. The response was best at the highest working temperature (450°C). These sensors did not react to the ethylene, carbon monoxide and methane at any of the studied temperatures. The humidity response for the tungsten oxide sensors was higher than in the case of the tin oxide, but if we compare it with the sensor response to the tested species, it could be considered to be negligible.

E) The last set consisted of the following, multi-quantity doped WO_3 MHP sensors

- ***WO_3 based on nano-metric grains (W_n_XX_0_50)***
- ***WO_3 doped with 1wt% Au (W_n_Au_1_50)***
- ***WO_3 doped with 2wt% Au (W_n_ A _2_50)***
- ***WO_3 doped with 4wt% Au (W_n_ Au_4_50)***

The two groups of graphics below (V.34 and V.35) present all the results obtained from the measurements of set E. The results are based on the measurements performed with two sensor chips. Each chip is composed by 4 individual sensors (one non-doped and tree doped). No graphic was presented for ethylene as no response was obtained during the measurements with this sensor set. In appendix B, detailed information about the results obtained can be achieved: the best doping for the measured specimen is highlighted and the best result is marked in red; the measured gases with no response are indicated in green; in some cases, where minimum sensitivity is desired (for example in the case of humidity) the optimal values are in blue.

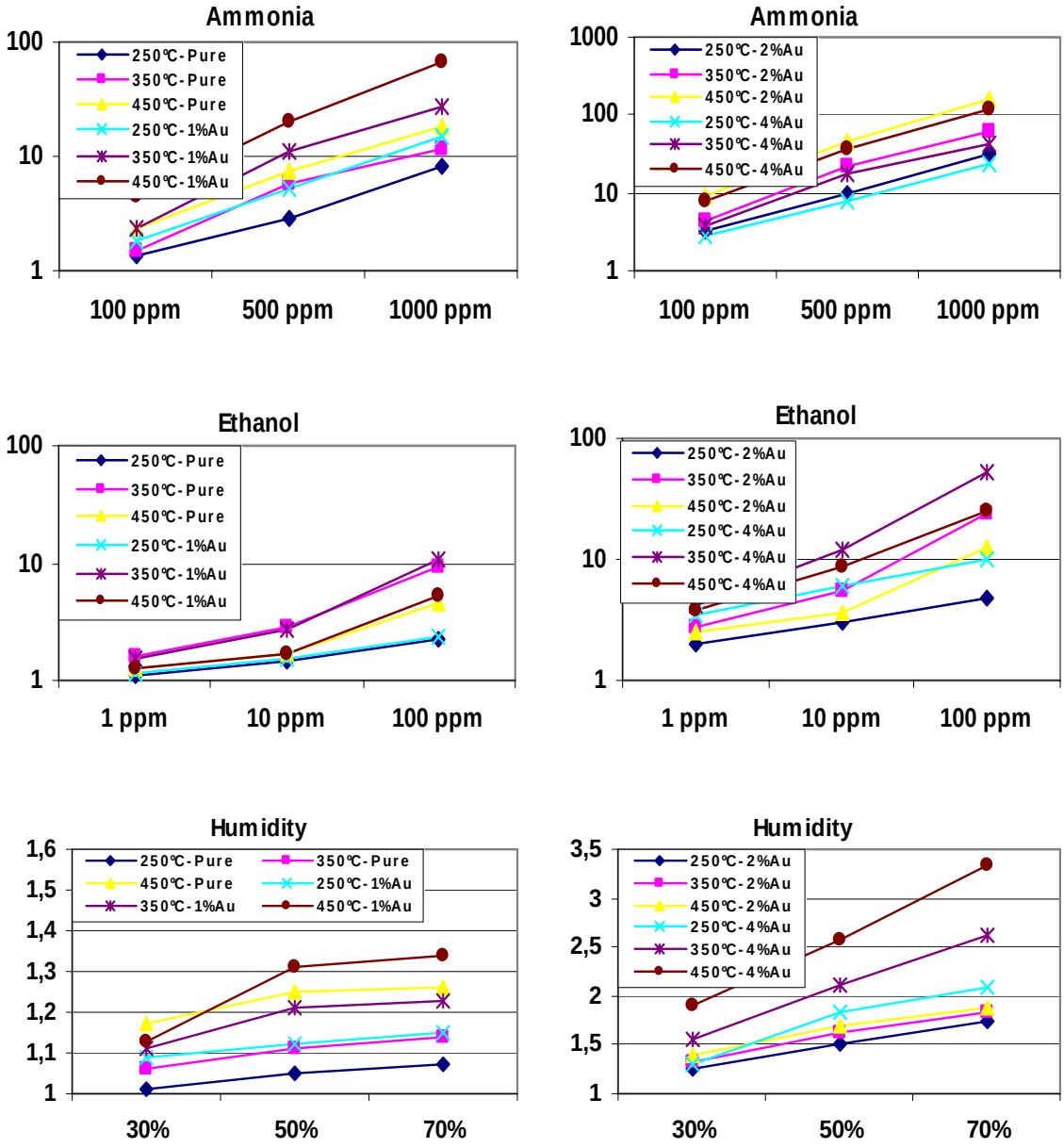

Figure V.34 WO_3 sensor responses to ammonia, ethanol and humidity (Sensors: W_n_XX_0_50, W_n_Au_1_50, W_n_ Au_2_50, W_n_ Au_4_50).

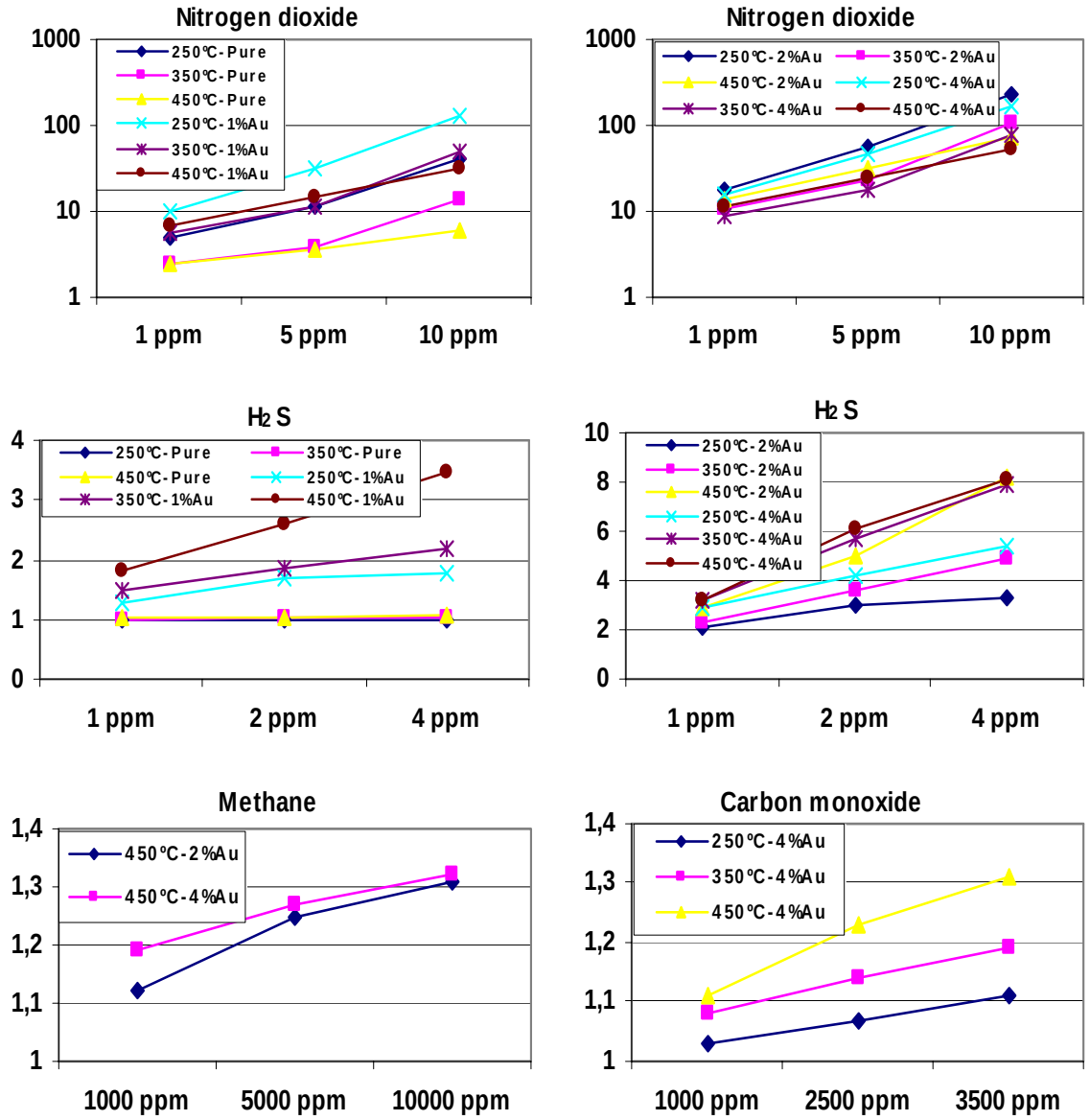

Figure V.35 WO_3 sensor responses to nitrogen dioxide, hydrogen sulphide, methane and carbon monoxide (Sensors: W_n_XX_0_50, W_n_Au_1_50, W_n_ Au_2_50, W_n_Au_4_50).

The investigation of the last sensor set, in which the tungsten layer was loaded with different quantities of gold, enables us to define the optimal doping concentration. The graphic shows that a gold loading of 2% leads to the best ammonia detection. When the metal concentration is increased, the sensitivity of the sensor decreases. The ethanol and H_2S, however, have the best response in the case of 4%Au loaded WO_3 sensor. The only difference between these two measured species is that for the ethanol the optimal working temperature was 350°C, while

for the hydrogen sulphide it was 450°C. The sensors doped with 2%Au, showed no reaction to CO, while for 4% Au loading, the tungsten oxide sensor did show a reaction. This sensor set also responded to CH_4 for the highest operating temperature 450°C and for Au loading of 2 and 4%.

Our study shows that the humidity dependence increases drastically when the sensor is highly doped with Au. Another disadvantage of the high doping is the drastically decreased selectivity. This is why we consider that the small doping quantity of approximately 1 or 2% of god loading is optimal for the sensor performance.

From the results above, it can be seen clearly that the doping study enables us to select the optimal doped active layer for each application. By combining four sensors it is possible to discriminate and quantify a variety of species. These results verify the capability of the fabrication technique launched in this study. Therefore, resistive gas sensors based on diverse metal oxides, screen-printed on micro-hotplates have a very powerful potential for hand-held gas monitors and other small, battery-powered gas analysers or e-noses.

V.4.3 Pure SnO_2/ WO_3 SOI micro-hotplate gas sensors

In order to decrease even more the power SOI solid-state gas-sensor with an original design of a poly-silicon loop-shaped micro-heater fabricated on a thin-stacked dielectric membrane is used. The properties of the substrate are detailed in Table V.11.

Parameters	Values
Substrate dimension	600 μm x 500 μm
Dimension of the active layer	200 μm x 200 μm
Thickness of the membrane	1 μm
Power consumption (at 400°C)	R_0=1.1 kΩ ± 5%

Table V.11. Characteristics of the SOI substrate

The micro-heater ensures high thermal uniformity and very low power consumption (20 mW for heating at 400°C). Sensitive films are based on tin and tungsten oxides. The first batch consisted of sensors deposited either by RF sputtering or drop coating. The response of the

sensors fabricated by drop coating was better than that of the sputtered ones. This suggests that the latest batch will respond better to the tested species because the screen-printing technology used for fabrication provides a high porosity active layer with homogeneous thickness. The completely CMOS-compatible TMAH-based bulk micro-machining techniques used during the fabrication process make it possible to integrate smart gas sensors in SOI-CMOS technology.

The sensitivity of 4 micro-sensors was studied (i.e. 2 sputtered during the first measurement cycle and 2 drop coated during the second measurement cycle). Sensors were operated at three different temperatures (150, 200 and 250°C) set by applying a current to their heating resistor. Both type of active layers (SnO_2 and WO_3) deposited with either r.f. sputtering or drop-coating, were sensitive to ethanol vapours (Figure V.36), while the drop-coated WO_3 ones, showed response to NO_2 (Figure V.37). The response to NO_2 of the WO_3 sensors was expected, because of the high affinity of this active material to the nitrogen species. The sensors showed insignificant response to ammonia, acetone and CO, which could be explained, with the lower operating temperature.

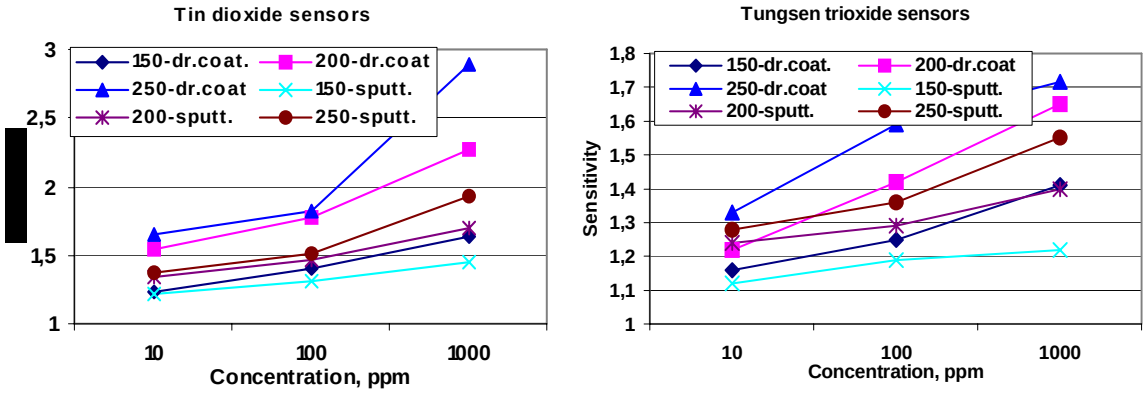

Figure V.36. Average sensitivity of the SnO_2 and WO_3 sensors to ethanol.

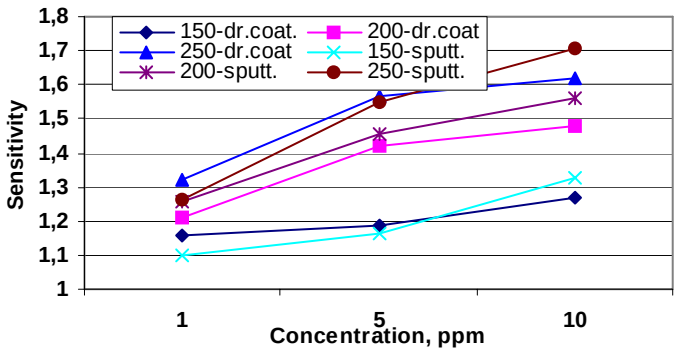

Figure V.37. Average sensitivity of the WO_3 sensors to NO_2

The response of the sensors to variations in the ambient moisture was also studied. It was observed that the sensor resistance decreased when the relative humidity was increased (see figure V.38). Furthermore, when the sensors were operated at higher temperatures, the change in their resistance caused by a change in the moisture level was higher.

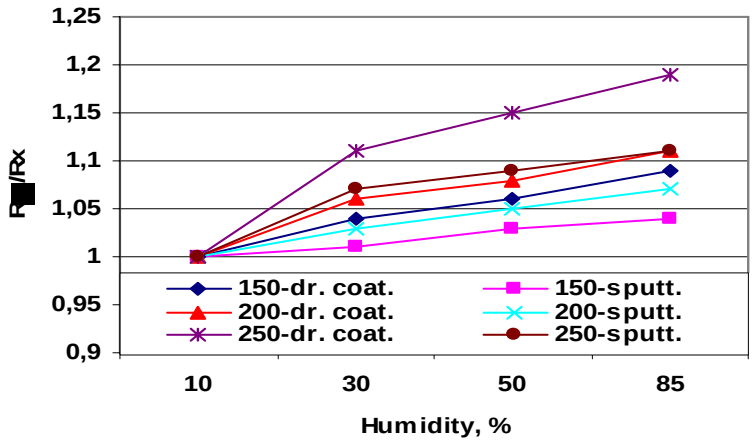

Figure V.38. Response of the drop-coated and sputtered sensors to humidity changes at different operating temperatures.

The sensor response time ranged between 30 and 45 s, depending on its operating temperature. It was defined as a time it took to reach 90 % of its steady value after exposure to a gas. Generally, the sensor response was faster when operated at higher temperature.

Once the functionality of the substrate was checked with active layers deposited via sputtering and drop-coating, thick film layers of pure SnO_2 and WO_3 were deposited via screen printing. The membranes remained undamaged, as once again the printing was made before the back side etching. Chemical test were planned in order to test the properties of the fabricated sensors, but due the technological problems could not be performed.

V.5 Applications with MHP arrays

Pattern recognition methods are very useful for classifying and quantifying gas/liquid species. Here we review the various methods used to extract important features from the responses of the MHP gas sensors and the pattern recognition algorithms implemented to recognise and quantify the gases and their mixtures. The pattern recognition methods used to analyse the experimental data and to classify and quantify the gases and mixtures are principal component analysis (PCA), linear discriminant analysis (LDA) and two neural networks such as the

multilayer perceptron (MLP) and the fuzzy ARTMAP. Their principal characteristics are summarised in Table V.12.

PARC	Learning	Linear	Parametric	Application	Comments
PCA	Non supervised	Yes	No	Feature extraction/ classification of unknown species	Data separated on basis of variance
LDA	Supervised	Yes	Yes	Classification of known species	Classified species
MLP	Supervised	No	No	Classification and quantitative mixture analysis	Artificial neural networks are opaque in nature
Fuzzy ARTMAP	Supervised	No	No	Classification and quantitative mixture analysis	Allows subjective classification

Table V.12. Classification scheme for pattern recognition (PARC) systems

In a supervised PARC method, a set of known data is introduced into the pattern recognition method, which classifies them according to known descriptors (classes) held in a knowledge base. Then, in the second stage, an unknown data input is tested against the knowledge base and the membership class is predicted. Other PARC methods do not need a separate training stage but learn the different classes from the response vectors automatically. These methods are non-supervised and they are much closer to the way that the human brain is believed to work.

A parametric technique is based upon the assumption that the sensor data can be described by a probability density function (PDF) that a posterior defines its spread of values (in most cases the assumption made is that data are normally distributed with a known mean and variance). Non-parametric methods do not assume any PDF for the sensor data and thus apply more generally.

V.5.1 LDA used for discrimination and quantification of simple volatiles and binary mixtures with non-doped SnO_2 sensors

The sensitivity to different concentrations of ethanol, acetone and ammonia vapours ad their binary mixtures was studied. The vapours were qualitatively and quantitatively analysed using linear discriminant analysis. The sensors with a 50μm inter-electrode gap were operated at 380°C and the sensors with a 100μm inter-electrode gap at 480°C.

LDA was performed using the responses of a 4-element micro-array. For each measurement, the feature extracted from the response of each sensor within the micro-array was the conductance change: $\Delta G = 1/R_g - 1/R_a$. For each micro-array, the response features were gathered to form a response matrix. Each response matrix had 4 columns (one column per sensor within the array) and 90 rows, which corresponded to the number of measurements ([3 single vapours + 3 binary mixtures] × 3 different concentrations × 5 replicates per measurement). In both cases, the first two discriminant factors accounted for more than 98% of the variance in the data. Figure V.39 shows the results of the LDA.

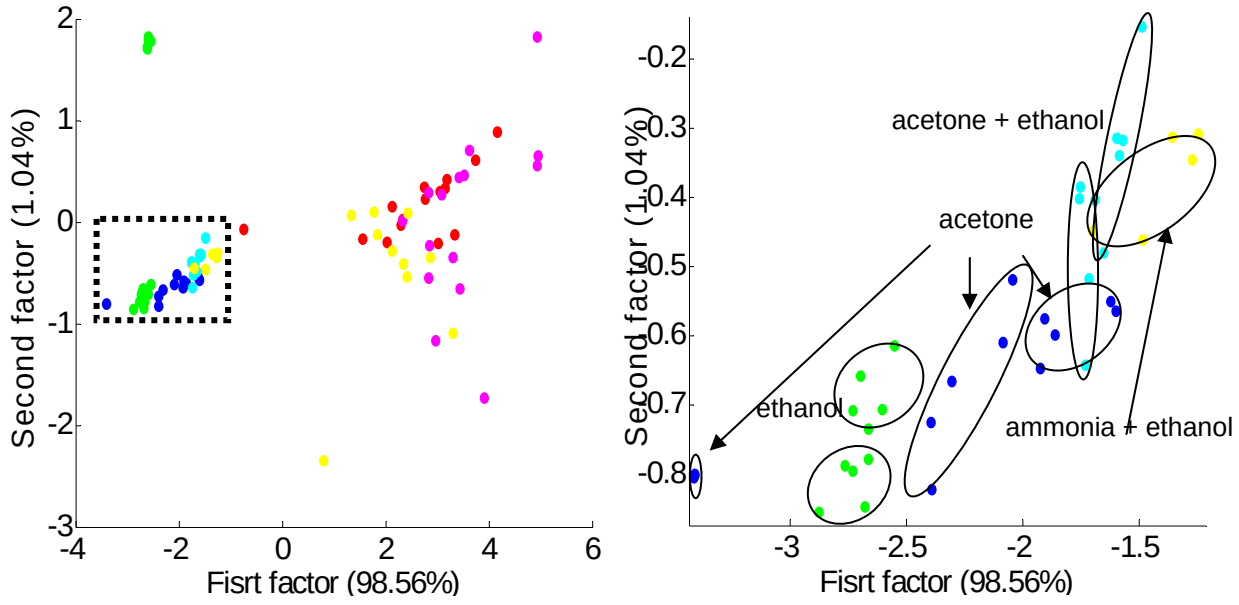

Figure V.39. Results of a linear discriminant analysis using an array of 4 tin oxide sensors. The plot on the right is an enlargement (dotted area) of the plot on the left.

Measurements of the same vapour (or vapour mixture) tend to cluster together. Furthermore, clusters are formed according to vapour concentration, which shows that it would be possible to identify and quantify the samples. Ellipses group measurements belonging to the same

category and have been added to help the eye. The clusters overlap considerably, suggesting that a linear pattern recognition method applied is not the most appropriate for vapour discrimination.

V.5.2 PCA, MLP and Fuzzy ARTMAP used for discrimination and quantification of simple volatiles and binary mixtures with non-doped SnO_2 sensors

- **PCA analysis**

We attempted to identify the various organic volatiles and their binary mixtures using a 4-element integrated sensor microarray. The microarray consisted of 2 tin oxide sensors with a 100μm inter-electrode gap operated at 480°C and 2 tin oxide sensors with 50μm inter-electrode gap operated at 380°C. The volatiles and their concentrations are summarised in table V.9. Each measurement was replicated three times. For each measurement, the feature extracted from the response of each sensor within the micro-array was the conductance change:

$$\Delta G = 1/R_g - 1/R_a \qquad \text{(V.1)}$$

All the response features were gathered to form a response matrix. The response matrix had 4 columns (one column per sensor within the array) and 54 rows, which corresponded to the number of measurements ([3 single vapours + 3 binary mixtures] × 3 different concentrations × 3 replicates per measurement). All the data processing methods were implemented using standard functions from MATLAB© [187].

A principal component analysis (PCA) was performed. For a description of how this linear pattern recognition method is applied to gas sensor data, see [188]. The data were mean-centred because this is the usual pre-processing method when the initial variables are homogeneous (e.g. the responses of four tin oxide micro-sensors). The first two principal components accounted for 99.43% of the variance in the data (principal components 1 and 2 accounted for 66.44% and 32.99% of data variance, respectively). This high degree of co-linearity between the sensors in the array could be anticipated because the sensors were coated with the same type of active layer (their main differences were in electrode type and operating temperature). Figure V.40-a shows the score plot of this PCA. Figures V. 40-b and V.40-c show magnifications of the zones inside the dotted contours in figure V.40-a.

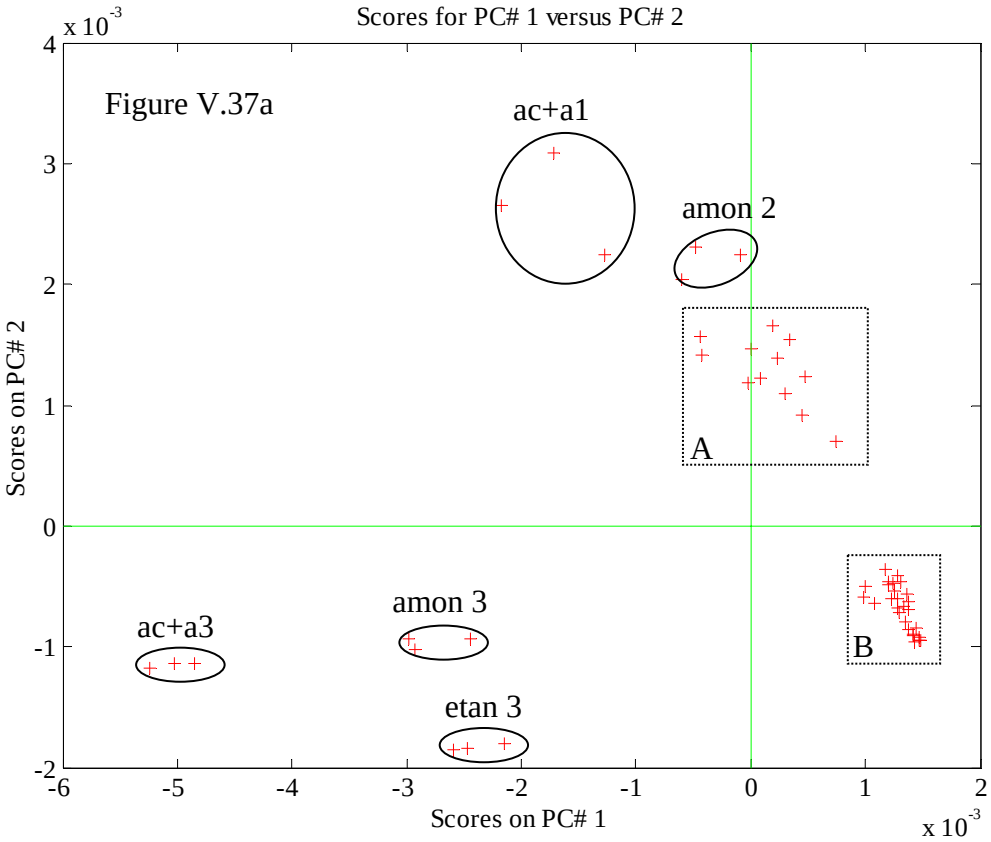
Scores for PC# 1 versus PC# 2
x 10^-3
Figure V.37a
ac+a1
amon 2
A
B
amon 3
ac+a3
etan 3
Scores on PC# 2
Scores on PC# 1
x 10^-3

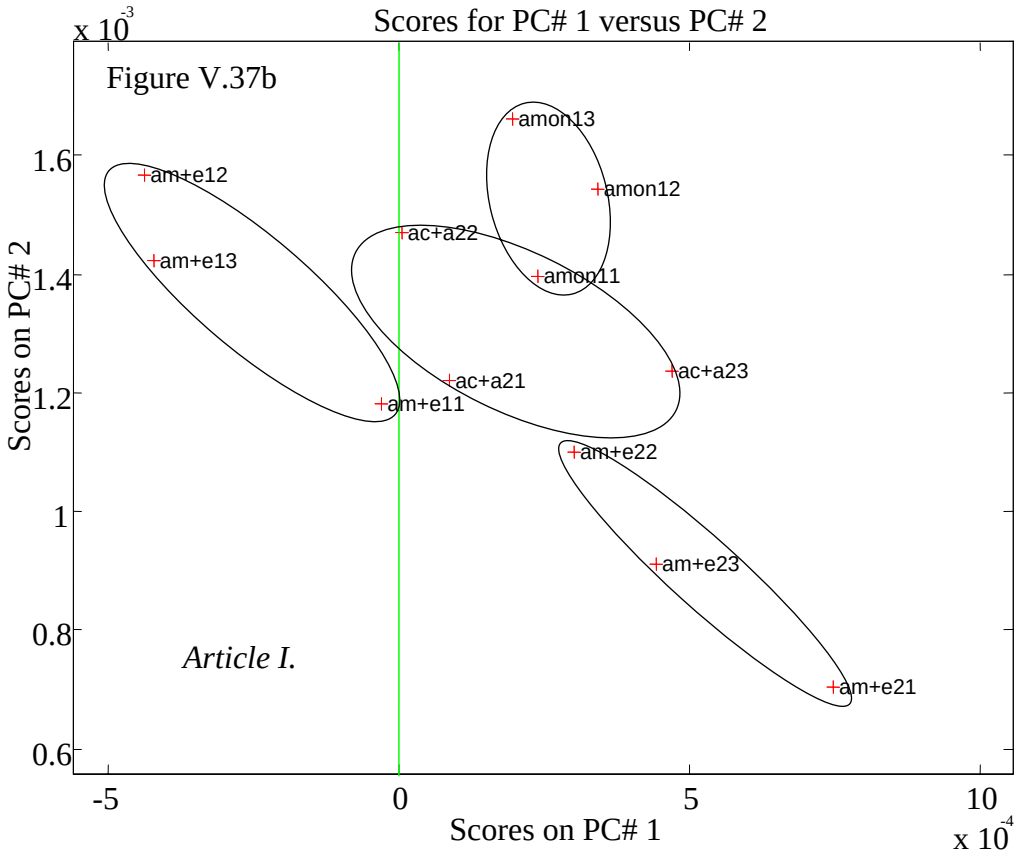
Scores for PC# 1 versus PC# 2
x 10^-3
Figure V.37b
amon13
amon12
am+e12
am+e13
ac+a22
amon11
ac+a21
ac+a23
am+e11
am+e22
am+e23
am+e21
Article I.
Scores on PC# 2
Scores on PC# 1
x 10^-4

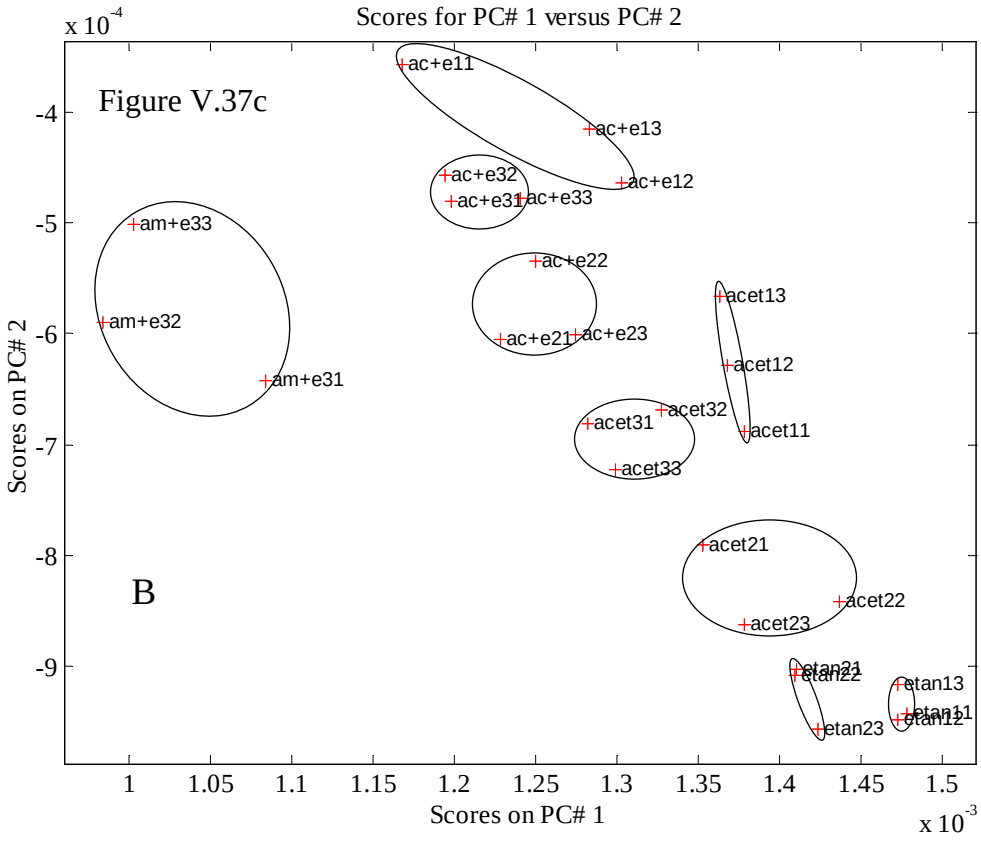

Figure V.40. Results of a PCA using the responses of a 4-element microsensor array (b and c show magnifications of the zones inside the dotted contours in a). Labels follow the structure: name_ij where i indicates the species concentration (1 is the lowest and 3 is the highest) and j is for the number of replicate measurements (1, 2 or 3). (Coding: etan: ethanol, acet: acetone, amon: ammonia, am+e: ammonia and ethanol mixtures, ac+e: acetone and ethanol mixtures, ac+a: acetone and ammonia mixtures)

As can be seen, replicate measurements cluster together, showing that the reproducibility of the results is good. The ellipses in this figure are intended only to help to identify the replicate measurements. The concentrations of ammonia vapours were higher than the concentrations of acetone or ethanol vapours, which is why the clusters for binary mixtures containing ammonia are always very near to the clusters corresponding to ammonia vapours. In particular, the cluster corresponding to an acetone and ammonia mixture clearly overlaps a cluster corresponding to ammonia in figure V.40-b. The complexity of the discrimination problem is further complicated by the wide range of vapour concentrations. The fact that sensor response is non-linear with vapour concentration explains why the clusters that correspond to higher concentrations of a vapour or vapour mixture do not appear along a line

in the principal component space (see figure V.40-b and c). These results suggest that it is worth trying non-linear pattern-recognition methods to better assess the vapour recognition ability of the micro-sensor array.

The multi-layer perceptron (MLP) and the fuzzy ARTMAP neural networks were applied as non-linear pattern recognition methods to solve the vapour identification problem. The MLP is the neural network that is by far the most commonly used by the gas sensor community and the fuzzy ARTMAP has the advantage that it can be trained very quickly and effectively, even when few samples are available for training [189, 190].

The performance of the neural methods was evaluated with a leave-one-out cross-validation approach using the 54-measurement dataset. With this strategy, the networks were trained 54 times using 53 measurements and tested against the measurement left out. The performance of a network was estimated as the average over the 54 tests.

- **MLP results**

The MLP neural network had 3 layers of feed-forward, fully connected neurones. The input layer had 4 neurones because the input data were the conductance changes of the 4 microsensors in the integrated array. The output layer consisted of 6 neurones, because the objective was to identify the vapours or vapour mixtures, and not determine their concentration. In other words, the objective was to classify the dataset into 6 different categories (there were 9 measurements in each category) and the activation of output neurone *i* means recognizing the input as belonging to category *i*. The number of neurones in the hidden layer was varied and the results were best when 10 neurones were used (Figure V.41).

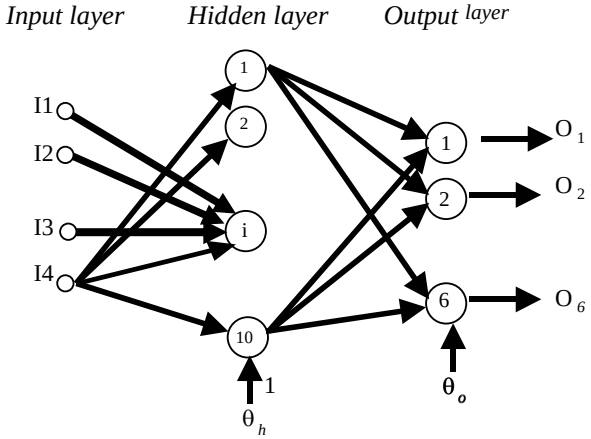

Figure V.41. MLP neural network with 3 layers

The overall identification success rate for the MLP was 77.78% (42 out of 54 measurements were correctly classified). Table V.13 shows the confusion matrix for this experiment. A perfect classification would result in all the measurements appearing on the main diagonal of the confusion matrix. The confusions occur between the following species:

a) The lowest and intermediate concentrations of ethanol and intermediate concentrations of acetone. This is in good agreement with the PCA results (see figure V.40-c) where the clusters for these species nearly overlap.

b) The lowest concentration of ammonia, intermediate concentrations of acetone and ammonia mixtures and lowest and intermediate concentrations of ammonia and ethanol mixtures. These confusions correspond to the measurements of the clusters, which overlap in Figure V.40-b.

MLP analysis		**Ethanol**	**Acetone**	**Ammonia**	**Ethanol + Acetone**	**Ethanol + Ammonia**	**Ammonia + Acetone**
Predicted as	**Ethanol**	6	3	-	-	-	-
	Acetone	3	6	-	-	-	-
	Ammonia	-	-	8	1	-	1
	Ethanol + Acetone	-	-	-	9	-	-
	Ethanol + Ammonia	-	-	-	-	7	2
	Ammonia + Acetone	-	-	1	-	2	6

Table V.13. Confusion matrix for the identification of 3 simple vapours and 3 binary mixtures using a 4-element tin oxide-based microarray and a multilayer perceptron neural network

The multiple errors in Table V.13 suggest that the multilayer perceptron neural network is not the most appropriate method for vapour discrimination.

- **Fuzzy ARTMAP results**

The fuzzy ARTMAP needs its inputs to vary between 0 and 1. Therefore, the data matrix was normalised by dividing its elements (all of which were positive) by the value of the maximum. Like MLP, the fuzzy ARTMAP had 4 inputs and 6 output neurones. Unlike MLP, the fuzzy ARTMAP automatically selects the number of hidden neurones during the training phase. Once again, the performance of the neural network in the identification of the 6 vapours and mixtures was evaluated using the leave-one-out approach. The number of committed nodes (equivalent to hidden neurones) during the leave-one-out tests varied between 6 and 14, which is not far from the 10 nodes needed by the MLP. However, the classification performance of the fuzzy ARTMAP was better than that of the MLP because 48 out of 54 samples were correctly classified, a success rate of 88.89%. Table V.14 shows the confusion matrix for the fuzzy ARTMAP. Vapour identification improves because the fuzzy ARTMAP is able to discriminate between acetone and ethanol vapours.

Fuzzy ARTMAP analysis		**Ethanol**	**Acetone**	**Ammonia**	**Ethanol + Acetone**	**Ethanol + Ammonia**	**Ammonia + Acetone**
Predicted as	**Ethanol**	9	-	-	-	-	-
	Acetone	-	9	-	-	-	-
	Ammonia	-	-	8	-	-	2
	Ethanol + Acetone	-	-	-	9	-	-
	Ethanol + Ammonia	-	-	1	-	7	1
	Ammonia + Acetone	-	-	-	-	2	6

Table V.14. Confusion matrix for the identification of 3 simple vapours and 3 binary mixtures using a 4-element tin oxide-based micro-array and a fuzzy ARTMAP neural network

Finally a semi-quantitative analysis was performed with a fuzzy ARTMAP neural network. This consisted of an 18-category classification (6 species and binary mixtures × 3 concentrations). Therefore, the neural network had 4 input neurones and 18 output neurones. Once again, a leave-one-out cross-validation was used to assess the performance of the method. The number of committed nodes during the leave-one-out tests varied between 18 and 24. The samples were identified and quantified with a 81.48% success rate (44 out of 54 samples were correctly classified). As well as the misclassified samples shown in table V.14, two samples of acetone vapours and two samples of acetone and ethanol mixtures were identified with wrong concentrations.

These promising results show that it is possible to identify gases and gas mixtures using integrated arrays of screen-printed micro-machined gas sensors operated at different temperatures.

V.5.2 PCA and Fuzzy ARTMAP used for discrimination and quantification of simple volatiles, binary mixtures and toxic gases with non-doped SnO_2 and WO_3 sensors

The above results clearly show that the qualitative and semi-quantitative analysis of the vapours was best when principal component analysis PCA and the fuzzy ARTMAP neural network were used. For this reason, a more exhaustive analysis was performed using these methods. We used SnO_2 and WO_3 sensors with a 50 μm electrode gap operated at 380^{o}C and SnO_2 and WO_3 sensors with a 100 μm electrode gap operated at 480^{o}C. The sensor operating temperatures were selected according to the sensitivity study conducted previously.

Two different gas analysis applications were developed. While the first application analysed vapours (acetone, ammonia and ethanol) and vapour mixtures, the second attempted to analyse gases (carbon monoxide and nitrogen dioxide). Therefore, the measurements were split into two datasets. Dataset 1 grouped the vapour measurements. The number of measurements in dataset 1 was equal to 90, which corresponded to 3 single vapours and 3 binary mixtures measured at 3 different concentrations (i.e. 18 different combinations) and each combination was replicated 5 times. Dataset 2 grouped the gas measurements. The number of measurements in dataset 2 was equal to 30 because 2 single gases at 3 different concentrations were measured and, once again, each measurement was replicated 5 times in order to increase the correctness of the result.

Before the PCA, the data were mean-centred. This is a common pre-processing method which considers that all the sensors are similar. For each dataset, two PCA were performed using the responses of a 4-element micro-array (tin oxide and tungsten oxide). For each measurement, the feature extracted from the response of each sensor within the micro-array was the conductance change: $\Delta G = 1/R_g - 1/R_a$. For each micro-array and dataset, the response features were gathered to form a response matrix. Each response matrix had 4 columns (one column per sensor within the array) and either 90 or 30 rows, which corresponded to the number of measurements in the two datasets.

- **Analysis of vapours and vapour mixtures**

Figure V.42 shows the results of the PCA performed on the responses to vapours and vapour mixtures of the tungsten oxide micro-arrays. Measurements of the same vapour (or vapour mixture) cluster together in the score plots. Furthermore, clusters are formed according to vapour concentration, which shows that it should be possible to identify and quantify the samples.

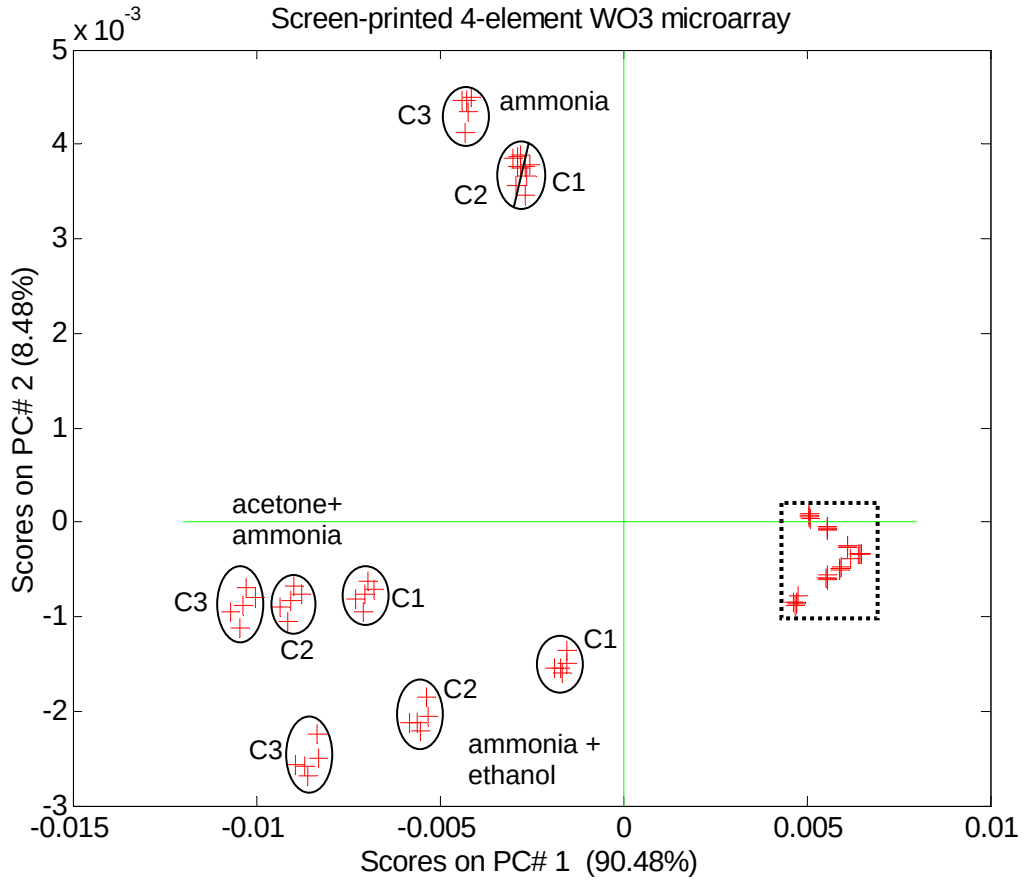

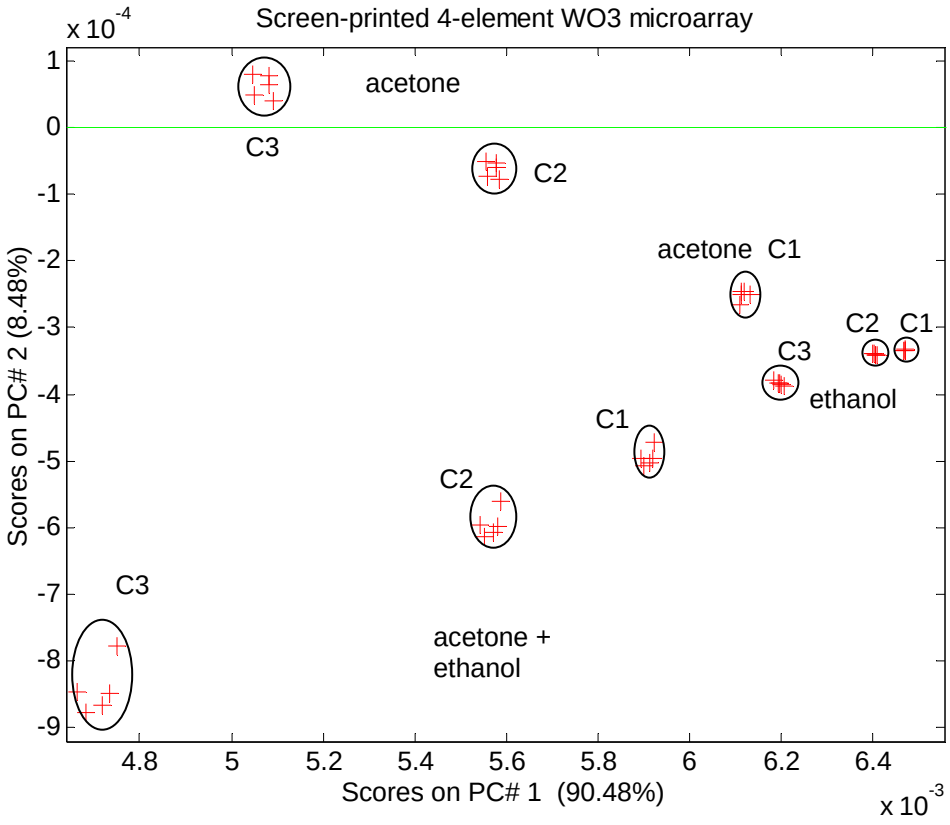

Figure V.42. Results of a PCA using the responses of a 4-element WO_3 microsensor array. C1, C2 and C3 correspond to the vapours or mixture concentrations shown in table V.9.

The sensors show good sensitivity in their responsiveness to ammonia, ethanol and acetone vapours. This explains why the clusters are well separated in figure V.42. The results (discussed above) were similar when the responses of the tin oxide micro-arrays were used to perform PCA.

A semi-quantitative analysis of the vapours was performed using fuzzy ARTMAP neural networks. This consisted of an 18-category classification (6 species and binary mixtures × 3 concentrations). Two different fuzzy ARTMAP models were built, which corresponded to the use of two micro-sensor arrays (i.e. tin or tungsten oxide). Since each measurement was replicated 5 times, a total of 90 measurements were available to train and validate the networks.

A leave-one-out cross-validation and the bootstrap method [191] were implemented to estimate the performance of the neural networks. With the leave-one-out method, the networks were trained 90 times using 89 measurements and tested against the measurement

left out. The performance of a network was estimated as the average over the 90 tests. To implement the bootstrap method, 100 training sets were formed by selecting 90 measurements at random with replacement from the data matrix. The test set of each training set consisted of those measurements not found in the training set. The performance of the fuzzy ARTMAP method was defined as the average performance over the 100 tests. The results for the leave-one-out cross-validation were as follows:

a) The responses of the tungsten oxide sensors were input to the network and the simultaneous identification and quantification success rate was 95.6%. Confusions occurred between samples corresponding to the lower and intermediate concentrations of ammonia. These misclassified samples corresponded to the overlapping in the PCA plot (see figure V.42). However, the quantification success rate increased to 100% when the responses from the tungsten oxide sensors were combined at the input of the neural networks.
b) The identification and quantification success rate was 100% when the responses of 4 tin oxide sensors were used.

Since there were few measurements for cross-validating the fuzzy ARTMAP models, a bootstrap procedure was implemented to better estimate the true success rate. The results of the bootstrap method used to estimate the performance in the simultaneous recognition and quantification of vapours are summarized in Table V.15. These results are very similar to the ones obtained when the leave-one-out approach was used.

Fuzzy ARTMAP analysis	**Performance**		**Statistics**	
	Best	**Worse**	**Mean**	**Standard dev.**
Screen-printed SnO_2 sensors	**100**	**80.9**	**83.7**	**4.19**
Screen-printed WO_3 sensors	**100**	**98.2**	**99.4**	**0.78**

Table V.15. Results of the bootstrap cross-validation of the fuzzy ARTMAP models built to semi-quantify the vapours and vapour mixtures

- **Analysis of toxic gases**

A process equivalent to the one described above was used to semi-quantitatively analyze carbon monoxide and nitrogen dioxide (dataset 2). Since the tungsten oxide-based sensors did not respond to carbon monoxide, only the tin oxide-based micro-arrays were used. Initially a

PCA was performed to see whether the micro-arrays were able to discriminate the gases. Figure V.43 shows the score plot of a PCA performed on the responses of a tin oxide micro-array.

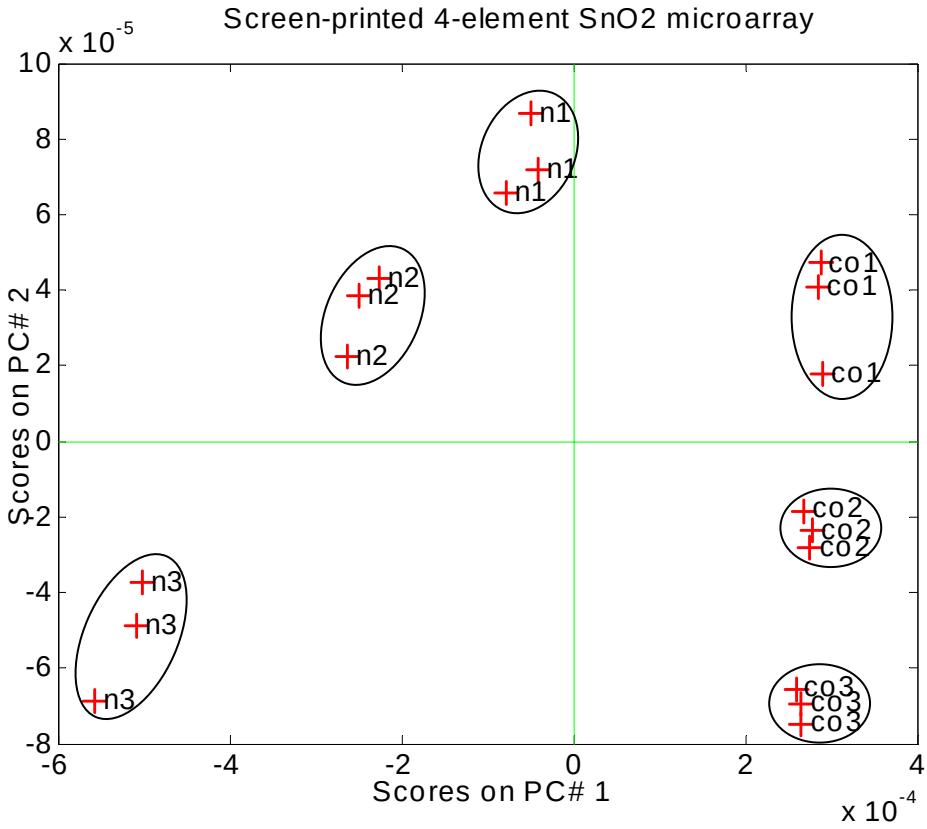

Figure V.43. Results of a PCA using the responses of a 4-element SnO_2 screen-printed micro-sensor array. The labels co1, co2, co3 and n1, n2, n3 correspond to increasing concentrations of carbon monoxide and nitrogen dioxide, respectively.

The gases are clearly separated and the replicate measurements of equal concentration cluster together. Once again, fuzzy ARTMAP models were built to simultaneously identify and quantify the gases. The rate of successful classifications, estimated by the leave-one out approach, was 100%.

V.5.4 A micro-sensor array for selective detection of ethylene, ammonia and ethanol

As we have stated before, the detection of ethylene gas is very important. It causes fruit to ripen and decay. Normally, fruits are stored in warehouses under controlled atmosphere (high humidity, low oxygen). Monitoring ethylene inside conservation chambers would extend the life cycle of fruits and increase quality. Ethylene gas is also used in ripening rooms to colour

up fruit, which is then moved to a regular cold storage room with other products. The monitoring of ethylene gas is very important for the fruit to reach the market in optimal conditions. Nowadays, the problem of continuously measuring ethylene levels during storage of climacteric fruit remains unsolved because ethylene detectors are bulky and very expensive.

While ethylene gas is used under controlled conditions as a ripening agent, even small amounts of ethylene gas during shipping and storage (20-100 ppm) can cause fruit decay. Below, we reports on the efforts to obtain a new generation of sensors, able to selectively detect ethylene in the presence of ethanol (indicator of fruit stress) and ammonia (leak from the cooling units). Our approach consists of designing an integrated sensor micro-array with a low number (4) of metal oxide sensors [192]. It is well known that metal oxides are poorly selective, however, overlapping sensitivities within a sensor array can be tuned by selecting appropriate materials loaded with noble metals. Tin oxide and tungsten oxide were the materials selected for the detection of ethylene and ammonia, respectively. The use of catalysts such as Au, Pt or Pd, was envisaged to increase sensitivity and improves selectivity to the target gases for the application considered.

The fabricated devices have been tested in the presence of ethylene, ethanol and ammonia (and their mixtures) at 3 different temperatures (250, 350 and 450ºC) and for three concentrations using a continuous flow system. The sensor response to interfering species like CH_4, H_2S and H_2O has been evaluated too. Figure V.44 shows a typical dynamic response of 4 different sensors within the same chip.

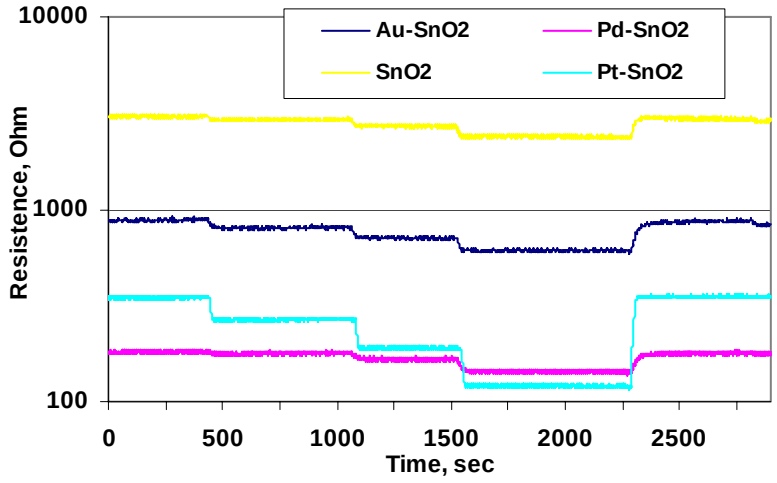

Figure V.44. Typical response of four SnO_2 sensors to 1, 5 and 10 ppm of C_2H_4 at 350ºC.

The first objective is to select the materials and catalysts for our application. The Pd-SnO_2 sensors showed the highest response to ammonia among the different tin oxide sensors tested. For example, their response was up to 6 times higher, than the un-doped SnO_2 sensors. Pure tungsten oxide was very sensitive to ammonia, too. From the experimental results we can conclude that if we want to detect ethanol, the Pt-doped sensors had the best sensitivity (10 times higher than the un-doped ones). The Pt doping promotes also the detection of ethylene. All SnO_2 sensors showed no response to methane and H_2S. For the selective detection of ethylene a sensor with un-doped WO_3 layer has to be included in the array, since no response to this gas was observed. On the other hand, the response to ethanol of the tungsten oxide sensors is much lower, than for the tin oxide sensors. Nevertheless, from humidity tests, we can conclude that the doping does not affect drastically sensitivity to moisture. Minimum response was observed for the non-doped layers, while the Pt doping catalyzes well this reaction. The selectivity of the proposed sensor matrix for ethylene detection is presented in figure V.45.

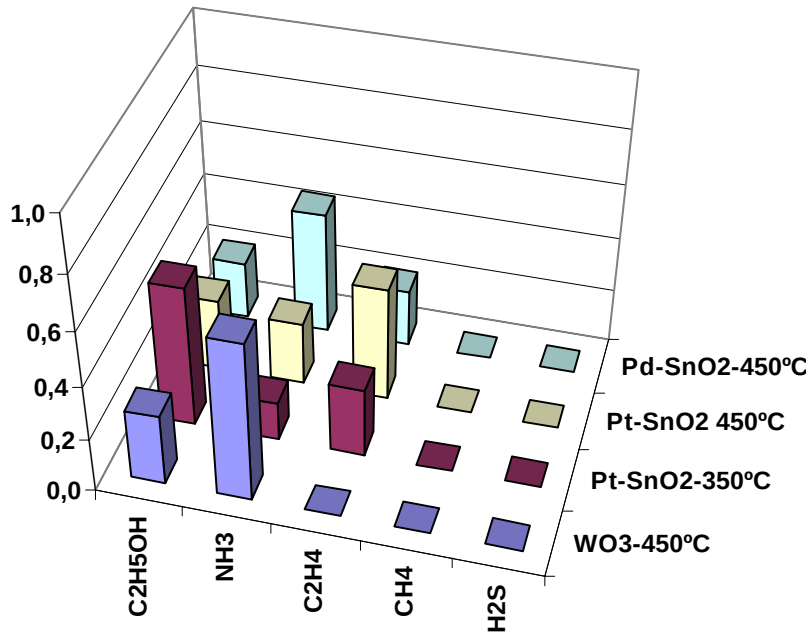

Figure V.45. Selectivity to some of the fabricated sensors to the tested gases.

A multivariate analysis of the measurements gathered using the 4-element array described in figure V.45 was performed. It was shown that ethylene can be distinguished from other gases and that the system would detect alarm levels of ethanol (fruit stress detection) and ammonia (leak detection).

SnO_2 and WO_3 based micro-hotplate thick-film sensor arrays have been fabricated via screen-printing. Some sensitive layers remained undoped, while others were doped with noble metals such as Pd, Pt and Au. Combining various active layers (tin and tungsten oxides) and various doping metals, very promising results were obtained for the selective ethylene detection.

V.6 Conclusions

This chapter presents the results of the fabrication, physical and chemical tests of sensors with substrates based on microhotplates and silicon-on-insulator. Performance (sensitivity, selectivity and power consumption) was excellent with the doped MHP gas sensors. It has been shown that sensors can be highly selective if the doping is carefully selected. Various methods and algorithms were also used to analyse the experimental data obtained from the non-doped MHP gas sensors. It has been demonstrated that the responses of a single chip, consisting of 4 sensors operating at different temperatures, permit excellent identification of the measured species. This is one of the important novelties of this doctoral thesis.

Simple vapours, binary mixtures and toxic gases were qualitatively and semi-quantitatively analysed by applying LDA, PCA, MLP and fuzzy ARTMAP neural networks to the response of the integrated micro-arrays. Results were best with PCA and fuzzy ARTMAP neural network methods. The PCA showed that a linear separation between the different species measured could be obtained in most cases. Two different fuzzy ARTMAP models were built for the simultaneous identification and quantification of the different species. The success rate was 95% for the semi-quantification of vapours and 100% for the semi-quantification of toxic vapours. These results confirm the viability and usefulness of the methods introduced in this study.

VI. CONCLUSIONS

This PhD thesis discusses the design, fabrication and characterization of thick-film gas sensors. It also deals with one of the most essential problems of these sensors: their lack of selectivity. The main objective was to create new sensor devices with improved selectivity. With this purpose a sensor substrate based on alumina with its essential elements (interdigitated electrodes, heater and temperature measuring meander) was developed. The active layers in this substrate were fabricated with the most popular metal oxides used for gas sensors (SnO_2 and WO_3). Some active layers remained unchanged, while others were modified with various methods. The sensing layers were doped with such techniques as sputtering or direct metal loading with a variety of noble metals (Pt, Pd, Ti and Au) so that the sensor sensitivity and selectivity would be better. To improve the surface adhesion diverse organic matrices, glass powders and binders were used. The influence of the catalytic filters was also studied. The fabricated sensors were tested with a wide range of gases and volatile compounds such as ammonia, acetone, benzene, ethanol, carbon monoxide, hydrogen sulphide, nitrogen dioxide and methane.

For sensors to have insignificant thermal inertia and low power consumption, the sensor substrate had to be changed. For this purpose, after the adhesion of the active layer on the standard silicon substrate had been checked, the microhotplate sensor substrate was introduced. Special nano-grain active phases, based on the above-mentioned metal oxides,

were prepared. The role of the doping type and the doping quantity was carefully studied. Because power consumption is very important for hand-held devices, at the end of the thesis we mention another promising sensor substrate, which has lower power consumption, and is based on silicon-on-insulator technology. Active layers of tin and tungsten oxide were also developed for this substrate.

Some of the most interesting conclusions drawn from the experiments made in this thesis are summarized below. Detailed information can also be found in chapter four and five, and in our publications summarized at the end of the thesis.

1. Screen printing technology was settled up.

The first basic conclusion of this thesis is that we learned to fabricate pastes of tin dioxide and tungsten trioxide with excellent adhesion, morphological and electrical properties. We become skilled at depositing thick film layers on a wide variety of substrates like alumina (for the preliminary sensor tests), microhotplates (used for the integrated sensor matrix fabrication) and silicon-on-insulator (employed for the production of low power consuming gas sensors). We discovered the effects of the different doping and found out the most favourable doping for the different gases studied. The produced tin dioxide sensors showed very good response to ethanol, while the developed tungsten trioxide gas sensors showed good results in detection of ammonia and nitrogen dioxide, which were some of the target gases in our study. We deposited numerous intrinsic and doped active layers with high fabrication yield on microhotplates. From the results obtained with the elaborated sensors we gained knowledge to set up sensor matrices based on sensors with different active layers, dopings, inter-electrode distance and operating temperatures. Using the cross-selectivity of the fabricated devices, we were capable, with the help of pattern recognition techniques, to distinguish with high success rate the tested gases. These techniques permit us to discriminate various polluting volatile organic compounds, distinguish between harmful gases like carbon monoxide and nitrogen dioxide and implement a practical micro-system for monitoring ethylene in warehouses.

2. A highly sensitive ethanol gas sensor based on Pt-doped SnO_2 surfaces was developed.

Two different methods of doping the SnO_2 active layer were studied. The active layer was doped with Pt using RF magnetron sputtering in one method and by mixing the SnO_2 paste with a Pt paste before the firing in the other. Sensors prepared with the second method were

five times more sensitive to ethanol than the sensors with the first method. The doping with Pt considerably improved the sensitivities of SnO_2 to ethanol in air, especially when the Pt atoms were homogeneously distributed throughout the tin oxide layer. The 3% Pt-doped samples are extremely sensitive to ethanol vapours and their responses are linear in the ppb range. Their detection limit is below 1 ppb for the optimal operation temperature of 300ºC. The sensitivity of these sensors is among the highest ever reported. To sum up, the Pt-doped SnO_2 material is less resistant, more sensitive and more responsive to ethanol than pure SnO_2. The fabricated sensors could be used in alcohol breathalyzers, foodstuff quality control and the on-line monitoring and control of small concentrations of ethanol.

3. Highly selective ammonia sensors with interchangeable *n*/*p* behaviour based Pt-doped SnO_2 were created.

Very specific results were obtained when the sensors with Pt paste were tested. They changed their conductance type from *n*-type to *p*-type during the measurements with ammonia. For temperatures lower then 350ºC, the sensors demonstrated the properties of semiconductor type *n* and for higher temperatures these properties changed to *p* type. The conductance type also changed at lower temperatures, but only for a concentration of 10 ppm. This effect may be because, at this temperature, Pt leads to the formation of NO_2 oxidizing species. With this information, a reliable ammonia sensor with excellent selectivity at high operating temperature was developed. The response to ammonia will be unambiguous, because of the specific *n* to *p* change in the sensor behavior.

4. Different doping methods were proposed to achieve better sensor selectivity.

Two different procedures for doping tin oxide with Pt and their influence on the morphology of films and on the performance of the resulting gas sensors was studied. Pt-doped tin oxide films significantly outperformed non-doped films in terms of sensitivity to ethanol vapours. In one set of samples, the screen-printed tin oxide layer was doped with Pt by using R.F. magnetron sputtering and a subsequent thermal treatment to promote the diffusion of Pt into the tin oxide layer. In the second set of samples, a Pt paste was added to the tin oxide paste before screen-printing onto the sensor substrate. The sensors prepared by this second method were five times more sensitive than the sensors prepared by the first method and twelve times more sensitive than non-doped sensors. XPS and SEM measurement showed that this behaviour could be associated with the distribution of the doping elements within the tin oxide layer. For the sensors doped by sputtering, the Pt atoms were found to remain mostly at the

surface of the active layer. On the other hand, the sensors produced by mixing the Pt and the SnO_2 pastes showed a more homogeneous distribution of the doping Pt atoms in the resulting films. The Pt-doped SnO_2 material is more sensitive and more responsive to ethanol than pure SnO_2. The method that enables the films to be homogeneously doped is preferred since it leads to the highest sensitivity to ethanol, but maintains moderate cross-sensitivity to water vapour.

5. The selectivity of SnO_2 and WO_3 layers was improved by adding promoters to the sensitive layers.

The effect of film adhesion promoters (Bi_2O_3 and Cu_2O) on the sensitivity of screen-printed tin and tungsten oxide sensors was investigated. The response of sensors containing small amounts of Bi_2O_3 and Cu_2O or Bi_2O_3 only to ammonia, nitrogen dioxide, ethanol, benzene, methane and carbon dioxide was measured. Tin oxide sensors containing only Bi_2O_3 were found to be sensitive and very selective to ethanol vapours. Tungsten oxide sensors with Bi_2O_3 and Cu_2O were found to be very sensitive to ammonia. However, they show important cross-sensitivity with nitrogen dioxide. Their selectivity to ammonia can be improved by selecting a high operating temperature and also by increasing the amount of Cu_2O in the active film (since Cu_2O enhances ammonia sensitivity). Tungsten oxide sensors containing only Bi_2O_3 are more sensitive to nitrogen dioxide than to ammonia when operated at low temperatures. To sum up, a highly selective nitrogen dioxide sensor using Bi_2O_3 was fabricated.

6. A platinum catalytic filter deposited on a WO_3 sensor was developed for the selective detection of benzene.

Placing a Pt catalytic filter on top of a WO_3 gas sensor makes it possible to selectively detect benzene in the ppm range, working at moderate temperatures. Two different catalytic filters were tested. The Pt catalytic filter proved to be best for benzene detection, where the WO_3 layer only detects gases after combustion in the catalytic filter. The benzene response is higher than with the filter fabricated with an alumina layer. The Pt filter reduces sensor sensitivity to ethanol and increases sensor response to benzene. The catalytic filter also affects NH_3 detection. As chemical reaction on its surface produces nitrogen oxides that oxidises the WO_3 surface. On the other hand, the Pt catalytic filter does not alter the NO_2 sensing capability of the tungsten trioxide.

7. A novel method for high-yield sensor micro-systems fabrication was implemented.

A new technological procedure was implemented for fabricating micro-machined gas sensors and gas sensing micro-systems. It combines the advantages of micro-machined silicon structures and screen-printed nano-particle tin oxide sensing films. The sensing layer is deposited before the silicon wafers are back-etched to create the membranes. This prevents damage to the membranes during film deposition and, therefore, the fabrication yield is excellent for integrated micro-sensors (around 95% of micro-sensors work properly after packaging). Silicon micro-machined structures are of interest because they dramatically reduce the power consumption of metal-oxide based gas sensors. Furthermore, the low thermal inertia of such structures enables the sensor operating temperature to be effectively cycled, which makes it possible to analyse multi-component gas mixtures. Screen-printed active layers are of interest because the microstructure of the film is well defined. The porosity (and surface area) of screen-printed films is higher than that of films deposited by CVD or sputtering techniques. Furthermore, thicker and more porous films are more resilient to aging than thin, compact layers. The silicon substrates had four thermally-insulated membranes and were coated with a 5 μm-thick nano-powder tin oxide (grain size was around 40 nm). Two of these membranes had interdigited electrodes and two had parallel electrodes. The sensitivity of these devices to different volatile organic compounds and their binary mixtures was investigated. Sensitivities to the species tested were good (e.g. up to 1000 for ammonia and mixtures containing ammonia). Micro-sensors with interdigited electrodes were more sensitive at lower operating temperatures than micro-sensors with parallel electrodes. The different single vapours and vapour mixtures measured were discriminated and quantified with high success rates using an integrated micro-array of four sensors operating at two different temperatures. These results confirm the viability of the fabrication technique introduced in this study. Thus, resistive gas sensors based on different metal oxides, screen-printed on micro-hotplates, show considerable potential for hand-held gas/vapour monitors and other small, battery-powered gas analyzers or e-noses.

8. A deposition technique was proposed to improve the performance of the micro-hotplate gas sensors.

Two deposition methods (r.f. sputtering and adapted screen-printing) and two materials (tin dioxide and tungsten trioxide) were used to grow sensing films onto integrated sensor micro-arrays. The sensor response to different single vapours, vapour mixtures and toxic gases was measured at different operating temperatures. The responsiveness of screen-printed sensors

was generally higher than that of sputtered sensors, which may be because of the higher surface-to-volume ratio of the screen-printed films. Qualitative and semi-quantitative analyses of simple vapours, binary mixtures and toxic gases were carried out by applying PCA and fuzzy ARTMAP neural networks to the response of the integrated micro-arrays. PCA showed that a linear separation between the different species measured could be obtained in most cases. Four different fuzzy ARTMAP models were built for the simultaneous identification and quantification of the different species. The success rate in the semi-quantification of vapours and the semi-quantification of toxic vapours was 95% and 100%, respectively. These results confirm that the screen printing method leads to better sensor performance than the sputtering method.

9. Selective gas detection using a single microhotplate chip with four different active layers was presented.

A batch of sensors with doped active layers is developed in order to widen the spectrum of gases and gas mixtures that can be analyzed. Tin and tungsten active layers, doped with different noble metals and in different quantities, were tested with a wide range of contaminants and toxic gases such as NH_3, H_2S, NO_2, CO, CH_4, etc. The results confirmed that if a single sensor chip with four different active layers is used, it is possible to obtain sensors with low power consumption and high selectivity. Another factor that can be used to increase the selectivity of the fabricated sensors even more is the operating temperature.

The most important conclusion from this thesis is that microhotplate gas sensors with differently doped active layers, together with pattern recognition techniques, can significantly increase the selectivity of metal oxide sensors. The results obtained in this study demonstrate that these sensors are suitable for developing small gas analysers and electronic noses with low-cost and reduced power consumption.

APPENDIX A

This appendix gives a brief review of the techniques that are commonly used to physically characterize active layers. The objective of this characterization is to obtain information about the material structure, which may be related to its detection properties. For this purpose we applied various techniques:

- ✓ Scanning Electron Microscopy (SEM) was used to obtain details about the film structure and the grain size.
- ✓ Energy-Dispersive X-ray Spectroscopy (EDS) was used for quantitative and qualitative analysis.
- ✓ Atomic Force Spectroscopy (AFM) was used to visualize the layer topography.
- ✓ X-ray Photoelectron Spectroscopy (XPS) gave us the bond characteristics and the composition profile.
- ✓ Raman Spectroscopy (RAMAN) gives information at molecular level allowing the vibrational and rotational analysis of chemical species.

A.1 Scanning electron microscopy (SEM)

To visualize the active layer topography SEM was used. SEM is the most common technique and is designed to provide images with high spatial resolution, usually with the secondary electron signal. The image displayed on a cathode ray tube (CRT) is created by scanning the

focused electron beam in a raster pattern across an area of the sample while synchronously scanning an analogous pattern on the CRT. The CRT brightness is modulated by the intensity of the signal of interest. Scanning electron microscopes usually use accelerating voltages between 5 and 30 kV. The major advantage of this technique is that it does not destroy the sample, except for the cases where the sample is not conductive and it must be covered with an Au conductive layer. The properties of the equipment used are summarized in table A.1

SEM model	Joel JSM 6400
Resolution	0.3 nm
Magnification	15-300 000 x
Kilo-voltage	from 0.5 to 40 kV
Sample rotation	360°
Sample inclination	90°
Back disperse electron detector	Yes

Table A.1. Technical characteristics of the SEM

A.2 Energy-dispersive X-ray spectroscopy (EDS or EDX)

At present, modern electron microscopy can give resolutions of less than 2 Å, which are sufficient to characterize the morphology and atomic structure of a metal cluster. An EDS technique was applied to make a quantitative composition analysis. This technique makes it possible to evaluate a specimen quickly, i.e. it enables the elements that form the cluster to be identified.

In its simplest form, quantitative analysis proceeds by determining the energies of x-ray emission. At low x-ray energies (less than 3 keV), peak separation and the limited resolution of the EDS spectrometer will probably restrict element identification to only one peak. But at low-energies, L or M lines will be accompanied by high-energy K or L lines in the 4-20 keV range, which can aid the identification [192]. Below 1 keV, quantitative EDS analysis is difficult. The main problem of the EDS used was that elements below Na (Z=11) could not be detected. Elements such as B, C, N and O will not be detected. The Be window that prevents the microscope chamber from becoming contaminated means that only elements below Na (Z=11) can be detected. Thus, in the case of oxides we will only detect their metallic component.

A.3 Atomic force microscopy (AFM)

AFM can image the surface topography, measure surface forces and adhesion, and determine mechanical properties. For contact imaging, the sample is scanned under an atomically sharp tip mounted on a cantilever. The deflection of the cantilever due to the force exerted by the sample on the tip is usually monitored optically. Typical forces are a few tenths of nN and are limited by adhesion. They are small enough for reproducible, non-destructive imaging of most surfaces. It is practical to use a feedback system that maintains a constant deflection of the cantilever by adjusting the z-piezo voltage. A plot of z (x,y), then, represents a surface of the constant force, and approximates the total charge density. The corrugation can be modelled by hard spheres in contact.

The AFM can also measure long-range interactions (non-contact mode). The advantage is that the tip now remains at a distance of some nano-meters from the sample so that there is no possibility of damaging either the tip or the surface. The tip is oscillated at a frequency that is slightly above its natural resonance frequency. A feedback system adjusts the tip-sample distance to keep the frequency shift constant at ~10-20 Hz. In this mode, however, the tip is not only influenced by Van der Waals forces (which dominate in the contact method), but also by charges on the surface and by capacitive forces. In order to be sensitive to surface morphology, the contact potential has to be compensated accurately, whereby the capacitive forces are minimized. In this case, atomic resolution may be achieved.

A.4 X-ray photoelectron spectroscopy (XPS)

XPS is used to determine the electronic structure of solid surfaces as well as to chemically identify surface components. It is a high-resolution method for determining the binding energies of electrons. Many photon or X-ray sources may be used but the most common are AlK_{α} (1486.6 eV) and MgK_{α} (1253.6 eV) radiation, both of which provide nearly monochromatic radiation with line widths of less than 1 eV. The Al or Mg X-ray sources actually produce a number of X-ray lines of which the $K_{\alpha 1,2}$ is the most intense. Each of the X-ray energies produced photoelectron transition, which mirror those produced by the K_{α} radiation. Since the intensity ratio and energy separation are known, the satellite photoelectron spectra may be removed with the appropriate software. The data from XPS has traditionally been taken as the number of electrons with energy, versus that energy. In current practice, XPS can detect all elements with $Z \geq 3$ (where Z is the atomic number) with little interference.

Using AlK_α or MgK_α radiation, the K-shell ionisation cross-section dominates for Z≤10 but above this atomic number the L-shell cross-section is significant and L photoelectrons may be used for analysis. The cornerstone of XPS is the measurement of the kinetic energy E_K of the outgoing electron. This energy is related to the electron binding energy E_B and to some external parameters:

$$E_K = h\nu - E_B - E_R - \Phi - \delta E \qquad \text{(A.1)}$$

Here, $h\nu$ is the photon energy of the incident X-rays, E_R is the recoil energy (this is a minor component, 0.1-0.001 eV, and is generally ignored), Φ is the spectrometer work function and δE describes the electronic charging of the spectrum which slightly reduces the energy of the photoelectrons (by up to 5 eV). E_K is determined experimentally, while $h\nu$ and Φ are known.

Contemporary XPS provides information about the environment of surface atoms. Core electrons are highly localized and their wave-functions are hardly affected by the surroundings. The binding energy of a core electron depends on the charge of the atom as well as on the background electrostatic potential in the core region.
Since the cross-section for the ionization of a core does not depend on the state of the valence electrons, the intensity of the emitted photoelectrons is proportional to the number of atoms in the detected volume. This is the basis of a quantitative XPS analysis. After a proper calibration, the chemical composition of the region investigated can be determined.

The XPS measurements were performed with a system equipped with a hemispherical electron energy analyser. The photon source was a monochromatic Al K_α line ($h\nu$ = 1486 eV). The resolution of the system (source + analyser) was 0.5 eV. Charging effects were neutralised using a flood gun operated at a kinetic energy of 2 eV.

A.5 Raman spectroscopy

Raman Spectroscopy is based on the diffusion processes given by the electronic polarization caused by ultraviolet or visible light. Detailed information about the principles of this spectroscopic technique is readily available [193, 194]. Raman analysis gives information at the molecular level and makes it possible to analyse the vibration and rotation of chemical species. Briefly, the radiation interacts with the molecular vibrational energy levels due to the light scattering phenomena, in which the electromagnetic radiation interacts with a pulsating

polarizable electron cloud. The diffusion effect means that this technique has several advantages. First, there is no need to prepare any samples so it is easier to implement. It also provides a nondestructive and quantitative microanalysis of structures and electronic properties. This technique has been widely used as well as XRD to identify the material structural phase and to analyse phase transitions. It can also be used to determine when the catalytic species are inside the semiconductor lattice, by analyzing the Raman peaks shift (see Cabot et al. [195] in their study on Pd-Pt/SnO_2 systems).

APPENDIX B

B.1 Table of results for sensors fabricated on Al_2O_3 substrate

B.1.1 SnO_2-doped sensors

- **Non doped SnO_2 sensor**
- **SnO_2 doped with Ag (sputtering)**
- **SnO_2 doped with Ti (sputtering)**
- **SnO_2 doped with Pt (sputtering)**
- **SnO_2 doped with Pt (paste**)

The gases measured are detailed in the following table.

Gases tested		
Ammonia	*Ethanol*	*Benzene*
Methane	*Relative humidity (10-85%)*	

Measured species

Tables B.1, B.2 and B.3 listed below present all the results obtained from the measurements. Methane is not included in the tables, because no reaction was detected during the test performed..

Non doped SnO_2		Sensitivity to temperature		
Gas	**Concentration (ppm)**	**250ºC**	**300ºC**	**350ºC**
Ethanol	**10**	5.14	7.26	3.04
	100	6.91	11.57	7.01
	1 000	19.94	62.30	38.92
Ammonia	**10**	1.14	1.06	2.45
	100	1.21	1.10	3.21
	1 000	1.51	1.31	3.60
Benzene	**10**	1.02	1.03	1.21
	100	1.05	1.35	1.69
	1000	1.16	1.67	2.62
Humidity	**25%**	1.24	1.52	1.68
	50%	1.48	1.66	1.78
	85%	1.56	1.88	1.92

Table B.1. Results of the measurements of non doped SnO_2

Tested sensors		Ag doped SnO_2			Ti doped SnO_2		
Gas	**Concentration (ppm)**	**250ºC**	**300ºC**	**350ºC**	**250ºC**	**300ºC**	**350ºC**
Ethanol	**10**	2.08	19.06	8.44	5.13	6.56	5.50
	100	3.44	31.02	19.65	10.07	13.88	27.97
	1 000	6.63	67.42	57.25	23.24	39.57	100.26
Ammonia	**10**	1.13	1.09	1.05	1.08	1.08	1.18
	100	1.24	1.31	1.17	1.09	1.11	1.31
	1 000	1.47	1.79	1.58	1.10	1.33	1.43
Benzene	**10**	1.02	1.07	1.44	1.01	1.21	1.22
	100	1.04	1.12	1.91	1.05	1.55	1.52
	1000	1.05	1.15	2.75	1.09	2.13	2.41
Humidity	**25%**	1.65	1.62	2.12	1.46	2.52	2.85
	50%	1.93	1.71	2.53	1.70	3.87	4.05
	85%	1.94	1.80	2.86	1.86	5.40	7.03

Table B.2. Results of the measurements of Ag and Ti doped SnO_2

Tested sensors		Pt (sputtering) doped SnO_2			Pt (paste) doped SnO_2		
Gas	**Concentration (ppm)**	**250ºC**	**300ºC**	**350ºC**	**250ºC**	**300ºC**	**350ºC**
Ethanol	**10**	2.95	2.55	32.77	20.16	78.51	9.10
	100	6.46	11.60	86.17	55.88	243.72	13.69
	1 000	19.06	30.35	247.98	120.07	524.66	19.10
Ammonia	**10**	1.06	1.26	1.28	1.56	7.34	2.43
	100	1.16	1.63	1.78	2.46	9.28	4.00
	1 000	1.29	2.15	3.36	6.01	11.32	6.00
Benzene	**10**	1.13	2.54	1.46	1.04	1.06	1.48
	100	1.26	5.18	2.51	1.39	1.28	2.29
	1000	1.65	11.12	4.69	2.49	2.06	4.77
Humidity	**25%**	1.44	1.44	2.32	1.71	2.12	3.30
	50%	1.62	1.64	3.23	1.67	1.70	1.72
	85%	1.75	2.00	3.88	4.44	4.80	4.89

Table B.3. Results of the measurements of Pt doped SnO_2

B.1.2 WO_3-doped sensors

- **Non doped WO_3 sensor**
- **WO_3 doped with Ag (15nm Ag layer via sputtering)**
- **WO_3 doped with Pt (Pt was introduced directly in the active layer**)
- **WO_3 doped with Pd (Pd was introduced directly in the active layer)**
- **WO_3 doped with Au (Au was introduced directly in the active layer)**
- **WO_3 doped with Au (15nm Au layer via sputtering)**
- **WO_3 doped with Au (25nm Au layer via sputtering)**

The gases measured are detailed in the following table.

Gases tested		
Ammonia	*Ethanol*	*NO_2*
Relative humidity (10-85%)		

Measured species

Tables B.4, B.5, B.6 and B.7 (see below) present all the results obtained from the measurements of this set.

Non doped WO_3		**Sensitivity to temperature**		
Gas	**Concentration (ppm)**	**250ºC**	**300ºC**	**350ºC**
Ethanol	**10**	1.35	2.78	2.07
	100	2.33	4.25	3.03
	1 000	3.34	7.97	5.24
Ammonia	**10**	1.19	1.20	1.07
	100	1.58	1.63	1.19
	1 000	2.71	2.98	1.53
NO_2	**1**	1.12	1.09	1.05
	5	3.29	3.15	1.53
	10	56.99	31.84	4.15
Humidity	**25%**	1.06	1.02	1.05
	50%	1.28	1.04	1.07
	85%	1.36	1.08	1.22

Table B.4. Results of the non- doped WO_3 measurements

Tested sensors		**Ag-doped WO_3**			**Pt-doped WO_3**		
Gas	**Concentration (ppm)**	**250ºC**	**300ºC**	**350ºC**	**250ºC**	**300ºC**	**350ºC**
Ethanol	**10**	1.12	2.97	3.92	1.45	2.86	1.87
	100	1.40	4.83	6.55	2.13	4.20	2.79
	1 000	1.94	9.99	13.68	3.15	7.40	5.07
Ammonia	**10**	1.04	1.00	1.02	1.38	2.27	1.76
	100	1.14	1.03	1.06	2.21	4.84	6.34
	1 000	1.46	1.09	1.14	2.50	5.23	18.72
NO_2	**1**	1.24	1.22	1.18	1.17	1.13	1.14
	5	3.94	5.27	3.22	3.53	3.50	2.13
	10	22.40	27.15	21.80	29.13	17.74	4.96
Humidity	**25%**	1.04	1.01	1.02	1.08	1.01	1.14
	50%	1.09	1.03	1.01	1.30	1.03	1.27
	85%	1.15	1.04	1.05	1.42	1.15	1.65

Table B.5. Results of the Ag- and Pt-doped WO_3 measurements

Tested sensors		Pd-doped WO_3			Au-doped WO_3 (paste)		
Gas	**Concentration (ppm)**	**250°C**	**300°C**	**350°C**	**250°C**	**300°C**	**350°C**
Ethanol	**10**	1.51	2.32	2.25	1.09	1.84	2.02
	100	3.17	6.66	7.21	1.28	2.50	2.94
	1 000	10.31	20.19	13.89	1.55	4.18	4.88
Ammonia	**10**	1.00	1.03	1.13	1.27	1.21	1.12
	100	1.03	1.04	1.19	1.88	1.64	1.38
	1 000	1.18	1.18	1.27	3.71	2.97	1.97
NO_2	**1**	1.29	1.10	1.08	1.26	1.17	1.04
	5	2.97	1.34	1.12	6.44	4.33	1.65
	10	21.77	2.16	1.21	62.90	40.92	5.09
Humidity	**25%**	1.21	1.03	1.10	1.02	1.01	1.05
	50%	1.98	1.08	1.18	1.33	1.07	1.05
	85%	3.14	1.11	1.90	1.75	1.10	1.18

Table B.6. Results of the Pd- and Au-doped WO_3 measurements

Tested sensors		Au-doped WO_3 (sputt. 15*nm*)			Au-doped WO_3 (sputt. 25*nm*)		
Gas	**Concentration (ppm)**	**250°C**	**300°C**	**350°C**	**250°C**	**300°C**	**350°C**
Ethanol	**10**	1.02	1.84	1.69	1.00	1.80	2.13
	100	1.05	2.66	2.23	1.02	2.62	2.92
	1 000	1.10	4.64	3.52	1.06	4.40	4.80
Ammonia	**10**	1.07	1.00	1.03	1.02	1.04	1.04
	100	1.20	1.04	1.09	1.06	1.12	1.11
	1 000	1.45	1.29	1.27	1.18	1.32	1.30
NO_2	**1**	1.33	1.50	1.49	1.26	1.37	1.42
	5	6.36	6.69	5.09	5.32	5.15	4.05
	10	11.94	11.52	8.75	11.20	8.89	6.80
Humidity	**25%**	1.04	1.08	1.10	1.03	1.00	1.11
	50%	1.22	1.09	1.14	1.22	1.14	1.15
	85%	1.57	1.18	1.19	1.64	1.20	1.22

Table B.7. Results of the Au-doped (via sputtering) WO_3 measurements

B.2 Table of results for sensors fabricated on MHP substrate

B.2.1 Non-doped SnO_2 sensors

- **Micro-grain SnO_2 sensor**
- **Nano-grain SnO_2 sensor**

The three tables below (B.8, B.9 and B.10) describe the first set, consisting of the SnO_2 MHP gas sensors. The best results are highlighted. The minimum values (where minimum value is needed) are in blue.

Layer	Grain	Electr.	T [°C]	Ethanol (ppm)			Acetone (ppm)			Ammonia (ppm)		
				C1	C2	C3	C1	C2	C3	C1	C2	C3
SnO_2	*μm*	50μm	110	1.02	1.22	1.91	1.00	1.19	1.90	1.01	1.07	1.93
			200	1.02	1.27	4.43	1.02	1.22	16.99	1.09	1.47	24.39
			380	1.03	1.54	14.81	**1.04**	**1.24**	**17.85**	1.13	19.39	148.22
		100μm	150	1.05	1.30	1.70	1.00	1.47	1.35	1.01	4.33	10.03
			250	1.17	1.68	1.87	1.22	3.50	4.33	1.28	14.81	20.49
			480	**1.19**	**4.69**	**15.95**	1.29	4.95	6.64	**1.32**	**46.79**	**168.48**
	nm	50μm	110	1.02	1.02	1.03	1.00	1.02	1.05	1.01	1.11	1.14
			200	1.37	1.43	1.73	1.31	1.35	1.39	1.20	1.64	21.68
			380	2.51	5.81	19.44	**2.41**	**21.58**	**22.67**	2.40	30.31	184.17
		100μm	150	1.06	1.19	1.20	1.00	1.28	1.34	1.01	1.32	1.35
			250	1.46	1.89	5.28	1.62	3.86	5.46	4.84	16.55	52.30
			480	**2.23**	**2.46**	**20.94**	1.72	1.50	8.34	**12.46**	**25.47**	**209.35**

Table B.8. Results of the measurements of simple volatile compounds

Layer	Grain	Electr.	T [°C]	Acetone+Ethanol (ppm)			Acetone+Ammonia (ppm)			Ammonia+Ethanol (ppm)		
				C1	C2	C3	C1	C2	C3	C1	C2	C3
SnO_2	*μm*	50μm	110	1.01	1.02	2.28	1.05	1.11	8.65	1.07	1.04	10.10
			200	1.08	1.17	5.00	1.41	1.71	47.55	1.60	1.95	33.09
			380	1.09	1.38	5.24	**1.80**	**4.43**	**187.40**	**1.73**	**4.12**	**188.75**
		100μm	150	1.01	1.42	1.67	1.02	2.72	5.84	1.03	3.19	4.09
			250	1.34	1.57	4.30	2.87	4.44	6.75	1.10	4.24	12.20
			480	**1.58**	**6.98**	**31.62**	4.78	7.81	32.15	3.60	9.69	12.32

		50µm	**110**	1.01	1.10	1.15	1.01	1.44	1.84	1.01	1.63	1.76
			200	1.25	1.43	1.68	1.28	1.97	5.098	1.27	2.36	4.98
			380	3.01	6.60	6.92	**11.25**	**61.82**	**243.62**	**13.54**	**44.34**	**252.93**
		100µm	**150**	1.01	1.50	1.77	1.02	3.21	5.35	1.01	1.23	4.03
			250	1.73	1.92	8.52	3.13	5.11	8.98	3.86	5.13	11.72
			480	**2.21**	**5.68**	**41.74**	4.28	7.59	41.79	5.48	14.35	16.51

Table B.9. Results of the measurements of binary mixtures

Layer	Grain	Electr.	T [°C]	NO_2 (ppm)			CO (ppm)			Humidity (%)		
				1	**5p**	**10**	**1000**	**2500**	**3500**	**30**	**50**	**70**
SnO_2	*µm*	50µm	**110°C**	1.40	1.83	1.97	1.00	1.00	1.00	**1.01**	**1.03**	**1.05**
			200°C	3.29	9.25	28.27	1.00	1.00	1.00	1.05	1.07	1.09
			380°C	1.48	2.32	10.57	1.00	1.10	1.05	1.20	1.22	1.29
		100µm	**150°C**	1.66	4.22	11.51	1.00	1.01	1.01	1.04	1.08	1.14
			250°C	**3.24**	**10.45**	**80.64**	1.02	1.17	1.30	1.06	1.09	1.10
			480°C	1.34	2.18	10.61	**1.05**	**1.40**	**1.66**	1.17	1.24	1.33
	nm	50µm	**110°C**	1.43	2.23	2.60	1.00	1.01	1.02	**1.04**	**1.09**	**1.13**
			200°C	3.36	11.29	37.32	1.01	1.06	1.13	1.07	1.10	1.15
			380°C	1.51	2.83	13.95	1.01	1.26	1.37	1.22	1.29	1.37
		100µm	**150°C**	1.69	5.15	15.19	1.00	1.01	1.31	1.06	1.11	1.16
			250°C	**3.63**	**12.75**	**106.44**	1.03	1.34	1.69	1.09	1.11	1.14
			480°C	1.50	2.66	14.00	**1.06**	**1.61**	**2.16**	1.24	1.34	1.40

Table B.10. Results of the measurements of toxic gases

B.2.2 Non-doped WO_3 sensors

- **Micro-grain WO_3 sensor**
- **Nano-grain WO_3 sensor**

The next three tables (B.11, B.12 and B.13) describe the second set, consisting of the WO_3 MHP gas sensors. Once again, the best results are highlighted. In some cases, where minimum sensitivity is desired (for example in the case of humidity) the optimal values are in blue.

Layer	Grain	Electr.	T [°C]	Ethanol (ppm)			Acetone (ppm)			Ammonia (ppm)		
				C1	C2	C3	C1	C2	C3	C1	C2	C3
WO_3	*μm*	50μm	**110**	1.24	2.62	12.94	1.12	1.73	1.94	1.13	2.09	2.92
			200	1.42	6.15	17.45	1.37	3.09	4.11	2.03	7.97	13.36
			380	2.01	11.45	34.03	1.83	4.67	8.59	2.47	9.8	34.33
		100μm	**150**	1.47	3.88	6.48	1.19	1.79	3.13	1.55	2.7	3.94
			250	1.93	4.56	12.65	1.55	4.03	9.46	2.15	9.37	17.61
			480	**2.39**	**7.92**	**40.91**	**2.01**	**7.38**	**14.66**	**3.19**	**13.23**	**46.31**
	nm	50μm	**110**	1.32	1.51	2.14	1.14	1.47	1.94	1.26	2.19	2.69
			200	2.95	6.92	12.88	1.91	3.40	5.15	2.34	8.91	10.96
			380	16.98	22.91	44.67	2.46	5.22	10.91	3.63	16.60	42.66
		100μm	**150**	1.51	2.00	2.51	1.23	1.63	2.15	1.74	2.34	3.47
			250	4.37	5.13	8.91	1.97	4.44	8.13	3.02	10.47	14.79
			480	**8.51**	**16.60**	**53.70**	**3.98**	**12.02**	**18.62**	**4.90**	**21.88**	**57.54**

Table B.11. Results of the measurements of simple volatile compounds

Layer	Grain	Electr.	T [°C]	Acetone+Ethanol (ppm)			Acetone+Ammonia (ppm)			Ammonia+Ethanol (ppm)		
				C1	C2	C3	C1	C2	C3	C1	C2	C3
WO_3	*μm*	50μm	**110**	1.38	2.06	2.69	1.50	1.62	3.44	1.71	2.74	6.07
			200	1.75	3.66	7.75	2.43	8.30	15.35	3.65	30.70	68.06
			380	3.40	7.30	9.11	3.21	14.10	21.18	**8.54**	**41.42**	**235.99**
		100μm	**150**	1.59	4.61	5.75	1.64	3.89	4.32	2.29	4.55	6.50
			250	4.08	5.80	16.20	3.44	11.20	13.37	5.77	19.37	96.13
			480	**5.02**	**17.12**	**31.58**	**6.54**	**22.60**	**36.42**	19.09	58.50	110.38
	nm	50μm	**110**	1.41	1.78	3.47	1.51	2.45	3.24	1.74	3.72	8.71
			200	2.51	4.47	8.19	1.86	9.55	16.22	3.31	37.15	50.12
			380	3.55	10.23	12.02	4.47	19.95	27.54	**8.13**	**91.20**	**316.23**
		100μm	**150**	1.62	4.57	5.62	1.66	4.47	5.62	2.34	5.50	8.71
			250	5.62	7.08	20.89	3.47	12.88	17.38	6.46	23.44	128.82
			480	**7.59**	**21.38**	**41.69**	**6.61**	**25.99**	**47.35**	21.38	70.79	147.91

Table B.12. Results of the measurements of binary mixtures

Layer	Grain	Electr.	T [°C]	NO_2 (ppm)			CO (ppm)			Humidity (%)		
				1	5	10	1000	2500	3500	30	50	70
WO_3	*µm*	50µm	110	1.85	2.48	3.55	1.00	1.00	1.00	**1.02**	**1.04**	**1.05**
			200	**8.74**	**12.70**	**12.58**	1.00	1.00	1.00	1.07	1.10	1.13
			380	2.62	5.30	6.45	1.00	1.00	1.00	1.15	1.21	1.23
		100µm	150	1.46	1.60	2.51	1.00	1.00	1.00	1.09	1.13	1.14
			250	6.27	8.01	10.53	1.00	1.00	1.00	1.12	1.21	1.22
			480	2.03	3.40	5.37	1.00	1.00	1.00	1.14	1.37	1.28
	nm	50µm	110	1.89	3.02	4.68	1.00	1.00	1.00	**1.11**	**1.26**	**1.32**
			200	**8.91**	**15.49**	**16.60**	1.00	1.00	1.00	1.15	1.33	1.44
			380	2.67	6.46	8.51	1.00	1.00	1.00	1.17	1.47	1.57
		100µm	150	1.69	1.95	3.31	1.00	1.00	1.00	1.21	1.31	1.49
			250	7.02	9.77	13.90	1.00	1.00	1.00	1.25	1.47	1.63
			480	2.27	4.15	7.09	1.00	1.00	1.00	1.28	1.66	1.72

Table B.13. Results of the measurements of toxic gases

B.2.3 Doped SnO_2 sensors

- **Non-doped SnO_2 sensors**
- **Au doped SnO_2 sensors**
- **Pd doped SnO_2 sensors**
- **Pt doped SnO_2 sensors**

The tables below (B.14, B.15 and B.16) present all the results obtained from the measurements of set C. The best doping for the measured specimen is highlighted and the best result is marked in red. The measured gases with no response are indicated in green. In some cases, where minimum sensitivity is desired (for example in the case of humidity) the optimal values are in blue.

Layer	T [°C]	Ammonia (ppm)			Ethanol (ppm)			Ethylene (ppm)		
		100	500	1000	1	10	100	1	5	10
SnO_2	250	1.07	1.51	2.96	1.37	2.14	3.50	1.01	1.06	1.27
	350	1.16	2.94	4.24	1.97	4.17	14.72	1.03	1.14	1.39
	450	1.78	3.87	5.71	1.60	2.46	6.99	1.05	1.18	1.56

SnO_2 +1%Au	**250**	1.43	2.65	5.43	1.47	2.30	3.75	1.20	1.42	2.78
	350	1.82	5.69	9.57	1.91	4.05	17.12	1.46	1.79	3.55
	450	3.40	10.49	23.89	1.64	2.52	8.38	1.84	3.04	4.79
SnO_2 +1%Pd	**250**	**1.77**	**3.27**	**6.71**	1.54	2.41	3.94	1.09	1.30	2.50
	350	**2.07**	**6.48**	**10.88**	2.08	4.41	18.66	1.39	1.71	3.34
	450	**3.90**	**12.02**	**29.37**	1.76	2.70	8.97	1.72	3.08	4.16
SnO_2 +1%Pt	**250**	1.61	2.98	6.11	**2.20**	**3.44**	**5.64**	**1.20**	**1.43**	**2.72**
	350	2.00	6.25	10.50	**3.43**	**7.28**	**62.00**	**1.50**	**1.84**	**3.54**
	450	3.59	11.07	25.22	**2.68**	**4.11**	**16.71**	**1.91**	**3.18**	**6.49**

Table B.14. Results of NH_3, C_2H_5OH and C_2H_4

Layer	**T [°C]**	**NO_2 (ppm)**			**CO (ppm)**			**H_2S (ppm)**		
		1	**5**	**10**	**1000**	**2500**	**3500**	**1**	**2**	**4**
SnO_2	**250**	3.41	7.25	24.27	1.01	1.14	1.2	1.00	1.00	1.00
	350	1.55	2.21	7.56	1.08	1.19	1.27	1.00	1.00	1.00
	450	1.42	1.93	2.91	1.12	1.25	1.31	1.00	1.00	1.00
SnO_2 +1%Au	**250**	**4.57**	**12.72**	**50.01**	1.35	2.00	2.20	1.00	1.00	1.00
	350	**2.43**	**4.28**	**17.06**	1.70	2.30	2.87	1.00	1.00	1.00
	450	**2.71**	**5.23**	**10.36**	2.14	3.39	4.66	1.00	1.00	1.00
SnO_2 +1%Pd	**250**	4.14	8.63	25.60	**1.52**	**2.25**	**2.48**	1.00	1.00	1.00
	350	2.12	2.81	11.03	**1.86**	**2.53**	**3.15**	1.00	1.00	1.00
	450	1.37	3.49	5.96	**2.26**	**3.58**	**4.92**	1.00	1.00	1.00
SnO_2 +1%Pt	**250**	4.35	10.11	27.63	1.45	2.14	2.36	1.00	1.00	1.00
	350	2.27	3.01	13.94	1.74	2.36	2.94	1.00	1.00	1.00
	450	1.49	3.80	6.20	2.07	3.28	4.52	1.00	1.00	1.00

Table B.15. Results of NO_2, CO and H_2S

Layer	**T [°C]**	**CH_4 (ppm)**			**Humidity %**		
		1000	**5000**	**10000**	**30**	**50**	**70**
SnO_2	**250**	1.00	1.00	1.00	**1.02**	**1.04**	**1.06**
	350	1.00	1.00	1.00	**1.06**	**1.08**	**1.10**
	450	1.00	1.00	1.00	**1.21**	**1.23**	**1.30**

SnO_2 +1%Au	**250**	1.00	1.00	1.00	1.03	1.06	1.08
	350	1.00	1.00	1.00	1.07	1.11	1.14
	450	1.00	1.00	1.00	1.23	1.28	1.36
SnO_2 +1%Pd	**250**	1.00	1.00	1.00	1.07	1.11	1.17
	350	1.00	1.00	1.00	1.09	1.12	1.13
	450	1.00	1.00	1.00	1.21	1.28	1.37
SnO_2 +1%Pt	**250**	1.00	1.00	1.00	1.08	1.13	1.20
	350	1.00	1.00	1.00	1.10	1.27	1.42
	450	1.00	1.00	1.00	1.22	1.57	1.75

Table B.16. Results of the measurements of CH_4 and H_2O

B.2.3 Doped WO_3 sensors

- **Non-doped WO_3 sensors**
- **Au doped WO_3 sensors**
- **Pd doped WO_3 sensors**
- **Pt doped WO_3 sensors**

Tables B.17, B.18 and B.19 present all the results obtained from the measurements of set D.

Layer	**T [°C]**	**Ammonia (ppm)**			**Ethanol (ppm)**			**Ethylene (ppm)**		
		100	**500**	**1000**	**1**	**10**	**100**	**1**	**5**	**10**
WO_3	**250**	1.34	2.84	7.96	1.10	1.45	2.26	1.00	1.00	1.00
	350	1.46	5.56	11.49	1.56	2.80	9.38	1.00	1.00	1.00
	450	2.26	7.35	18.32	1.26	1.64	4.40	1.00	1.00	1.00
WO_3 +1%Au	**250**	1.83	5.06	14.93	1.15	1.52	2.33	1.00	1.00	1.00
	350	2.35	10.92	26.51	1.48	2.66	10.50	1.00	1.00	1.00
	450	4.42	20.25	66.65	1.26	1.65	5.08	1.00	1.00	1.00
WO_3 +1%Pd	**250**	**2.32**	**6.34**	**18.86**	1.18	1.56	2.36	1.00	1.00	1.00
	350	**2.73**	**12.64**	**30.79**	1.58	2.85	11.04	1.00	1.00	1.00
	450	**5.19**	**23.56**	**78.00**	1.32	1.73	5.25	1.00	1.00	1.00
WO_3 +1%Pt	**250**	2.16	5.87	17.54	**1.64**	**2.19**	**3.26**	1.00	1.00	1.00
	350	2.70	12.38	30.35	**2.54**	**4.61**	**35.43**	1.00	1.00	1.00
	450	4.88	22.03	73.39	**1.97**	**2.58**	**9.44**	1.00	1.00	1.00

Table B.17. Results of NH_3, C_2H_5OH and C_2H_4

Layer	T [°C]	NO_2 (ppm)			CO (ppm)			H_2S (ppm)		
		1	5	10	1000	2500	3500	1	2	4
WO_3	250	4.94	11.60	41.26	1.00	1.00	1.00	1.00	1.00	1.00
	350	2.40	3.76	13.99	1.00	1.00	1.00	1.00	1.01	1.03
	450	2.34	3.47	5.82	1.00	1.00	1.00	1.01	1.02	1.05
WO_3 +1%Au	250	**9.94**	**30.53**	**127.53**	1.00	1.00	1.00	**1.28**	**1.67**	**1.75**
	350	**5.65**	**10.91**	**47.34**	1.00	1.00	1.00	**1.47**	**1.83**	**2.17**
	450	**6.71**	**14.12**	**31.08**	1.00	1.00	1.00	**1.77**	**2.54**	**3.43**
WO_3 +1%Pd	250	6.82	15.68	49.42	1.00	1.00	1.00	1.05	1.09	1.11
	350	3.73	5.42	23.17	1.00	1.00	1.00	1.08	1.21	1.28
	450	2.57	7.13	13.54	1.00	1.00	1.00	1.15	1.24	1.38
WO_3 +1%Pt	250	7.58	19.43	56.43	1.00	1.00	1.00	1.08	1.17	1.20
	350	4.23	6.15	30.98	1.00	1.00	1.00	1.14	1.28	1.50
	450	2.95	8.22	14.90	1.00	1.00	1.00	1.20	1.47	1.55

Table B.18. Results of NO_2, CO and H_2S

Layer	T [°C]	CH_4 (ppm)			Humidity %		
		1000	5000	10000	30	50	70
WO_3	250	1.00	1.00	1.00	**1.01**	**1.03**	**1.04**
	350	1.00	1.00	1.00	**1.06**	**1.09**	**1.12**
	450	1.00	1.00	1.00	**1.14**	**1.20**	**1.22**
WO_3 +1%Au	250	1.00	1.00	1.00	1.08	1.12	1.13
	350	1.00	1.00	1.00	1.11	1.20	1.21
	450	1.00	1.00	1.00	1.13	1.26	1.35
WO_3 +1%Pd	250	1.00	1.00	1.00	1.09	1.24	1.30
	350	1.00	1.00	1.00	1.13	1.31	1.42
	450	1.00	1.00	1.00	1.15	1.45	1.55
WO_3 +1%Pt	250	1.00	1.00	1.00	1.19	1.29	1.47
	350	1.00	1.00	1.00	1.23	1.45	1.86
	450	1.00	1.00	1.00	1.47	1.93	2.23

Table B.19. Results of the measurements of CH_4 and H_2O

B.2.4 Au doped WO_3 sensors

- **Non-doped WO_3 sensors**
- **1%Au doped WO_3 sensors**
- **2%Au doped WO_3 sensors**
- **4%Au doped WO_3 sensors**

Tables B.20, B.21 and B.22 present all the results obtained from the measurements of set E.

Layer	T [°C]	Ammonia (ppm)			Ethanol (ppm)			Ethylene (ppm)		
		100	500	1000	1	10	100	1	5	10
WO_3	250	1.36	2.87	8.05	1.11	1.47	2.29	1.00	1.00	1.00
	350	1.48	5.63	11.63	1.58	2.84	9.50	1.00	1.00	1.00
	450	2.30	7.46	18.60	1.28	1.67	4.47	1.00	1.00	1.00
WO_3 +1%Au	250	1.85	5.12	15.09	1.16	1.54	2.36	1.00	1.00	1.00
	350	2.38	11.07	26.86	1.50	2.70	10.64	1.00	1.00	1.00
	450	4.49	20.56	67.67	1.28	1.68	5.16	1.00	1.00	1.00
WO_3 +2%Au	250	**3.22**	**9.84**	**30.82**	2.02	2.96	4.82	1.00	1.00	1.00
	350	**4.43**	**22.61**	**59.70**	2.79	5.51	23.65	1.00	1.00	1.00
	450	**8.90**	**44.46**	**162.59**	2.54	3.63	12.40	1.00	1.00	1.00
WO_3 +4%Au	250	2.82	7.91	22.93	**3.42**	**5.89**	**9.84**	1.00	1.00	1.00
	350	3.74	17.61	43.13	**4.20**	**12.26**	**52.56**	1.00	1.00	1.00
	450	7.71	35.45	120.08	**3.83**	**8.86**	**24.79**	1.00	1.00	1.00

Table B.20. Results of NH_3, C_2H_5OH and C_2H_4

Layer	T [°C]	NO_2 (ppm)			CO (ppm)			H_2S (ppm)		
		1	5	10	1000	2500	3500	1	2	4
WO_3	250	5.00	11.73	41.72	1.00	1.00	1.00	1.01	1.01	1.01
	350	2.43	3.81	14.17	1.00	1.00	1.00	1.01	1.02	1.04
	450	2.38	3.52	5.91	1.00	1.00	1.00	1.03	1.04	1.07
WO_3 +1%Au	250	10.05	30.87	128.93	1.00	1.00	1.00	1.29	1.69	1.77
	350	5.73	11.06	47.97	1.00	1.00	1.00	1.49	1.85	2.20
	450	6.81	14.34	31.55	1.00	1.00	1.00	1.80	2.58	3.48

WO_3 +2%Au	**250**	**17.51**	**57.34**	**223.31**	1.00	1.00	1.00	2.15	3.05	3.31
	350	**10.67**	**22.59**	**104.61**	1.00	1.00	1.00	2.27	3.58	4.89
	450	**13.50**	**31.01**	**71.81**	1.00	1.00	1.00	2.87	5.02	8.19
WO_3 +4%Au	**250**	15.31	46.09	166.15	**1.03**	**1.07**	**1.11**	**2.91**	**4.24**	**5.38**
	350	9.01	17.59	75.59	**1.08**	**1.14**	**1.19**	**3.17**	**5.72**	**7.87**
	450	11.70	24.73	53.04	**1.11**	**1.23**	**1.31**	**3.22**	**6.06**	**8.09**

Table B.21. Results of NO_2, CO and H_2S

Layer	**T [°C]**	**CH_4 (ppm)**			**Humidity %**		
		1000	**5000**	**10000**	**30**	**50**	**70**
WO_3	**250**	1.00	1.00	1.00	**1.01**	**1.05**	**1.07**
	350	1.00	1.00	1.00	**1.06**	**1.11**	**1.14**
	450	1.00	1.00	1.00	**1.17**	**1.25**	**1.26**
WO_3 +1%Au	**250**	1.00	1.00	1.00	1.09	1.12	1.15
	350	1.00	1.00	1.00	1.11	1.21	1.23
	450	1.00	1.00	1.00	1.13	1.31	1.34
WO_3 +2%Au	**250**	1.00	1.00	1.00	1.26	1.52	1.74
	350	1.00	1.00	1.00	1.33	1.62	1.83
	450	**1.12**	**1.25**	**1.31**	1.40	1.69	1.88
WO_3 +4%Au	**250**	1.00	1.00	1.00	1.31	1.83	2.09
	350	1.00	1.00	1.00	1.56	2.12	2.63
	450	**1.19**	**1.27**	**1.32**	1.91	2.57	3.34

Table B.22. Results of the measurements of CH_4 and H_2O

REFERENCES

1. L. Dori, S. Nicoletti and I. Elmi, A gas chromatographic-like system for the separation and monitoring of benzene, toluene and xylene compounds at the ppb level using solid state metal oxide gas sensors, Sensors and Materials Journal, 12, pp.163-174, 2000.

2. T. Aishima, Discrimination of liquor aromas by pattern recognition analysis of responses from a gas sensor array, Anal. Chim. Acta, 243, pp. 287-292, 1991.

3. Figaro Gas Sensor Company, Gas sensor catalogue and technical information, 2000.

4. W. Göpel, G. Reinhardt, Metal oxide sensors: New devices through tailoring interfaces on the atomic scale, Sensors and Actuators Update vol.1, H. Baltes, W. Göpel, J. Hesse, Eds., Weinheim, 1996.

5. V. M. Jiménez, J. P. Espinós and A. R. González-Elipe, Effect of texture and annealing treatments in SnO2 and Pd/SnO_2 gas sensor materials, Sens. Actuat. B, 61, pp. 23-32, 1999.

6. Y. Shimizu, T. Maekawa, Y. Nakamura and M. Egashira, Effects of gas diffusivity and reactivity on sensing properties of thick film SnO2 based sensors, Sens. Actuat. B, 46, pp. 163-168, 1998.

7. N. Yamazoe, Y. Kurokawa and T. Seiyama, Effects of additives on semiconductor gas sensors, Sens. Actuat. B, 4, pp. 283-289, 1983.

8. D. Kohl, The role of noble metals in the chemistry of solid-state gas sensors, Sens. Actuat. B, 1, pp. 158-165, 1990.

9. J. Mizsei, How can sensitive and selective semiconductor gas sensor be made?, Sens. Actuat. B, 23, pp. 173-176, 1995.

10. Y. Shimizu, E. Kanazawa, Y. Takao and M. Egashira, Modification of H_2-sensitive breakdown voltages of SnO_2 varistors with noble metals, Sens. Actuat. B, 52, pp. 38-44, 1998.

11. N. Yamazoe, Y. Kurokawa and T. Seiyama, Effects of additives on semiconductor gas sensors, Sens. Actuat. B, 4, pp. 283-289, 1993.

12. N. Yamazoe, New approaches for improving semiconductor gas sensors, Sens. Actuat. B, 5, pp. 7-19, 1991.

13. A. R. Phani, S. Manorama and V. J. Rao, The nature of surface behavior of tin oxide doped sensors: X-ray photoelectron spectroscopy studies before and after exposure to liquid petroleum gas, Journal of Physics and Chemistry of Solids, 61, pp. 985-993, 2000.

14. O. Renault, A. V. Tadeev, G. Delabouglise and M. Labeau, Integrated solid-state gas sensors based on SnO_2 (Pd) for CO detection, Sens. Actuat. B, 59, pp. 260-264, 1999.

15. A. V. Tadeev, G. Delabouglise and M. Labeau, Influence of Pd and Pt additives on the microstructural and electrical properties of SnO_2-based sensors, Materials Science and Engineering, B57, pp. 76-83, 1998.

16. N. Bârsan, J. R. Stetter, M. Findlay, Jr. and W. Göpel, High-Performance Gas Sensing of CO: Comparative Tests for Semiconducting (SnO_2-Based) and for Amperometric Gas Sensors, Analytical Chemistry, 71 (13), pp. 2512-2517, 1999.

17. W. K. Choi, S. K. Song, J. S. Cho, Y. S. Yoon, D. Choi, H.-J. Jung and S. K. Koh, H_2 gas-sensing characteristics of SnOx sensors fabricated by a reactive ion-assisted deposition with/without an activator layer, Sens. Actuat. B, pp. 40, 21, 1997.

18. D. Rosenfeld, R. Sanjinés, W.H. Schreiner and F. Lévy, Gas sensitive and selective SnO_2 thin polycrystalline films doped by ion implantation, Sens. Actuat.B,15-16, pp. 406-409,1993.

19. T. B. Fryberger and S. Semancik, Conductance Response of Pd/SnO_2 Model Gas Sensors to H_2 and O_2, Sens. Actuat. B, 2, pp. 305-309, 1990.

20. I. Hayakawaa, Y. Iwamotoa, K. Kikutab and S. Hiranob, Gas sensing properties of platinum dispersed-TiO_2 thin film derived from precursor, Sens. Actuat.B,62, pp. 55-60,2000.

21. H.P. Kim, J. Choi, H. Cheong, J. Kim and J. Kim, Sensing mechanism of SnO_2-based sensors for alcohols, Sensors and Acuators B, 13-14, pp. 511-512, 1993.

22. P.Clifford, Selective gas detection and measurement system, US Patent 4542640, 1985.

23. N. Yamazoe, New approaches for improving semiconductor gas sensors, Sens. Actuat. B, 5, 7-19, 1991.

24. C. Xu, J. Tamaki, N. Miura and N. Yamazoe, Grain size effects on gas sensitivity of porous SnO_2-based elements, Sens. Actuat. B, 3, pp. 147-155, 1991.

25. A. Cabot, J. Arbiol, J. R. Morante, U. Weimar, N. Bârsan and W. Göpel, Analysis of the noble metal catalytic additives introduced by impregnation of as obtained SnO_2 sol-gel nanocrystals for gas sensors, Sens. Actuat. B, 70, pp. 87-100, 2000.

26. M. Labeau, B. Gautheron, G. Delabouglise, J. Peña, V. Ragel, A. Varela, J. Román, J. Martínez, J. M. González-Calbet and M. Vallet-Regí, Synthesis, structure and gas sensitivity properties of pure and doped SnO_2, Sens. Actuat. B, 15-16, pp. 379-383, 1993.

27. R. Cavicchi, V. Sukharev and S. Semancik, Time-dependent conductance of Pd-dosed SnO_2 (110), Surface Science, 418, pp. L81-L88, 1998.

28. PhD Thesis of Jordi Arbiol i Cobos, Metal additive distribution in TiO_2 and SnO_2 Semiconductor gas sensor nano-structured materials, 2001.

29. Y. Shimizu, M. Egashira, Basic aspects and challenges of semiconductor gas sensors, MRS Bulletin, 24 (6), pp. 18-24, 1999.

30. C. Xu, T. Jun, N. Miura, N. Yamazoe, Correlation between gas sensitivity and crystallite size in porous SnO_2-based sensors, Chemical Letters, 3, pp. 441-444, 1990.

31. P.T. Moseley and B. Tofield, Solid state gas sensors, Adam Hilger, Bristol, U.K., 1987.

32. P.T. Moseley, A.M. Stoneham and D.E. Williams, Techniques and mechanisms in gas sensing, Adam Hilger, Bristol, U.K., 1991.

33. Xu, J. Tamaki, N. Miura and N. Yamazoe, Grain size effects on gas sensitivity of porous SnO_2-based elements, Sens. Actuat. B, 3, pp. 147-155, 1991.

34. W. Göpel, New materials and transducers for chemical sensors, Sens. Actuat. B, 18-19, pp. 1-21, 1994.

35. V. Demarne and R. Sanjines, Gas sensors principles, operation and development, Kluwer Academic, ed. G. Sberveglieri, Dordrecht, the Netherlands, pp. 89-116, 1992.

36 M. Haruta, Size and support-dependency in the catalysis of gold, Catalysis Today, 36, pp. 53-166, 1997.

37. H.M. Lin, C.M. Hsu, N.Y. Yang, P.Y. Lee and C.C. Yang, Nanocrystalline WO_3-based H_2S sensors, Sens. Actuat. B, 22, pp. 63-68, 1994.

38 M. Penza, C. Martucci and G. Cassano, NO_x gas sensing characteristics of WO_3 thin films activated by noble metals (Pd, Pt, Au) layers, Sens. Actuat. B, 50, pp. 52-59, 1998.

39. T. Maekawa, J. Tamaki, N. Miura and N. Yamazoe, Gold-loaded tungsten oxide sensor for detection of ammonia in air, Chem. Lett., 2, pp. 639-642, 1992

40. Y. Shimizu and M. Egashira, Basic aspects and challenges of semiconductor gas sensors, MRS Bulletin, pp. 18-24, June 1999.

41. N. Yamazoe, New approaches for improving semiconductor gas sensors, Sens. Actuat. B, 5, pp. 7-19, 1991.

42. F.J. Gutierrez, L. Arés, M.C. Horrillo, I. Sayago, J.A. Agapito and L. López, Use of complex impedance spectroscopy in chemical sensor characterisation, Sens. Actuat. B, 4, pp. 359-363, 1991.

43. H. Amrani, P. Payne and K. Persaud, Multi-frequency measurements of organic conducting polymers for sensing of gases and vapours, Sens. Actuat.B, 33, pp. 137-141, 1996.

44. E. Llobet, X. Vilanova, J. Brezmes, J.E. Sueiras and X. Correig, Transient response of thick-film tin oxide gas sensors to multicomponent gas mixtures, Sens. Actuat. B, 47, pp. 104-112, 1998.

45. E. Llobet, X. Vilanova, J. Brezmes, J.E. Sueiras, R. Alcubilla and X. Correig, Model for the steady-state and transient behaviour of thick-film tin oxide gas sensors in the presence of gas mixtures, Journal of the Electrochemical Society, 145, pp. 1772-1779, 1998.

46. E. Llobet, J. Brezmes, X. Vilanova, J.E. Sueiras and X. Correig, Qualitative and quantitative analysis of volatile organic compounds using transient and steady-state responses of a thick-film tin oxide gas sensor array, Sens. Actuat. B, 41, pp. 13-22, 1997.

47. M. Roth, R. Hartinger, M. Schwaiger, M. Gräber, H.E. Endres, Drift reduction of gas sensors by temperature modulation and signal processing, 3rd IFAC Symposium on Intelligent Components and Instrumentation for Control Applications, Annecy, 1997.

48. R.J.R. Uhlhorn and A.J. Burggraaf, Gas separation with inorganic membranes, in R.R. Bhave (ed.), Inorganic Membranes: Synthesis, Characteristics and Applications, Van Nostrand Reinhold, New York, U.S.A., pp. 155, 1991.

49. P. Althainz, A. Dahlke, J. Goschnick and H.J. Ache, Low temperature deposition of glass membranes for gas sensors, Thin Solid Films, 241, pp. 344-347, 1994.

50. C.O. Park, S.A. Akbar, J. Hwang, Selective gas detection with catalytic filter, Materials Chemistry and Physics, 73, pp. 56-60, 2002.

51. M.A. Portnoff, R.G. Grace, A.M. Guzman, P.D. Runco and L.N. Yannopoulos, Enhancement of MOS gas sensor selectivity by on-chip catalytic filtering, Technical Digest of the 3rd International Meeting on Chemical Sensors, Cleveland, U.S.A., pp. 96-97, September 24-26, 1990.

52. C.D. Feng, Y. Shimizu and M. Egashira, Effect of gas diffusion process on sensing properties of SnO_2 thin film sensors in a SiO_2/SnO_2 layer-built structure fabricated by sol-gel process, J. Electrochem. Soc., 141, pp. 220-225, 1994.

53. T. Schwebel, M. Fleischer and H. Meixner, CO-Sensor for domestic use on high temperature stable Ga_2O_3 thin films, IEEE Transducers '97 on Solid-State Sensors and Actuators, pp. 547-550, Chicago, U.S.A., 1997.

54. C.H. Kwon, D.H. Yun, H.K. Hong, S.R. Kim, K. Lee, H.Y. Lim and K.H. Yoon, Multi-layered thick-film gas sensor array for selective sensing by catalytic filtering technology, Sens. Actuat. B, 65, pp. 327-330, 2000.

55. T. Börjesson, U. Stöllman and J. Schnürer, Off-odours compounds produced by moulds on oatmeal agar. Identification and relations to other growth characteristics, J. Agric. Food Chem., 41, pp. 2104-2111, 1993.

56. E. Schaller, S. Zenhäusern, T. Zesiger, J.O. Bosset and F. Escher, Use of preconcentration techniques applied to a MS-based electronic nose, Analysis, 28, pp. 743-749, 2000.

57. J. W. Gardner and P.N. Bartlett, Electronic noses: Principles and applications, Oxford University Press, 1999.

58. C.K. Persaud and G.H. Dodd, Nature, 299, pp. 352-355, 1982.

59. J.W. Gardner, Detection of vapours and odours from a multi-sensor array using pattern recognition. Part 1: Principal component and cluster analysis, Sens. Actuat. B, 4, pp. 109-115, 1991.

60. D. Kohl, The role of noble metals in the chemistry of solid-state gas sensors, Sens. Actuat. B, 1, pp. 158-164, 1990.

61. H.V. Shurmer, J.W. Gardner and P. Carcoran, Intelligent vapour discrimination using a composite 12-element sensor array, Sens. Actuat. B, 1, pp. 256-260, 1990.

62. C. Cané, I. Gràcia, A. Götz, L. Fonseca, E. Lora-Tamayo, M.C. Horrillo, I. Sayago, J.I. Robla, J. Rodrigo and J. Gutiérrez, Detection of gases with arrays of micromachined tin oxide gas sensors, Sens. Actuat. B, 65, pp. 244-246, 2000.

63. W. Yan, C. Diao, Z. Tang amd X. Li, The study of gas sensor array signal processing with improved BP algorithm, Sens. Actuat. B, vol. 66, pp. 283-285, 2000.

64. J.W. Gardner and P.N. Bartlett, Monitoring of fish freshness using tin oxide sensors, in Sensors and Sensory Systems for an Electronic Nose, Kluwer Academic Publishing, pp. 257-272, 1992.

65. H.K. Hong, C.H. Kwon, S.R. Kim, D.H. Yun, K. Lee and Y.K. Sung, Portable electronic nose system with gas sensor array and artificial neural network, Sens. Actuat. B, vol. 66, pp. 49-52, 2000.

66. Fis (gas sensor company), Gas Sensor Catalogue and Technical Information (Fis, Inc.). http://www.fisinc.co.jp, 2000.

67. S. R. Morrison, Chemical sensors, in Semiconductor sensors, Ed. By S. M. Sze, John Wiley & Sons, Inc., 1994.

68. F. Cosandey, G. Skandan and A. Singhal, Materials and processing issues in nanostructured semiconductor gas sensors, JOM-e, 52, 2000.

69. A.K. Mukhopaghyay, P. Mitra, A. Chatterjee, H.S. Maiti, A new method of preparing tin dioxide thin film sensors, Journal of Materials Science Letters, 17, pp. 625-627, 1998.

70. www.directindustry.com (Thick film gas sensor producers).

71. N. M. White, J. D. Turner, Thick-film sensors: past, present and future, Measurement Science and Technology, 8, pp. 1-20, 1997.

72. B. Hoffheins, Solid state, resistive gas sensors, Handbook of Chemical and Biological Sensors, ed. R. F. Taylor and J. S. Schultz, IOP, Bristol, 1996.

73. RTC-01 Combustible gas sensor specifications (Schaumburg, IL: Sinostone).

74. J. L. Youngblood, Development of a hydrogen sulfide sensor: a case study, Sensors Expo. Proc., Peterborough, NH: Helmers Publishing, Inc., pp. L0782-L0792, 1986.

75. Steinel's website, http://www.steinel.ch

76. I. Igarashi, New technology of sensors for automotive applications, Sens. Actuat. B, 10, pp. 181-193, 1986.

77. H.J. Beie, A. Gnörich, Oxygen gas sensors based on CeO_2 thick and thin films, Sens. Actuat. B, 4, pp. 393-399, 1991.

78. H. Maixner, J. Gerblinger, U. Lampe, M. Fleischer, Thin-film gas sensors based on semiconducting metal oxides, Sens. Actuat. B, 23, pp. 119-125, 1995.

79. M. Akiyama, Z. Zhang, J. Tamaki, N. Miura, N. Yamazoe, Tungsten oxide-based semiconductor sensor for detection of nitrogen oxides in combustion exhaust, Sens. Actuat. B, 14, pp. 619-620, 1993.

80. K. Satake, A. Katayama, H. Ohkoshi, T. Nakahara, T. Takeuchi, Titania NO_x sensors for exhaust monitoring, Sens. Actuat. B, 20, pp. 111-117, 1994.

81. T. Seiyama, A. Kato, K. Fujishi, M. Nagatami, A new detector for gaseous components using semiconductive thin films, Analytical Chemistry, 34, pp. 1502-1503, 1962.

82. M. Nitta, M. Haradome, Semiconductor gas sensors, Japanese Journal of Applied Physics, 48, pp. 977-984, 1979.

83. N. Yamazoe, Y. Kurokawa, T. Seiyama, Effects of additives on semiconductor gas sensors, Sens. Actuat. B, 4, pp. 283-289, 1983.

84. W. Göpel, K. Schierbaum, H.D. Wienhöfer, J. Maier, Defect chemistry of tin (IV) oxide in bulk and boundary-layers, Solid State Ionics, 32/33, pp. 440-443, 1989.

85. B. Ruhland, T. Becker, G. Müller, Gas-kinetic interaction of nitrous oxides with SnO_2 surfaces, Sens. Actuat. B, 50, pp. 85-94, 1998.

86. B. Kamp, R. Merkle, J. Maier, Chemical diffusion of oxygen in tin dioxide, Sens. Actuat. B, 77, pp. 534-542, 2001.

87. J. W. Gardner, A non-linear diffusion-reaction model of electrical conduction in semiconductor gas sensors, Sens. Actuat. B, 1, pp. 166-170, 1990.

88. X. Vilanova, E. Llobet, X. Correig, Model for the electrical conductance transient behaviour in thick film SnO_2 semiconductor gas sensors, 18th International Semiconductor Conference, Sinaia, Rumania, IEEE, pp. 473-476, 1995.

89. X. Vilanova, E. Llobet, R. Alcubilla, J. Sueiras, X. Correig, Analysis of the conductance transient in thick-film tin oxide gas sensors, Sens. Actuat. B, 31, pp. 175-180, 1996.

90. E. Llobet, J. Brezmes, X. Vilanova, L. Fondevila, X. Correig, Quantitative vapour analysis using the transient response of non-selective thick-film oxide gas sensors, Transducers'97, International Conference on Solid-State Sensors and Actuators, Chicago, June 16-19, pp. 971-974, 1997.

91. E. Llobet, J. Brezmes, X. Vilanova, J. E. Sueiras, X. Correig, Qualitative and quantitative analysis of volatile organic compounds using transient and steady-state responses of a thick-film tin oxide gas sensor array, Sens. Actuat. B, 41, pp. 13-21, 1997.

92. E. Llobet, X. Vilanova, J. Brezmes, J. E. Sueiras, X. Correig, Transient response of thick-film tin oxide gas-sensors to multicomponent gas mixtures, Sens. Actuat. B, 47, pp. 104-112, 1998.

93. D. H. Yun, C. H. Kwon, H.-K. Hong, H. W. Shin, S.-R. Kim, K. Lee, Abnormal current-voltage characteristics of WO_3-doped SnO_2 oxide semiconductors and their applications to gas sensors, Sens. Actuat. B, 35-36, pp. 48-51, 1996.

94. W. Hellmich, G. Müller, C. B.-v. Braunmühl, T. Doll, I. Eisele, Field-effect-induced gas sensitivity changes in metal oxides, Sens. Actuat. B, 43, pp. 132-139, 1997.

95. R. Rella, A Serra, P. Siciliano, L. Vasanelli, G. Licciulli, A. Quirino, Tin oxide-based gas sensors prepared by the sol-gel process, Sens. Actuat. B, 44, pp. 462-467, 1997.

96. G. Molas, E. Llobet, F. Masana, J. CAlderer, X. Vilanova, J. Brezmes, J. E. Sueiras, X. Correig, Fabrication of highly selective SnO_2 ethanol sensors, 3th Conference on Electronic Devices, 15-16 February, Granada, Spain, pp. 41-44, 2001.

97. J. H. Park, K. H. Kim, Improvement of long-term stability in SnO_2-based gas sensor for monitoring offensive odor, Sens. Actuat. B, 56, pp. 50-58, 1999.

98. S. W. Lee, P. P. Tsai, H. Chen, Comparison study of SnO_2 thin and thick-film gas sensors, Sens. Actuat. B, 67, pp. 122-127, 2000.

99. A. A. Tomchenko, V. V. Khatko, I. L. Emilianov, WO_3 thick-film gas sensors, Sens. Actuat. B, 46, pp. 8-14, 1998.

100. A. A. Tomchenko, I. L. Emilianov, V. V. Khatko, Tungsten trioxide-based thick-film NO sensor: design and investigation, Sens. Actuat. B, 57, pp. 166-170, 1999.

101. A. A. Tomchenko, Structure and gas-sensitive properties of WO_3-Bi_2O_3 mixed films, Sens. Actuat. B, 68, pp. 48-52, 2000.

102. Y.K. Chung, M.H. Kim, W.S. Um, H.S. Lee, J.K. Song, S.C. Choi, K.M. Yi, M.J. Lee, K.W. Chung, Gas sensing properties of WO_3 thick film for NO_2 gas dependent on process conditions, Sens. Actuat. B, 60, pp. 49-56, 1999.

103. J.I. Yang, H. Lin, S.-D. Han, Influence of binders on the sensing and electrical characteristics of WO_3-based gas sensors, Sens. Actuat. B, 60, pp. 71-77, 1999.

104. D. Lee, S. Han, J. Huh, D. Lee, Nitrogen oxides-sensing characteristics of WO_3-based nanocrystalline thick film gas sensor, Sens. Actuat. B, 60, pp. 57-63, 1999.

105. D.-S. Lee, J.-W. Lim, S.-M. Lee, J.-S- Huh, D.-D. Lee, Fabrication and characterization of micro-gas sensor for nitrogen oxides gas detection, Sens. Actuat. B, 64, pp. 31-36, 2000.

106. G. Huyberechts, M. Van Muylder, M. Honoré, J. Desmet, J. Roggen, Development of a thick film ammonia sensor combined with a ventilation rate sensor for livestock buildings, Sensors IV, Technology, Systems and Applications, ed. K. T. V. Grattan, A. T Augousti, IOP Publishing Ltd., Bristol, pp. 85-90, 1993.

107. T. Maekawa, J. Tamaki, N. Miura, N. Yamazoe, Gold-loaded tungsten oxide sensor for detection of ammonia in air, Chemistry Letters, pp. 639-642, 1992.

108. Y. Takao, K. Miyazaki, Y. Shimizu, M. Egashira, Semiconductor ammonia gas sensors with double-layered structure, Transducer'93, International Conference on Solid-State Sensors and Actuators, Yokohama, Japan, pp. 360-363, 1993.

109. D. H. Yun, C. H. Know, H.-K. Hong, S.-R. Kim, K. Lee, H. G. Song, J. E. Kim, Highly sensitive and selective ammonia gas sensor, Transducers'97, International Conference on Solid-State Sensors and Actuators, Chicago, June 16-19, pp. 959- 962, 1997.

110. E. Llobet, G. Molas, P. Molinàs, J. Calderer, X. Vilanova, J. Brezmes, J. E. Sueiras, X. Correig, Fabrication of highly selective tungsten oxide ammonia sensors, Journal of the Electrochemical Society, 147, pp. 776-779, 2000.

111. C. N. Xu, N. Miura, Y. Ishida, K. Matsuda, N. Yamazoe, Selective detection of NH_3 over NO in combustion exhaust by using Au and MoO_3 doubly promoted WO_3 element, Sens. Actuat. B, 65, pp. 163-165, 2000.

112. X. Wang, N. Miura, N. Yamazoe, Study of WO_3-based sensing materials for NH_3 and NO detection, Sens. Actuat. B, 66, pp. 74-76, 2000.

113. B. T. Marquis, J. F. Vetelino, A semiconductor metal oxide sensor array for the detection of NO_x and NH_3, Sens. Actuat. B, 77, pp. 100-110, 2001.

114. M. Penza, G. Cassano, F. Tortorella, Gas recognition by activated WO_3 thin-film sensors array, Sens. Actuat. B, 81, pp. 115-121, 2001.

115. W.-H. Tao, C.-H. Tsai, H_2S sensing properties of noble metal doped WO_3 thin film sensor fabricated by micromachining, Sens. Actuat. B, 81, pp. 237-247, 2002.

116. J. L. Solis, S. Saukko, L. B. Kish, C. G. Granqvist, V. Lantto, Nanocrystalline tungsten oxide thick-films with high sensitivity to H_2S at room temperature, Sens. Actuat. B, 77, pp. 316-321, 2001.

117.Y. Shimizu, N. Matsunaga, T. Hyoto, M. Egashira, Improvement of SO_2 sensing properties of WO_3 by noble metal loading, Sens. Actuat. B, 77, pp. 35-40, 2001.

118. S. Matsushima, Y. Teraoka, N. Miura, N. Yamazoe, Electronic interaction between metal additives and tin dioxide in tin dioxide-based gas sensors, Japanese Journal of Applied Physics, 27, pp. 1798-1802, 1988.

119. K. Fukui, Alcohol selective gas sensors, US Patent 4849180, 1989.

120. T. Makaewa, Y. Anno, J. Tamaki, N. Miura, N. Yamazoe, Y. Asano, K. Hayashi, Development of semiconductor gas sensors to discern flavours of consommé soup, Sens. Actuat. B, 13, pp. 713-714, 1993.

121. M. C. Carotta, M. Ferroni, D. Gnani, V. Guidi, M. Merli, G. Martinelli, M.C. Casale and M. Notaro, Nonostructured pure and Nb-doped TiO_2 as thick film gas sensors for environmental monitoring, Sens. Actuat. B, 58, pp. 310-317, 1999.

122. A. Diéguez, A. Vilà, A. Cabot, A. Romano-Rodríguez, J. R. Morante, J. Kappler, N. Bârsan, U. Weimar and W. Göpel, Influence on the gas sensor performances of the metal chemical states introduced by impregnation of calcinated SnO_2 sol-gel nanocrsytals, Sens. Actuat. B, 68, pp. 94-99, 2000.

123. P. Albers and J. Kiwi, Highly dispersed platinum on TiO_2 obtained via autoreduction of the precursor species, Journal of Molecular Catalysis, 58, pp. 115-126, 1990.
124. K. Sekizawa, H. Widjaja, S. Maeda, Y. Ozawa and K.Eguchi, Low temperature oxidation of methane over Pd catalyst supported on metal oxides, Catalysis Today, 59, pp. 69-74, 2000.
125. P. Claus, H. Berndt, C. Mohr, J. Radnik, E.- J. Shin and M. A. Keane, Pd/MgO: Catalyst characterization and phenol hydrogenation activity, Journ. of Catalysis, 192, pp. 88-97, 2000.
126. J. C. Kennedy III and A. K. Datye, Photothermal heterogeneous oxidation of ethanol over Pt/TiO_2, Journal of Catalysis 179, pp. 375–389, 1998.
127. J. C. Yang, Y. C. Kim, Y. G. Shul, C. H. Shin and T. K. Lee, Characterization of photoreduced Pt/TiO_2 and decomposition of dichloroacetic acid over photoreduced Pt/TiO_2 catalysts, Applied Surface Science, 121/122, pp. 525-529, 1997.
128. N. Yamazoe, Chemical sensors R&D-Japan, Sens. Actuat. B, 6, pp. 9-15, 1992.
129. M. Prudenziati (ed) Thick-film sensors, (Amsterdam: Elsevier Science) 1994.
130. N. M. White and J. D. turner, Thick-film sensors: past, present and future, Meas. Science Technology 8 pp. 1-20, 1997.
131. J. E. Brignell, N. M. White, A. Cranny, Sensor applications of thick-film technology, IEE Proc. I, 135, pp. 77-84, 1998.
132. M. Prudenziati and B. Morten, The state of the art in thick-film sensors, Journal of Microelectronic, 23, pp.133, 1992.
133. P. Holmes R. G. Loasby, Handbook of thick film technology (Glasgow: Electrochemical Publications) 1976.
134. G Martinelli and M. C. Carotta, Thick-film gas sensors, Sens. and Actuators. B, 23 pp. 157-161, 1995.
135. W. Wepper, Solid state electrochemical gas sensors, 12, pp. 107, 1987.
136. Y.K. Chung, M.H. Kim, W.S. Um, H.S. Lee, J.K. Song, S.C. Choi, K.M. Yi, M.J. Lee and K.W. Chung, Gas sensing properties of WO_3 thick film for NO_2 gas dependent on process condition, Sens. Actuat. B, 60, pp. 49-56, 1999.
137. G. Zhang, M. Liu, Effect of particle size and dopant on properties of SnO_2-based gas sensors, Sens. Actuat. B, 69, pp. 144-152, 2000.
138. M.J. Willett, V.N. Burganos, C.D. Tsakiroglou, and A.C. Payatakes, Gas sensing and structural properties of variously pre-treated nanopowder tin (IV) oxide samples, Sens. Actuat. B, 53, pp. 76-90, 1998.
139. A.A. Tomchenko, Structure and gas-sensitive properties of WO_3-Bi_2O_3 mixed thick films, Sens. Actuat. B, 68, pp. 48-52, 2000.

140. A. Cabot, J. Arbiol, A. Cornet and J.R. Morante, Bi_2O_3 as selective sensing material for NO detection. 9th Conference IMCS, Boston, 2002.

141. Y.S. Chung and H.G. Kim, Effect of oxide glass on the sintering behavior and electrical properties in Ag thick films, IEEE Transac. on Components, Hybr., and Manufact. Technology, 11, 1988.

142. C. Cantalini, M.Z. Atashbar, Y. Li, M.K.Ghatasala, Characterisation of sol-gel prepared WO_3 thin films as gas sensor, J.Vac. Sci. Technol. A, 17, 1999.

143. Da. Lee, S. Han, J. Huh, Du. Lee, Nintrogen oxides-sensing characteristics of WO_3-based nanocrystalline thick film gas sensor, Sens. Actuat. B, 60, pp. 57-63, 1999.

144. H.S. Varol, A. Hinsch, SnO_2, Sb dip coated films on anodized aluminum selective absorber plates, Sol. Ener. Mat. Cells, 40, pp. 273-283, 1996.

145. B.Orel, A. Surca, Structural and FTIR spectroscopic studies of gel-xerogel-oxide transitions of SnO_2 and SnO_2:Sb powders and dip-coated films prepared via inorganic sol-gel route, J. Non-Cryst. Sol., 167, pp. 272-288, 1994.

146. R. Rella, A. Serra, P. Siciliano, L. Vasanelli, G. De, A. Licciulli and A. Quirini, Tin oxide based gas sensors prepared by sol-gel process, Sens. Actuat. B, 80, pp. 267-271, 2001.

147. A. Khodadadi, S.S. Mohajerzadeh, Y. Mortazavi and A. Miri, Cerium oxide/SnO_2-based semiconductor gas sensors with improved sensitivity to CO, Sens. Actuat. B, 44, pp. 462-467, 1997.

148. Datasheet of Figaro sensor 822: http://www.figarosensor.com/products/822pdf.pdf

149. S. Matsushima, T. Maekawa, J. Tamaki, N. Miura, N. Yamazoe, Role of additives on alcohol sensing by semiconductor gas sensor, Chemical Letters (1989) pp. 845-848

150. N. Yamazoe, New approaches for improving semiconductor gas sensors, Sens. Actuators, B, Chem 5 (1991) pp. 7-19

151. V. Gopal Reddy, W. Cao, O. K. Tan and W. Zhu, Preparation of $Fe_2O_3(0.9)$–$SnO_2(0.1)$ by hydrazine method: application as an alcohol sensor, Sens. Actuators, B, Chem 81 (2002) pp. 170-175

152. T. Maekawa, J. Tamaki, N. Miura, N. Yamazoe and S. Matsushima, Development of SnO_2-based ethanol gas sensor, Sens. Actuators, B, Chem 9 (1992) pp. 63-69

153. B. Ruhland, Th. Becker, G. Müller, Gas-kinetik interactions of nitrous oxides with SnO_2 surfaces, Sens. Actuat. B, Chem. 50, pp. 85-94, 1998.

154. I. Kocemba, S. Szafran, J. Rynkowski and T. Paryjczak, The properties of strongly pressed tin oxide-based gas sensors, Sens. Actuat. B, 79, pp. 28-32, 2001.

155. R. Long, R. Yang, Noble metal (Pt, Rh, Pd) promoted Fe-ZSM-5 for selective catalytic oxidation of ammonia to N_2 at low temperatures, Catalysis Letters, 78, pp. 353-357, 2002.

156. J. Gland and V. Korchak, Ammonia oxidation on a stepped platinum single crystal surface, Journal of Catalysis, 53, pp. 9-23, 1978.

157. T. Pignet and L. D. Schmidt, Kinetics of NH_3 oxidation of Pt, Rh, and Pd, Journal of Catalysis, 40, pp. 212-219, 1975.

158. D. Williams, Conduction and gas response of semiconductor gas sensors, Solid State Gas Sensors, Adam Hilger, Bristol, pp. 71, 1987.

159. P. Moseley, D. Williams, Oxygen surface species on semiconducting oxides, Solid State Gas Sensors, Adam Hilger, Bristol, pp. 46, 1987.

160. K. Shimazu, R. Goto, K. Tada, Electrochemical reduction of nitrate ions on tin-modified platinum and palladium electrodes, Chemistry letters, 2, pp. 204-205, 2002.

161. M. Zhang, B. Zhou and K. Chuang, Catalytic deep oxidation of volatile organic compounds over fluorinated carbon supported platinum catalysts at low temperatures, Appl. Catalysis, B, Env. 13, pp. 123-130, 1997.

162. Y. Li, J. Armor, Selective NH_3 oxidation to N_2 in a wet stream, Appl. Catalysis, B Env. 13, pp. 131-139, 1997.

163. P. Papaefthimiou, T. Ioannides, and X. Verykios, Catalytic incineration of volatile organic compounds present in industrial waste streams, Appl. Thermal Engng. 18, pp. 1005-1012, 1998.

164. W. Menz, J. Mohr, O. Paul, Microsystem technology, Wiley-Vch Verbag GmbH, Germany, 2001.

165. S. Fung, Z. Tang, P. Chan, J. Sin, P. Cheung, Thermal analysis and design of micro-hot plate for integrated gas-sensor applications, Sensors and Actuators A, 54, pp. 482-487, 1996.

166. A. Götz, I. Gràcia, C. Cané, E. Lora-Tamayo, Thermal and mechanical aspects for the designing micromachined low-power gas sensors, Journal of Micromachining and Microengineering, 7, pp. 247-249, 1997.

167. Sberveglieri, W. Hellmich, G. Müller, Silicon hotplates for metal oxide gas sensor element, Microsystem Technologies 3, pp. 183-190, 1997.

168. J. Suehle, R. E. Cavicchi, M. Gaitan, S. Semancik, Tin oxide gas sensor fabricated using CMOS micro-hotplates and in situ processing, IEEE Electr. Dev. Lett., 14, pp. 118-120, 1993.

169. N. Najafi, K. D. Wise, R. Merchange, J. W. Schwank, An integrated multi-element ultrathin film gas analyser, Proceedings of the 1992 Workshop on Sensors and Actuators, Hilton Head, pp. 19-22, 1992.

170. N. Najafi, K. D. Wise, J. W. Schwank, A micromachined ultra-thin-film gas detector, IEEE Transaction on Electron Devices, 41, pp. 1770-1777, 1994.

171. S. Semancik, R. Cavicchi, M. Gaitan, J. Suehle, Temperature-controlled, micromachined arrays for chemical sensor fabrication and operation, US Patent no. 5345213, 1994.

172. S. Semancik, R. E. Cavicchi, Kinetically-controlled chemical sensing using micromachined structures, Accounts of Chemical Research, 31, pp. 279-287, 1998.

173. G. Faglia, E. Comini, A. Cristalli, G. Sberveglieri, L. Dori, Very low power consumption micromachined CO sensors, Sens. Actuat. B, 55, pp. 140-146, 1999.

174. M. Schweizer-Berberich, M. Zdralek, U. Weimer, W. Gopel, T. Viard, D. Martinez, A. Seube, A. Peyre-Lavigne, Pulsed mode of operation and artificial neural network evaluation for improving the CO selectivity of SnO_2 gas sensors, Sens. Actuat. B, 65, pp. 91-93, 2000.

175. S. Semancik, R. E. Cavicchi, M. C. Wheeler, J. E. Tiffany, G. E. Poirier, R. M. Walton, J. S. Suehle, B. Panchapakesan, D. L. DeVoe, Microhotplate platforms for chemical sensor research, Sens. Actuat. B, 77, pp. 579-591, 2001.

176. M.C. Horrillo, I. Sayago, L. Arés, J. Rodrigo, J. Gutiérrez, A. Götz, I. Gràcia, L. Fonseca, C. Cané, E. Lora-Tamayo, Detection of low NO_2 concentrations with low power micromachined tin oxide gas sensors, Sensors Actuators B, 58, pp. 325-329, 1999.

177. D.G. Rickerby, N. Wätchter, M.C. Horrillo, J. Gutiérrez, I. Gràcia, C. Cané, Structural and dimensional control in micromachined integrated solid state gas sensors, Sensors Actuators B, 69, pp. 314-319, 2000.

178. E. Llobet, P. Ivanov, X. Vilanova, J. Brezmes, J. Hubalek, K. Malysz, I. Gracia, C. Cané and X. Correig, Screen-printed nanoparticle tin oxide films for high-yield sensor microsystems , Sens. Actuat. B-Chemical, 96, pp. 94-104, 2003.

179. J. Laconte , V. Wilmart , J.P. Raskin and D. Flandre, Fully CMOS compatible low-power microheater, Design, Test, Integration and Packaging of MEMS/MOEMS - DTIP 2002, Cannes Mandelieu, France, May 5-8, pp. 634-644, 2002.

180. V. A. Chandhary, I. S. Mulla, S. R. Sainbar, A. A. Belhebar, K. Vijayamohanan, Surface-ruthenated tin oxide as a novel hydrocarbon sensor, Sensors and Actuators A, 65, pp. 197-202, 1998.

181. D. S. Vlachose, C. A. Papadopoulos, J. N. Avaritsiotis, Characterization of the catalyst-semiconductor interaction mechanism in metal-oxide gas sensors, Sens. Actuat. B, 44, pp. 458-461, 1997.

182. I. Simon, N. Barsan, M. Bauer, U. Weimar, Micromachined metal oxide gas sensors: opportunities to improve sensor performance, Sens. Actuat. B, 73, pp. 1-26, 2001.

183. S. Semancik, R. Cavicchi, Kinetically controlled chemical sensing using micromachined structures, Accounts of Chemical Research, 31, pp. 279-287, 1998.

184. D. G. Rickerby, M. Horrillo, J. P. Santos, P. Serrini, Microstructural characterization of nanograin tin oxide gas sensors, Nanostructured Materials, 9, pp. 43-52, 1997.

185. D. G. Rickerby, N. Wächter, M. C. Horrillo, J. Gutiérrez, I. Gràcia, C. Cané, Structural and dimensional control in micromachined integrated solid state gas sensors, Sens. Actuat. B, 69, pp. 314-319, 2000.

186. J.W. Gardner, A non-linear diffusion-reaction model of electrical conduction in semiconductor gas sensors, Sens. Actuat. B, 1, pp. 166-170, 1990.

187. Neuralex Toolbox for Matlab®, Documentation, The MathWorks, Inc., 2000.

188. R. Ionescu, E. Llobet, X. Vilanova, J. Brezmes, J.E. Suerias, J. Calerer, X. Correig, Quantitative analysis of NO_2 in the presence of CO using a single tungsten oxide semiconductor sensor and dynamic signal processing, Analyst, 127, pp. 1237-1246, 2002.

189. G. Carpenter, S. Grossberg, N. Markuzon, J. Reynolds, and D. Rosen, Fuzzy ARTMAP: A neural network architecture for incremental supervised learning of analog multidimensional maps, IEEE Trans. Neural Nets., 3, pp. 698-703, 1992.

190. E. Llobet, E.L. Hines, J.W. Gardner, P.N. Bartlett, T.T. Mottram, Fuzzy ARTMAP based electronic nose data analysis, Sens. Actuat. B 61, pp. 183-190, 1999.

191. S.M. Weiss, C.A. Kulikowski, Computer Systems that Learn, Chapter 2, Morgan Kaufmann Publishers, Inc., San Francisco, CA, 1991.

192. D. Kohl, The role of noble metals in the chemistry of solid-state gas sensors, Sens. Actuat. B, 1, pp. 158-165, 1990.

192. J. I. Goldstein, D. E. Newbury, P. Echlin, D. C. Joy, A. D. Romig Jr., C. E. Lyman, C. Fiori, E. Lifshin, Scanning electron microscopy and X-ray microanalysis, A text for biologists, material scientists, and geologists, Plenum Press, New York, 1992.

193. K. Nakamoto, Infrared and Raman Spectra of Inorganic and Coordination Compounds, John Wiley and Sons Inc., New York, 1986.

194. J. G. Grasselli and B. J. Bulkin, Analytical Raman Spectroscopy, John Wiley and Sons Inc., New York, 1991.

195. A. Cabot, A. Diéguez, A. Romano-Rodríguez, J. R. Morante and N. Bârsan, Influence of the catalytic introduction procedure on the nano-SnO_2 gas sensor performances. Where and how stay the catalytic atoms, Sens. Actuat. B, 79, pp. 98-106, 2001.

LIST OF PUBLCATIONS

1. P. Ivanov, E. Llobet, X. Vilanova, J. Brezmes, J. Hubalek, K. Malysz, X. Correig,

A route toward more selective and less humidity sensitive screen-printed SnO_2 and WO_3 gas sensitive layers,

Published in Sensors and Actuators B-Chemical, 100, (2004), pp.221-227

2. P. Ivanov, E. Llobet, X. Vilanova, J. Brezmes, J. Hubalek and X. Correig,

Development of high sensitivity ethanol gas sensor based on Pt-doped SnO_2 surfaces,

Published in Sensors and Actuators B-Chemical, 99 (2004) pp. 201-206

3. P. Ivanov, M. Stankova, E. Llobet, X. Vilanova, I. Gràcia, C Cané and X. Correig,

Microhotplate sensor arrays based on sputtered and screen printed metal oxide films for selective detection of volatile compounds

Published in Sensors & Transducers Magazine, Vol. 36, Issue 10 (2003), pp. 16-23

4. E. Llobet, **P. Ivanov**, X. Vilanova, J. Brezmes, J. Hubalek, K. Malysz, I. Gràcia, C. Cané and X. Correig,

Screen-printed nanoparticle tin oxide films for high-yield sensor microsystems,

Published in Sensors and Actuators B-Chemical, 96 (2003) pp. 94-104

5. C. Bittencourt, E. Llobet, **P. Ivanov**, X. Correig, X. Vilanova, J. Brezmes, J. Hubalek, K. Malysz, J.J. Pireaux, J. Calderer,

Influence of the doping method on the sensitivity of Pt-doped screen-printed SnO_2 sensors,
Published in Sensors and Actuators B-Chemical, 97 (2004) pp. 67-73

6. M. Stankova, **P. Ivanov**, E. Llobet, J. Brezmes, X. Vilanova, I. Gràcia, C. Canè, J. Hubalek, K. Malysz, X. Correig,

Sputtered and screen-printed metal oxide-based integrated micro-sensor array for the quantitative analysis of gas mixtures,
Published in Sensors and Actuators B-Chemical (In press)

7. K. Malysz, J. Prásek, X. Vilanova, J. Hubálek, **P. Ivanov**, E. Llobet, J. Brezmes, X. Correig, Z. Sverák,

On the use of a catalytic filter to selectively detect benzene with a tungsten oxide sensor,
Published in Sensors and Actuators B-Chemical (In press)

8. P. Ivanov, M. Stankova, E. Llobet, X. Vilanova, I. Gràcia, C. Cané J. Calderer and X. Correig,

Nano-particle metal oxide films for micro-hotplate gas sensors,
Submitted to IEEE Sensors Journal

9. A. Vergara, E. Llobet, J. Brezmes, **P. Ivanov**, X. Vilanova, I. Gràcia, C. Cané and X. Correig,

Optimized temperature modulation of micro-hotplate gas sensors through pseudorandom binary sequences,
Published in IEEE Sensors Journal (In press)

10. M. Stankova, X. Vilanova, J. Calderer, E. Llobet, **P. Ivanov**, I. Gràcia, C. Cané and X. Correig,

Detection of SO_2 and H_2S in CO_2 stream by means of WO_3-based microhotplate sensors,
Published in Sensors and Actuators B-Chemical (In press)

11. C. Bittencourt, E. Llobet, **P. Ivanov**, X. Vilanova, X. Correig, M.A.P. Silva, L.A.O. Nunes and J.J. Pireaux,

Ag induced modifications on WO_3 films studied by AFM, Raman and X-ray photoelectron spectroscopy,

Submitted to Journal of Condensed Matter

12. P. Ivanov, J. Laconte**,** J. P. Raskin, M. Stankova, E. Sotter, E. Llobet, X. Vilanova, D. Flandre, X. Correig

SOI-CMOS compatible low-power gas sensor using sputtered and drop-coated metal-oxide active layers, pp. 137-142

Submitted to Journal of Microsystem Technologies

13. P. Ivanov, E. Llobet, M. Stankova, A. Vergara, X. Vilanova, J.Hubalek, I. Gracia, C. Cané, X. Correig

Towards a microsystem for monitoring ethylene in warehouses

Submitted to Sensors and Actuators B-Chemical

14. P. Ivanov, M. Vilaseca, E. Llobet, X. Vilanova, J. Hubalek, J. Coronas, J. Santamaría, X. Correig

Influence of zeolite films on the sensitivity of SnO_2 and Pt-SnO_2 thick film gas sensors

Submitted to Sensors and Actuators B-Chemical

15. A. Vergara, E. Llobet, J. Brezmes, **P. Ivanov**, X. Vilanova, I. Gracia, C. Cané, X. Correig,

Optimised temperature modulation of metal oxide micro-hotplates gas sensors through multi-level PRS

Submitted to Sensors and Actuators B-Chemical

INTERNATIONAL CONGRESSES

1. June 2003, European Material Research Society, Sprig Meeting, Strasbourg, France,
P. Ivanov, E. Llobet, X. Vilanova, J. Brezmes, J. Hubalek, K. Malysz, X. Correig,

A route toward more selective and less humidity sensitive screen-printed SnO_2 and WO_3 gas sensitive layers, pp. N-12

2. September 2003, Smart Sensors and MEMS, NATO Advanced Study Institute, Povoa de Varzim, Portugal,
P. Ivanov, M. Stankova, E. Llobet, X. Vilanova, X. Correig, J. Hubalek, K. Malysz, I. Gràcia, C. Cané,

Microhotplate sensor arrays based on sputtered and screen-printed metal oxide films for selective detection of volatile compounds, pp. 291

3. September 2003 Eurosensors XVII, 17th European Conference on Solid-State Transducers, Guimaraes, Portugal,
M. Stankova, **P. Ivanov**, E. Llobet, J. Brezmes, X. Vilanova, I. Gràcia, C. Cané, J. Hubalek, K. Malysz, X. Correig,

Sputtered and screen-printed metal oxide –based integrated micro-sensor arrays for the quantitative analysis of gas mixture, pp. 667-668

4. September 2003 Eurosensors XVII, 17th European Conference on Solid-State Transducers, Guimaraes, Portugal,
K. Malysz, J. Prásek, X. Vilanova, J. Hubálek, **P. Ivanov**, E. Llobet, J. Brezmes, X. Correig, Z. Sverák

On the use of a catalytic filter to selectively detect benzene with a tungsten oxide sensor, pp. 665-666

5. October 2003 IEEE Sensors 2003, The second IEEE international conference on sensors, Toronto, Canada,
P.Ivanov, E. Llobet, X. Vilanova, M. Stankova, J. Brezmes, X. Correig, J. Hubalek, K. Malysz,I. Gràcia, C. Cané,

Screen-printed nano-grain WO_3 films for micro-hotplate gas sensors, pp. 100-101

6. October 2003 IEEE Sensors 2003, The second IEEE international conference on sensors, Toronto, Canada,
A. Vergara, E. Llobet, , J. Brezmes, M. Stankova, **P. Ivanov**, I. Gràcia, C. Cané, X. Correig

MLS-based temperature modulation of μ-hotplates, pp. 440-441

7. May 2004 Symposium on Design, Test, Integration and Packaging of MEMS/MOEMS, Conference of microfabrication, integration and packaging, Montreux, Switzerland,
P. Ivanov, J. Laconte**,** J. P. Raskin, M. Stankova, E. Sotter, E. Llobet, X. Vilanova, D. Flandre, X. Correig

SOI-CMOS compatible low-power gas sensor using sputtered and drop-coated metal-oxide active layers, pp. 137-142

8. September 2004 Eurosensors XVIII, 18th European Conference on Solid-State Transducers, Rome, Italy,
P. Ivanov, E. Llobet, M. Stankova, A. Vergara, X. Vilanova, J. Hubalek, I. Gracia, C. Cané, X. Correig

Towards a microsystem for monitoring ethylene in warehouses

9. September 2004 Eurosensors XVIII, 18th European Conference on Solid-State Transducers, Rome, Italy,

P. Ivanov, M. Vilaseca, E. Llobet, X. Vilanova, J. Hubalek, J. Coronas, J. Santamaría, X. Correig

Influence of zeolite films on the sensitivity of SnO_2 and Pt-SnO_2 thick film gas sensors

10. September 2004 Eurosensors XVIII, 18th European Conference on Solid-State Transducers, Rome, Italy,

A. Vergara, E. Llobet, J. Brezmes, **P. Ivanov**, X. Vilanova, I. Gracia, C. Cané, X. Correig,

Optimised temperature modulation of metal oxide micro-hotplates gas sensors through multi-level PRS

NATIONAL CONGRESSES

1. February 2003, 4th Conference on Eletronic Devices, Calella de la Costa, Spain,
P. Ivanov, E. Llobet, X. Vilanova, J. Brezmes, X. Correig, J. Hubálek, K. Malysz, I. Gràcia and C. Cané,

Screen-printed nano-grain tin oxide films for micro-hotplate gas sensors, pp. 145

2. June 2003, Ph.D Students' Meeting on Electron Devices and Microelectronics, Tarragona, Spain
P. Ivanov, E. Llobet, X. Vilanova, J. Hubalek, K. Malysz, X. Correig

Improvement of the selectivity of screen-printed SnO_2 and WO_3 gas sensitive layers

3. June 2004, Nanoelectronic and Photonic Systems Workshop, Tarragona, Spain
P. Ivanov, E. Llobet, X. Vilanova, X. Correig

Improvement of the selectivity of SnO_2 and Pt-SnO_2 thick film gas sensors via zeolite films

RESUMEN DE LA TESIS DOCTORAL

En la Comunidad Europea se ha tomado conciencia del problema causado por la contaminación del medio ambiente. La lista inicial de contaminantes que deben ser controlados con mayor atención incluye aquellas especias susceptibles de afectar en mayor medida a la salud pública en los ecosistemas humanos. En referencia a la contaminación atmosférica, dicha lista incluye partículas en suspensión, óxidos de nitrógeno, dióxido de sulfuro, vapores de benceno, ozono y especies causantes de malos olores como el sulfhídrico y los vapores de amoniaco. Entre las especies citadas anteriormente, los óxidos de nitrógeno, el sulfhídrico y los vapores de amoniaco constituyen serios contaminantes del medio ambiente. Los óxidos de nitrógeno aparecen como resultado de la combustión de combustibles fósiles en plantas de generación de energía eléctrica, en calderas de calefacción/agua caliente, automóviles, etc. pueden causar una seria contaminación ambiental ya que son responsables de la lluvia ácida y la contaminación por ozono. La aparición de vapores de amoniaco en la atmósfera es debida a causas diversas como fugas en sistemas de refrigeración basados en la absorción NH_3-H_2O, procesos de combustión a presión atmosférica y altas temperaturas (p.e. para la reducción catalítica o no catalítica de NO_x) y calefactores de queroseno de uso doméstico, entre otros. Sin embargo, la mayor parte de los vapores de amoniaco emitidos en la atmósfera en Europa provienen de las instalaciones para la cría y el engorde de

animales. Se ha comprobado que las emisiones de sulfhídrico están asociadas al nivel de emisión de vapores de amoniaco en las instalaciones citadas anteriormente. NH_3 y H_2S contribuyen significativamente a la contaminación atmosférica y a la generación de malos olores. Además, los niveles de dichos contaminantes en el interior causan problemas de salud a los animales, lo que redunda en una disminución de la productividad.

Los métodos existentes en la actualidad que permiten la detección fiable de estos gases se basan en técnicas ópticas (p.e. fluorescencia de foto-fragmentación). Dichos métodos, aunque precisos, son excesivamente caros. En muchos casos, en que existe la necesidad de realizar un control continuo y los requerimientos de bajo coste, la utilización de sensores químicos de estado sólido es una buena solución. La investigación y desarrollo de sensores químicos de estado sólido ha mostrado un importante crecimiento en los últimos años. Este tipo de dispositivos está asumiendo una importancia creciente en la detección de gases debido a su tamaño reducido, bajo coste, capacidad de realizar medidas continuas y especialmente, a la mejora constante de sus prestaciones. Todo ello los convierte en una opción prometedora para el desarrollo de equipos analizadores de bajo coste.

El trabajo realizado en esta tesis doctoral consiste en el desarrollo de sensores químico-resistivos de capa gruesa destinados a la detección gases contaminantes en la atmósfera. Para lograr este objetivo, se ha puesto a punto la tecnología de fabricación de sensores de capa gruesa. Especial interés se ha mostrado por la detección de vapores de amoníaco. En este trabajo contemplamos dos objetivos principales. En primer lugar se han fabricado sensores de gases de capa gruesa robustos y de bajo coste basados en óxido de estaño y de tungsteno. Con estos materiales ya se han obtenido resultados prometedores para la detección de NH_3. Se han depositado capas gruesas sobre soportes con electrodos, para medir la resistencia de las capas. Tres diferentes tipos de sensores han sido estudiados. En el primer caso, el conjunto se ha realizado sobre substratos alúmina en los que se han elaborado todos los elementos necesarios para el funcionamiento del dispositivo (electrodos, elemento calefactor, resistencia de medida de la temperatura del sensor y la capa activa) por medio de técnicas serigráficas. Se han examinado las distintas

condiciones de deposición de la capa activa sobre el sensor y se ha estudiado la inclusión de dopantes (Pt, Ti, Ag, etc.). Se han diseñado máscaras serigráficas y se han preparado las pastas necesarias. Se han obtenido capas dopadas por sputtering (para ello se han diseñado máscaras de sombra especiales) y también añadiendo los dopantes en la pasta, antes de la deposición de la capa activa. Con ello se ha podido investigar de forma sistemática el comportamiento de los sensores en función de las condiciones de deposición de la capa activa. El sensor fabricado permite miniaturización y admite su integración en una matriz de sensores.

En el caso de los otros tipos de sensores se ha realizado sólo la deposición de la capa activa, encima de substratos ya fabricados. Se han utilizado substratos de silicio con resistencia de poli-silicio micro-mecanizado (microhotplates) y substratos de tipo SOI-CMOS (silicon-on-insulator). Para lograr este objetivo, se ha a punto la tecnología de impresión de capa gruesa sobre micro-mecanizado y se han hecho pruebas con SOI-CMOS. Se ha diseñado un juego máscara serigráfica que permiten deposición de capa gruesa sobre una oblea de 3 o 4 pulgadas. De este modo se ha podido obtener una capa uniforme sobre todos los sensores, que forman parte de la oblea. Esta está compuesta por 95 o 235 dados y cada dado por su parte contiene un conjunto inseparable de 2 o 4 sensores. Se han realizado pruebas con distintas malla de plástico y de metal para poder lograr una buena alineación entre la mascara y la oblea y una alta definición de la capa depositada. Se han obtenido sensores basados en capas de óxido estaño y óxido de tungsteno dopado y no dopado. Se ha evaluado la respuesta de los sensores desde el punto de vista de la sensibilidad, selectividad y de la velocidad de respuesta. Se han realizado pruebas para determinar la inercia térmica y la potencia consumida.

A todos mlos sensores fabricados se ha hecho caracterización estructural de las capas depositadas. Con gran rigor se han correlacionado los métodos de síntesis y deposición de las fases activas con la morfología y estructura final después de la deposición, pues diferentes morfologías superficiales de una misma fase suelen generar actividades catalíticas muy diferenciadas. Esto ha tenido gran relevancia en los casos en que se han introducido agentes dopantes como el Pt, Ti, Ag, Au, etc. que pueden ubicarse en los bordes del grano cristalino de la fase mayoritaria según la morfología superficial dando

una distribución del agente dopante más o menos conveniente a la selectividad que se pretende obtener. Se han utilizado diversas técnicas para estudiar la estructura, morfología, composición y propiedades superficiales de las capas de óxido de estaño y de tungsteno. Para llevar a cabo dicha caracterización se han utilizado técnicas de difracción (XRD), espectroscopia foto-electrónica de rayos X (XPS), espectroscopia vibracional (espectroscopia Raman), microscopias electrónicas (SEM y TEM) y AFM.

Se ha caracterizado el comportamiento estático de los sensores fabricados. Para ello estos han sido soldados con máquina de ultrasonido y encapsulados. Para la caracterización del comportamiento estático se ha utilizado un sistema automatizado de medida en flujo continuo que permite medir gases simples o mezclas binarias y un sistema de inyección mediante jeringa cromatográfica. En concreto se han medido las respuestas a los siguientes gases y vapores: amoniaco, sulfhídrico, dioxido de carbono, metano, etileno, etanol y benceno (metano, sulfhídrico y vapor de agua son interferentes importantes para la medida de amoníaco, en cuanto al etanol constituye un vapor patrón en la caracterización de sensores de óxidos metálicos).

El segundo objetivo ha consistido en aplicar técnicas asociadas a los sistemas de olfato electrónico, como son la utilización de una matriz de sensores con selectividades parcialmente solapadas, para desarrollar una nariz electrónica capaz de discriminar entre distintos gases. Las matrices fabricadas han sido capaces de hacer una medición continuada de gases y volátiles orgánicos y han podido rechazar interferencias causadas tanto por variaciones de temperatura y humedad en el ambiente de medida como por la presencia de otros gases (p.e. metano y sulfhídrico). Se ha investigado el comportamiento de los sensores, añadiendo varios dopantes en la capa activa.

Los sensores de gases fabricados junto a las técnicas de procesado de señal para agrupaciones de sensores, conduce a un gran número de aplicaciones. Se pueden destacar los sectores de ganadería (mejora de la productividad y del bienestar de los animales), medio ambiente (detección de emisiones de de gases en la atmósfera), sistemas de refrigeración (sistemas basados en ciclos de absorción con amoniaco), seguridad doméstica e industrial (monitorización de calderas y reducción de emisiones de NO_x).